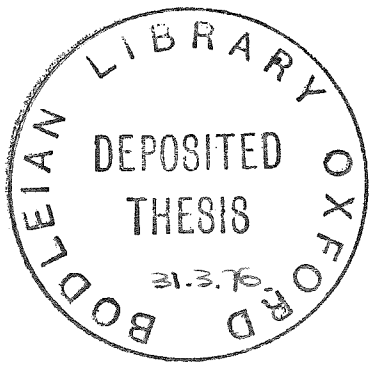
THE EFFECT OF NITROGEN AND OXYGEN ON THE MECHANICAL PROPERTIES OF MOLYBDENUM

Douglas James Capp

Wolfson College



A thesis submitted in supplication for the degree of

Doctor of Philosophy

Oxford University

Michaelmas Term, 1975

ABSTRACT

An investigation has been made of the effects of nitrogen and oxygen in solid solution on the mechanical properties of molybdenum single crystals. This is believed to be the first investigation of its type, involving the controlled addition of interstitial solutes to a Group VIa metal.

The establishment of a standard route for the preparation of molybdenum single crystals of well characterised purity has been undertaken as a necessary preliminary to the investigation of interstitially doped material. High purity molybdenum with a resistance ratio >5,000 and a total interstitial content <10 at.ppm has been prepared by the successive zone-melting, decarburisation and high vacuum annealing of commercial purity material. Resistance ratio measurements and chemical analysis have been used to define the purification mechanisms which operate during these treatments.

A high speed quenching technique has been developed for doping molybdenum mechanical test specimens with nitrogen and oxygen. Compression specimens may be prepared with only small concentrations of interstitials in solid solution ($\sim$10 at.ppm) but comparatively large concentrations (>100 at.ppm) may be quenched into solution in wire tension specimens. The nitrogen doped molybdenum is more thoroughly characterised than the oxygen doped molybdenum.

Residual resistivity and lattice parameter measurements have indicated some anomalous features of the behaviour of nitrogen and oxygen in molybdenum. The specific residual resistivity of oxygen in molybdenum is much lower than that generally observed for interstitial solutes in refractory metals. This indicates a weak electronic interaction of oxygen with molybdenum which may be analagous to that of substitutional solutes. The lattice parameter changes caused by nitrogen and oxygen in molybdenum do not show a linear concentration dependence. The observed concentration dependence is in qualitative agreement

with the clustering behaviour of interstitials in these supersaturated solid solutions. The specific lattice parameter changes associated with unclustered nitrogen and oxygen atoms in molybdenum are an order of magnitude greater than those observed for interstitial atoms in Group Va metals. No other reliable measurements have been reported for Group VIa metals but this would suggest a much stronger elastic interaction of interstitial atoms with Group VIa than Group Va metals.

A comprehensive study of the deformation behaviour of molybdenum-nitrogen alloys has been conducted involving the variation of temperature, composition and crystal orientation. A more abridged deformation study of molybdenum-oxygen alloys has also been completed.

Interstitial alloying has been shown to have a strong effect on the deformation behaviour of molybdenum throughout the concentration range 10 at. ppm to >100 at.ppm. The effects are complex and appear to be associated with both interstitials segregated to dislocations and those in bulk solid solution. The doping of molybdenum with low concentrations of interstitials produces a dramatic coarsening of the surface slip traces but no significant change in the slip geometry. The principal effect on the stress-strain behaviour is the introduction of a discontinuous yield. This is believed to be a consequence of the pinning of the grown-in dislocations by interstitial atoms. At high concentrations of interstitials changes in the flow behaviour at large strains occur. The most notable of these is a reduction in the work hardening rate which indicates that interstitial atoms in bulk solid solution are influencing the dynamic behaviour of dislocations. Nitrogen produces larger changes in the deformation behaviour of molybdenum than does oxygen. This agrees with other observations of the comparative effects of nitrogen and oxygen on the deformation behaviour of tantalum (Smialek and Mitchell 1970).

There is a large lattice contribution to the low temperature flow stress of molybdenum. Nitrogen and oxygen cause an increase in both the temperature dependence of the yield stress, defined by direct deformation and the

temperature dependence of the flow stress, defined by differential temperature change tests. The magnitude of the increase is dependent on the orientation of the deformation axis. The increase in the thermal component of the flow stress caused by nitrogen in molybdenum is more than twice that previously determined for nitrogen in niobium (Taylor and Bowen 1970). The larger frictional hardening effect of the atom clusters which are present in the supersaturated molybdenum-nitrogen solid solutions may be partly responsible for this difference. But the lattice parameter measurements indicate that the mean elastic dilatation of the lattice caused by individual nitrogen atoms is an order of magnitude greater in molybdenum than in Group Va metals. This might also be expected to produce a larger increase in the lattice friction stress of molybdenum than of Group Va metals. These results indicate important differences between the deformation characteristics of interstitial alloys of molybdenum and Group Va metals. Similar studies of other Group VIa metal-interstitial alloys are necessary to verify the general validity of these conclusions about the comparative effects of interstitials on the deformation behaviour of Group Va and VIa metals.

References:

Smialek R.L. and Mitchell T.E. 1970, Phil. Mag. 22, 1105.

Taylor G. and Bowen D.K. 1970, Proc. 2nd Int. Conf. on Strength of Metals and Alloys, Asilomar, ASM, p. 78.

TABLE OF CONTENTS

		Page No.
Chapter 1	GENERAL INTRODUCTION	1
	PART A	
	THE PREPARATION AND CHARACTERISATION OF MOLYBDENUM-NITROGEN AND MOLYBDENUM-OXYGEN ALLOYS	4
Chapter 2	INTRODUCTION	6
Chapter 3	LITERATURE REVIEW	8
Chapter 4	EXPERIMENTAL APPARATUS AND PROCEDURE	29
Chapter 5	RESULTS	44
Chapter 6	DISCUSSION	55
	PART B	
	THE DEFORMATION BEHAVIOUR OF MOLYBDENUM-NITROGEN AND MOLYBDENUM-OXYGEN ALLOYS	70
Chapter 7	INTRODUCTION	72
Chapter 8	LITERATURE REVIEW	74
Chapter 9	EXPERIMENTAL APPARATUS AND PROCEDURE	99
Chapter 10	RESULTS	119
Chapter 11	DISCUSSION	133
Chapter 12	GENERAL CONCLUSIONS	170
ACKNOWLEDGEMENTS		174
REFERENCES		175

TABLE OF SYMBOLS

T_M	melting point (^oK)
T	temperature
C	concentration
p	pressure (torr.)
R	Gas constant (cal./mole ^oK)
R.R.	resistance ratio
ρ_R	residual resistivity
ρ_i	specific residual resistivity of solute, i (ohm cm/at.ppm.)
$\Delta\rho_Q$	quenched-in resistivity
a_o	lattice parameter of pure metal
$\Delta a/a_o$	specific lattice parameter change $(at.ppm.)^{-1}$
$\underline{b}$	Burgers vector
τ^*	effective stress
σ	normal stress ($kg/mm.^2$)
τ	shear stress ($kg/mm.^2$)
ε	normal strain
v^*	activation volume

Chapter 1

GENERAL INTRODUCTION

The susceptibility of the body centred cubic (b.c.c.) transition metals to brittle fracture at low temperatures is a long-standing problem which has been the subject of much investigation. The problem is particularly acute in the Group VIa refractory metals where the transition from ductile to brittle behaviour frequently occurs at or above room temperature. This transition is believed to be closely related to the rapid rise in the yield and flow stress which occurs in b.c.c. metals at low temperatures ($\lesssim 0.2\ T_M$). It is also well established that interstitial impurities have a generally deleterious effect on ductility. But there is considerable uncertainty as to the nature of the embrittling mechanism and particularly, as to the role of interstitial atoms in solid solution.

Understandably, much of the interest in basic deformation mechanisms in b.c.c. metals has concentrated on the low temperature region and has been closely concerned with the origin of the strong temperature dependence of the flow stress. There is ample evidence to indicate that a thermally activated dislocation mechanism is controlling the deformation at low temperatures. However, there has been a persevering controversy over the relative importance of the extrinsic hardening effect of residual interstitial impurities and the intrinsic lattice friction stress on dislocations in determining the low temperature strength.

Much of the early work concerned with this question was undertaken on polycrystalline material of moderate purity. But more recently several investigations have been reported where ultrapure Group Va metal single

crystals have been doped with small concentrations of interstitial solutes. These experiments have provided more reliable information about the general deformation of dilute interstitial alloys and specifically about the influence of interstitial solutes on the low temperature flow stress. No analagous investigations involving the controlled addition of interstitials to Group VIa metals have been reported. The low terminal solid solubilities of interstitial elements in these metals make it difficult to prepare alloys with interstitials in solid solution.

There is considerable interest in the comparative effects of interstitials on the deformation behaviour of Group Va and VIa metals. Group VIa metals show certain deformation characteristics which are quite different to those of Group Va metals. It is not clear to what extent these may be attributed to the different lattice potentials of the 'pure' metals and to what extent to the different effects of residual interstitial impurities.

The investigation reported here and the parallel investigation of molybdenum-carbon alloys undertaken by Mr. H.W. Evans are, as far as the author is aware, the first systematic studies of the effects of interstitial solutes in solid solution on the deformation behaviour of a Group VIa metal. This work falls in an area of common interest to the research group in the Oxford department studying basic deformation mechanisms in b.c.c. metals and alloys, and the refractory metals group at Harwell which is concerned with a more general investigation into the properties of refractory metals. An investigation of molybdenum-nitrogen alloys was most attractive because of the background deformation studies undertaken on pure molybdenum at Oxford (Vesely 1972, 1973a,b) and the solubility, diffusivity and ageing studies of nitrogen in molybdenum completed at Harwell (Evans and Eyre 1969, Evans et al. 1970, Eyre and Evans 1972). Some exploratory work on the molybdenum-oxygen system, undertaken in the initial stages of the present investigation, recommended an additional, though necessarily less comprehensive, study of the deformation behaviour of molybdenum-oxygen alloys.

The research project resolved itself into two distinct phases; the preparation and characterisation of the molybdenum and molybdenum-interstitial alloys which are reported in PART A, and the deformation studies conducted on these alloys which are reported in PART B.

PART A

THE PREPARATION AND CHARACTERISATION OF MOLYBDENUM-NITROGEN AND MOLYBDENUM-OXYGEN ALLOYS

		Page No.
Chapter 2	INTRODUCTION	6
Chapter 3	LITERATURE REVIEW	8
3.1	The Purification of Molybdenum	8
3.2	Material Characterisation	12
3.3	The Thermodynamics and Kinetics of Molybdenum-Gas Reactions	19
3.4	Interstitial Doping Techniques	27
Chapter 4	EXPERIMENTAL APPARATUS AND PROCEDURE	29
4.1	Electron Beam Zone-Melting Furnace	29
4.2	Controlled Atmosphere Quenching Furnace	30
4.3	Resistivity Measuring Apparatus	32
4.4	Material	35
4.5	Crystal Growth by Zone-Melting	35
4.6	Decarburisation and High Vacuum Annealing	39
4.7	Doping Treatments	39
4.8	Gamma Activation Analysis	42
Chapter 5	RESULTS	44
5.1	As Zone-Melted (A.Z.M.) Crystals	44
5.2	Decarburised and High Vacuum Annealed (H.V.A.) Crystals	45
5.3	Vacuum Quenched Crystals	46

		Page No.
5.4	Nitrogen Doped Crystals	46
5.5	Oxygen Doped Crystals	50
5.6	Lattice Parameter Measurements	53
Chapter 6	DISCUSSION	55
6.1	The Preparation and Characterisation of High Purity Molybdenum	55
6.2	The Preparation and Characterisation of Nitrogen and Oxygen Doped Molybdenum	57
6.3	Summary	67

Chapter 2

INTRODUCTION

The careful characterisation of base material purity should be regarded as a necessary preliminary to any study of the effects of specific impurities on the mechanical or physical properties of a 'pure' material. It is of particular importance in an investigation of the influence of nitrogen and oxygen in solution on the deformation behaviour of molybdenum, since carbon, which is one of the most difficult elements to reduce to low levels, is also expected to exert a strong influence.

Much of the previous work on the influence of interstitial impurities on the mechanical properties of b.c.c. metals has been beset with difficulties arising from the failure to purify and characterise adequately starting materials. This has been due in part to the limitations of the generally available analytic techniques for the determination of interstitial elements but also, to the tendency to regard zone-melting as a hallmark of material purity. In the case of molybdenum, where zone-melting frequently yields material containing considerable and variable concentrations of the interstitial impurity carbon, relatively few attempts have been made to utilise supplementary treatments to ensure the removal of carbon. It was consequently felt that an investigation of the mechanical properties of molybdenum-nitrogen and molybdenum-oxygen alloys should be prefaced by a characterisation study of pure molybdenum. This was undertaken in a joint investigation with Mr. H.W. Evans. It was primarily concerned with clarifying the purification mechanisms of molybdenum with a view to establishing an optimum route for the preparation of high purity material.

Techniques for the preparation of molybdenum containing nitrogen, oxygen and carbon in solid solution have previously been developed for resistometric and transmission electron microscopic studies of their ageing behaviour (e.g. Burck et al. 1969, Evans et al. 1970). In the present study, the well established susceptibility of molybdenum to fracture at low temperatures made it desirable to prepare specimens initially for compression rather than tension testing. Because this required the preparation of alloy specimens of much larger dimensions than in previous investigations, some further development and evaluation of the doping techniques were necessary.

Initially, the experimental effort was concentrated on establishing the maximum concentrations of nitrogen which could be retained in solution in large diameter specimens suitable for compression testing. There was a secondary interest in this work in verifying the nitrogen equilibrium solubility data determined by Evans and Eyre (1969). Later, some attempts were made to prepare molybdenum-oxygen alloys. The first concern here was to obtain some approximate thermodynamic and kinetic information for the molybdenum-oxygen system. This was necessary to permit the further exercise of determining the concentrations of oxygen which could be retained in solid solution in mechanical test specimens.

Chapter 3

LITERATURE REVIEW

3.1 The Purification of Molybdenum

Zone-melting is usually the first purification step employed in the preparation of high purity molybdenum. It has been shown to remove a large proportion of many impurities present in commercially 'pure' molybdenum (Belk 1959a, Stein 1967, Eyre et al. 1970). These impurities include relatively volatile substitutional impurities (e.g. iron, nickel, aluminium, copper) and much of the purification occurs by their vaporisation. The degree of purification effected by this mechanism is ultimately limited by the presence of low vapour pressure impurities, tungsten being the principal element of this type in molybdenum. Both tungsten's low volatility and its unfavourable equilibrium distribution coefficient (Barthel and Eichler 1967) for zone-refining, are consistent with the failure of zone-melting to reduce its concentration. Both Oppermann et al. (1967) and Evans and Eyre (1968b) confirmed this experimentally using chemical analysis and resistance ratio (R.R.) measurements. When the starting material was subjected to special chemical pretreatments to remove tungsten, very high R.R.'s ($>10^5$) were obtained (Oppermann et al. 1967).

While the ultimate R.R. and purity of zone-melted molybdenum is largely determined by its tungsten content, it would appear that the R.R. and purity attained in practice are frequently strongly influenced by the presence of another impurity, carbon. Carbon is the main interstitial impurity present in arc cast and, in some instances, powder metallurgical

commercial molybdenum but its concentration may vary from <10 to >1000 at.ppm. depending on the individual supplier and production variables. Belk (1959b), in a study of the zone-melting of a comparatively high carbon content material (800 at.ppm.), found chemical analytic evidence suggesting the removal and/or redistribution of carbon by a zone-refining mechanism. Further work yielded stronger evidence for the zone-refining of carbon where the carbon concentration in the final solidified zone was frequently found to be higher than in the starting material (Belk 1959a). In a similar investigation of the zone-melting of molybdenum with a high carbon content (~3000 at.ppm.) Kovtun et al. (1966) used R.R. measurements to infer a strong impurity gradient along their crystals. Preliminary carbon analysis results and the not unfavourable distribution coefficient of carbon in molybdenum led them to conclude that part of the R.R. gradient was due to the zone-refining of carbon. They also undertook a systematic study of the influence of zone traverse speed and number of zone passes on purification and found, in contradiction with other results (Stein 1967), that the purity achieved was particularly sensitive to these parameters. However, Stein's (1967) conclusion that there was a poor correlation between R.R., zone-melting parameters and analytically determined purity took no account of the possibility of an inhomogeneous distribution of carbon in his zone-melted crystals. The point on which all these workers (Belk 1959a,b, Kovtun 1966, Stein 1967) were implicitly in agreement was that, for molybdenum with comparatively high carbon concentrations (say $\geq$500 at.ppm.), zone-melting is an inefficient means of removing the carbon.

At lower carbon concentrations it would appear that the rate of carbon removal and/or redistribution does not limit the purity achieved in zone-melting. Evans and Eyre (1968b)found that the zone-melting of commercial molybdenum containing 160 at.ppm. carbon produced essentially carbon free material (<4 at.ppm.). Very low post zone-melting carbon concentrations have been reported in other investigations using high purity molybdenum

(Vesely 1968b, Korenko et al. 1974) and it might be assumed that the concentrations in their starting material were sufficiently low to permit its removal under suitable zone-melting conditions. Kovtun's (1966) findings indicate that the latter comprise a minimum number of zone passes at a maximum zone speed for a given initial carbon concentration. Any extension of the zone-melting operation to lower zone speeds or larger numbers of zone passes would appear to improve the overall purity only through further evaporation of volatile impurities.

Some successful attempts have been made to improve the general purity of zone-melted molybdenum by subjecting it to further high vacuum anneals. Evans and Eyre (1969) obtained an increase in the R.R. after prolonged annealing at >2000°C and $<10^{-6}$ torr. which was probably associated with impurity outgassing and volatisation. However, post (and some pre-) zone-melting treatments have usually been specifically directed at removing carbon. Anneals in a stream of purified hydrogen were first employed for this purpose but the decarburisation reaction

$$[C]_{Mo} + 2(H_2)_g \rightleftharpoons (CH_4)_g$$

is such that prolonged treatment times and concomitantly large volumes of hydrogen are required in practice (Few and Manning 1952, Stein 1967, Evans and Eyre 1968b, Lau and Dorn 1968). In the only investigation where sufficient analytic sensitivity was available to ensure carbon concentrations were reduced to <10 at.ppm. the treatments were performed on commercial purity molybdenum before zone-melting (Evans and Eyre 1968b)

More recently two types of treatments have been successfully used to decarburise molybdenum. Touboul et al. (1971, 1973) obtained residual carbon concentrations of <3 at.ppm. in molybdenum by annealing in a dynamic atmosphere of 2×10^{-5} torr. oxygen at 1800°C. Under these conditions a kinetic steady state equilibrium is achieved at the surface between the reactions

below

$$[C]_{Mo} + [O]_{Mo} \rightleftharpoons (CO)_g$$

$$Mo + x\,[O]_{Mo} \rightleftharpoons (MoO_x)_g$$

$$\tfrac{1}{2}\,(O_2)_g \rightleftharpoons [O]_{Mo}$$

The rate of metal loss due to volatilisation of oxide is small (<10μ/hour) and the incident flux of oxygen molecules is sufficient to eliminate all the carbon arriving at the surface. The rate controlling step in both the dissolution of any carbide precipitates present at the annealing temperature and, in the subsequent removal of carbon from solution, was shown to be the diffusion of carbon in the metal. Annealing in a flowing stream of moist hydrogen (5 torr. water vapour, 100 torr. hydrogen) in the temperature range 1235-1760°C has also been shown to reduce carbon concentrations to <0.02 at.ppm. (Kunze and Reichelt 1970). The chemical equilibrium at the gas/metal interface is

$$[C]_{Mo} + (H_2O)_g \rightleftharpoons (CO)_g + (H_2)_g$$

where the rate of formation and volatilisation of the oxide is sufficiently small to permit the oxidation reaction to be ignored. Kunze and Reichelt (1970) experimentally determined that the decarburisation kinetics were here also controlled by the rate of carbon diffusion in the bulk metal. From a practical standpoint, this type of decarburisation treatment has the advantage of involving much shorter treatment times than the dry hydrogen anneals and less risk of metal loss due to oxide evaporation than the oxygen treatments.

3.2 Material Characterisation

There is a variety of physical, chemical and mechanical methods which may be used to determine impurity levels in high purity metals. Physical methods (e.g. residual resistivity, lattice parameter, internal friction and anelastic relaxation measurements) are mainly sensitive to impurity concentrations in solution while mechanical and chemical measurements (e.g. hardness tests, radiochemical and conventional chemical analysis) reflect total impurity concentrations. Purity characterisation in the concentration range <100 at.ppm., which is of particular importance for interstitial impurities in b.c.c. metals, requires the combined application of the most sensitive of these techniques.

Residual resistivity (ρ_R) measurements are widely employed to establish impurity levels in high purity metals. In practice, the resistance ratio (R.R.) is usually measured which greatly simplifies the experimental technique and permits the calculation of ρ_R from the equation

$$R.R. = \frac{R \text{ (typically at } 273^{\circ}K)}{R \text{ (typically at } 4.2^{\circ}K)} = \frac{\rho(273^{\circ}K)}{\rho(4.2^{\circ}K)} = \frac{\rho_T + \rho_R}{\rho_R}$$

where R is the resistance of the specimen

ρ is the resistivity of the material

ρ_T is the resistivity component due to thermal scattering

ρ_R is the resistivity component due to scattering by chemical and physical defects

ρ_T and ρ_R are assumed to be independent and additive (Matthieson's Rule)

In the case of very high purity metals there is a possibility that at $4.2^{\circ}K$, where both the thermal and defect scattering are small, the electron mean free path may approach the transverse dimensions of the

specimen and give rise to a size effect. Where data is available, as it is for molybdenum (Elefant 1971), the relation

$$\rho_A/\rho_R = 1 + \alpha\, l/d$$

where l is the mean free path of electrons

d is the specimen thickness or diameter

ρ_A is the apparent residual resistivity

$\alpha = 1$ for $l/d > 0.5$
$\rightarrow 0.57$ as $l/d \rightarrow 0$

may be used to calculate the magnitude of, and compensate for, this effect (Köthe 1972).

Dislocations, grain boundaries, vacancies, precipitate strain fields etc. all contribute to the residual resistivity but in well annealed single crystals the contribution from impurity atoms in solution is usually dominant. Thus ρ_R gives a measure of the overall impurity levels in solution where, for total solution concentrations < 1 at.%

$$\rho_R = \sum_i \rho_i C_i \quad \text{(Nordheim's Rule)}$$

where ρ_i is the specific residual resistivity of impurity species i

C_i is the concentration of impurity species i

The magnitude of ρ_i effectively determines the sensitivity of the R.R. measurement for a particular impurity species. It would appear that ρ_i depends more upon the valence than size difference between the impurity and host atoms. Typically, substitutional atoms of the same valence as the host metal have ρ_i values an order magnitude less than interstitial impurities but as the valence difference of the substitutional atoms increases, ρ_i approach

those of interstitial atoms. For example, in molybdenum ρ_i (ohm cm/at.ppm.) for substitutional tungsten and tantalum are 7-8 x 10^{-12} (Evans and Eyre 1968b, Oppermann et al. 1967) and 4 x 10^{-11} (Van Torne and Thomas 1966) respectively; for interstitial nitrogen it is 2.4 x 10^{-10} (Evans and Eyre 1969). The comparatively large values of ρ_i for interstitial impurities in refractory metals (see Table A1) permit the detection of solution concentrations of <1 at.ppm. by simple and unexceptionally sensitive resistivity measuring apparatus.

A major limitation of R.R. measurements is that they do not allow the direct identification of specific impurities in solution. The non-specific nature of the technique means that where significant concentrations of two or more impurities occur in solution, only a conservative upper limit can be placed on their individual concentrations. This is of particular importance for the refractory metals where one is uncertain whether to ascribe the residual resistivity to the relatively innocuous substitutional impurities or to the deleterious interstitials which may be present. Usually, there is only one major substitutional impurity remaining after the normal purification treatments have been given to the Group Va and VIa metals e.g. tantalum in niobium, tungsten in molybdenum. So, if both the concentration and the specific residual resistivity of that substitutional impurity are known, the total interstitial concentration may be calculated. Chemical analysis must be employed to obtain the substitutional impurity concentration but this information is frequently easier to obtain than direct analytic data for the interstitial elements.

The other major difficulty with the R.R. measurement is its general insensitivity to impurity precipitates. This means that the procedure described above must be cautiously applied to the Group VIa metals which have very low terminal solubilities for interstitial elements. For example, Oppermann et al. (1967) found that in molybdenum with a total carbon content of 8 at.ppm., <1 at.ppm. was in solid solution and contributing to the

Solute Element	V	Nb	Ta	Mo	W
O	57,50 (1) (9)	42 (1)	55 (1)		
N	54 (1)	38 (1)	52 (1)	24 (2)	
C			55 (3)		38 (4)
Ti					17 (5)
Zr		11 (8)			
Nb					1.2 (5)
Ta		2.5 (8)		4 (6)	
Mo					4 (5)
W		11 (8)		0.7,0.8 (10)(7)	
Fe					20 (5)

Table A1 Specific Residual Resistivities of Solutes in Refractory Metals
10^{-11} ohm cm/at.ppm.

(1) Hörz et al. 1965
(2) Evans and Eyre 1969
(3) Hörz et al. 1974
(4) Krautz et al. 1968
(5) Schultz 1964
(6) Van Torne and Thomas 1966
(7) Oppermann et al. 1967
(8) Meyerhoff 1971
(9) Bressers et al. 1975
(10) Evans and Eyre 1968b

residual resistivity. This difficulty, which arises in the Group Va metals to a lesser degree, may be circumvented to the extent that fast cooling or quenching is capable of retaining the interstitial atoms in solid solution. But for confident control of interstitial impurities to low levels it is necessary to supplement R.R. measurements with chemical analysis, which yields information about interstitial impurity concentrations both in and out of solid solution.

Only the most highly specialised chemical analysis techniques and measuring systems have sufficient sensitivity to give reliable data for interstitial impurities down to the low concentrations of interest in the refractory metals (<10 at.ppm.). The more conventional analytic methods for determining gaseous and interstitial impurities (e.g. mass spectrometry, vacuum and inert gas fusion) are capable of approaching these sensitivities, but only where the measuring system has been specifically developed for the analysis of interstitial elements and where the optimum sample size, counting times etc., can be achieved (e.g. Weaver 1972). Frequently, the conditions necessary to attain such sensitivities place new constraints on the information which can be obtained. For example the minimum sample size may be such that important inhomogeneities in the material are masked.

There are two other major analytic techniques which, although cost and availability prevent their widespread use, are most suitable for the determination of many interstitial elements at very low concentrations.

Gamma activation analysis involves the production of radioactive species from the interstitial impurity atoms present by irradiation in a high density gamma flux. By subsequently burning the sample and selectively recovering specific radioactive species the concentration of the individual interstitials may be determined (Baker and Williams 1968). The technique is well suited to determinations at <100 at.ppm. and in fact at higher concentrations interference effects between different interstitial species may give erroneous results. Typically, Touboul et al. (1971) could detect

<1 at.ppm. carbon in molybdenum using radioactivation.

A more sensitive (<0.1 at.ppm.), though less direct tracer technique has been used by Stein et al. (1963) to determine carbon in iron and by Kunze and Reichelt (1970) to determine carbon in molybdenum. Carbon 14 (C^{14}) was introduced into the material in large concentrations with respect to the non-active carbon already present. By monitoring the removal of carbon (by counting or radiography) in subsequent decarburisation treatments, and assuming that the active and non-active carbon remain in a constant proportion, the total carbon concentration may be determined. This method has the advantage over activation analysis of being non-destructive but does rely on the availability of a suitable means of introducing a uniform concentration of the tracer into the sample.

Neither the activation nor tracer technique involve apparatus or reagent blanks so that it is only the counting time and half life of the radioisotope which limit the sensitivity. Activation analysis also averts the specimen surface contamination problems frequently associated with conventional techniques (e.g. Friedrich et al. 1968). The surface material can be removed after activation and any contaminating elements subsequently introduced are non-radioactive and hence remain undetected.

Lattice parameter measurements are one of the two remaining important types of physical measurements which are of particular value for the monitoring of solute concentrations in high purity metals. The change in lattice parameter (Δa) reflects the mean displacement of atoms from their lattice sites in the parent metal caused by the solute atoms. The magnitude of the mean displacement increases as the size difference between the solute and solvent atoms (size factor) increases. Although Vegard's Law ($\Delta a \propto C$) is strictly obeyed for very few, if any, metallic solid solutions, an approximate linear dependence at low concentrations has been observed for many interstitial solid solutions. The major substitutional impurities in the Group Va and VIa metals have very small size factors and even at concentrations >100 at.ppm.

have a negligible effect on the lattice parameter. Interstitial impurities cause very much larger lattice parameter changes ($\Delta a = 10^{-7} - 10^{-6}$ Å/at.ppm.). But because lattice parameters can only be measured with approximately $\pm 10^{-5}$ Å precision, the method only allows interstitial concentrations to be monitored down to the 10-100 at.ppm. However, at higher concentrations where parameter changes have been calibrated against chemical analysis data, the technique has been usefully employed (e.g. Jung and Trenzinger 1974).

The other physical monitoring method which finds most application in the determination of interstitial solute concentrations in b.c.c. metals is the internal friction technique. A simple torsion pendulum allows detection down to approximately 100 at.ppm. with $\pm$ 10 at.ppm. precision; more sophisticated arrangements can detect lower concentrations. At low concentrations there is a simple relation of proportionality between the Snoek peak heights and concentration. The occurrence of several peaks each associated with a particular interstitial species permits the simultaneous monitoring of all interstitials present. This affords internal friction measurements a major advantage over the other physical monitoring techniques which are non-specific for individual atom species. As the concentrations increase subsidiary peaks arise which are associated with the interstitials interacting to form pairs and eventually larger clusters. In iron and the Group Va metals the origin and concentration dependence of these peaks have been well established (Powers and Doyle 1959) but only one detailed study of a Group VIa - interstitial system has been made (Ma and Son 1964). At the very high concentrations which can be retained in solid solution in the Group Va metals (typically $\geqslant$1 at.%) the interstitial interactions become so complicated that stress and strain relaxation rather than internal friction techniques must be employed. There is also the possible additional complication of substitional-interstitial interactions (Fast 1950). This points to the desirability of utilising the internal friction method only when the concentration dependence of the Snoek peaks has been determined for

material of the same base purity.

3.3 The Thermodynamics and Kinetics of Molybdenum-Gas Reactions

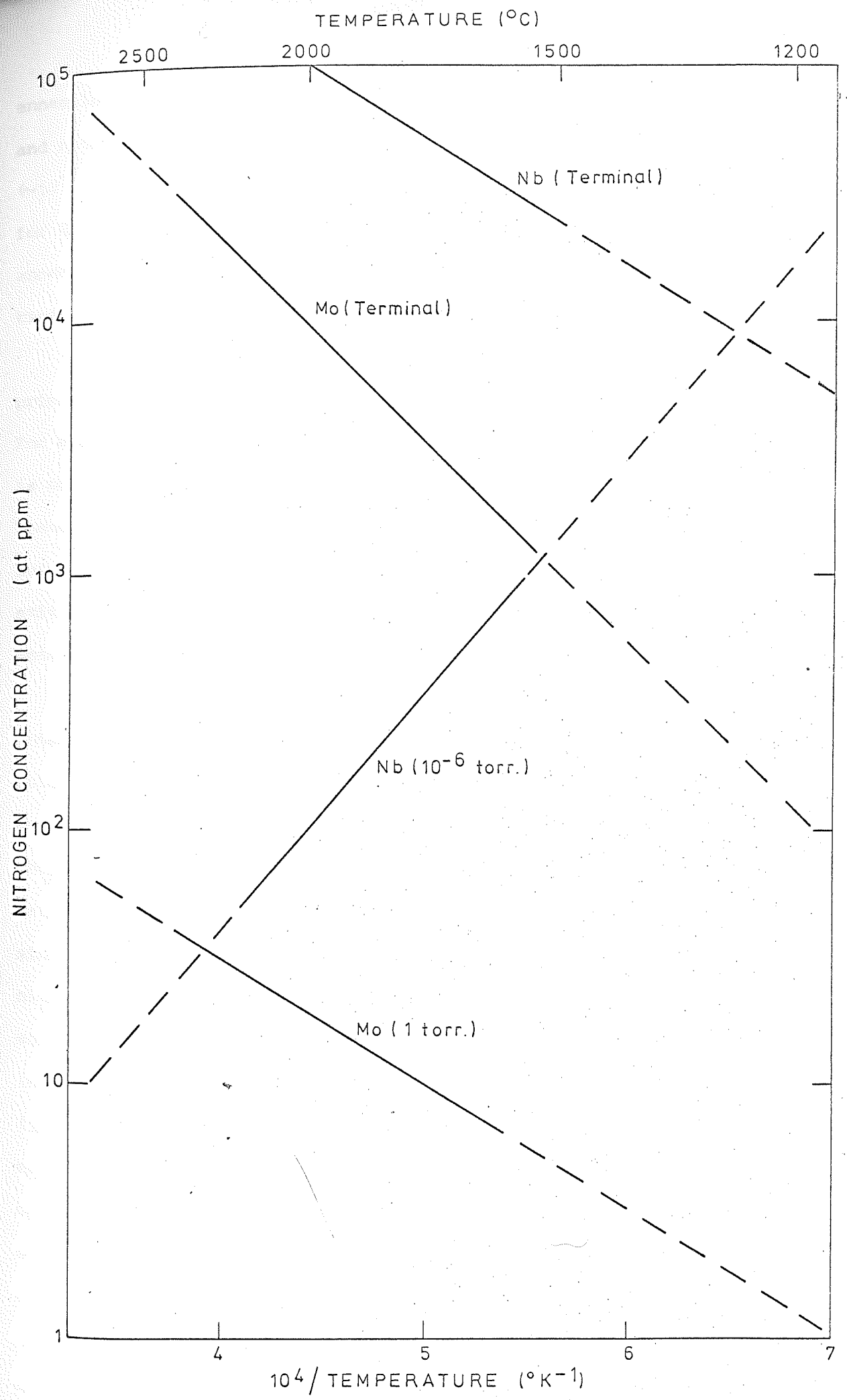
Measurements of densities, lattice parameters and diffusivities indicate that elements with small atomic radii such as hydrogen, oxygen, nitrogen and carbon occupy interstitial sites in the b.c.c. transition metals. With the exception of carbon the above mentioned interstitial impurities are gases and carbon is frequently introduced into a metal sample from a hydrocarbon gas. Thus, a knowledge of both the equilibrium and rate constants of the relevant gas-metal reactions is important for an understanding of the behaviour of interstitial impurities in refractory metals.

All the thermodynamic data have been determined for the Group Va primary solid solution-gas equilibria, either from direct experiments or thermodynamic calculations. The data for the Group VIa metals are not complete and only a qualitative description and prediction of behaviour can be given for some of the reactions. The chemical reactions themselves are similar for all the refractory metals but there are large differences in the values of the equilibrium constants.

Both the magnitude and the temperature dependence of the solubilities are markedly different for the Group Va and VIa metals. For example, Fig.A1 shows that at high temperatures the pressure of nitrogen gas in equilibrium with a given concentration of nitrogen in solid solution in niobium is approximately six orders of magnitude less than that for molybdenum. Furthermore, the heat of solution of nitrogen in molybdenum is positive and in niobium negative so that the equilibrium concentrations in molybdenum increase, and in niobium decrease, with increasing temperature. This has obvious significance for the purification procedures which are effective for the Group Va and VIa metals. For example, ultra high vacuum ($\leq 10^{-10}$ torr.)

Figure A1 Terminal and Equilibrium Solubilities of Nitrogen in Molybednum and Niobium

(Data: Fromm and Jehn 1972)


TEMPERATURE (°C)
2500
2000
1500
1200
10^5
10^4
10^3
10^2
10
1
NITROGEN CONCENTRATION (at. ppm)
Nb (Terminal)
Mo (Terminal)
Nb (10^{-6} torr.)
Mo (1 torr.)
4
5
6
7
10^4 / TEMPERATURE ($°K^{-1}$)

annealing treatments are necessary to reduce the concentration levels of oxygen and nitrogen in Group Va metals to levels achieved by relatively poor vacua ($\sim 10^{-5}$ torr.) in the Group VIa metals. Also, vacuum annealing is most effective for Group Va metals at temperatures approaching the melting point but the annealing temperatures for the Group VIa metals are best kept as low as is kinetically practicable.

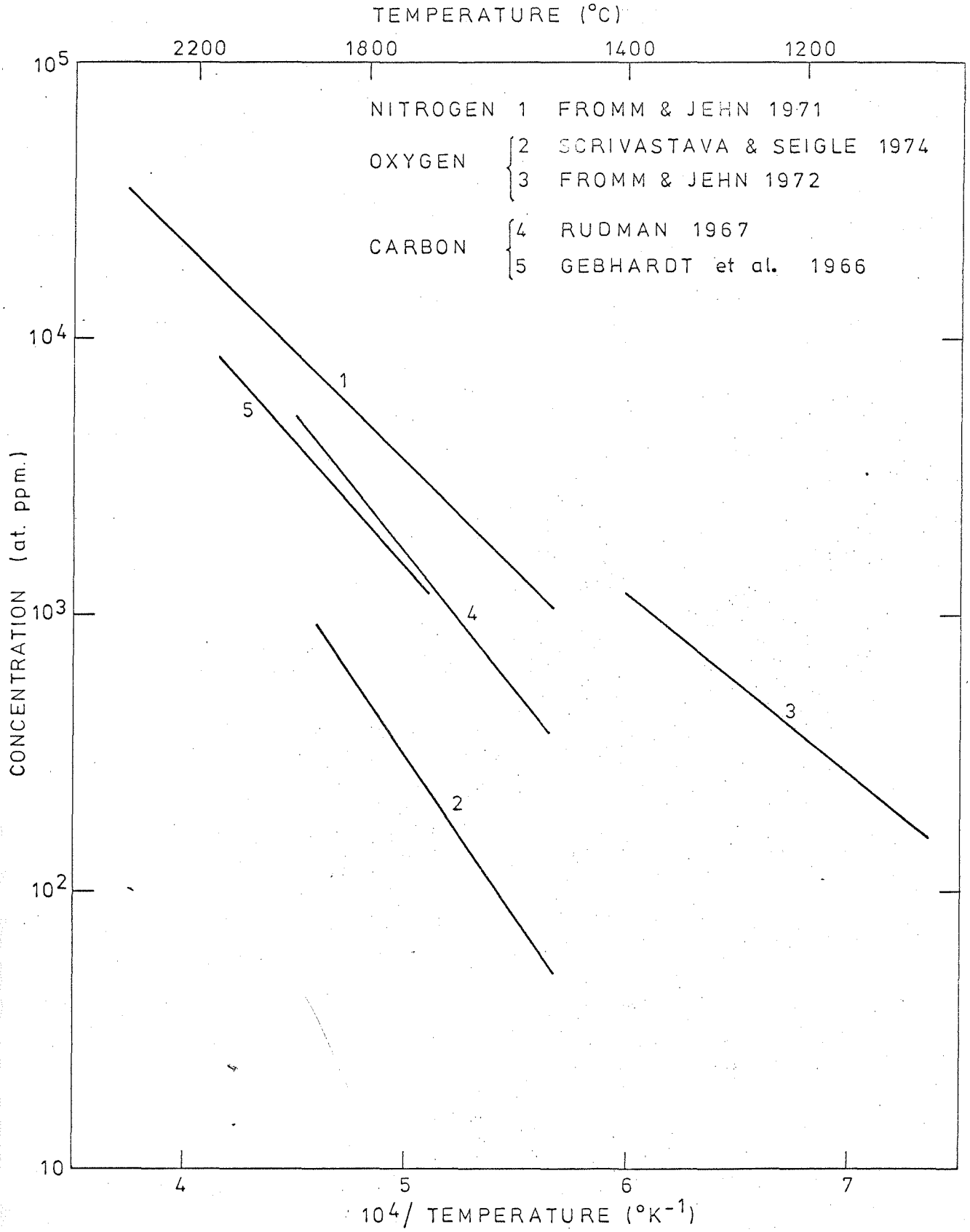
The differences in the terminal compositions of Group Va and Group VIa metal primary solid solutions are much less than those of the equilibrium solubilities. For example, the high temperature terminal solubility of nitrogen in molybdenum is only an order of magnitude less than that of nitrogen in niobium (see Fig.A1). These differences appear to have little significance for purification treatments but do indicate that at room temperature there is a greater likelihood of interstitial impurities being present as second phase precipitates in the Group VIa metals.

Table A2 contains the better established solid solubility data for the interstitial elements nitrogen, oxygen and carbon in molybdenum. The terminal solubility lines are plotted in Fig.A2. Fromm and Jehn's (1971) nitrogen values were calculated from equilibrium data and the formation energy of the nitride (Mo_2N) and are only accurate to within an order of magnitude. The nitrogen saturation solubility is of little practical importance at high temperatures since gas pressures from 10-10,000 atmospheres are necessary to achieve these nitrogen concentrations. The solidus lines for the molybdenum-carbon primary solid solution can be obtained by equilibrating molybdenum and molybdenum carbide (Mo_2C) at high temperatures; the results of Rudman (1967) and Gebhardt et al. (1966) are in good agreement. Scrivastava and Seigle (1974), using the same method, determined the solubility limits of oxygen in molybdenum. Their results do not compare favourably with those of Fromm and Jehn (1972) but the latter were only tentative data from preliminary unpublished work. Extrapolation of the results of all workers (including these of Fromm and Jehn (1972)) to low temperatures does indicate very low terminal solubilities of interstitials in molybdenum. For example, at $\sim 850^{\circ}C$ the terminal solubilities of oxygen,

REACTION	ΔG^{o} (Cal/mole)	EQUILIBRIA (at.ppm., ^{o}K, torr.)	TEMPERATURE RANGE (^{o}C)	REFERENCE (*Calculated)
$Mo_2N = 2Mo + [N]_{Mo}$	36200 - 6.8T	$\log C_N = 7.49 - \frac{7910}{T}$	1600 - 2400	Fromm and Jehn 1971*
$\frac{1}{2}MoO_2 = \frac{1}{2}Mo + [O]_{Mo}$	55400 - 11.65T	$\log C_O = 8.55 - \frac{12117}{T}$	1500 - 1900	Scrivastava and Seigle 1974
$\frac{1}{2}MoO_2 = \frac{1}{2}Mo + [O]_{Mo}$	22300 + 8.65T	$\log C_O = 5.79 - \frac{4870}{T}$	1100 - 1400	Fromm and Jehn 1972
$Mo_2C = 2Mo + [C]_{Mo}$	45500 - 10.0T	$\log C_C = 8.19 - \frac{9945}{T}$	1500 - 2000	Rudman 1967
$Mo_2C = 2Mo + [C]_{Mo}$	41500 - 7.8T	$\log C_C = 7.7 - \frac{9070}{T}$	1700 - 2100	Gebhardt et al. 1966
$\frac{1}{2}(N_2)_g = [N]_{Mo}$	19100 + 2.06T	$\log C_N = \frac{1}{2} \log p_{N_2} + 3.11 - \frac{4148}{T}$	1000 - 1900	Weaver 1972
$\frac{1}{2}(N_2)_g = [N]_{Mo}$	22600 + 5.03T	$\log C_N = \frac{1}{2} \log p_{N_2} + 3.48 - \frac{4940}{T}$	1600 - 2400	Fromm and Jehn 1971
$\frac{1}{2}(N_2)_g = [N]_{Mo}$	18400 + 6.22T	$\log C_N = \frac{1}{2} \log p_{N_2} + 3.20 - \frac{4030}{T}$	1400 - 2200	Evans and Eyre 1969
$\frac{1}{2}(O_2)_g = [O]_{Mo}$	-10760 + 9.1T	$\log C_O = \frac{1}{2} \log p_{O_2} + 2.52 + \frac{2357}{T}$	1500 - 1900	Scrivastava and Seigle 1974*
$(CH_4)_g = 2(H_2)_g + [C]_{Mo}$	49900 - 34.2T	$\log C_C = \log p_{CH_4} - 2 \log p_{H_2} + 16.38 - \frac{10,900}{T}$	1700 - 2100	Gebhardt et al. 1966*

Table A2 Thermodynamic Data for Molybdenum-Interstitial Solid Solutions

Figure A2 Terminal Solid Solubilities of Interstitial Elements in Molybdenum


TEMPERATURE (°C)
2200
1800
1400
1200
NITROGEN 1 FROMM & JEHN 1971
OXYGEN 2 SCRIVASTAVA & SEIGLE 1974
3 FROMM & JEHN 1972
CARBON 4 RUDMAN 1967
5 GEBHARDT et al. 1966
CONCENTRATION (at. ppm.)
10^5
10^4
10^3
10^2
10
1
2
3
4
5
4
5
6
7
10^4/ TEMPERATURE (°K^-1)

nitrogen and carbon are much less than 10 at.ppm.

Equilibrium concentration isobars for nitrogen and oxygen in primary solid solution in molybdenum are plotted in Fig.A3. It would appear that true thermodynamic equilibrium conditions are only achieved at high temperatures (>1400°C) though Weaver's (1972) results indicate equilibrium at lower temperatures for molybdenum-nitrogen solid solutions. Weaver (1972) has also shown that the only reliable heat of solution values for nitrogen in molybdenum are those determined by Evans and Eyre (1969) and Fromm and Jehn (1971). Evans and Eyre (1969) obtained resistivity values proportional to the solubility which they then calibrated against the transient permeation data of Frauenfelder (1968). The latter were undoubtedly influenced by nitrogen trapping effects at carbides present in their material and this may explain the high solubility values of Evans and Eyre (1969).

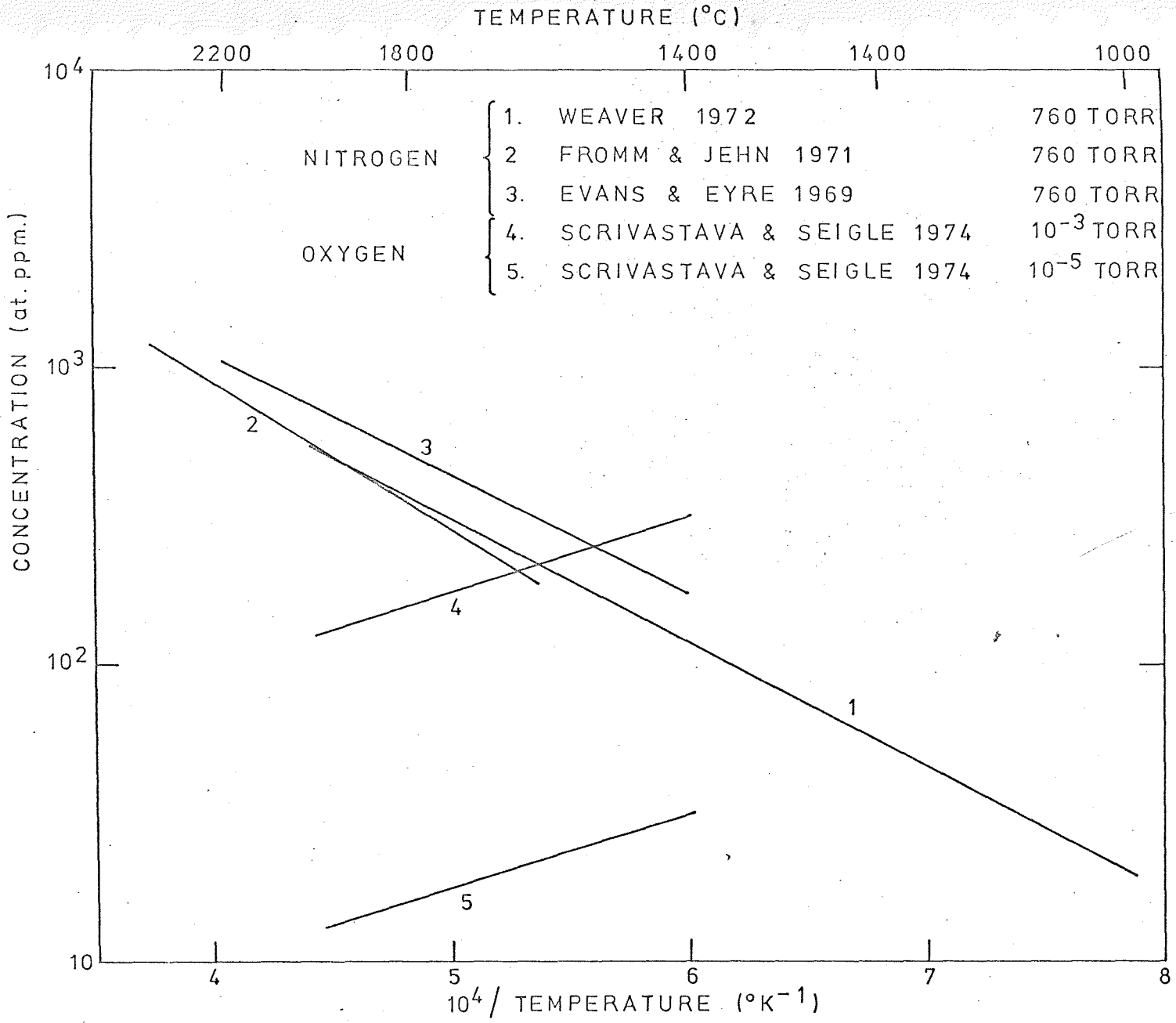
The oxygen equilibrium solubility data of Scrivastava and Seigle (1974) were calculated from saturation solubilities and the formation energy of the oxide (MoO_2), assuming that the solution is regular and that oxygen occupies octahedral sites in molybdenum. However, when molybdenum is annealed in low oxygen partial pressures (10^{-3} - 10^{-5} torr.) at high temperatures (>1000°C) oxide formation and evaporation at the specimen surface prevent equilibrium conditions being attained. Instead, there is competition between the two reactions below.

$$Mo + x[O]_{Mo} \rightleftharpoons (MoO_x)_g$$

$$\tfrac{1}{2}(O_2)_g \rightleftharpoons [O]_{Mo}$$

After a short transient period a kinetic steady state is achieved between oxygen absorption and oxide evaporation where the oxygen concentration in the primary solid solution is a well defined function of the temperature and oxygen partial pressure. Sufficient data is not available to establish this

Figure A3 Equilibrium Solid Solubilities of Nitrogen and Oxygen in Molybdenum


TEMPERATURE (°C)
2200
1800
1400
1400
1000
10^4
10^3
10^2
10
CONCENTRATION (at. ppm.)
NITROGEN
1. WEAVER 1972 760 TORR
2 FROMM & JEHN 1971 760 TORR
3. EVANS & EYRE 1969 760 TORR
OXYGEN
4. SCRIVASTAVA & SEIGLE 1974 10^{-3} TORR
5. SCRIVASTAVA & SEIGLE 1974 10^{-5} TORR
1
2
3
4
5
4
5
6
7
8
10^4 / TEMPERATURE (°K^{-1})

function for molybdenum, but for niobium and tantalum, where a quantitative treatment is possible, the steady state concentrations of oxygen in solution are found to be many orders of magnitude less than the equilibrium concentrations (Fromm and Jehn 1972). Thus, Scrivastava and Seigle's (1974) equilibrium values put a conservative upper limit on the steady state concentrations which will be attained during annealing in oxygen atmospheres. For low temperature, high partial pressure oxygen anneals a comparison of the equilibrium and terminal solubility values (see Figs.A2 and A3) indicates the possibility of oxide precipitation in molybdenum.

Hörz (1972) has proposed that during the annealing of molybdenum in water vapour at high temperatures a kinetic steady state is established between the reactions below.

$$(H_2O)_g \rightleftharpoons (H_2)_g + [O]_{Mo}$$

$$x[O]_{Mo} + Mo \rightleftharpoons (MoO_x)_g$$

The reverse of the first reaction does not occur at a significant rate for low hydrogen partial pressures which, for instance, are secured by a flowing water vapour atmosphere. Kunze and Reichelt (1970) have shown that in moist hydrogen atmospheres (750 torr. hydrogen, 12 torr. water vapour) the oxidation rate is very small and the recomposition of water vapour occurs at a rate which permits the establishment of true thermodynamic equilibrium for this reaction. In contrast, a kinetic equilibrium between the oxidation and water vapour decomposition reactions operates when niobium and tantalum are annealed in moist hydrogen atmospheres.

The knowledge of reaction kinetics which allows the estimation of the time to reach the equilibrium or steady state concentrations of interstitial elements in refractory metals, is more advanced for the Group Va than Group VIa metals. There is sufficient data available for both to

indicate certain differences between the two groups which parallel, and to some extent derive from, their contrasting thermodynamic behaviour.

To consider the general case of the outgassing of a diatomic gas from a metal sample, there are a number of steps which can or must occur. These are illustrated schematically in Fig.A4 where it can be seen that some occur in series and some in parallel. In the former instance the slowest step is rate controlling and, in the latter, the fastest. The possibility of mixed control where two steps proceed at similar rates and, of a shift in control with variations in temperature, pressure, sample size and reaction time should be considered.

In the metal-nitrogen systems where true thermodynamic equilibria obtain, the kinetics are comparatively simple. For example, for the tantalum-nitrogen reaction, the ingassing rate is controlled by chemisorption at the surface and outgassing is subject to mixed control between chemi-desorption and the recombination of nitrogen atoms (Hörz 1972). Solid diffusion control has been shown experimentally to operate for the outgassing of nitrogen from molybdenum (Fromm and Jehn 1970). Hörz (1972) has argued that the ingassing reaction for molybdenum and nitrogen should be controlled by the decomposition of nitrogen molecules and solid diffusion but this has not been verified experimentally.

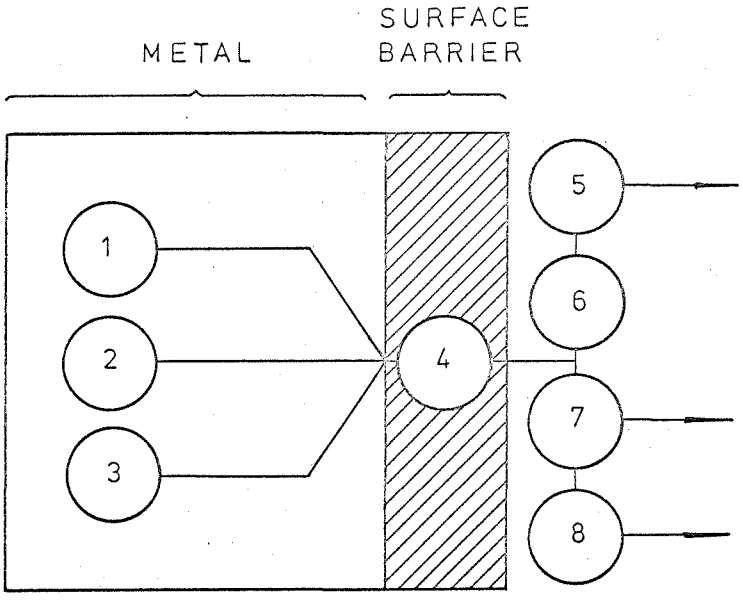
The kinetics of oxygen-metal reactions are more complicated and only for the Group Va metals has any quantitative data been obtained. For example, the kinetics of the oxygen ingassing and outgassing reactions for niobium-oxygen solid solutions given below, have been investigated under conditions for which the reverse reactions occur at negligible rates (Hörz 1968, 1969).

$$\tfrac{1}{2}\,(O_2)_g \rightleftharpoons [O]_{Nb} \qquad \text{Ingassing}$$

$$Nb + [O]_{Nb} \rightleftharpoons (NbO)_g$$

$$Nb + 2[O]_{Nb} \rightleftharpoons (NbO_2)_g \qquad \text{Outgassing}$$

Figure A4 Schematic Diagram Showing Possible Rate Controlling Steps for the Outgassing of a Diatomic Gas



1 LATTICE DIFFUSION

2 GRAIN BOUNDARY DIFFUSION

3 PIPE DIFFUSION

4 PASSAGE THROUGH SURFACE/ SURFACE BARRIER

5 DESORPTION OF GAS MOLECULES

6 RE-COMBINATION OF GAS ATOMS

7 CHEMICAL / PHYSICAL DESORPTION OF GAS ATOMS

8 FORMATION & EVAPORATION OF GAS-METAL COMPOUND

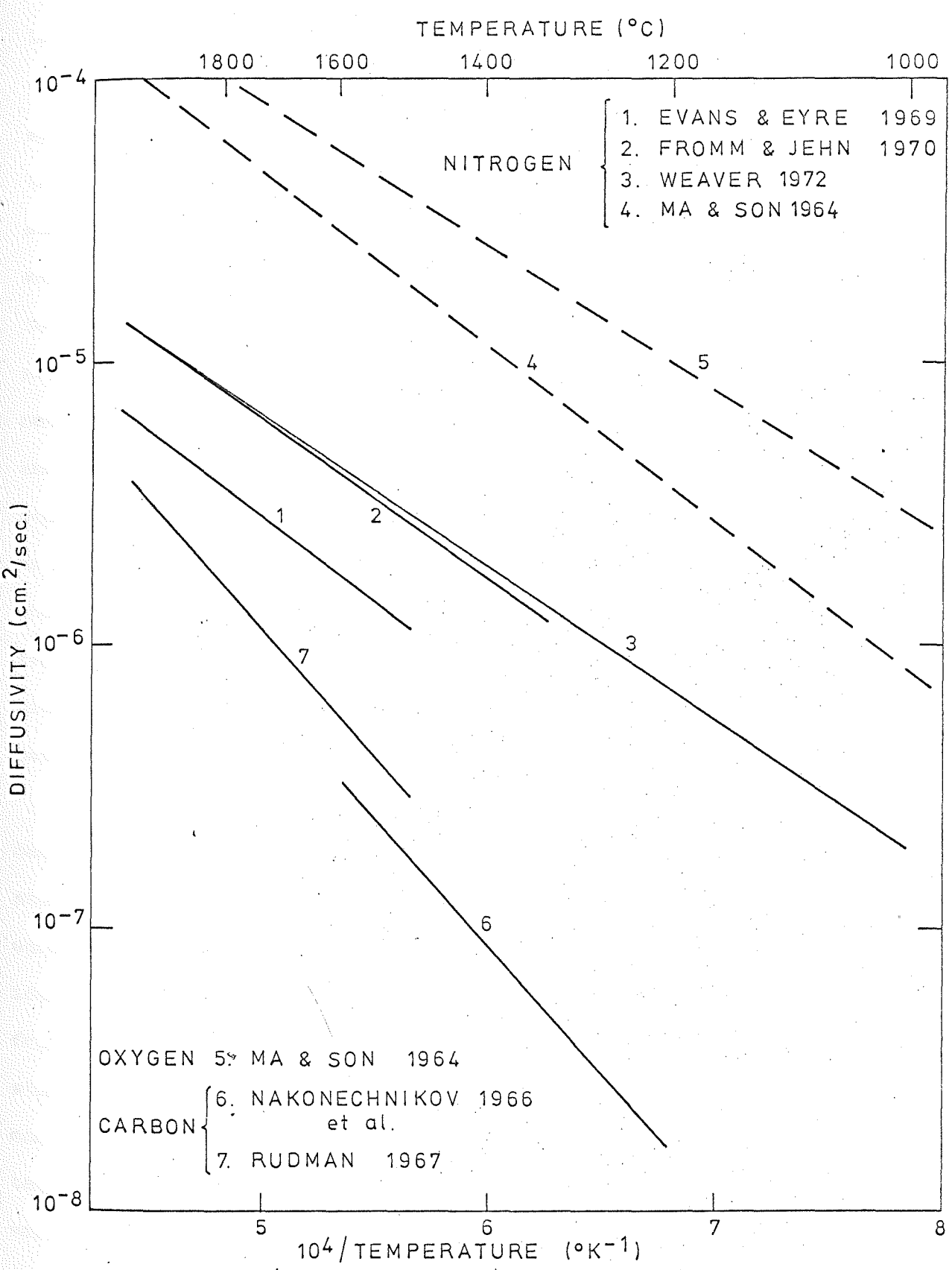
The outgassing kinetics were found to be complex but essentially determined by the rate of evaporation of one or both of the oxides. The rate of ingassing was controlled by gas transport to, or chemisorption on, the metal surface depending on the pressure and the temperature conditions. However, at high temperatures (>1800°C) and oxygen pressures (>5 x 10^{-5} torr.) both ingassing and outgassing reactions occur simultaneously and in thin specimens (say <1 mm.) a kinetic equilibrium is established between the two in a few minutes (Fromm and Jehn 1967). There is little kinetic information available for the oxygen ingassing and outgassing reactions for Group VIa metals such as molybdenum. Kinetic steady state equilibria are known to be established when molybdenum is annealed in oxygen atmospheres >10^{-5} torr. and temperatures >1000°C (Hörz 1972). At high temperatures (>1700°C) and for thin specimens, the times required to establish steady state concentrations of oxygen will be short (of the order of a few minutes) but for lower temperatures and/or larger specimen thicknesses the equilibration times and kinetics are not known.

The carburisation kinetics of molybdenum have not been determined but decarburisation in both moist hydrogen (Kunze and Reichelt 1970) and oxygen (Touboul et al. 1971) atmospheres is controlled by the diffusion of carbon in the solid.

The kinetics of the majority of the ingassing and outgassing reactions described above are determined by gas transport and/or surface reaction steps. In the case of molybdenum, solid diffusion control operates only for the desorption of nitrogen and carbon. However, at large sample thicknesses there is a probability that solid diffusion will be partly or wholly controlling for the remaining gas reactions. Solid diffusivity data is therefore required to estimate the reaction times necessary to establish thermodynamic equilibria. Fig.A5 gives the more reliable diffusivity data for nitrogen, carbon and oxygen in molybdenum.

The agreement between Weaver's (1972) and Fromm and Jehn's (1970)

Figure A5 Diffusivity of Interstitials in Molybdenum


TEMPERATURE (°C)
1800
1600
1400
1200
1000
10^{-4}
10^{-5}
10^{-6}
10^{-7}
10^{-8}
DIFFUSIVITY (cm.^{2}/sec.)
NITROGEN
1. EVANS & EYRE 1969
2. FROMM & JEHN 1970
3. WEAVER 1972
4. MA & SON 1964
OXYGEN 5. MA & SON 1964
CARBON
6. NAKONECHNIKOV 1966 et al.
7. RUDMAN 1967
1
2
3
4
5
6
7
5
6
7
8
10^4/TEMPERATURE (°K^{-1})

nitrogen diffusivities is excellent. Evans and Eyre (1969) obtained significantly lower values mainly due to their higher migration energy. Later work by Evans et al. (1970), involving anelastic relaxation measurements, yielded three migration energies associated with nitrogen clusters in supersaturated solid solution. If the lowest of these relaxation energies (23.1 $\pm$ 2.3 kcal/mole) is associated with the migration of single nitrogen atoms, it is in agreement with Fromm and Jehn's (1970) and Weaver's (1972) values (viz. 26 and 24.5 kcal/mole respectively) within the uncertainties of the measurement. The only other reasonably reliable relaxation data for nitrogen was obtained by Ma and Son (1964) using internal friction measurements. Their values have been extrapolated to high temperatures and plotted in Fig.A5. They are an order of magnitude greater than the other worker's values but, considering the temperature range and accuracy of Ma and Son's data, they are in agreement within the experimental error. It should be remembered that the pre-exponential factor could be in error by a factor of two depending upon the actual site and diffusion path of the nitrogen atoms. In addition, there is the possibility that the diffusion path changes over the wide temperature range covered by the extrapolation.

The high temperature carbon diffusivity data of Rudman (1967) and Nakonechnikov et al. (1966) are in good agreement. The internal friction study of Piguzov et al. (1967) yielded an activation energy in reasonable agreement with the high temperature values. Their work, however, failed to identify conclusively the species associated with the several internal friction peaks observed. Consequently, Ma and Son's (1964) more thorough study which gave different temperatures for the oxygen peaks, is regarded as more reliable. Their oxygen diffusivity values extrapolated to high temperatures are shown in Fig.A5. The same qualifications apply to these values as were previously applied to the nitrogen diffusivities determined by the same workers. In view of the apparent overestimation of the pre-exponential factor for nitrogen, Ma and Son's (1964) data may be regarded as defining an

upper limit for oxygen diffusivities. A lower limit for the same was shown by Scrivastava and Seigle (1974) to be set by the carbon diffusivity values of Rudman (1967).

3.4 Interstitial Doping Techniques

The doping of Group Va metals with interstitial elements is usually achieved by simply annealing in a gaseous atmosphere under appropriate temperature and pressure conditions to levels not exceeding the terminal solid solubility at ambient temperatures. In some instances an alternative method, such as anodisation followed by an homogenising anneal (Smialek and Mitchell 1970a) is more attractive. By subsequently cooling from the annealing temperature at a rate sufficient to prevent outgassing or ingassing of material in the vicinity of the specimen surface (furnace cooling is usually satisfactory) specimens of uniform concentration and any dimension required by the subsequent testing and investigation may be prepared. This method has been used by Taylor and Bowen (1970) and Bressers et al. (1975) to prepare niobium-nitrogen and vanadium-oxygen solid solution alloy specimens, of 3 and 4 mm. diameter respectively, for compression testing. Smialek and Mitchell (1970a) and Szkopiak(1970) have also doped 2 mm. diameter tantalum and 1.25 mm. diameter niobium specimens with carbon and nitrogen respectively, in this manner.

Similar gas atmosphere anneals may be used to introduce interstitial elements into Group VIa metals such as molybdenum. Uniform concentrations of nitrogen may be established in molybdenum samples by anneals in a nitrogen atmosphere under the necessary time, temperature and pressure conditions to achieve thermodynamic equilibrium. Molybdenum-oxygen alloys may be prepared by anneals in oxygen or water vapour atmospheres using the conditions necessary to establish kinetic steady state concentrations. If carbon is to be introduced into a molybdenum sample by annealing in a flowing hydrocarbon gas, a supplementary high vacuum anneal is necessary to ensure homogeneity

because neither kinetic nor thermodynamic equilibrium can be achieved during the gas anneal.

Since the room temperature saturation solubilities of interstitial elements in molybdenum are very small, the interstitials must be secured in supersaturated solid solution if the material is to be studied at low temperatures. This requires the high speed quenching of the doped material from the annealing temperature and therefore imposes limitations on the geometry of the specimens which may be prepared. Previous ageing studies of molybdenum-interstitial alloys have only required the preparation of thin foil and wire specimens ($\leq$1 mm.) by this method (Burck et al. 1969, Eyre and Evans 1972). Very high quench rates (approximately 10^4 - 10^5 ^{o}C/sec) may be achieved for specimens of these dimensions but the extension of the technique to larger specimens, such as those required for mechanical compression testing (typically, 2-3 mm. diameter), reduces the quench speeds obtained. This reduces the concentrations of interstitial atoms which can be secured in supersaturated solid solution.

Chapter 4

EXPERIMENTAL APPARATUS AND PROCEDURE

4.1 Electron Beam Zone-Melting Furnace

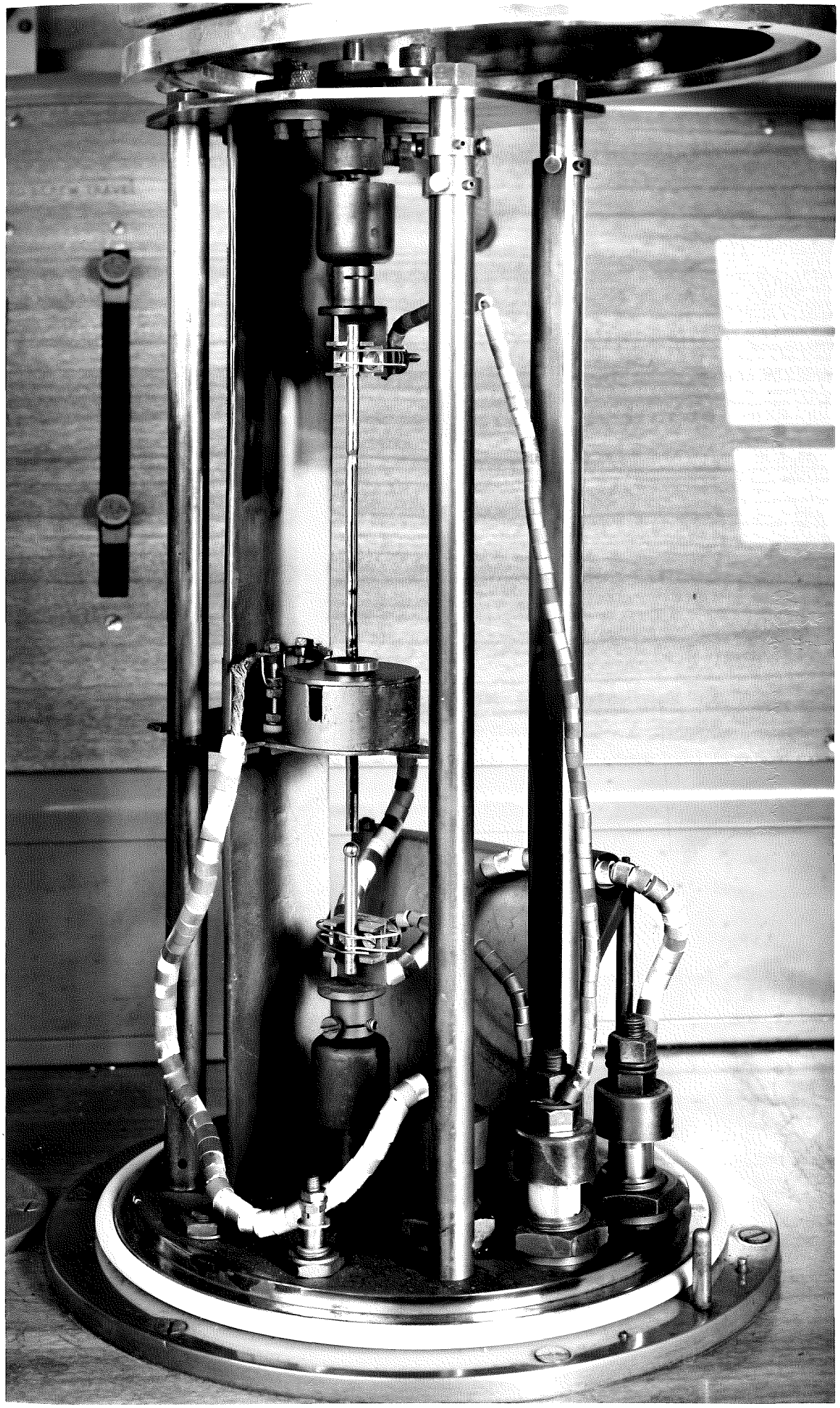
The general principles of this type of crystal growing system have been described in basic papers by Calverley et al. (1957) and Birbeck and Calverley (1959).

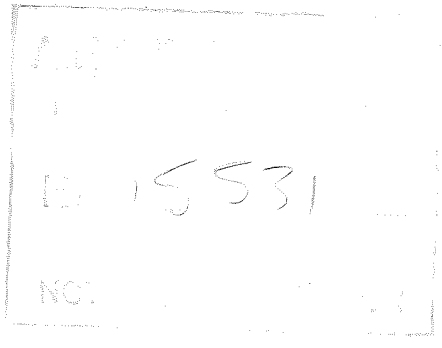
A Miles Hivolt Mark II zone-melting unit was used to grow the molybdenum single crystal for this investigation. The work chamber of the unit is shown in Fig.A6. The electron gun was mounted on a platform which could be translated up and down a vertical mounted crystal rod at speeds of 1-20 mm./min. The molybdenum rods were mounted in V-notch, spring-loaded grips at the base and top of the chamber. The bottom grips were attached to a movable post which could be raised and lowered to fuse and part lengths of crystal. The top grips could be translated laterally to align the rod held in them with the axis of the electron gun and the seed in the base grip.

A molybdenum wire filament was employed in the gun. This had a shorter life than the more usually employed tungsten but did eliminate the possibility of the tungsten content of the molybdenum being increased during zone-melting. The output of the high voltage supply to the gun could be varied between 0 and 10 kV and the current supply to the filament between 0 and 50 amps. An emission stabiliser control circuit was incorporated in the unit to facilitate the manual control of the conditions in the molten zone.

The work chamber was pumped by a liquid nitrogen trapped 6 in. mercury

Figure A6 Work Chamber of Zone-Melting Furnace




15531

diffusion pump with a pumping speed of 650 l/sec. The operating vacuum in the work chamber was typically 10^{-5} torr. Both the gettering of gases by molybdenum vapour condensing on the furnace walls, and the general baking out of the internal components of the chamber, caused the vacuum to improve progressively during the zone-melting operation.

4.2 Controlled Atmosphere Quenching Furnace

A medium frequency induction heated furnace was used for the decarburisation, high vacuum annealing and doping treatments. A general view of the furnace, which was constructed by Mr. H.W. Evans, is shown in Fig.A7. A detailed diagram of the tube furnace itself is given in Fig.A8.

A 1 in. outside diameter, 6 in. long molybdenum tube with a 1/16 in. wall thickness was employed as a susceptor. The specimens contained within the susceptor were heated by radiation but did not suscept directly with the medium frequency field. The susceptor was enclosed by four concentric molybdenum heat shields which reduced the radiation losses and allowed temperatures >2000°C to be attained. Both the susceptor and heat shields were decarburised before use in annealing treatments.

The furnace temperature was measured with a molybdenum sheathed, beryllia insulated, tungsten-rhenium thermocouple. This had been calibrated by Harwell Instrument Test Laboratories and was estimated to be accurate to within $\pm$ .75% of the measured value in the temperature range 500-2100°C. The temperature was found to be constant to within $\pm$ 1% in an ~4 cm. zone in the central region of the susceptor length. The mean temperature of this zone was not monitored directly during the doping anneals but was precalibrated against the input to the medium frequency coil. The calibration was found to be independent of the nitrogen gas pressure used during the nitrogen anneals. But it was particularly sensitive to the wall thickness of the susceptor which was reduced, due to oxidation, during the oxygen anneals. Recalibration of the susceptor after the oxygen anneals indicated the temperature dropped 20-100°C due to the thinning of

Figure A7 General View of Quenching Furnace

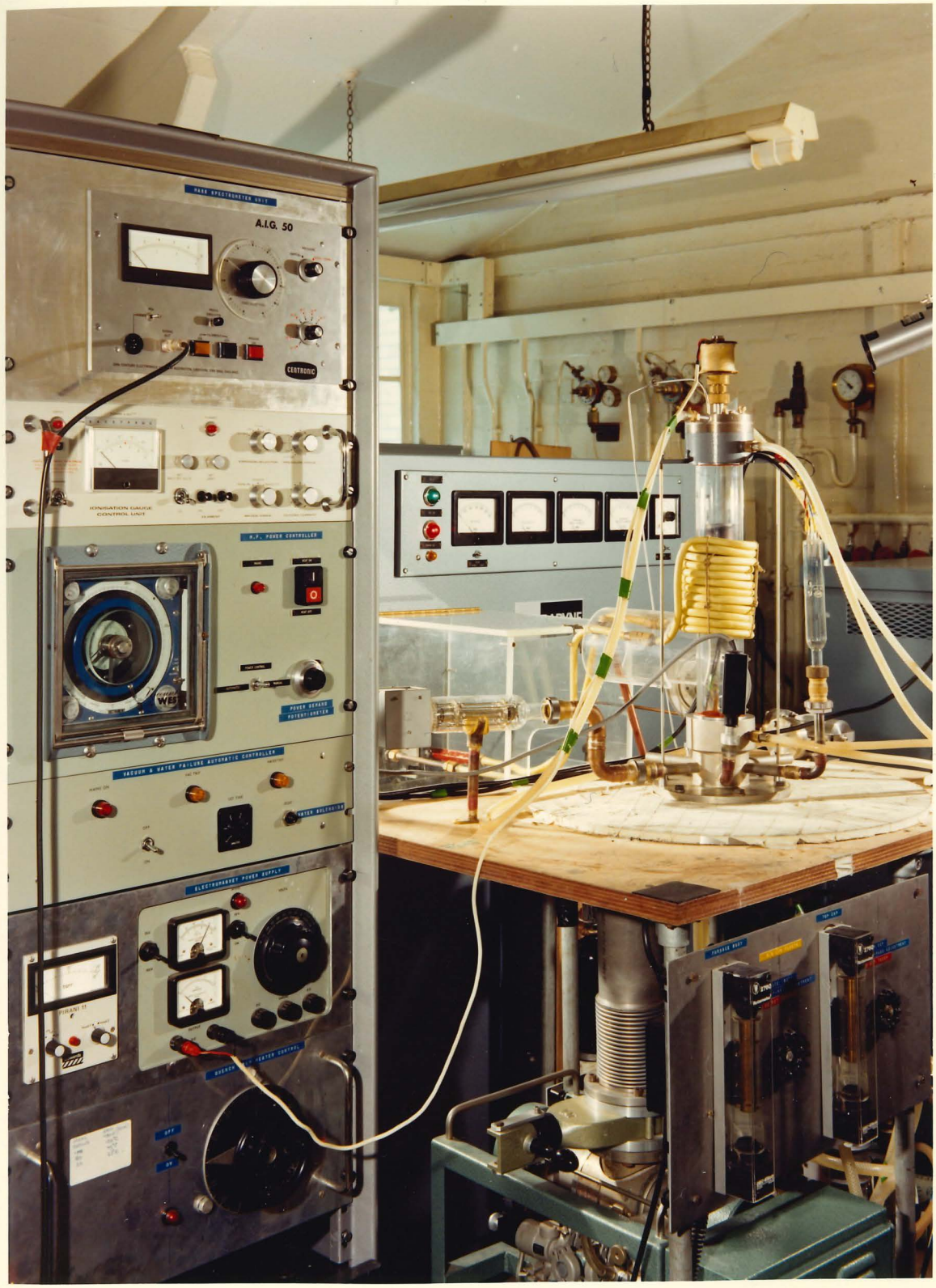
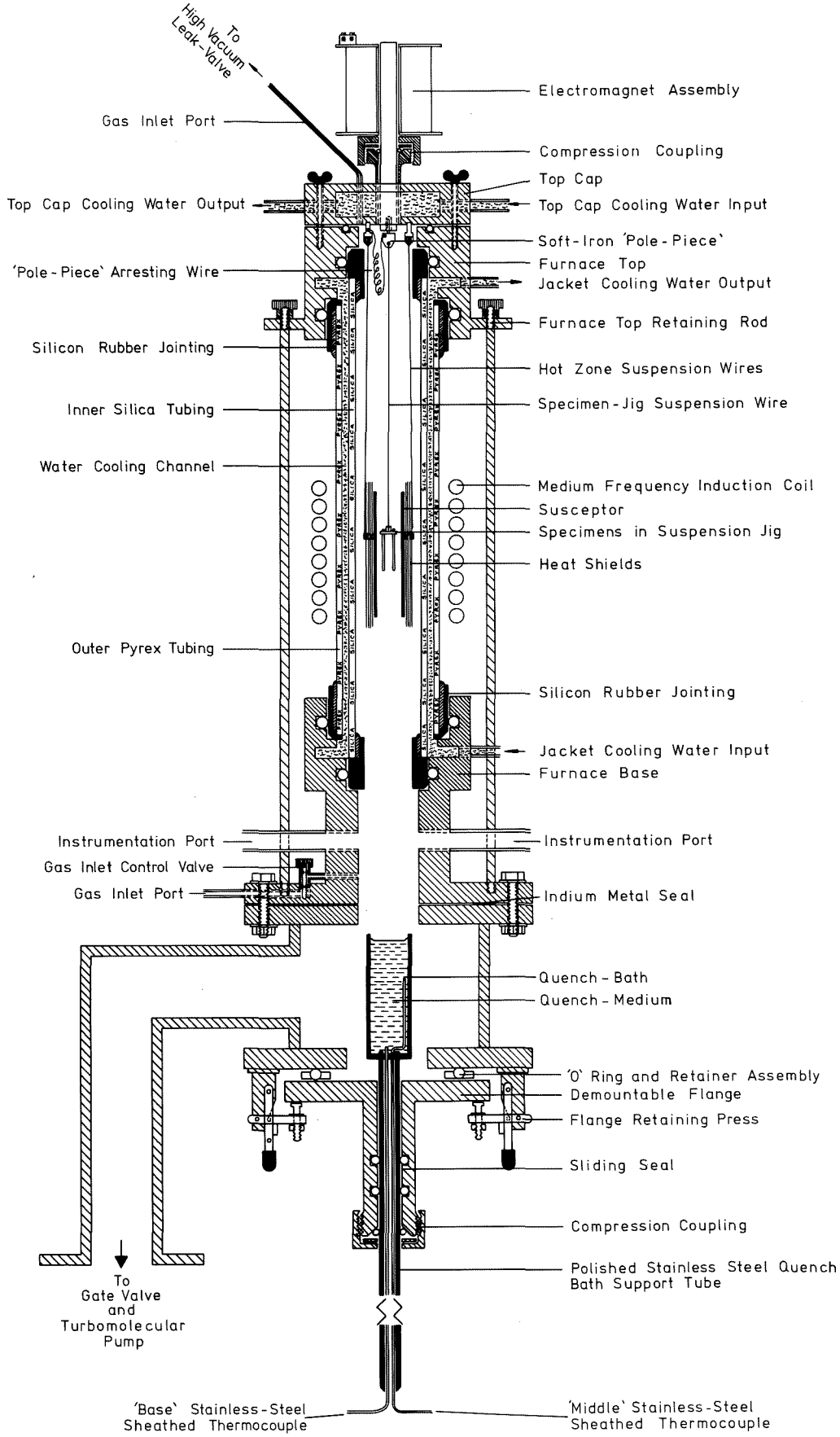

A.I.G. 50
CENTRONIC
IONISATION GAUGE
CONTROL UNIT
R.F. POWER CONTROLLER
POWER DEMAND
POTENTIOMETER
VACUUM & WATER FAILURE AUTOMATIC CONTROLLER
ELECTROMAGNET POWER SUPPLY

Figure A8 Diagram of Quenching Furnace



CONTROLLED ATMOSPHERE HIGH TEMPERATURE QUENCHING FURNACE.

the susceptor walls. In the later oxygen anneals the initial thickness of the susceptor walls was increased from 1/16 in. to 1/8 in. which reduced the magnitude of the temperature drop to ~10°C.

The furnace was pumped by a Pfeiffer TVS 250 turbo molecular pump which had a pumping speed of 70 l/sec. and a working range which extended from atmospheric pressure to high vacua. With the furnace at maximum temperature, pressures of $<10^{-5}$ torr. could be readily attained. When the pump was isolated from the tube furnace by means of an intervening gate valve, the 'leak' rate of the furnace was ~2-5 x 10^{-5} torr./min. All pressure gauges were coupled to the instrumentation ports at the base of the furnace. A Penning and Bayard-Alpert type ion gauge were used to monitor pressures in the high vacuum range. At higher pressures a Pirani and anaerobic gauge were employed. A high vacuum leak valve was connected to the gas inlet port of the top cap. This allowed dynamic atmospheres in the pressure range ~10^{-1} - 10^{-5} torr. to be maintained. A back filling inlet port at the base of the furnace also permitted higher pressure, static gas atmospheres to be introduced.

A quench bath containing a type metal alloy, with a melting point of 58°C and the composition given below, was mounted at the base of the furnace.

49% bismuth	12% tin
18% lead	21% indium

The bath could be raised to a position immediately beneath the susceptor by means of a sliding O-ring seal. When the bath was in the fully retracted position radiation from the susceptor was sufficient to melt the alloy, the temperature of which rose to a limiting value of 95°C.

Specimens were mounted in a molybdenum jig which was essentially a strip of decarburised molybdenum perforated with ~3 mm. diameter holes. By spot-welding a molybdenum wire tab on the end of a cylindrical specimen it

could be suspended in a vertical and free hanging position beneath the jig. This ensured the specimens entered the quench bath vertically and were sufficiently widely spaced to prevent the quench rate of the individual specimens being influenced by the close proximity of other specimens. It was found that only when these conditions were met could reproducible quenching results be obtained.

The jig and specimens were in turn suspended in the constant temperature zone of the susceptor by a molybdenum or tungsten wire and a magnetically clamped soft iron 'pole-piece'. The pole-piece was latched by a wire to the top cap such that, when it was unclamped to allow the specimens to fall from the hot zone, they were arrested before they impacted on the bottom of the raised quench bath. The fall distance of the specimens from the hot zone to the bath was ~4 in. The temperature drop of the specimens due to radiation loss during the fall was estimated to be $< 20^{\circ}C$.

4.3 Resistivity Measuring Apparatus

Fig.A9 shows the apparatus used to measure resistance ratios and hence, residual resistivities. This was housed in an air-conditioned room where the temperature was controlled to $20 \pm 1^{\circ}C$ because of the temperature sensitivity of much of the electronic equipment involved.

A four point resistor, potentiometric measuring system was used to determine the R.R's. Usually the ratio of the resistance at $273^{\circ}K$ (specimen immersed in an ice bath) to that at $4.2^{\circ}K$ (specimen immersed in a helium bath) was measured and the residual resistivity calculated using a resistivity value at $273^{\circ}K$ of 5.0×10^{-6} ohm cm. (Holmwood and Glang 1965). A block diagram of the measuring system is given in Fig.A10 and the specifications of the system components are given in Table A3.

A direct current was passed through the usually cylindrical resistivity specimen via contacts at its ends and the potential difference (V_1) measured

Figure A9 General View of Resistivity Measuring Apparatus

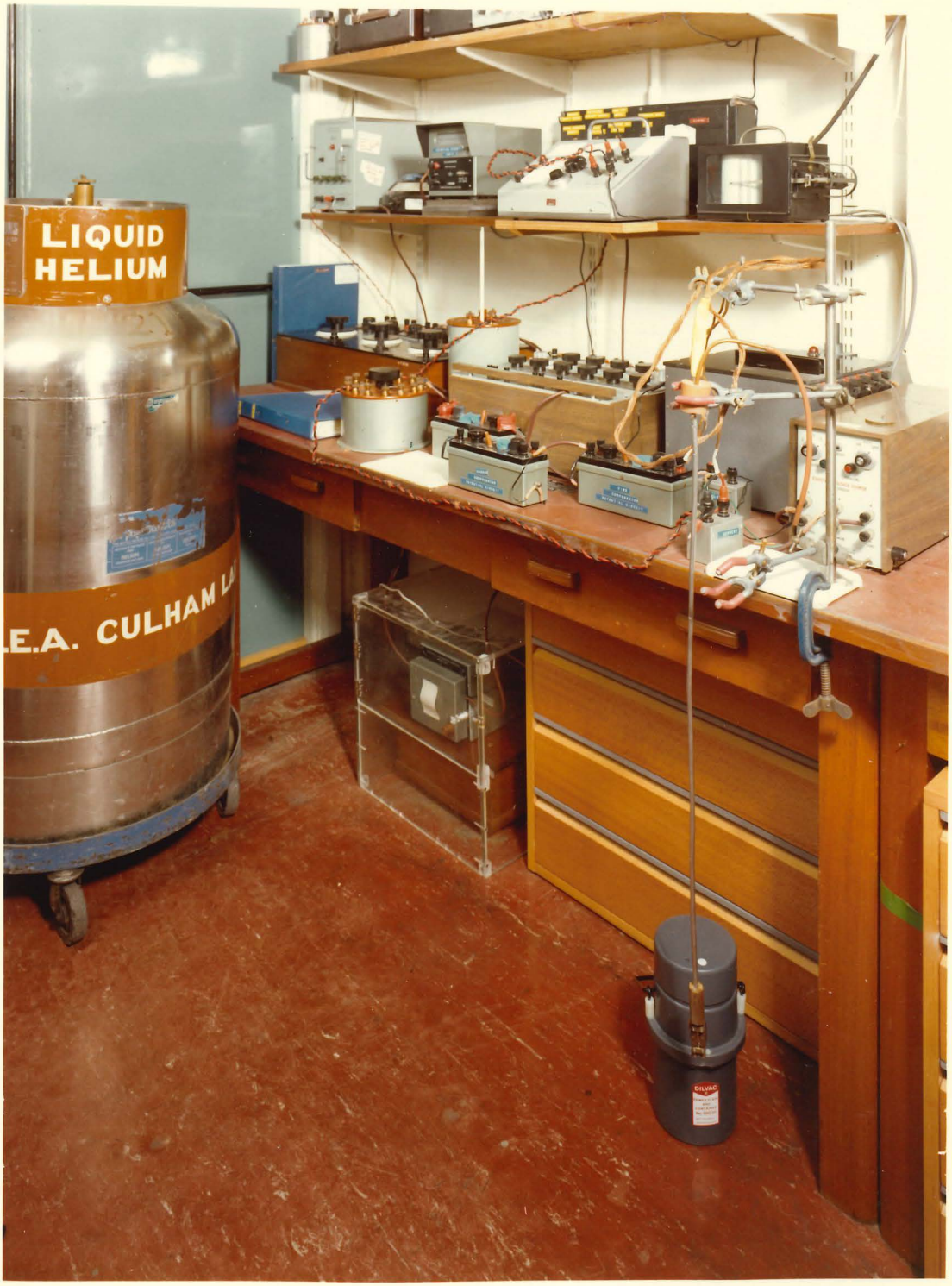
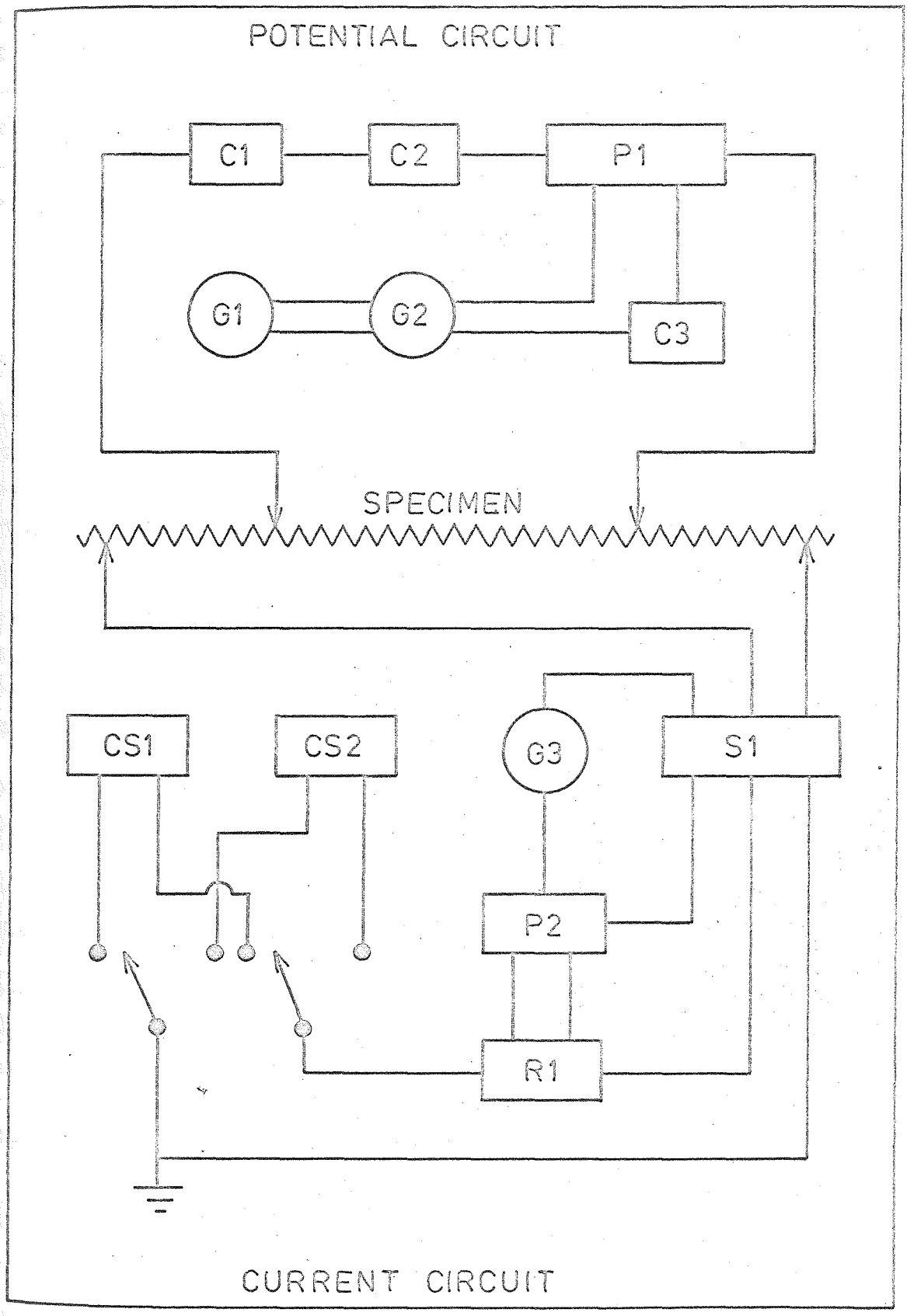

LIQUID
HELIUM
E.A. CULHAM

Figure A10 Block Diagram of Resistivity Measuring System
(For Legend see Table A3)


POTENTIAL CIRCUIT
C1
C2
P1
G1
G2
C3
SPECIMEN
CS1
CS2
G3
S1
P2
R1
CURRENT CIRCUIT

C1	Thermal Compensator	0-5 μV	Tinsley Type 5214A
C2	" "	0-0.5 μV	" " "
C3	" "	0-1.6 μV	" " "
P1	Double Decade Resistance Nanovolt Potentiometer	0-0.02 V ± 2 nV*	Guildline Type 9176G
	Standard Cell Battery	- *	Tinsley Type 5644
	Constant Voltage Source	12 V ± 3 x 10^{-6} V	Guildline Type 9780/12
P2	Vernier Potentiometer	0-2 V ± .001% or 10 μV	Cambridge
G1	Galvanometer	1 mm./nV	Tinsley Type MS245E
G2	Galvanometer Amplifier	-	" " 5214
G3	Galvanometer	10 mm./ V	Cambridge
S1	Thermoelectric Free Reversing Switch	Brake and make	Tinsley Type 4092
CS1	Constant Voltage Supply Unit	40 V 0-250 mA	Harwell
CS2	Constant Current Supply Unit	40 V 5 A	Solartron PSU AS
R1	Standard Resistance	0.1 ohm ± .003%	Cropico Type RS2

*Calibrated against National Physics Laboratory Standards

Table A3 Specification of Resistivity Measuring System Components

between two leads contacting the specimen at intermediate positions. The current (viz. 200.0 ± 0.1 mA at 273°K and 2.00 ± .001 A at 4.2°K) were chosen so that, for the range of specimen geometries employed, negligible resistance heating of the specimen occurred in the fixed temperature baths. For the 4.2°K measurement in particular, the thermal gradients in the potential leads connecting the specimen to the nanovolt potentiometer gave rise to large (several μV) thermal emf.'s. So, V_1 was in fact the sum of the actual potential drop along the specimen (V_s) and these thermal emf.'s (V_T). In the absence of any heavy thermal lagging, V_T was very sensitive to the boil off rate of helium and hence, changed considerably when the current through the specimen was turned on and off. It was therefore found unsatisfactory to determine V_s by balancing out V_T with thermal compensators prior to switching on the current. Instead, after measuring V_1 the current was reversed and the potential drop across the leads (V_2) measured.

Since $$V_1 = V_T + V_s$$

and $$V_2 = V_T - V_s$$

then $$V_s = \frac{V_1 - V_2}{2}$$

where V_T is constant during the period of the two measurements.

The accuracy with which the R.R. was measured was in most instances determined by the accuracy with which V_s was measured at 4.2°K. With rapid balancing of the nanovolt potentiometer, V_s (4.2°K) could be determined with a precision of ± 2 nV. But the accuracy of the measurement was of the order of ± 5 nV because of thermal emf.'s within the nanovolt potentiometer itself. The accuracy of the residual resistivity so determined was a function of specimen geometry. It would typically vary from $\pm 10^{-10}$ ohm cm. (i.e. ± 10%) for a high vacuum annealed, 2.5 mm. diameter (compression size) specimen to $\pm 5 \times 10^{-12}$ ohm cm. (i.e. ± .0005%) for a heavily doped, 1 mm. diameter

(tension size) specimen.

Two types of potential contacting systems requiring two types of resistivity probe heads were employed. In the first system ~1 mm. diameter wire tabs were spot welded onto the resistivity specimens at any chosen interval and these connected to the potential leads by freezing both in a pool of low melting point (~15°C), gallium-indium-tin alloy. This system was most suited to those specimens which were eventually sectioned into compression test specimens because the spot weld contacts could be positioned outside the test specimen gauge lengths. In the second system spring-loaded gold tabs, mounted at a fixed separation of ~1.5 cm. on the resistivity probe head, were used to make the potential contacts. This system was used to measure the resistivity of tension test specimens where no marking of the specimen surface could be tolerated. The potential contacts in both systems were located >5 mm. from the current contacts in a region where the lines of equipotential would be uniformly distributed.

4.4 Material

Arc-cast molybdenum supplied by the Climax Molybdenum Company in the form of 3/16 in. diameter centreless ground rods was employed in this investigation. The rods had been prepared from two batches of material whose supplier's specified compositions are given in Table A4. Analysis results obtained by activation analysis and spark source mass spectrography are presented in Tables A5 and A6. The resistance ratio of the as received material varied from 70 to 90.

4.5 Crystal Growth by Zone-Melting

Prior to the melting of the as received molybdenum rod, a preliminary outgassing pass at ~2000°C was made along its length. It was then fused to

Batch Number	ELEMENT (at.ppm.)					
	Ni	N	H	O	Fe	C
C8076	<16	<24	<96	<66	<52	<400
C7424	<16	<24	<96	<12	<17	<320

Table A4 Supplier's Specified Composition for As Received Material

Batch Number	ELEMENT (at.ppm.)				
	Fe*	Si*	O*	C	W
C8076	< 34	< 64	< 70	480 ± 4	48 ± 2
C7424	< 20	< 37	< 36	320 ± 4	48 ± 2
*Results for small samples indicated considerable heterogeneity along the rod					

Table A5 Activation Analysis Results for As Received Material

Batch C7424 MATERIAL	ELEMENT (at.ppm.)									
	Mg	S	Ca	Sc	V	Cr	Mn	Co	Ni	Cu
As Received	<240	<0.6	<14.4	<2.1	0.2-2	0.2-2	0.19-1.9	0.03-0.3	<48	0.09-.9
Zone-Melted	<0.8	<3.2	<2.4	<0.07	0.1-1	0.15-1.5	0.1-1	0.1-1	<2	0.02-.2
	Ge	Zr	Nb	Rh	Pd	Sn	Sb	Te	Re	Os
As Received	<0.8	<65	0.6-6	<2	<0.1	0.3-3	<0.05	<1.3	<1.3	<5
Zone-Melted	<0.26	<0.6	-	<0.1	<0.6	0.03-.3	<0.05	<1.3	-	-

All elements from atomic No's 3-92 (with the exception of C, N, O, Si, Fe, W) were determined.

Unquoted elements were below the limits of detection (0.001-0.01 wt.ppm.)

The concentration of a range of elements could only be fixed by a conservative upper limit because of interference from complex ions

Table A6 Results of Spark Source Mass Spectrographic Analysis

a single crystal seed which was mounted in the bottom grips. When a stable molten zone ~1 cm. long had been secured it was passed from the bottom to the top of the rod. A series of crystals was grown where from 2 to 8 passes were made in the upwards direction. Several different traverse speeds in the range 2-8 mm./min. were also employed.

At the completion of the final pass the crystal was parted from the unmelted stub in the top grips to minimise any thermal stressing of the crystal as it cooled. Approximately 2 cm. lengths were then discarded from the bottom and top of the zone-melted crystal where some contamination from the seed and unmelted top stub may have occurred. The remaining ~12 cm. crystal length was then etched in a 40:20:20 sulphuric, nitric and hydrofluoric acid solution and the etch bands examined to ensure it was a single crystal.

Samples for the analysis of carbon and silicon by gamma and neutron activation techniques respectively were cut at ~3 cm. intervals along the crystals. Further samples for oxygen and iron analysis by gamma and neutron activation respectively were also cut from the tops and bottoms of the crystals.

The remaining crystal sections were then centreless ground to several diameters in the range 0.5-3.0 mm. Not greater than .002 in. reductions were used during the grinding and the final 1 mm. of the diameter was removed in .0005 in. steps. This standard grinding procedure was adopted throughout the investigation to guarantee a constant damage layer depth. Laue photography was employed to determine the depth of grinding damage. When a 25μ layer of material had been electropolished from the specimen surface, there was no detectable streaking of the Laue spots. So, this amount of material was removed from the surface of all the centreless ground crystals by electropolishing in a 70:30 sulphuric acid and methanol solution. The R.R.'s of these specimens were then measured before subjecting them to further treatments.

4.6 Decarburisation and High Vacuum Annealing

The ground and polished crystal rods were annealed in low partial pressures (2-6 x 10^{-5} torr.) of oxygen at temperatures from 1600°C to 1900°C to remove residual carbon. The temperature and pressure conditions were varied so as to secure the most rapid decarburisation of the molybdenum but with a minimum loss of material from the specimen due to oxidation. At the conclusion of the decarburisation treatments the crystals were high vacuum annealed at $<10^{-5}$ torr. and 1800-1900°C to remove oxygen.

The composition of the furnace atmosphere was monitored during the treatments and both R.R. measurements and gamma activation analysis were employed to follow the progress of the decarburisation and deoxidation. At the conclusion of the deoxidation treatment several vacuum quenches were made as an ultimate test of material purity.

4.7 Doping Treatments

A series of doping treatments was undertaken where batches of high vacuum annealed crystal rods, 3.0-3.5 cm. long, were quenched from nitrogen and oxygen atmospheres. The primary purpose of these quenches was to establish the maximum concentration of nitrogen and oxygen which could be secured in solid solution in specimens of suitable dimensions for compression (2.5-3.0 mm. diameter) and tension (~1.0 mm. diameter) testing. A thin control wire or foil, whose quench-rate was expected to be comparatively large, was quenched simultaneously with tension and compression size specimens. The annealing conditions were varied until the quenched-in resistivities obtained in the specimens of different thickness were approximately the same. This was taken to define the concentration level at which the quench rate in the larger diameter specimens was sufficient to retain the nitrogen or oxygen in solid solution.

Several 1 mm. thick discs of high vacuum annealed molybdenum suitable for lattice parameter measurements and activation analysis were also doped in some of the treatments. The number of specimens which could be simultaneously quenched was limited by the internal diameter of the susceptor and the alignment accuracy of the quenching system. Typically 6 tension size specimens or 3 compression size specimens could be successfully quenched together. After loading the specimens and pumping the furnace down cold the following annealing and quenching procedure was followed.

The specimens and susceptor were initially outgassed at a temperature $\geq 1800^{\circ}C$ and pressure $\leq 10^{-5}$ torr. for ~60 min. before the temperature was adjusted to the required value and the doping atmosphere introduced. British Oxygen Company grade X nitrogen and oxygen with the maximum impurity levels given in Table A7 were used.

Impurity Gas	Nitrogen	Oxygen
N_2	-	<200
O_2	< 2	-
CO_2	< 1	< 1
CO	< 1	< 1
HC	< 1	< 2
H_2	< 1	< 2
H_2O	< 5	< 5
Ar	<10	<100

Table A7 Impurity Content of Doping Gas (vol.ppm.)

Quenches were made from nitrogen atmospheres over a wide range of pressures (10^{-2} - 300 torr.) and temperatures (1500-1900°C). For doping

treatments at nitrogen pressures $\leqslant 10^{-1}$ torr. a dynamic atmosphere was employed. To secure larger pressures of nitrogen ($\geqslant$1 torr.), a dynamic atmosphere of ~0.1 torr. was first established. The turbo molecular pump gate valve was then closed and the furnace was back-filled with nitrogen to the required static pressure. This procedure minimised the amount of impurity gases 'leaking' into the system. However, at pressures $\geqslant$10 torr. the partial pressures of gaseous impurities introduced with the doping gas itself were comparable to those already present in the residual vacuum.

All the oxygen quenches were conducted from dynamic atmospheres. At the higher temperatures ($\geqslant$1800°C) or pressures ($\geqslant 10^{-4}$ torr.) the rapid oxidation of the specimens and internal components of the furnace limited the length of the annealing treatments. Also, the use of an 1/8 in. wall thickness susceptor with only a 3/4 in. internal diameter to reduce the temperature decay during the treatments, severely restricted the number and size of specimens which could be treated simultaneously.

After the appropriate annealing time, the quench bath was raised, the pole-piece unlatched and the specimens dropped from the hot zone into the quench bath. The furnace power was cut off by a pressure trip which was activated by the vaporisation of the quenching alloy when the specimens entered the bath. Depending on the thermal mass of the batch of specimens quenched, the temperature of the bath rose from 95°C to 100-120°C when the specimens entered the bath. Approximately 1 min. after quenching, the quench bath was retracted and the specimens remained suspended ~4 in. below the susceptor. Radiation from the hot susceptor caused some initial heating of the specimens. By locating a thermocouple 4 in. below the susceptor and simulating the heating and cooling cycle of the quenching sequence, the temperature of the specimen was estimated to rise to approximately 120-140°C before cooling to ambient temperature.

After the specimens were removed from the furnace they were warmed to melt the quenching alloy. This was readily removed by wiping the specimens

with a wet tissue. They were then given a light electropolish. ESCA analysis indicated there was no contamination of the specimen surface by the quenching alloy. All the doped specimens were stored in card ice at $\sim -78^{\circ}C$ until R.R. and lattice parameter measurements, or mechanical tests were made.

4.8 Gamma Activation Analysis

Carbon, nitrogen and oxygen were determined by high energy gamma photon activation analysis at Harwell. The availability of this analytic facility, particularly suited to the determination of low concentrations of interstitials elements, was a great advantage in the characterisation of the molybdenum and molybdenum-interstitial alloys employed in this investigation. The technique, as outlined below, is applicable to the determination of these elements in a wide range of materials but Harwell have had considerable experience in its application to molybdenum.

All three elements were determined by the production and measurements of their neutron deficient isotopes. These are formed by the reaction $A_X^N (\gamma,n) A_X^{N-1}$ when the elements are bombarded with high energy gamma photons produced, in Harwell's case, using a 45 MeV electron linear accelerator (Baker and Williams 1968). It is necessary to radiochemically separate the sought element from the sample matrix in order to measure its characteristic β^+ radiation and subsequently compare it with the activity induced in simultaneously irradiated standards.

Carbon

The isotope C^{11} (half life 20 min.), formed by the reaction $C^{12}(\gamma,n) C^{11}$, is separated from the matrix by burning the sample in oxygen at $1400^{\circ}C$. The $C^{11}O_2$ evolved is collected by absorption on soda asbestos and its β^+ activity measured.

Nitrogen and Oxygen

The isotopes formed are O^{15} (half life 2 min.) and N^{13} (half life 10 min.). An inert gas fusion technique is used to separate these from the matrix. The sample is heated to a high temperature in a graphite crucible and the evolved CO^{15} and N_2^{13} are swept through a chemical separation train (Hislop and Williams 1971) by a stream of helium. The activities of the components of the train are measured in order to determine oxygen and/or nitrogen. Two types of heating techniques may be used.

(i) Induction heating where the sample and a copper/carbon flux are heated to ~2200°C for 3 min. and 10 min. in the case of oxygen and nitrogen determinations respectively.

(ii) Impulse heating where the sample is heated to ~3000°C for 20 secs.

Both the precision and accuracy of carbon and oxygen analysis results have been verified by the analysis of standard reference materials. The reliability of the nitrogen results is not well established and, in fact, the activation analysis technique has rarely been applied before to determinations in molybdenum.

Chapter 5

RESULTS

5.1 As Zone-Melted (A.Z.M.) Crystals

The dependence of the carbon content and resistance ratio of the A.Z.M. crystals on the zone-melting variables is shown in Figs.A11 and A12. As expected, the R.R. increased and by inference the total impurity content decreased as the number of zone passes made was increased. Fig.A11 shows this result for specimens taken from the centre of the A.Z.M. crystal lengths. The carbon content in the central region of the crystals also generally decreased with increasing numbers of zone passes. As shown in Fig.A12 the carbon level increased and the R.R. decreased from the bottom to the top (i.e. the zone traverse direction) of the A.Z.M. crystals.

The carbon contents of the two batches of starting material were different (see Tables A4 and A5) and this caused additional variations in the levels present in the A.Z.M. crystals. Typically, the carbon concentration at the centre of 3-5 zone pass crystals was 50-300 at.ppm. This increased to 400-2400 at.ppm. at the tops of the crystals. These concentrations are much greater than the terminal solubility of carbon at low temperatures (<10 at.ppm. at 1000^{o}C) and so a large proportion of the carbon would be precipitated in the furnace cooled A.Z.M. crystals.

No systematic variation was found in the oxygen, silicon and iron levels with the zone traverse speed and number of zone passes employed or with the position along the crystal length. The ranges of concentrations determined in the A.Z.M. crystals were 3-35 at.ppm. oxygen, 3-10 at.ppm. silicon and 4-12 at.ppm. iron. These levels are lower than those in the

Figure A11 Variation in Carbon Content and Resistance Ratio of A.Z.M. Crystals with Number of Zone Passes

Zone speed 8 mm./min.
Batch C7424 material

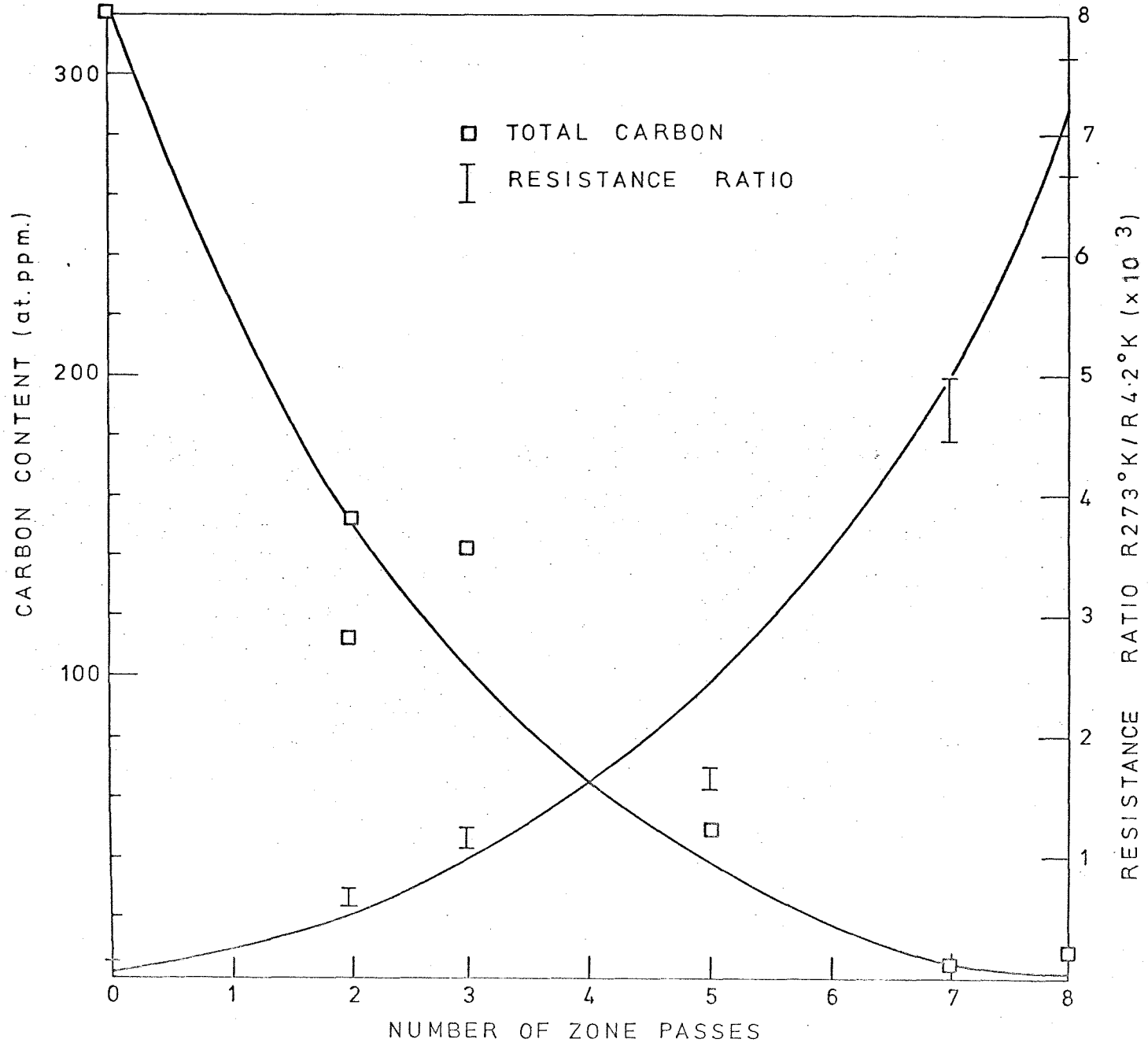
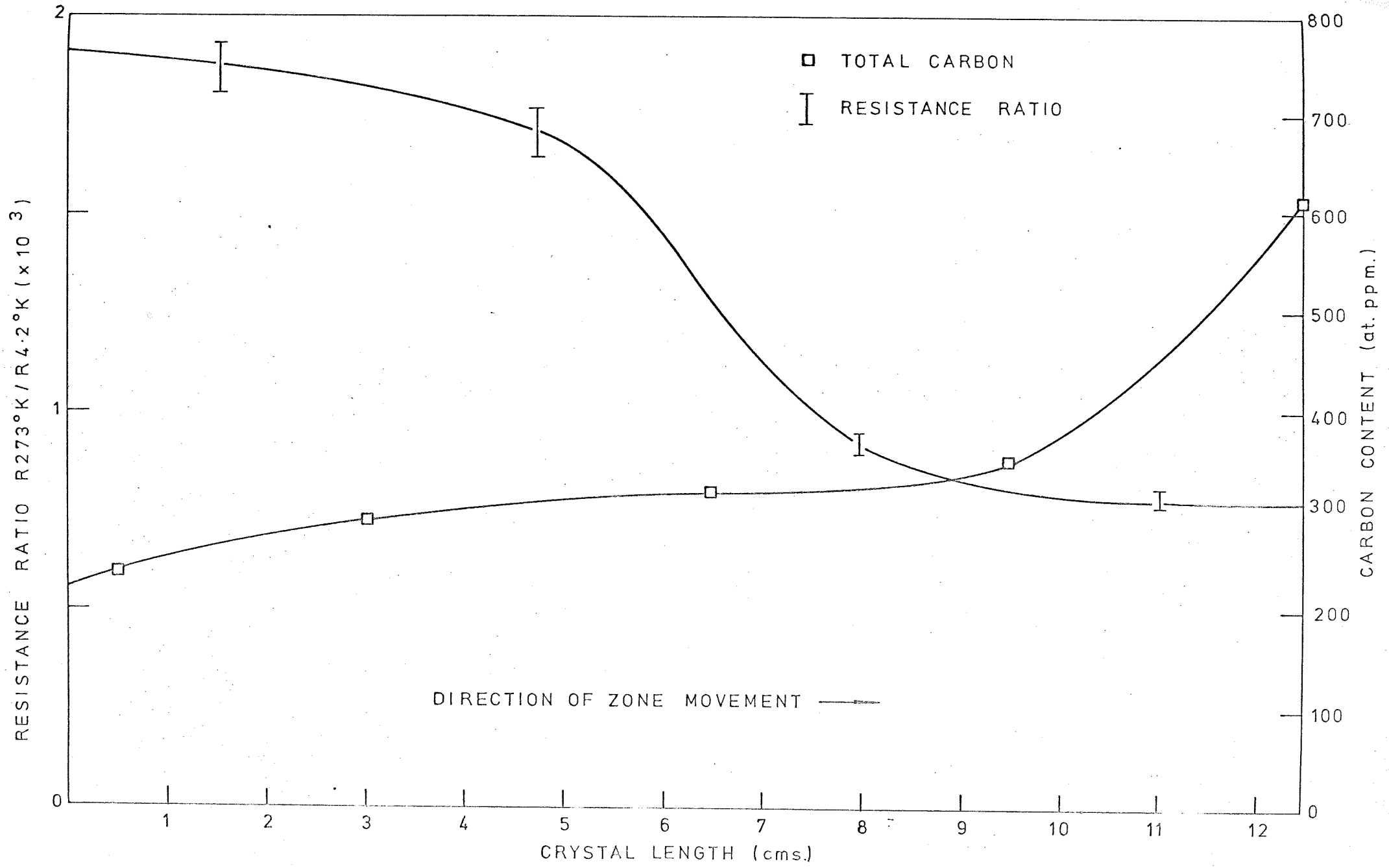

TOTAL CARBON
RESISTANCE RATIO
CARBON CONTENT (at. ppm.)
RESISTANCE RATIO R273°K/R4·2°K (x10⁻³)
NUMBER OF ZONE PASSES
300
200
100
0
1
2
3
4
5
6
7
8

Figure A12 Variation in Carbon Content and Resistance Ratio with Axial Position in an A.Z.M. Crystal

Zone passes 4
Zone speed 8 mm./min.
Batch C7424 material


TOTAL CARBON
RESISTANCE RATIO
RESISTANCE RATIO R273°K / R4·2°K (x10 3)
CARBON CONTENT (at. ppm.)
DIRECTION OF ZONE MOVEMENT
CRYSTAL LENGTH (cms.)
2
1
0
800
700
600
500
400
300
200
100
0
1
2
3
4
5
6
7
8
9
10
11
12

as received molybdenum (see Table A5). It would appear that the major reduction in the concentrations of these elements occurred by outgassing and evaporation during the initial zone passes. The tungsten content of the molybdenum was not significantly changed by zone-melting. This is consistent with the findings of previous investigations (Oppermann et al. 1967, Evans and Eyre 1968b).

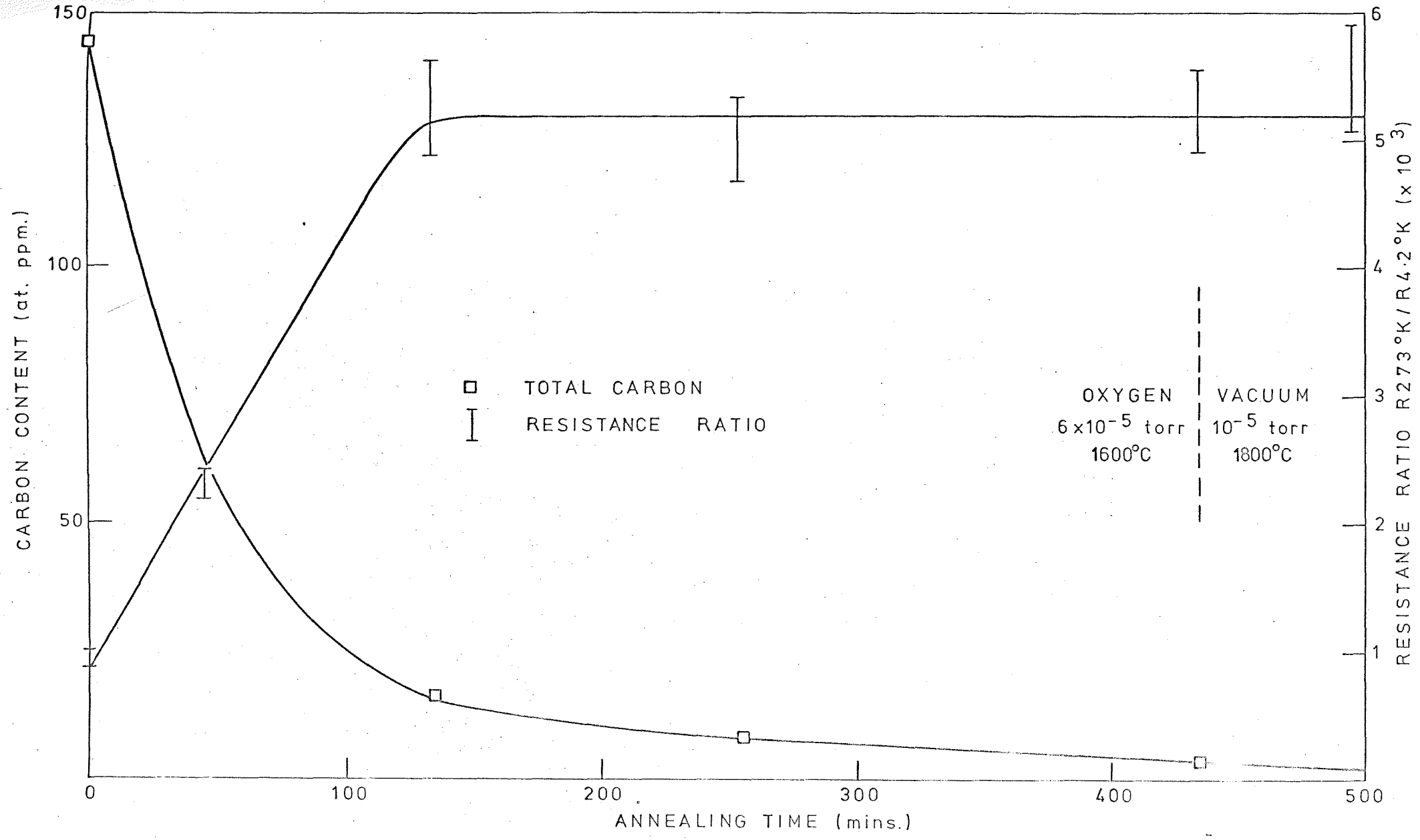
5.2 Decarburised and High Vacuum Annealed (H.V.A.) Crystals

The decay in the partial pressure of carbon monoxide in the furnace atmosphere during the decarburisation treatments indicated the carbon content of the molybdenum was being progressively reduced. This was confirmed by the carbon analysis results and R.R. measurements. The decrease in the total carbon content and increase in R.R. with increasing oxygen annealing times is shown for a typical decarburisation treatment in Fig.A13. The resistance ratio tended to saturate when the total carbon content was reduced to <20-30 at.ppm. This insensitivity of the R.R. to the variation in the carbon content during the latter stages of the oxygen anneal suggests that, after furnace cooling of the crystals, little carbon remained in solid solution. So the significant reduction in total carbon content indicated by the analysis results would be accompanied by only a small reduction in the carbon concentration in solution. It is emphasised that it is only the latter which directly determines the R.R.

The oxygen annealing times required to reduce the total carbon content to <4 at.ppm. (i.e. the sensitivity of the gamma activation analysis) were consistent, given the scatter in the carbon diffusivity data (see Section 3.3), with a solid diffusion controlled decarburisation reaction. Only a small, if at all significant, increase in the R.R. occurred when the decarburised crystals were high vacuum annealed to remove oxygen introduced during the oxygen anneal. Gamma activation analysis indicated the residual oxygen

Figure A13 Variation in Carbon Content and Resistance Ratio with Annealing Time during the Decarburisation of an A.Z.M. Crystal

Zone passes 4
Zone speed 8 mm./min.
Batch C8076 material


150
100
50
0
100
200
300
400
500
6
5
4
3
2
1
CARBON CONTENT (at. ppm.)
RESISTANCE RATIO R273°K/R4.2°K (x 10 3)
ANNEALING TIME (mins.)
TOTAL CARBON
RESISTANCE RATIO
OXYGEN
6 x 10-5 torr
1600°C
VACUUM
10-5 torr
1800°C

concentration in the H.V.A. material was < 6 at.ppm.

As shown in Fig.A14 decarburisation considerably reduced the axial variation in R.R. shown by the A.Z.M. crystals. Fig.A15 and A16 also indicate the dependence of the R.R. of the decarburised crystals on zone melting parameters. The R.R. was observed to increase with an increasing number of zone passes at a given zone speed, and in general to decrease with an increasing zone speed for a given number of passes. The maximum R.R. achieved was a weak function of the purity of the starting material but the results indicate that decarburised crystals of optimum purity could be obtained by making 4-7 zone passes at 6-8 mm./min.

5.3 Vacuum Quenched Crystals

An increase in the residual resistivity of $3\text{-}5 \times 10^{-10}$ ohm cm. occurred when decarburised and deoxidised crystals were quenched from vacua of $\leqslant 10^{-5}$ torr. in which water vapour was the major component. Transmission electron microscopic examination of the vacuum quenched specimens showed essentially particle free material and no large increase in dislocation density over that in the furnace cooled, H.V.A. material. This indicated that the quenched-in resistivity was not due to quenching strains. Isochronal annealing of several vacuum quenched specimens gave a single recovery stage at $\sim 800^{\circ}C$ with no detectable reduction in the resistivity below $400^{\circ}C$ (see Fig.A17). This recovery behaviour is very similar to that observed for molybdenum which has been doped with oxygen by quenching from an oxygen atmosphere where a single annealing peak occurs at $830^{\circ}C$ (Burck et al. 1969).

5.4 Nitrogen Doped Crystals

Table A8 gives the annealing conditions and quenched-in resistivities ($\Delta\rho_Q$) for the final nitrogen doping treatments where the mechanical test

Figure A14 Axial Variation in Resistance Ratio of a Decarburised Crystal

Zone passes 8
Zone speed 8 mm./min.
Batch C7424 material

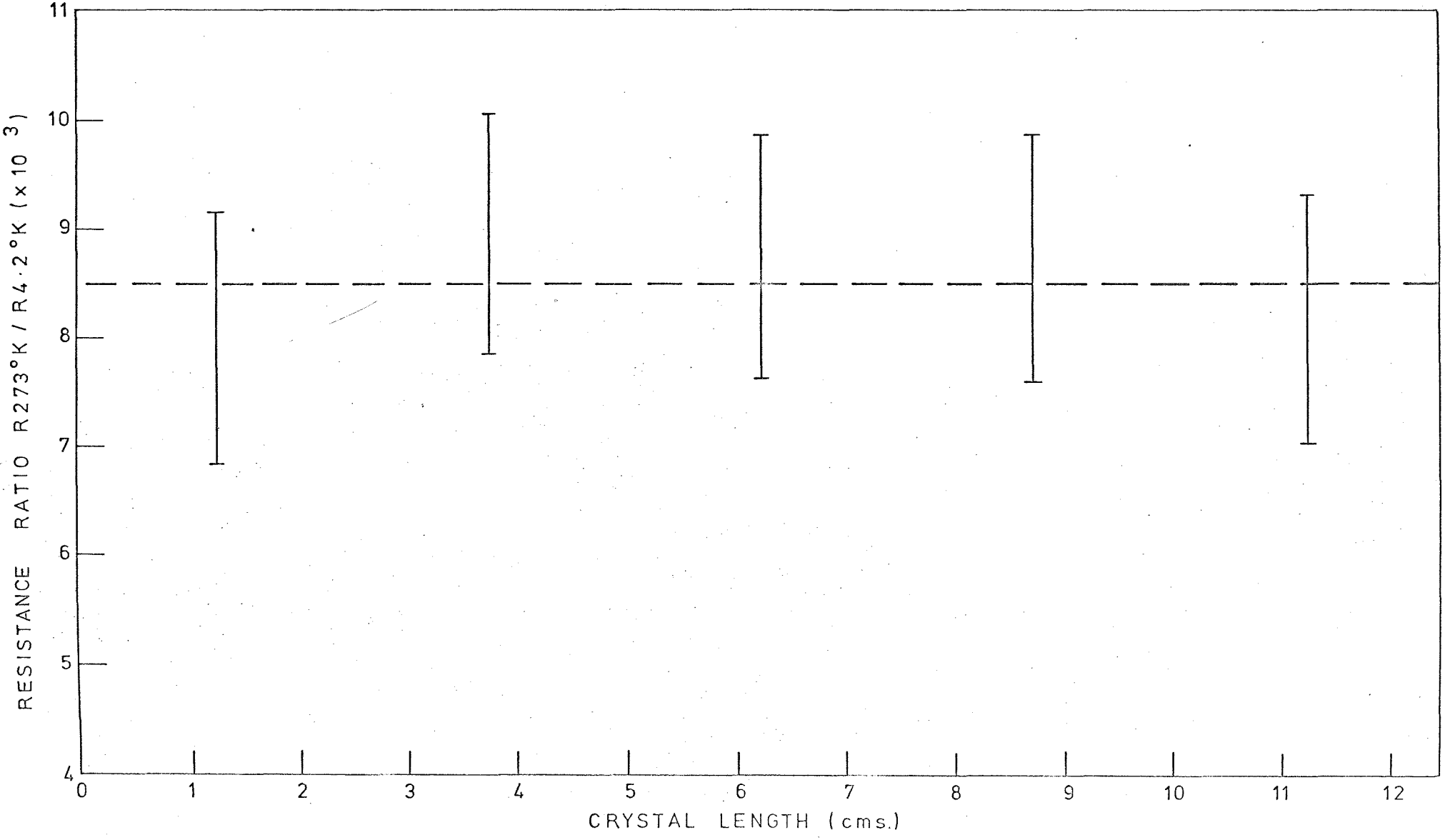

RESISTANCE RATIO R273°K / R4.2°K (x 10 3)
11
10
9
8
7
6
5
4
0
1
2
3
4
5
6
7
8
9
10
11
12
CRYSTAL LENGTH (cms.)

Figure A15 Variation in Resistance Ratio of Decarburised Crystals with Number of Zone Passes

Zone speed 8 mm./min.
Batch C7424 material

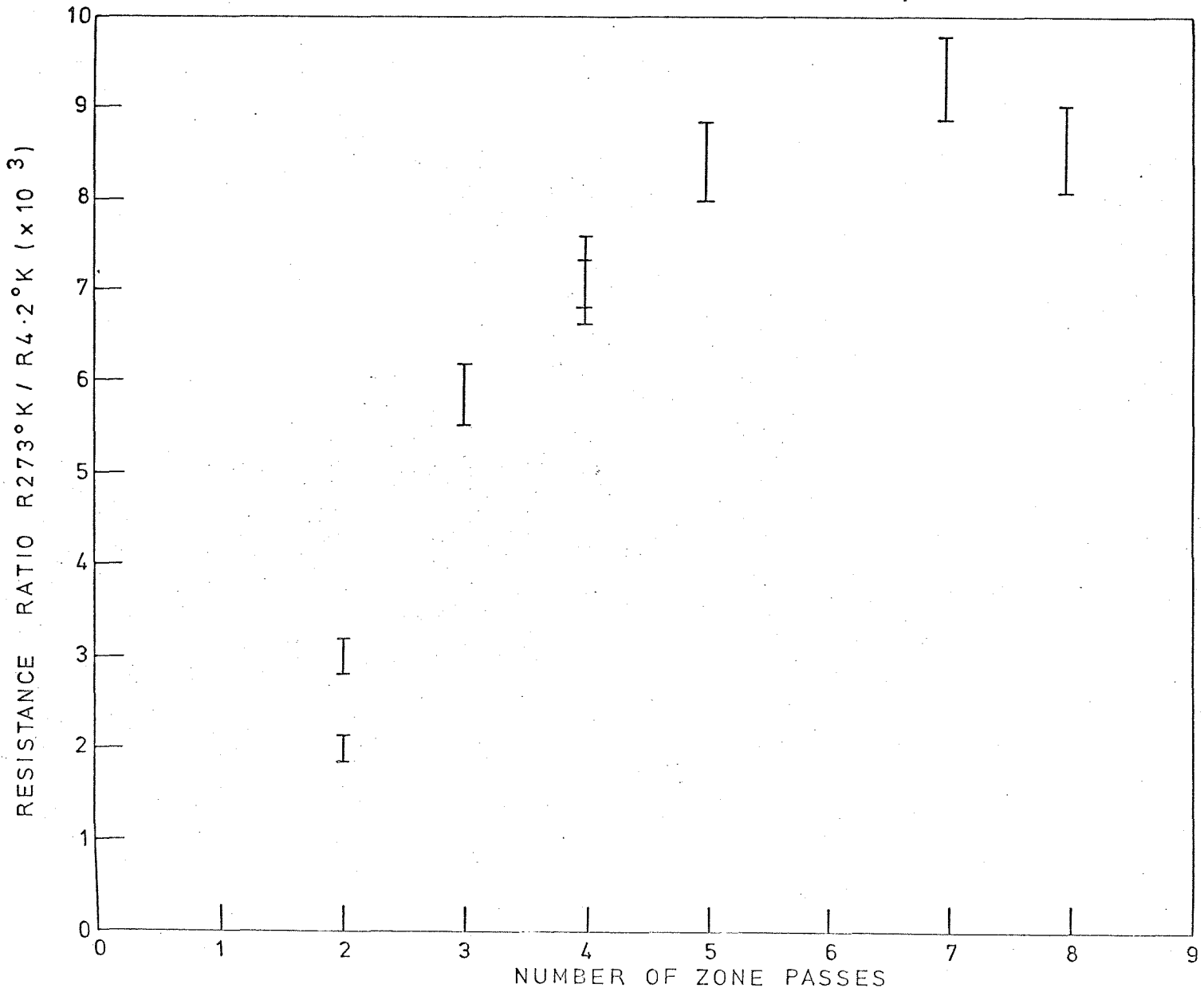

RESISTANCE RATIO R273°K / R4·2°K (x 10 3)
NUMBER OF ZONE PASSES
0
1
2
3
4
5
6
7
8
9
10

Figure A16 Variation in Resistance Ratio of Decarburised Crystals with Zone Speed

Zone passes 4
Batch C8076 material

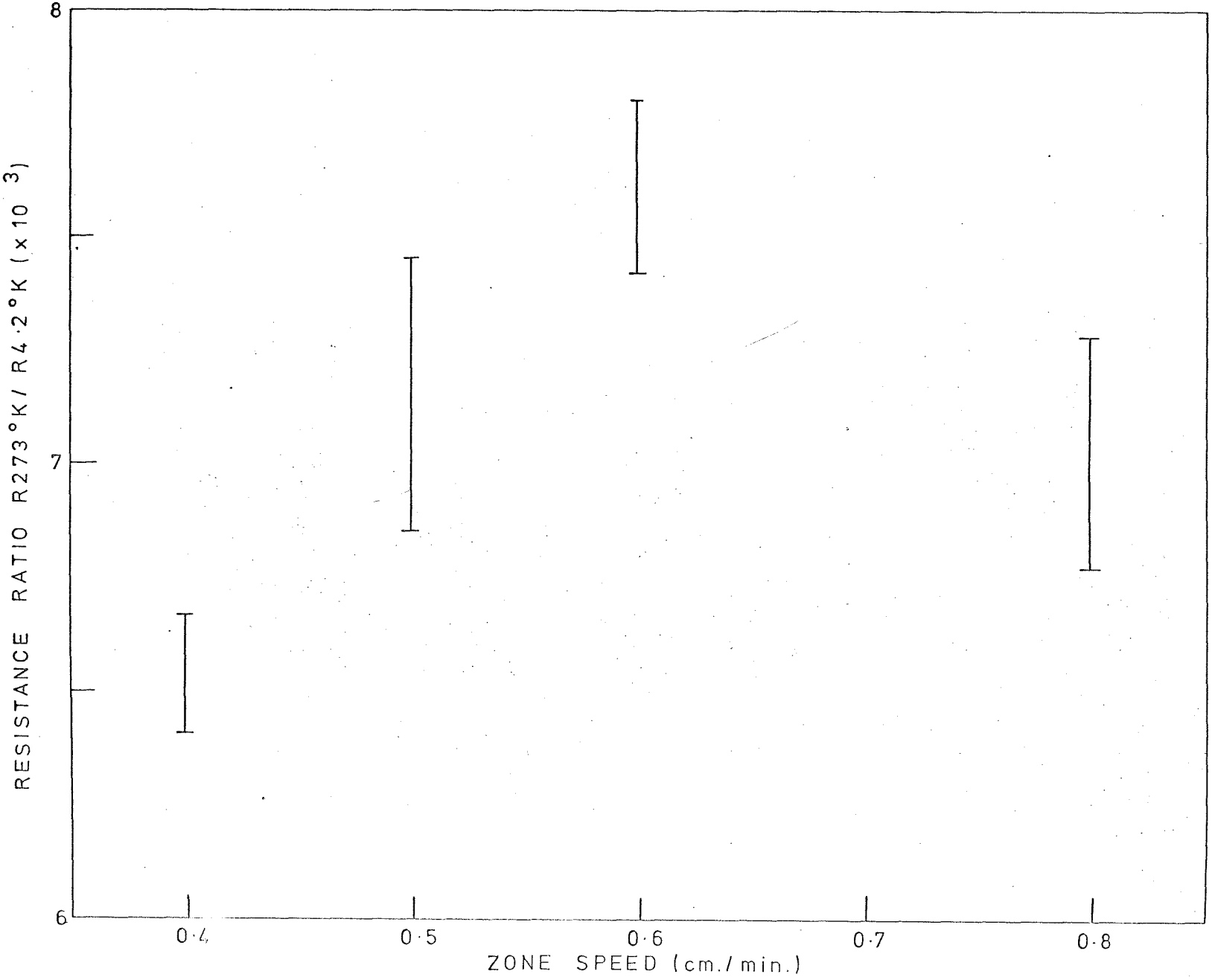
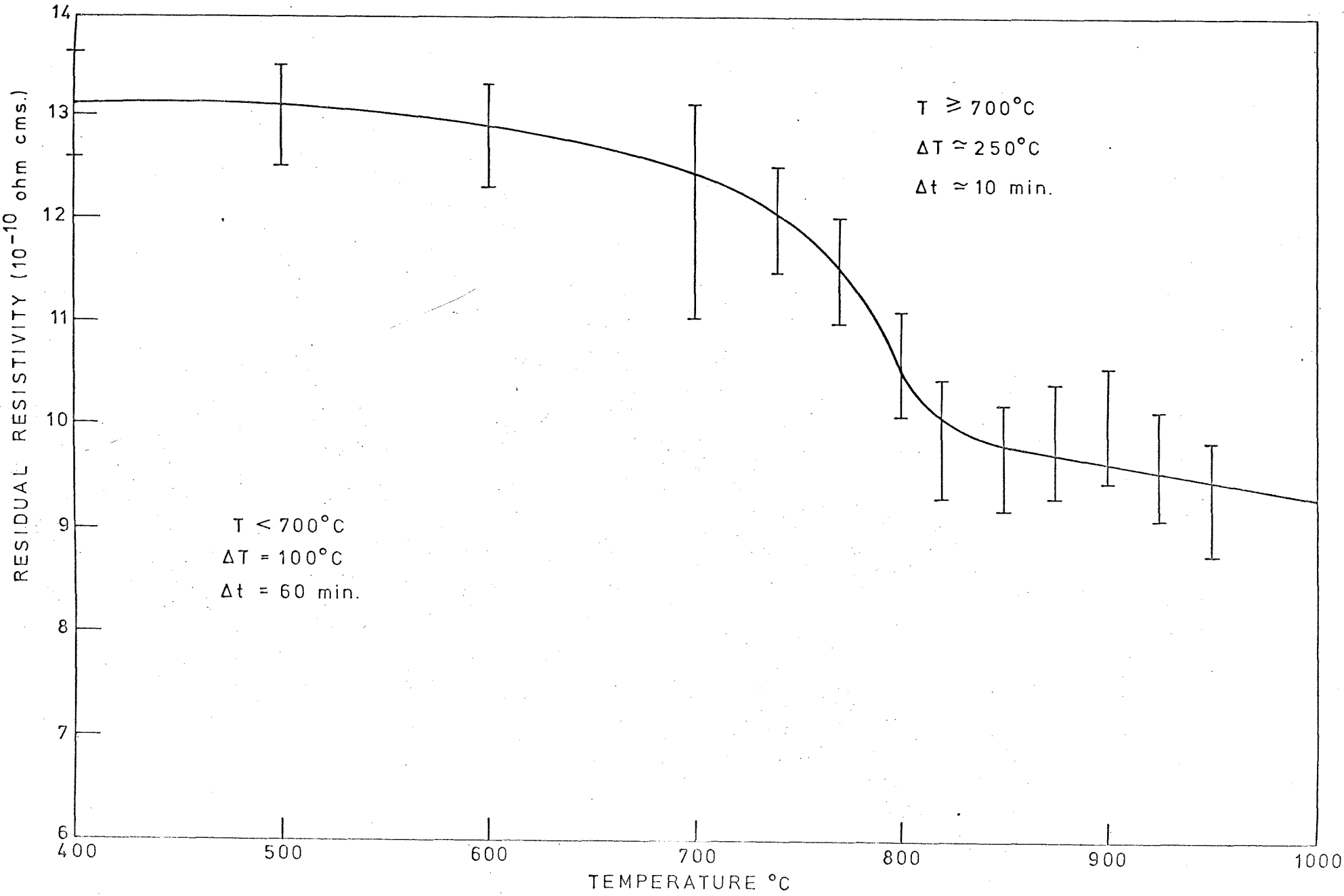

8
7
6
RESISTANCE RATIO R273°K / R4·2°K (x 10 3)
0·4
0·5
0·6
0·7
0·8
ZONE SPEED (cm./min.)

Figure A17 Isochronal Recovery Behaviour of a Vacuum Quenched Crystal
(Quenched-in Resistivity, $\Delta\rho_Q = 5 \times 10^{-10}$ ohm cm.)


RESIDUAL RESISTIVITY (10^{-10} ohm cms.)
14
13
12
11
10
9
8
7
6
400
500
600
700
800
900
1000
TEMPERATURE °C
T ≥ 700°C
ΔT ≃ 250°C
Δt ≃ 10 min.
T < 700°C
ΔT = 100°C
Δt = 60 min.

TREATMENT	TEMPERATURE (°C)	PRESSURE (torr.)	TIME (mins.)	SPECIMEN DIAMETER (mm.)	$\Delta\rho_Q$ (10^{-10} ohm cm.)
ND21	1800	6×10^{-2}	150 (50)	0.5 2.5	30.0 ± 0.5 27.8 ± 1.5 [10.6]
ND23	1785	6×10^{-2}	100 (55)	1.0 2.5 2.5	27.4 ± 1.2 24.2 ± 1.2 25.0 ± 3.8 [10.3]
ND24	1900	200	60 (10)	0.25* 1.1 1.1 1.1	776.0 ± 1.7 746.0 ± 1.0 763.1 ± 3.5 756.5 ± 1.2 [751]
ND25	1900	30	65 (10)	1.1 1.1 1.1 1.1 1.1 1.1 1.1	328.0 ± 2.5 328.2 ± 2.5 331.0 ± 1.2 343.0 ± 3.5 331.3 ± 1.3 350.1 ± 2.2 349.8 ± 1.3 [291]
ND26	1900	30	60 (10)	1.1 1.1 1.1	326.2 ± 1.3 326.4 ± 1.3 321.1 ± 1.3 [291]
ND27	1900	~1	180 (10)	1.1 1.1 1.1	115.9 ± 2.4 118.1 ± 2.4 121.2 ± 1.3 [53]

() Time to establish uniform concentration, calculated using nitrogen diffusivity data of Evans and Eyre (1969).

[] Quenched-in resistivities estimated from results of Evans and Eyre (1969).

* Polycrystalline foil

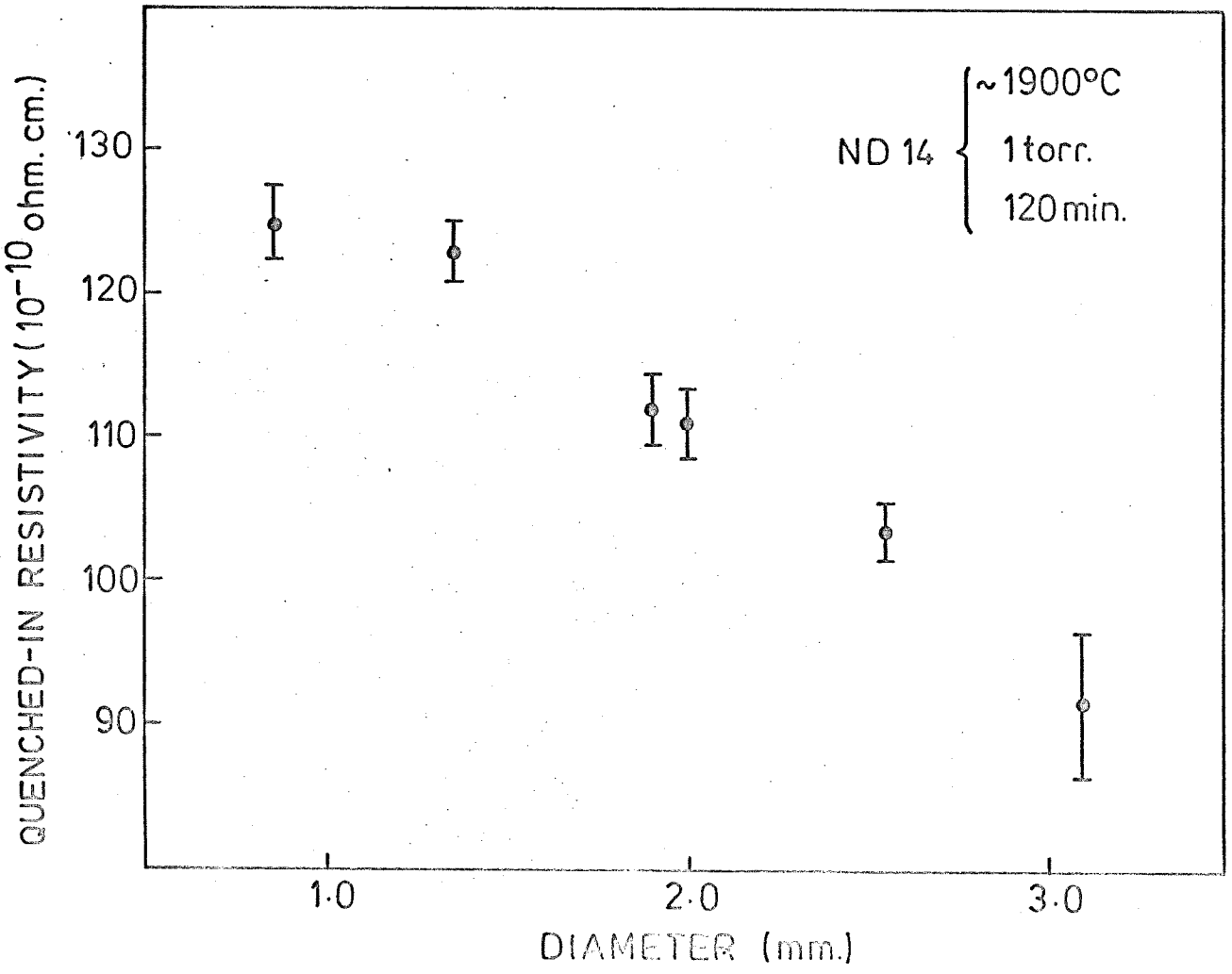
Table A8 Treatment Conditions and Quenched-in Resistivities ($\Delta\rho_Q$) for Nitrogen Doped Mechanical Test Specimens

specimens were prepared. The calculated annealing times required to establish a uniform concentration of nitrogen in the largest specimens doped in each treatment, are also given in Table A8. These assume the nitrogen ingassing reaction is solid diffusion controlled. Evans and Eyre's (1969) nitrogen diffusivity values were employed since these were obtained in the same type of experimental system and are lower than other workers values (see Fig.A5). It is evident that the actual treatment times employed were sufficient to establish a uniform equilibrium concentration of nitrogen in the specimens.

The mechanical test specimens were doped with a range of nitrogen concentrations up to the maximum level which could be retained in solution. There was more than an order of magnitude difference between the maximum concentrations which could be retained in solution in the compression and tension specimens. This indicates a strong dependence of the quench rate on the specimen thickness.

In treatment ND21 and 23 the 2.5 mm. diameter compression specimens were doped with the maximum nitrogen concentrations which could be secured in solution. Assuming Nordheim's rule is obeyed ($\Delta\rho_Q \propto C$) and the specific residual resistivity of nitrogen (ρ_N) is 2.4×10^{-10} ohm cm/at.ppm. (Evans and Eyre 1969), the $\Delta\rho_Q$ obtained in these treatments corresponds to a concentration of ~10 at.ppm. At higher concentrations $\Delta\rho_Q$ in the thin control specimens was significantly greater than that in the compression size specimens. For example, Fig.A18 shows the variation in $\Delta\rho_Q$ with diameter for a batch of specimens doped with ~50 at.ppm. nitrogen (assuming $\rho_N = 2.4 \times 10^{-10}$ ohm cm/at.ppm.). The comparatively small $\Delta\rho_Q$ for the specimens with diameters >1 mm. implied that autoageing was occurring during the quench. This was confirmed by transmission electron microscopic (T.E.M.) examination of the centre of discs cut from the cross-section of the 2.55 and 3.1 mm. diameter specimens. Small precipitates were visible on dislocations which were acting as preferential sites for nucleation. No precipitation or

Figure A18 Quenched-in Resistivity versus Diameter for Specimens Doped with ~50 at.ppm. Nitrogen


QUENCHED-IN RESISTIVITY (10^{-10} ohm. cm.)
130
120
110
100
90
1·0
2·0
3·0
DIAMETER (mm.)
ND 14
~1900°C
1 torr.
120 min.

decoration of dislocations was apparent in T.E.M. discs cut from the 2.5 mm. diameter compression specimens doped in treatments ND21 and 23.

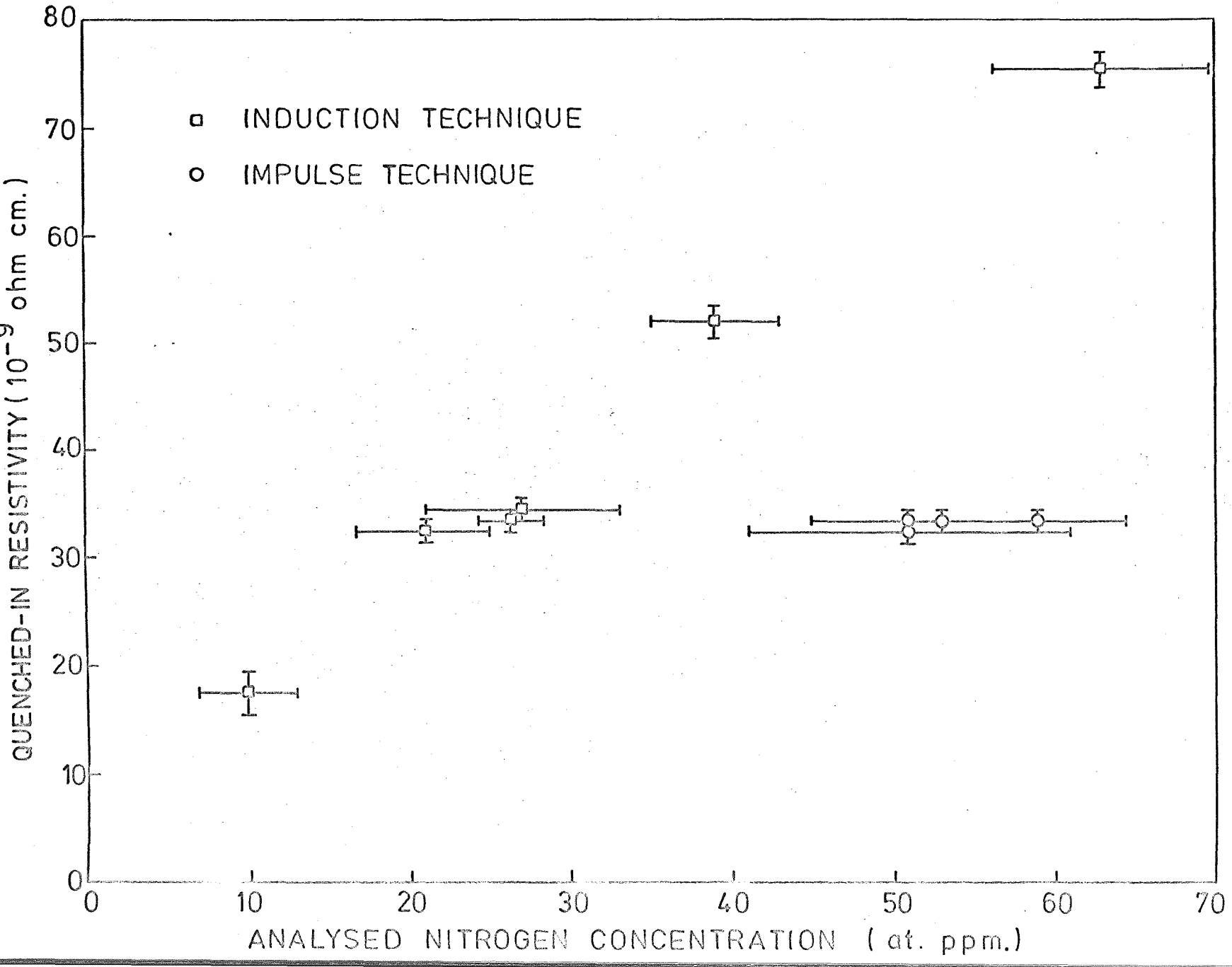
A maximum concentration of ~300 at.ppm. nitrogen (assuming $\rho_N = 2.4 \times 10^{-10}$ ohm cm/at.ppm.) was quenched into solution in the tension specimens doped in treatment ND24. This indicates a very high quench rate ($10^4 - 10^5$ °C/sec.) comparable to those attained for molybdenum in similar quenching apparatus (Evans and Eyre 1968a).

At high pressures the $\Delta\rho_Q$, obtained for those specimens where the quench rate was sufficient to retain the nitrogen in solution, were in good agreement with those determined by Evans and Eyre (1969). However, an extrapolation of the latter's data to lower pressures (<20 torr.), assuming Sievert's law is obeyed ($C \propto p^{\frac{1}{2}}$), gives much lower $\Delta\rho_Q$ values than observed in this investigation (see treatments ND21, 23 and 27 in Table A8). This discrepancy may be in part a consequence of the pressure measurement errors in the range 0.5-1.0 torr. where neither the anaerobic nor the Pirani gauge are reliable. But, a 500% error which would be necessary to give the observed deviation from Sievert's law is unlikely.

Gamma activation analysis was conducted on several thin resistivity specimens where the nitrogen was known to be in solution. This was one of the first attempts made to analyse nitrogen in molybdenum by this method. Both induction and impulse heating techniques were employed in these analyses to confirm that the N^{13} was being recovered from the sample with 100% efficiency. The results are presented in Fig.A19 where they are plotted against the quenched-in resistivities.

The impulse technique gave results consistently higher than those obtained by the induction technique. Since there is no possibility of contamination of the sample with N^{13} occurring during the heating, this implies that the N^{13} was being recovered with less than 100% efficiency during the induction heating. It also necessarily casts doubt on the recovery efficiency for the impulse technique.

Figure A19 Analysed Concentration versus Quenched-in Resistivity for Nitrogen Doped Crystals


INDUCTION TECHNIQUE
IMPULSE TECHNIQUE
QUENCHED-IN RESISTIVITY (10^{-9} ohm cm.)
ANALYSED NITROGEN CONCENTRATION (at. ppm.)
0
10
20
30
40
50
60
70
80

5.5 Oxygen Doped Crystals

The results of some of the initial, exploratory quenches made from oxygen atmospheres are given in Table A9. The treatment conditions and $\Delta\rho_Q$ for the actual mechanical test specimens are given in Table A10.

In thin specimens where the quench rate was established to be sufficient to retain the oxygen in solution, $\Delta\rho_Q$ increased rapidly as the oxygen annealing pressure was increased. There was also a general trend of an increasing $\Delta\rho_Q$ with increasing temperature; but at high temperatures $\Delta\rho_Q$ showed a comparatively weak temperature dependence. The absolute magnitudes of the $\Delta\rho_Q$'s observed in these quenches were in good agreement with the results of the only previously reported oxygen quenching experiment conducted by Burck et al. (1969) (see Table A9).

Oxygen concentrations, corresponding to $\Delta\rho_Q$ of $\sim 50 \times 10^{-10}$ ohm cm., were quenched into solution in 1 mm. diameter tension specimens. However, the quench rate of the 2.5 mm. diameter compression specimens was only sufficient to retain much lower oxygen concentrations, corresponding to $\Delta\rho_Q$ of $\sim 10 \times 10^{-10}$ ohm cm., in solid solution. At oxygen concentrations corresponding to $\Delta\rho_Q > 20 \times 10^{-10}$ ohm cm. (see treatments OD6-11 in Table A9), $\Delta\rho_Q$ showed a strong dependence on specimen diameter. This strongly suggested that autoageing was occurring during the quenching of the larger diameter specimens. T.E.M. examination of the largest diameter specimens doped in treatments OD9 and 10 provided direct confirmation of this. Distinctive, lamellae-like precipitates almost exclusively associated with dislocations were seen.

The absence of any kinetic data for the molybdenum-oxygen gas reaction meant that there was some doubt about the uniformity of the oxygen concentration in some of the specimens. Although the high temperature diffusivity of oxygen in molybdenum has not been determined, there is good evidence that oxygen diffuses more rapidly than carbon (Scrivastava and

TREATMENT	TEMPERATURE (°C)	PRESSURE (torr.)	TIME (mins.)	SPECIMEN DIAMETER (mm.)	$\Delta\rho_Q$ (10^{-10} ohm cm.)
OD3	~1500	4×10^{-3}	65 (~900)	0.85 ~3.0	8.4 ± 1.0 7.4 ± 1.0
OD4	1450-1500	4×10^{-3}	120-180 (1200)	0.85 ~3.0	5.8 ± 1.0 4.8 ± 1.0
OD6	1770-1800	10^{-3}	60 (190)	0.80 2.0 ~3.0	46.6 ± 1.1 24.6 ± 1.4 19.9 ± 1.0
OD8	1725-1750	10^{-3}	90-120 (240)	0.75 2.5 ~3.0	39.4 ± 1.1 19.4 ± 1.3 16.8 ± 0.9
OD9	1695-1725	10^{-3}	360 (280)	0.75 2.0 ~3.0	25.1 ± 0.7 13.4 ± 1.7 10.5 ± 1.0
OD10	~1760	10^{-3}	185 (~190)	0.75 2.0 ~2.9	62.5 ± 1.3 24.9 ± 1.7 20.0 ± 0.4
OD11	1850-1900	3.5×10^{-5}	205 (90)	1.0 2.5 2.5	21.7 ± 0.7 13.5 ± 2.0 15.9 ± 2.6
OD12	~1810	10^{-4}	60 (~20)	0.7 1.0 1.1 1.1	25.7 ± 0.2 24.3 ± 0.3 24.6 ± 0.3 22.7 ± 0.5
*	2350	9×10^{-4}	-	0.5	45-55

() Time to establish uniform concentration assuming oxygen diffusivity = carbon diffusivity (Rudman 1967)

* Quenched-in resistivity obtained by (Burck et al. 1969)

Table A9 Treatment Conditions and Quenched-in Resistivities ($\Delta\rho_Q$) for Initial Oxygen Doping Anneals

TREATMENT	TEMPERATURE (°C)	PRESSURE (torr.)	TIME (mins.)	SPECIMEN DIAMETER (mm.)	$\Delta\rho_Q$ (10^{-10} ohm cm.)
OD14	~1830	1.5×10^{-5}	200 (~100)	1.0 2.5 2.5	14.6 ± 3.1 10.0 ± 1.3 11.8 ± 2.2
OD15	~1810	$\sim10^{-3}$	60 (~20)	0.7 1.1	43.9 ± 0.2 39.6 ± 0.2
OD16	1900-2000	$\sim10^{-3}$	65 (15)	0.7 1.1 1.1 1.1 1.1 1.1	53.4 ± 0.2 49.5 ± 0.4 44.1 ± 0.4 46.8 ± 0.5 50.0 ± 0.5 46.5 ± 0.2

Table A10 Treatment Conditions and Quenched-in Resistivities ($\Delta\rho_Q$) for Oxygen Doped Mechanical Test Specimens

Seigle 1974). The ingassing times necessary to establish uniform steady state concentrations in the specimens have been calculated assuming solid diffusion control and using Rudman's (1967) carbon diffusivity values. These are given in Tables A9 and A10 and show that in treatments OD3-8 inadequate annealing times may have been partly responsible for the smaller $\Delta\rho_Q$ in the large diameter specimens. In the remaining doping treatments (OD9-16) the annealing times may be more confidentally concluded to have been sufficient to fully ingas all the specimens.

At the low temperatures and high oxygen pressures employed in treatments OD3 and 4 in particular, the terminal and equilibrium solid solubility data for oxygen in molybdenum (see Figs.A2 and A3) indicate the possibility of oxide precipitation occurring during the annealing treatments prior to quenching. Consequently, in the final doping treatments for the mechanical test specimens, higher annealing temperatures were employed. No precipitates were found in T.E.M. specimens cut from the 2.5 mm. diameter

compression specimens doped in treatment OD14. However, no T.E.M. examination was undertaken on the tension specimens doped in the other treatments. In treatment OD16 the oxidation rate, associated with the high temperatures and pressures, was the maximum which could be tolerated (~100μ/hour). So, it was not possible to increase the temperature or pressure to ascertain if higher oxygen concentrations than those obtained in this treatment could be quenched into solution.

Gamma activation analysis was conducted on both thin wire and disc specimens where it had been established that the oxygen was in solid solution. The results are shown in Fig.A20 where they are plotted against the quenched-in resistivities. The analysed oxygen concentration showed an approximately linear dependence on resistivity. A least squares fit has been made to estimate a value for the specific residual resistivity of oxygen (ρ_o) of $0.5 \pm 0.1 \times 10^{-10}$ ohm cm/at.ppm. The error is two standard deviations (i.e. 95% confidence limits). This value of ρ_o is significantly smaller than the ρ_i values generally observed for interstitial elements in the refractory metals (see Table A1).

5.6 Lattice Parameter Measurements

The lattice parameters of several H.V.A., nitrogen and oxygen doped single crystal, disc specimens were measured using a high precision X-ray diffraction technique (Baker et al. 1968). The results of the measurements, are presented in Fig.A21 where a number of previously determined values obtained on pure molybdenum are also given. Both Evans' (1967) values obtained on a zone-melted and decarburised molybdenum single crystal and the most reliable values quoted by Smith (1960) are in excellent agreement with the parameter determined here for H.V.A. molybdenum. Nitrogen and oxygen doping caused the expected increase in lattice parameter but in neither case did this increase show a linear dependence on concentration. The magnitude

Figure A20 Analysed Concentration versus Quenched-in Resistivity for Oxygen Doped Crystals

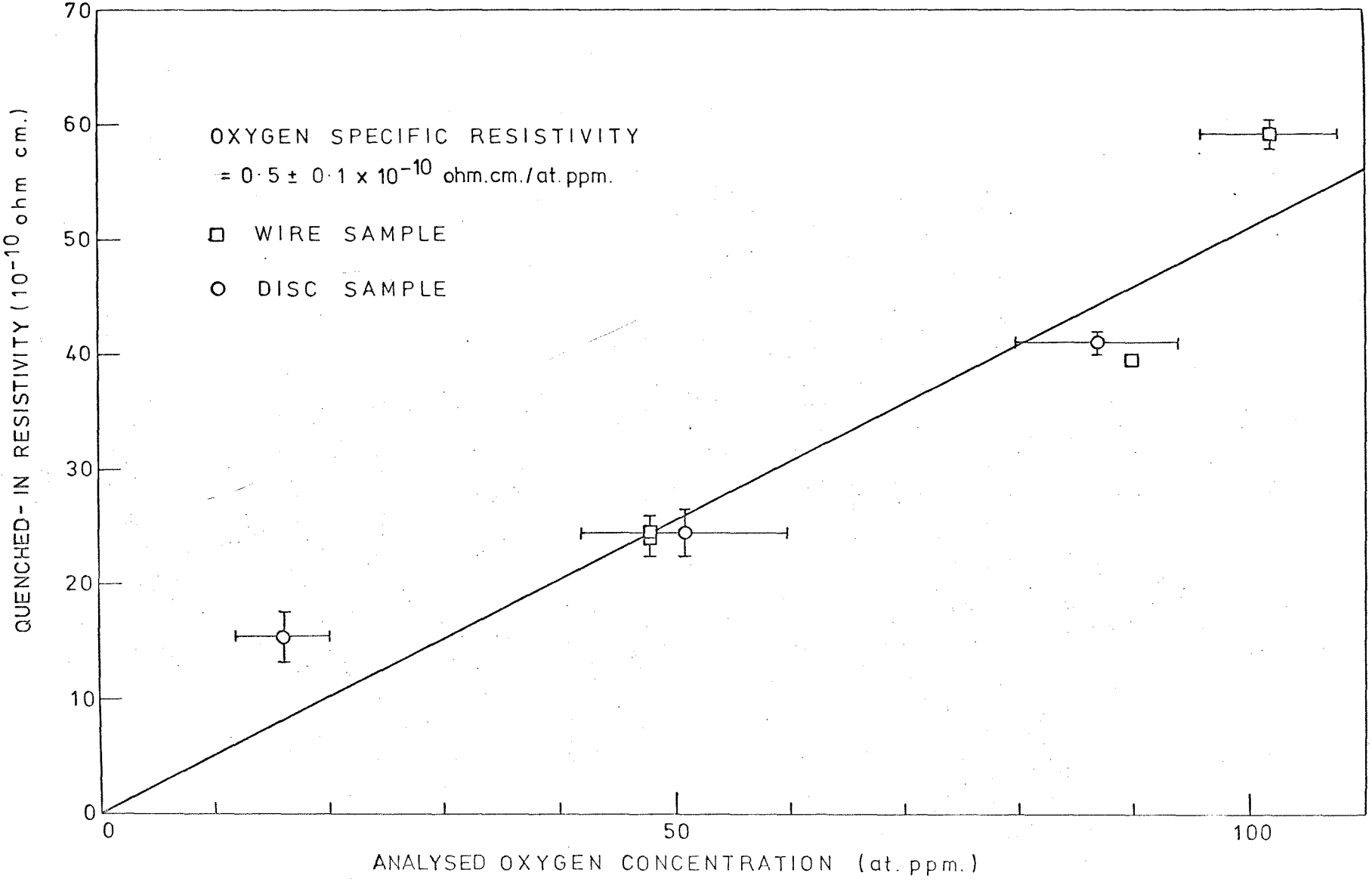
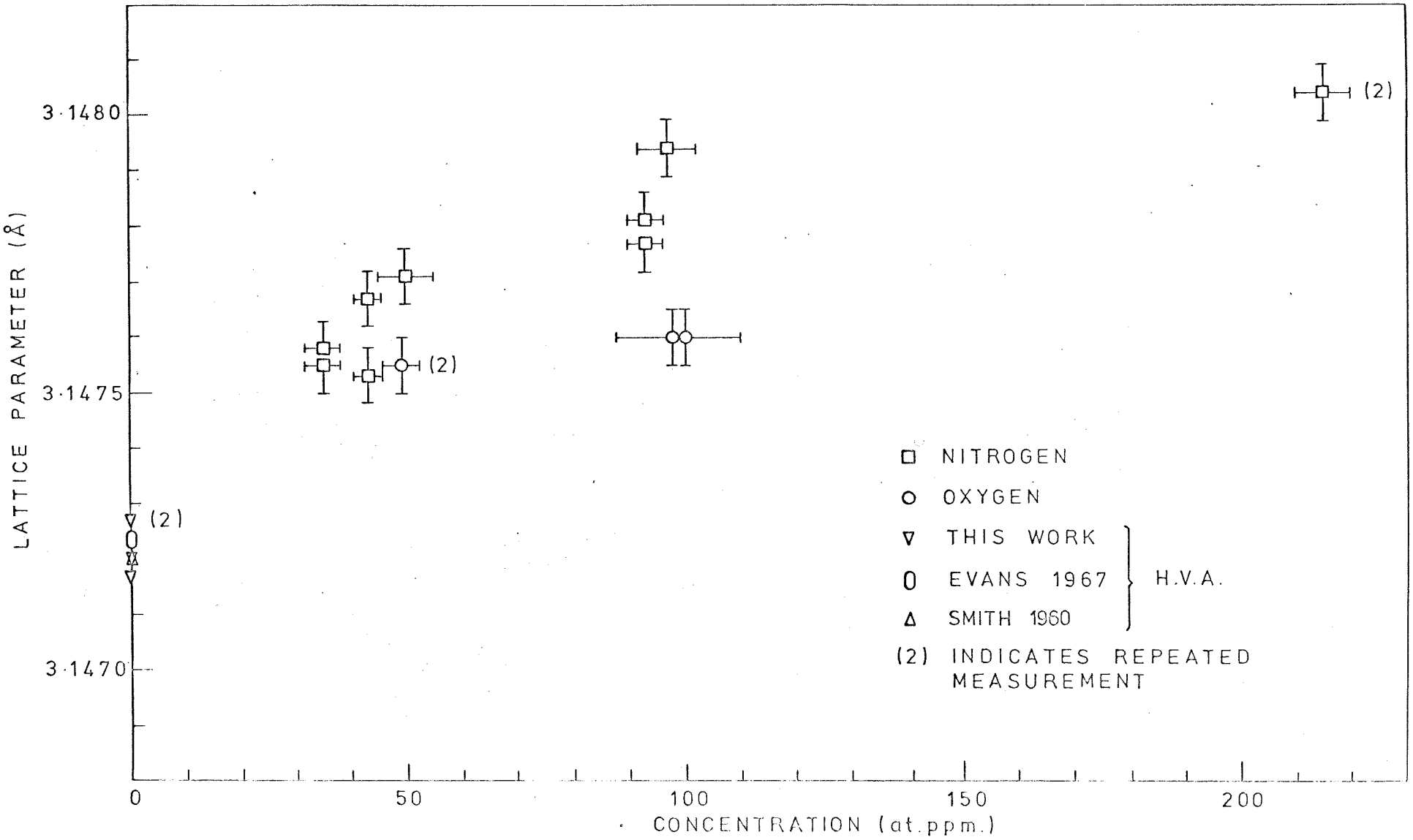

OXYGEN SPECIFIC RESISTIVITY
= 0·5 ± 0·1 x 10⁻¹⁰ ohm.cm./at.ppm.
WIRE SAMPLE
DISC SAMPLE
QUENCHED-IN RESISTIVITY (10⁻¹⁰ ohm cm.)
ANALYSED OXYGEN CONCENTRATION (at.ppm.)
0
10
20
30
40
50
60
70
0
50
100

Figure A21 Lattice Parameter versus Concentration for Nitrogen and Oxygen Doped Crystals

Using (400) reflection, copper K_α radiation ($\lambda = 1.54050\text{Å}$)


3·1480
3·1475
3·1470
LATTICE PARAMETER (Å)
(2)
(2)
(2)
0
50
100
150
200
CONCENTRATION (at.ppm.)
NITROGEN
OXYGEN
THIS WORK
EVANS 1967
SMITH 1960
H.V.A.
(2) INDICATES REPEATED MEASUREMENT

of the change was also anomalous, being more than a factor of ten greater than that generally observed in refractory metal-interstitial alloys.

The errors indicated in Fig.A21 for the lattice parameter ($\pm$ 5 x 10^{-5} Å) were due to variations across the specimen diameter. Some broadening of the Bragg peak occurred on doping which was probably due to a change in the crystallite size or to the formation of randomly distributed interstitial clusters. At large concentrations (~100 at.ppm.) nitrogen appeared to cause a larger increase in the parameter than did oxygen but, given the scatter of the data, this difference may not be significant.

Chapter 6

DISCUSSION

6.1 The Preparation and Characterisation of High Purity Molybdenum

The general increase in the R.R. of the molybdenum crystals as the number of zone passes was increased and the zone speed was reduced is consistent with the progressive removal of impurities by outgassing and volatilisation. Most of the substitutional impurities (see Tables A5 and A6) have higher vapour pressures than molybdenum and so will be lost by evaporation during zone-melting. Of the elements having a lower vapour pressure (e.g. niobium, osmium, rhenium, tungsten and carbon) most are present at low concentration levels in the starting material. The two notable exceptions are tungsten and carbon. The activation analysis results for tungsten indicate that zone-melting does not cause any significant change in the concentration or distribution of tungsten. This is consistent with the unfavourable equilibrium distribution coefficient of tungsten in molybdenum for zone-refining (Barthel and Eichler 1967). The ultimate deterioration in the R.R. after a large number of zone passes (see Fig.A15) or at the lowest zone speeds (see Fig.A16) is possibly due to recontamination of the crystals by the residual atmosphere in the zone-melting furnace.

The positive carbon gradient, in conjunction with the negative R.R. gradient, from the bottom to the top of the A.Z.M. crystals (see Fig.A12) shows that carbon is being redistributed along the length of the molybdenum crystals during the zone-melting operation. The removal of the R.R. gradient by the decarburisation treatments implies that the gradient can be attributed

solely to the axial variation in the carbon concentration. It follows, therefore, that carbon is the only element undergoing a significant redistribution by a zone-refining mechanism. Additional confirmation that zone-refining does operate to segregate the carbon is provided by the analysis results which give carbon levels at the tops of the crystals which are often higher than that of the starting material. These results also suggest that carbon removal by oxidation is not occurring to any great extent during zone-melting.

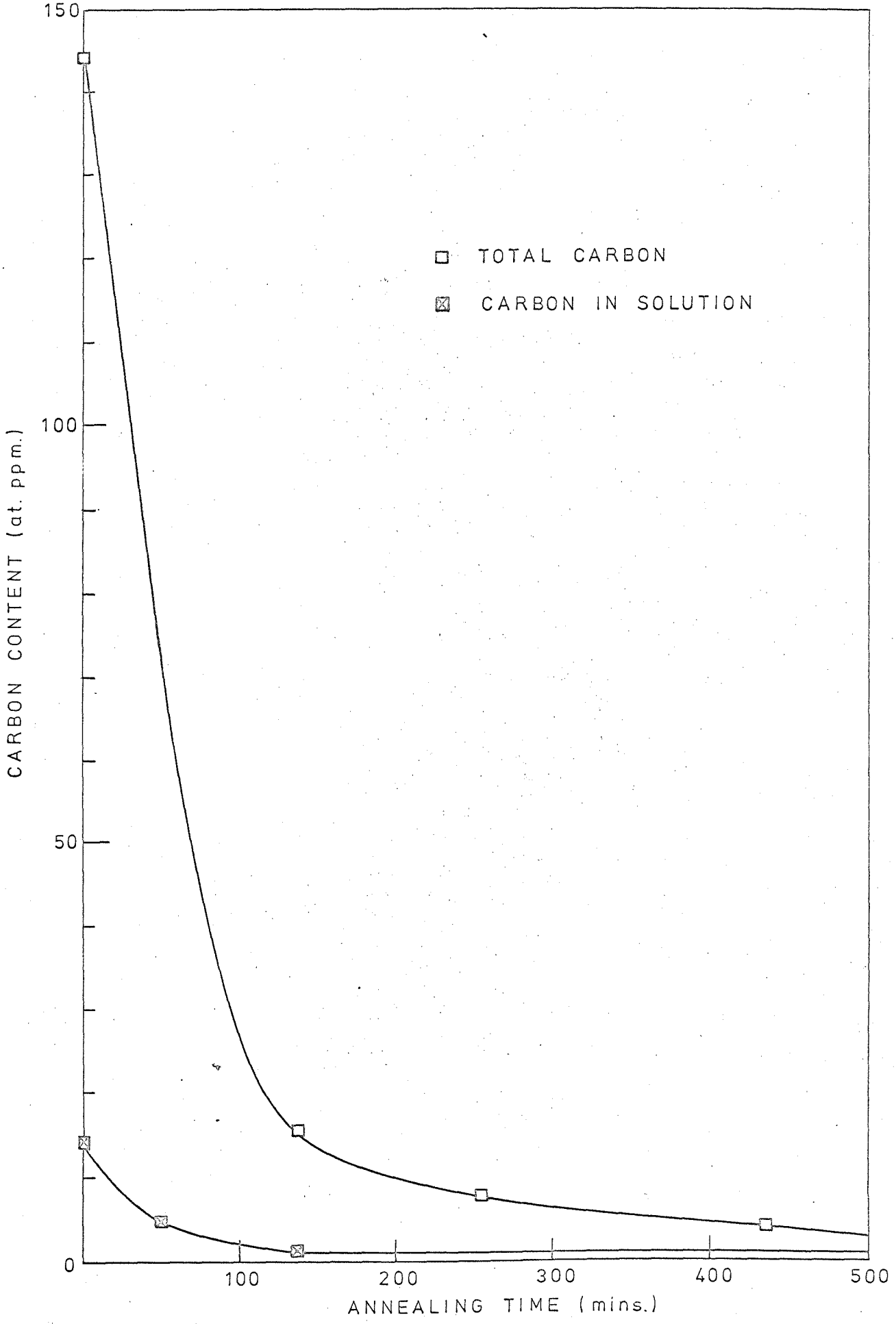
If the residual resistivities of the partially decarburised crystals are divided by the specific residual resistivity of carbon in molybdenum (assumed to be $\sim 3 \times 10^{-10}$ ohm cm/at.ppm. (Burck et al. 1969)), the concentration of carbon in solution can be compared with the total, analysed carbon concentration. A plot of the total carbon concentration and the carbon concentration in solution against decarburisation annealing times is given in Fig.A22. It can be seen that in the furnace cooled material most of the carbon is present in precipitate form, even at very low total carbon concentrations (<8 at.ppm.).

The maximum R.R. achieved in the furnace cooled, H.V.A. molybdenum crystals was ~10,000 which corresponds to a residual resistivity of $\sim 5 \times 10^{-10}$ ohm cm. The major contribution to the latter is made by the 48 ± 2 at.ppm. of tungsten present. Taking the specific residual resistivity of tungsten to be $7\text{-}8 \times 10^{-12}$ ohm cm/at.ppm. (see Table A1), the tungsten contributes $\sim 3\text{-}4 \times 10^{-10}$ ohm cm. to the total residual resistivity. The remaining $1\text{-}2 \times 10^{-10}$ ohm cm. is the combined contribution of the other substitutional impurities such as silicon and iron, which the analysis indicates are present at low concentrations, and interstitial impurities in solution (< 2 at.ppm.).

The equilibrium solubility data for nitrogen in molybdenum (see Fig.A3) implies that total nitrogen concentrations of <<1 at.ppm. are present after high vacuum annealing. The activation analysis results define a maximum carbon concentration of 4 at.ppm. in the H.V.A. crystals but, as discussed above, only a small proportion of the total carbon present is in solution in

Figure A22 Variation in Total Carbon Concentration and Carbon Concentration in Solution with Decarburisation Annealing Time

Zone passes 4
Zone speed 8 mm./min.
Batch C7424 material


150
100
50
0
CARBON CONTENT (at. ppm.)
TOTAL CARBON
CARBON IN SOLUTION
100
200
300
400
500
ANNEALING TIME (mins.)

the furnace cooled material. The additional 3-5 x 10^{-10} ohm cm. residual resistivity component in the high vacuum quenched crystals is probably associated with residual oxygen in equilibrium with the water vapour present in the annealing atmosphere. Any residual carbon quenched into solution would be expected to cluster and precipitate at temperatures well below the ~800°C ageing peak observed. Assuming an oxygen specific residual resistivity of 0.5 x 10^{-10} ohm cm. (see Section 5.5), the maximum quenched-in resistivity corresponds to ~10 at.ppm. total oxygen. This is in fair agreement with the maximum of 6 at.ppm. defined directly by activation analysis. As the terminal solubility data for oxygen (see Fig.A2) would predict, most of this oxygen must be precipitated in the furnace cooled H.V.A. crystals.

6.2 The Preparation and Characterisation of Nitrogen and Oxygen Doped Molybdenum

The quenched-in resistivities obtained in the nitrogen doping treatments are, in general, in agreement with those determined by Evans and Eyre (1969) in a more comprehensive series of quenching experiments. However, no quenches at pressures <30 torr. were undertaken in the latter investigation. So, although the $\Delta\rho_Q$'s obtained in the present investigation indicate a deviation from Sievert's law at pressures <20 torr., they do not directly contradict the $\Delta\rho_Q$ results obtained in the earlier investigation.

The pressure and temperature dependence of the quenched-in resistivities determined by Evans and Eyre (1969) are given below

$$\Delta\rho_Q = 3.84 \times 10^3 \, p^{\frac{1}{2}} \exp(-18400 \pm 200/RT)$$

where $\Delta\rho_Q$ (10^{-10} ohm cm.)

p (torr.)

R (cals/mole °K)

T (°K)

By assuming $\Delta\rho_Q = \rho_N \cdot C$, they were able to calibrate their results against the transient permeation data of Frauenfelder (1968) to obtain a specific residual resistivity for nitrogen (ρ_N) of 2.4×10^{-10} ohm cm/at.ppm. However, it has been shown that Frauenfelder's (1968) results, which were not obtained on high purity molybdenum, are erroneous (Weaver 1972). In Weaver's (1972) outgassing experiments, where decarburised, zone-melted molybdenum of comparable purity to that employed by Evans and Eyre (1969) was employed, the following expression for the equilibrium solubility of nitrogen was obtained.

$$C = 1.3 \times 10^{3}\, p^{\frac{1}{2}} \exp(-19100 \pm 520/RT)$$

where C (at.ppm.)

The heat of solution obtained is in excellent agreement with that of Evans and Eyre (1969). Thus, by evaluating a mean value of $\Delta\rho_Q/C$ in the common temperature range of the two sets of data (viz. 1400-1900°C), a more reliable value of $\rho_N = 3.5 \times 10^{-10}$ ohm cm/at.ppm. is obtained. This value has been used to calculate the nitrogen concentrations from the $\Delta\rho_Q$'s for all the nitrogen doped specimens prepared in this investigation.

The activation analysis results given in Fig.A19, which imply much larger ρ_N values (~6-12 $\times 10^{-10}$ ohm cm/at.ppm.), have not been used to calibrate the residual resistivities. The application of the gamma activation technique to nitrogen determinations is still in a developmental stage and its accuracy has not as yet been confirmed by results obtained on standard reference materials. Furthermore, the poor agreement between the impulse and induction results obtained in this investigation, indicates that neither set of results may be considered reliable.

The accuracy of oxygen analysis results obtained using the gamma activation technique has been confirmed by the analysis of analytic standards.

Also the technique has been routinely applied at Harwell to oxygen determinations specifically in molybdenum. So the results presented in Fig.A20 and the oxygen specific residual resistivity (ρ_O = 0.5 x 10^{-10} ohm cm/at.ppm.) calculated from them are considered to be of good reliability. The oxygen concentrations of all the oxygen doped molybdenum specimens have been calculated from the quenched-in resistivities using this value of ρ_O.

A comparison of ρ_O with other values of the specific residual resistivity (ρ_i) of interstitials in molybdenum and other refractory metals (see Table A1), shows the former to be at least a factor of five smaller. In fact, several substitutional solutes have ρ_i's which are larger than ρ_O. This anomalously low value of ρ_O indicates that the electronic interaction of oxygen with the molybdenum lattice is much weaker than that for most interstitials with refractory metals. It also suggests that the interaction may be in some ways analagous to that of substitutional solutes.

The $\Delta\rho_Q$'s for the thin specimens doped in treatments OD9-16 (see Tables A9 and A10), where the oxygen is believed to be in uniform solid solution, may be converted to oxygen concentrations using ρ_O = 0.5 x 10^{-10} ohm cm/at.ppm. This permits a comparison of these quenched-in oxygen concentrations with the equilibrium solubilities calculated by Scrivastava and Seigle (1974) (see Table A2 and Fig.A3). The oxygen concentrations quenched into solution in the oxygen doping treatments are consistently lower than the calculated equilibrium solubilities. This is consistent with the thermodynamic equilibrium concentrations defining an upper limit for the kinetic steady state concentrations, which are established during oxygen anneals at these temperatures and pressures (Hörz 1972). The steady state concentrations estimated from the $\Delta\rho_Q$'s are, however, less than an order of magnitude smaller than the equilibrium concentrations. This behaviour is very different to that of Group Va metals where the steady state concentrations of oxygen are several orders of magnitude less than the equilibrium concentrations.

The approximate maximum concentrations of nitrogen and oxygen which

could be quenched into solution in the mechanical test specimens are summarised in Table A11. These concentrations have been calculated from the $\Delta\rho_Q$'s using

	NITROGEN	OXYGEN
TENSION (1 mm. diameter)	~200 (~5%)	≳100 (~10%)
COMPRESSION (2.5 mm. diameter)	~10 (~10%)	~20 (~25%)

Table A11 Maximum Interstitial Concentrations Quenched into Solution in Mechanical Test Specimens (at.ppm.)

$\rho_N = 3.5 \times 10^{-10}$ ohm cm/at.ppm. and $\rho_O = 0.5 \times 10^{-10}$ ohm cm/at.ppm. The percentages given in brackets indicate the approximate differences between the concentrations quenched into the thin control, wire or foil specimens and the respective tension and compression specimens. The magnitude of this difference gives some relative measure of the probability of interstitial atoms not being retained in solution.

It is apparent that the certainty that all the interstitial atoms were retained in solution in the tension specimens is greater than that for the compression specimens. Likewise, the certainty that all the nitrogen atoms were retained in solution in the tension and compression specimens is greater than that for the oxygen atoms in the respective test specimens. The latter observation is consistent with the limited thermodynamic and kinetic data for oxygen and the concomitant uncertainty as to the form and distribution of the oxygen in the test specimens.

The order of magnitude difference between the interstitial concentrations which could be quenched into solution in the compression and tension specimens implies a strong dependence of the quench rate on the specimen diameter.

Since the primary purpose of the doping experiments was to ascertain what concentrations of nitrogen and oxygen could be retained in solution in these different diameter specimens, it is important to rationalise this implied variation in quench rate.

The magnitude of the interstitial concentration which could be quenched into solution in the 1 mm. diameter tension specimens is in good agreement with the results of previous quenching experiments (Burck et al. 1969, Evans and Eyre 1969). For example, Evans and Eyre (1969) were able to quench 300 at.ppm. nitrogen (NB. all nitrogen concentrations subsequently quoted assume $\rho_N = 3.5 \times 10^{-10}$ ohm cm/at.ppm.) into 0.75 mm. diameter wires using a mercury quench bath. Quench rates of $10^4 - 10^5$ ^oC/sec. have been measured for specimens of these thicknesses quenched into similar liquid metal baths (Köthe 1972, Hall 1974).

Hall (1974) has also determined that, for specimens thicknesses $\lesssim$0.2 mm., heat transfer in the quench is largely surface controlled. With increasing thickness there is a shift in control to heat conduction in the solid, where $Q \propto 1/d^2$ (Q - quench rate, d - specimen diameter). Thus, to a good approximation an increase in specimen diameter from 1 mm. to 3 mm. would correspond to an order of magnitude reduction in the quench rate from say, 10^4 ^oC/sec. to 10^3 ^oC/sec. Flinn (1962) has developed an expression for the number of atom jumps (N) during a quench from a quenching temperature (T) at a quench rate (Q).

$$N = \frac{D_o R T^2}{a^2 E_m Q} \cdot \exp\left(\frac{-E_m}{RT}\right)$$

where D_o is the pre-exponential diffusion factor

E_m is the activation energy for diffusion

a is the lattice parameter

Now, the mean number of jumps ($\bar{N}$) for the first clustering of interstitial atoms may be related to the concentration by the expression (Damask and Dienes, 1963)

$$\bar{N} = 1/bC$$

where C is the atom fraction of interstitial solute

b ~1 for interstitials in a b.c.c. metal

Thus, equating N and $\bar{N}$ gives

$$C = \frac{a^2 E_m Q}{D_o R T^2} \cdot \exp\left(\frac{E_m}{RT}\right)$$

$\propto$ Q for a given metal, interstitial species and quenching temperature.

C is now the concentration at which the first clustering of atoms occurs. This may be approximately equated with the maximum concentration which can be quenched into solution. So, the order of magnitude reduction in the quench rate which occurs on increasing the specimen diameter from 1 mm. to 3 mm. would be predicted to produce an order of magnitude reduction in the maximum concentration quenched into solution.

Both nitrogen and oxygen doping caused an increase in the lattice parameter of molybdenum. This would be predicted for solute atoms which occupy interstitial sites and is invariably observed for interstitial solutes in b.c.c. metals. There were, however, two unexpected features of the lattice parameter results shown in Fig.A21. Firstly, the lattice parameter change did not show the approximate linear dependence on solute concentration which is frequently observed in both interstitial and substitutional alloys. Instead, the specific lattice parameter change $(\Delta a/a_o \text{ (at.ppm.)})^{-1}$, where a_o = lattice parameter of the pure metal) decreased as the interstitial

concentration increased. Secondly, at low concentrations $\Delta a/a_o$ was an order of magnitude greater than those $\Delta a/a_o$ values previously determined for refractory metal-interstitial alloys. Only at high concentrations (>50-100 at.ppm.) did the $\Delta a/a_o$ values determined here approach those of other interstitial alloys. Both these phenomena appear to be closely related to the clustering of interstitial atoms which has been shown to occur in the supersaturated molybdenum-interstitial alloys.

The reduction in $\Delta a/a_o$ as the interstitial content of the molybdenum was increased indicates that the mean dilatation of the lattice, caused by the introduction of an interstitial atom, is smaller at high concentrations than at low concentrations. This behaviour may be explained by an increasing tendency for atoms to cluster as the concentration of the alloy and therefore, the degree of supersaturation is increased.

There is strong evidence to suggest that the binding energy of clustered interstitial atoms is of an elastic and not of a chemical nature (Fast 1971). So, the clustering of atoms may then be considered a consequence of the mutual relaxation of their elastic strain fields. This implies that clustering reduces the mean dilatation of the lattice and hence reduces $\Delta a/a_o$. It also explains the comparative insensitivity of the specific residual resistivity (ρ_i) to clustering, which is indicated by the linear dependence of the residual resistivity on interstitial concentration. Since ρ_i appears to reflect the electronic rather than elastic interaction of solute atoms and the metal lattice (Schultz 1968), the largely elastic interactions associated with clustering, would not be expected to change ρ_i greatly.

Evans et al. (1970) have obtained evidence from the isochronal recovery and stress relaxation behaviour of molybdenum-nitrogen alloys which indicates that small clusters of nitrogen atoms occur in the as quenched material. The concentration dependence of the temperature and the magnitude of the isochronal resistivity recovery peaks, which were correlated with different size atom clusters, also showed that the degree of clustering increased as the

concentration of the alloys increased.

A similar trend would be expected in the as quenched molybdenum-nitrogen alloys prepared in the present investigation. Also some post quench clustering, which probably occurred in the highest nitrogen concentration (~200 at.ppm.) molybdenum specimens, would have accentuated this trend. As described in Section 4.7, all specimens were heated to 120-140°C immediately after the quench. In alloys with nitrogen concentrations >100 at.ppm. some recovery of the resistivity occurs at these temperatures (Evans et al. 1970). This has been ascribed to the clustering of the single nitrogen atoms, which are present in the as quenched alloys, to form precipitate nuclei. Although much larger than the atom clusters present in the as quenched alloys, these nuclei do not become visible as precipitates ($\gtrsim$15 Å) until aged at much higher temperatures ($\gtrsim$300°C) (Eyre and Evans 1972).

The very high temperature (830°C) of the initial resistivity recovery stage for molybdenum-oxygen alloys (Burck et al. 1969), means that no post quench ageing of the oxygen doped specimens could have occurred. However, Ma and Son (1964), in an internal friction study of quenched molybdenum-oxygen alloys, have shown that an increasing proportion of oxygen is present in the form of di-oxygen clusters, as the concentration of the alloys increases. This investigation was conducted using low base purity material and comparatively large oxygen concentrations (~600 at.ppm.). But there is no reason to conclude that the oxygen quenched into supersaturated solid solution in the present investigation should not show a similar clustering trend.

No reliable theoretical prediction of the magnitude of the elastic relaxation associated with the clustering of the interstitial atoms in molybdenum is possible. The strong concentration dependence of $\Delta a/a_o$ is, however, in qualitative agreement with the concentration dependence of the clustering behaviour in the molybdenum-nitrogen and the molybdenum-oxygen alloys.

The magnitude of the $\Delta a/a_o$ values determined in this investigation and

those found in several other investigations of refractory metal-interstitial alloys are presented in Table A12. Because the lattice parameter did not show a linear dependence on concentration, a range of values have been given for nitrogen and oxygen in molybdenum. The $\Delta a/a_o$ values observed at large concentrations of nitrogen and oxygen approach those for the other interstitial alloys but this comparison is complicated by the clustering which occurs in the molybdenum-nitrogen and molybdenum-oxygen alloys. The $\Delta a/a_o$ at low concentrations (0-50 at.ppm.), which may be argued to reflect the lattice dilatation due to single nitrogen and oxygen atoms in molybdenum, is an order of magnitude larger than the $\Delta a/a_o$'s for other interstitial alloys. This indicates a much stronger elastic interaction of nitrogen and oxygen with molybdenum than is generally observed for other metals.

In Fig.A23 the results, obtained by Speiser et al. (1952), in the only previously reported investigation of the lattice parameter change in a Group VIa metal-interstitial alloy, are compared with the present results. A comparison is not possible over a common concentration range, but the large discrepancy between the two sets of results cannot be explained by a concentration dependence of the specific lattice parameter change. Although Speiser et al.'s (1952) $\Delta a/a_o$ value is in good agreement with the $\Delta a/a_o$'s for the Group Va metals (see Table A12), it is considered to be unreliable. Commercial purity molybdenum, likely to contain interacting interstitial and substitutional impurities, was employed in their investigation. This may explain the anomalous a_o value obtained by an extrapolation of their data to zero carbon concentration. This value (3.1466 Å) is significantly smaller than the most reliable values quoted by Smith (1960) and that determined here for high purity molybdenum (3.1472 Å). It is also unlikely that the quench rates achieved were sufficient to retain the comparatively large concentrations of carbon in solution. Much of the carbon would have been precipitated or in a highly clustered form. This would explain the small effect of carbon on the lattice parameter in comparison with that observed for nitrogen and oxygen in

	NITROGEN	OXYGEN	CARBON
Mo	3-35 (1)	3-25 (1)	2.3 (2)
Nb	2.5 (5) 1.3 (6)	1.2 (3) 0.8 (4)	0.6* (7)
Ta	1.5 (9) 1.4 (8) 1.8 (10)	1.4 (8)	8.8* (8)
*Very approximate			

Table A12 Specific Lattice Parameter Changes for Interstitials in Refractory Metals 10^{-7}/at.ppm.

(1) This work

(2) Speiser et al. (1952)

(3) Taylor and Doyle (1967a)

(4) Seybolt (1954)

(5) Taylor and Doyle (1967b)

(6) Dürrschnabel and Hörz (1963)

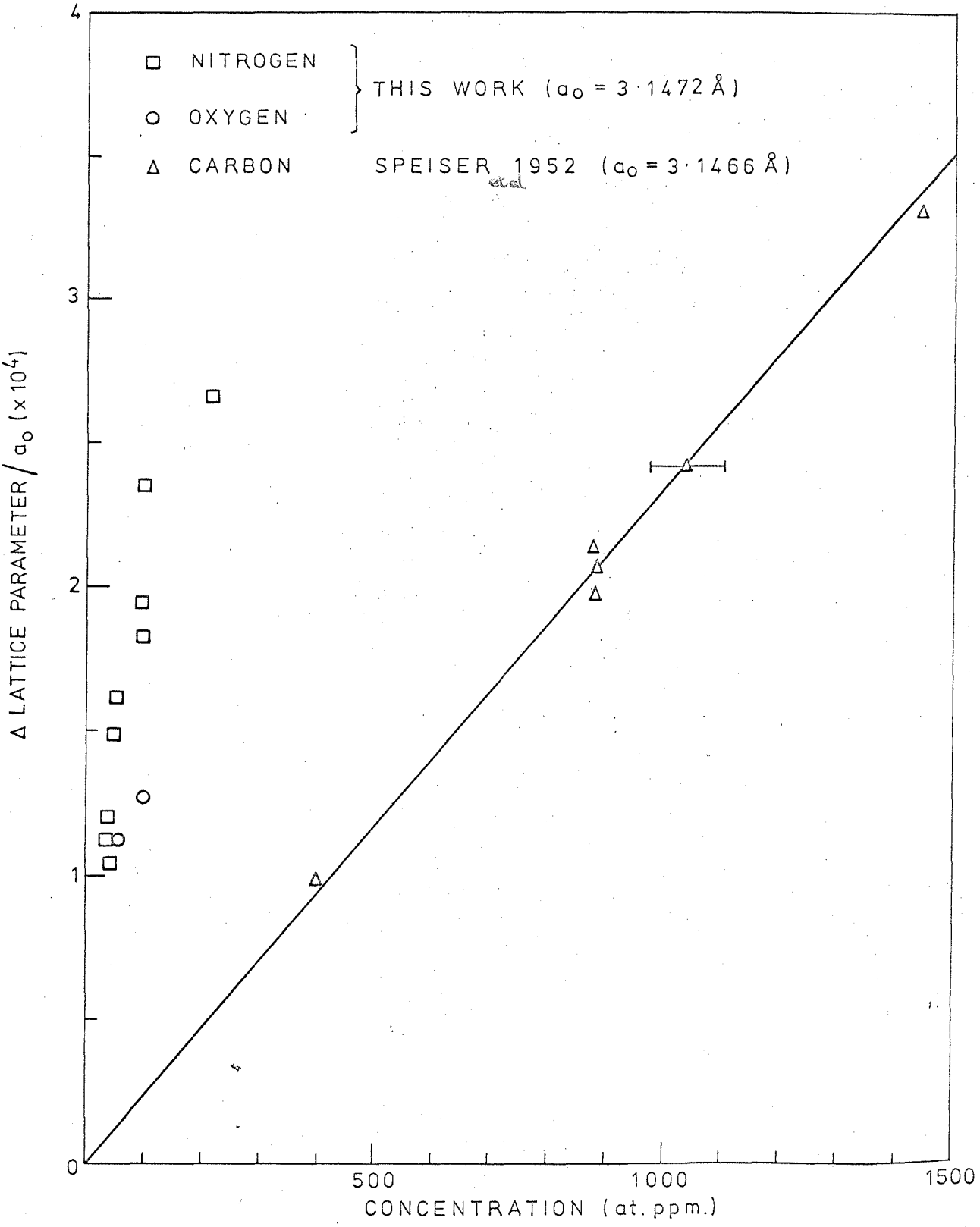
(7) Taylor and Doyle (1967c)

(8) Vaughan et al. (1961)

(9) Trenzinger et al. (1974)

(10) Gebhardt et al. (1958)

Figure A23 Comparison of Lattice Parameter Change for Nitrogen, Oxygen and Carbon in Molybdenum


NITROGEN
OXYGEN
CARBON
THIS WORK (a_o = 3·1472 Å)
SPEISER et al 1952 (a_o = 3·1466 Å)
Δ LATTICE PARAMETER / a_o (x 10^4)
CONCENTRATION (at. ppm.)
0
1
2
3
4
500
1000
1500

the present study.

The difference between the $\Delta a/a_o$ values for nitrogen and oxygen doped molybdenum and those for interstitially doped Group Va metals is more significant. There is a substantial number of self-consistent results, many of which were obtained using high purity metals (e.g. Trenzinger et al. 1974), which indicate both the magnitude and the linear concentration dependence of the lattice parameter, determined for the Group Va metals, are reliable. All these results were obtained for alloys with interstitial concentrations >2000 at.ppm. The large interstitial solubilities in Group Va metals means there is little possibility of precipitation occurring until much larger concentrations (>10,000 at.ppm.). Also the first di-interstitial clusters are only detected at concentrations of ~5,000 at.ppm. and the degree of clustering shows a comparatively weak concentration dependence. So, the order of magnitude difference between the molybdenum and the Group Va metal $\Delta a/a_o$ values signifies that the lattice dilatation caused by individual interstitial atoms in molybdenum (and probably in other Group VIa metals) is also an order of magnitude greater than that in Group Va metals. This contrasting behaviour is not unexpected in view of other dramatic differences in the physical and chemical properties of Group Va and VIa metals, e.g. the notably larger Young's moduli and the orders of magnitude smaller, interstitial terminal solubilities for Group VIa metals.

6.3 Summary

(i) An optimum preparation route has been established for the preparation of high purity molybdenum single crystals with resistance ratios >5,000 and a total interstitial content <10 at.ppm.

(ii) A zone-refining mechanism operates to segregate carbon during the zone-melting operation but other impurities are removed by outgassing and volatilisation. The degree of purification is ultimately

limited by the concentration of low vapour pressure impurities (principally tungsten) in the starting material and the concentration of gaseous impurities (principally oxygen) in equilibrium with the residual vacuum.

(iii) In view of the low terminal solid solubilities of interstitials in molybdenum, the resistance ratio of furnace cooled material may not fully reflect the total levels of these impurities. The resistance ratio of vacuum quenched material where the residual interstitials are in solid solution is a more significant index of material purity.

(iv) A high speed quenching technique has been developed for the doping of molybdenum mechanical test specimens with nitrogen and oxygen. Compression specimens may be prepared with only small concentrations of interstitials (~10 at.ppm.) in solid solution. Comparatively large concentrations of interstitials (>100 at.ppm.) may be quenched into solution in tension specimens.

(v) The specific residual resistivity of oxygen in molybdenum is much lower than that generally observed for interstitial solutes in refractory metals. This indicates a weak electronic interaction of oxygen with molybdenum which may be analagous to that of substitutional solutes.

(vi) The lattice parameter changes caused by nitrogen and oxygen in molybdenum do not show a linear concentration dependence. The observed concentration dependence is in qualitative agreement with the clustering behaviour of interstitials in these super-saturated solid solutions.

(vii) The specific lattice parameter changes associated with unclustered nitrogen and oxygen atoms in molybdenum, are an order of magnitude greater than those observed for interstitial atoms in Group Va metals. No other reliable measurements have been reported for

Group VIa metals but this would suggest a much stronger elastic interaction of interstitial atoms with Group VIa metals than Group Va metals.

PART B

THE DEFORMATION BEHAVIOUR OF MOLYBDENUM-NITROGEN AND MOLYBDENUM-OXYGEN ALLOYS

		Page No.
Chapter 7	INTRODUCTION	72
Chapter 8	LITERATURE REVIEW	74
8.1	The Slip Geometry	74
8.2	The Theories of the Yield	79
8.3	The Orientation Dependence of the Yield and Flow Stress	83
8.4	The Temperature Dependence of the Yield and Flow Stress	88
8.4.1	Recent Experimental Evidence	89
8.4.2	Theories	91
Chapter 9	EXPERIMENTAL APPARATUS AND PROCEDURE	99
9.1	Seeding and Orientation Determination	99
9.2	Compression Testing Machine	100
9.3	Tension Testing Machine	103
9.4	Methods of Obtaining Test Temperatures	105
9.5	Preparation and Testing of Compression Specimens	106
9.6	Preparation and Testing of Tension Specimens	109
9.7	Processing of Mechanical Test Data	111
9.8	Differential Temperature Change Testing	113
9.9	Reproducibility of Mechanical Test Results	116
9.10	Slip Trace Analysis	117

	Page No.
Chapter 10 RESULTS	119
10.1 Introduction	119
10.2 Crystals Deformed in Compression	122
10.2.1 <149> and <113> Crystals	122
10.2.2 <122> Crystals	123
10.3 Crystals Deformed in Tension	124
10.3.1 Nitrogen Doped <149> Crystals	124
10.3.2 Oxygen Doped <149> Crystals	126
10.3.3 Doped <001>, <011> and <111> Crystals	127
10.4 Slip Geometry and Morphology	129
10.4.1 <149> Crystals Deformed at 290°K	129
10.4.2 <149> Crystals Deformed at 77°K	130
10.4.3 <122> Crystals Deformed at 77°K	131
Chapter 11 DISCUSSION	133
11.1 The General Effects of Interstitials on the Deformation Behaviour	133
11.2 The Temperature Dependence of the Yield and Flow Stress	137
11.3 The Concentration Dependence of the Yield and Flow Stress	142
11.4 The Orientation Dependence of the Deformation Behaviour	148
11.4.1 The Yield and Flow Behaviour	148
11.4.2 The Temperature Dependence of the Yield and Flow Stress	152
11.5 The Comparative Effects of Oxygen and Nitrogen	155
11.6 The Effects of Interstitials on the Slip Geometry	159
11.6.1 <149> Crystals	159
11.6.2 <122> Crystals	164
11.7 General Discussion	165
11.8 Summary	168

Chapter 7

INTRODUCTION

The complex behaviour of b.c.c. metals under stress makes it desirable, in an investigation of the deformation behaviour of interstitial alloys, to examine the influence of temperature, strain rate, orientation and deformation sense besides, of course, interstitial concentration. The results of the preparation and characterisation studies reported in PART A indicated some important limitations on the number and range of these variables which could be considered.

Only comparatively small concentrations of interstitials could be successfully quenched into solution in compression size specimens. This prevented any comprehensive testing program, involving alloys with a range of interstitial concentrations, being conducted in compression. To examine the deformation behaviour of alloys containing larger concentrations of interstitials it was necessary to resort to the testing of thin wires in tension. This allowed mechanical test data to be obtained on crystals with several different nitrogen concentrations. However, the greater vulnerability of the doped material to brittle fracture when tested in tension restricted the amount of flow data which could be obtained at the lowest test temperatures.

Most of the mechanical testing was conducted on molybdenum-nitrogen alloys which were the more thoroughly characterised and more readily prepared. The successful preparation of oxygen doped mechanical test specimens where the oxygen was believed to be in solid solution allowed a parallel, though less comprehensive, deformation study of molybdenum-oxygen alloys to be undertaken. The deformation behaviour of the molybdenum-oxygen single crystals

was of particular interest in view of some of their anomalous physical properties (e.g. the very low specific residual resistivity of oxygen reported in PART A). Other exceptional features of the behaviour of oxygen in molybdenum, such as its severe embrittling effect on polycrystalline material (Touboul et al. 1971) and its unusual stability in solid solution at high temperatures (Burck et al. 1969), also recommended such a study.

Chapter 8

LITERATURE REVIEW

8.1 The Slip Geometry

The slip direction in b.c.c. transition metals has been generally observed to be the <111> direction. Slip has been observed to occur on {110} and {112} planes which are regarded as probable atomic slip planes. The {123} and higher Miller indice irrational slip planes indicated in many investigations are believed to involve composite microscopic or atomic slip on the {110} and {112} planes. Both slip line analysis and transmission electron microscopy have been used in studies of the influence of the temperature, orientation, sense of the applied stress and alloying on the slip geometry and morphology of the Group Va metals, vanadium, niobium and tantalum and the Group VIa metals, molybdenum and tungsten. Each metal shows highly individualistic slip behaviour but some general features and trends are apparent. There is also increasing evidence that the Group Va and VIa metals show certain distinctive slip characteristics which justify the classification of their slip behaviour on a Group basis. However, no simple relationship between the stress or strain level and the slip geometry is apparent and it would seem the slip behaviour can be most successfully analysed in terms of the general form of the flow curve.

At room temperature the central triangle, easy glide orientation (oriented for slip on the $[111](\bar{1}01)$ system with respect to the [001] - [011] - $[\bar{1}11]$ reference triangle which will be employed here) displays a stress-strain curve with the same form as that associated with the three stage work hardening behaviour of f.c.c. metals but, with an additional stage 0 'microstrain'.

Deformation in the stage O region is not associated with a single slip system. Slip traces corresponding to many 'unexpected' systems with low Schmid factors are observed (e.g. Vesely 1968b, Luft and Kaun 1973). In addition, transmission electron microscopic observations indicate that all four Burger's vectors (b's) operate (e.g. Foxall et al. 1967, Vesely 1973a). The slip geometry is not very sensitive to either the sense of deformation or the orientation, although for some symmetry orientations, e.g. <001>, all slip systems have the same Schmid factors and no unexpected systems operate.

The stage O region in Group Va metals such as niobium is small, with slip commencing on the primary system after ~½% strain at room temperature. Group VIa metals such as molybdenum show a more extensive stage O of ~2-3% at room temperature. Furthermore, in contrast with the Group Va metals where the stage O region is reduced at lower temperatures, molybdenum must be strained 6-9% at 77°K before the onset of primary slip.

The most detailed studies of stage O slip behaviour have been made on molybdenum (Vesely 1968a,b, Richter 1971, Matsui et al. 1974, Jeffcoat 1975). Vesely (1968a,b), who investigated the slip behaviour of both thin foils and bulk specimens, observed that the operative slip systems were strongly influenced by the local orientation of the specimen surface. It was suggested that the low mobility of screw dislocations at the low stress levels of stage O inhibited the operation of bulk sources. This is in general accord with the stage O edge exhaustion hardening models (see Section 8.2) where screw dislocations are assumed to be immobile and thus no dislocation sources can operate during the microdeformation. Vesely (1968b), however, proposed that sources near the surface could operate and that their ease of operation was determined by the slip distance of their screw components to the surface. So, the slip system which would operate at any point on the specimen surface was predicted to be that for which the local b made the largest angle with the local surface normal and whose slip plane was most nearly perpendicular to the surface.

It is possible to represent these criteria on a stereogram as shown in Fig.B1 for a circular cross-section specimen with a central triangle orientation. The four closed curves ('Vesely' curves) corresponding to each of the four $\underline{b}$'s represent the traces of the planes which provide the minimum slip distance to the surface at any position around the specimen circumference. They may be defined as the locus of the direction of intersection of two planes A and B, where:

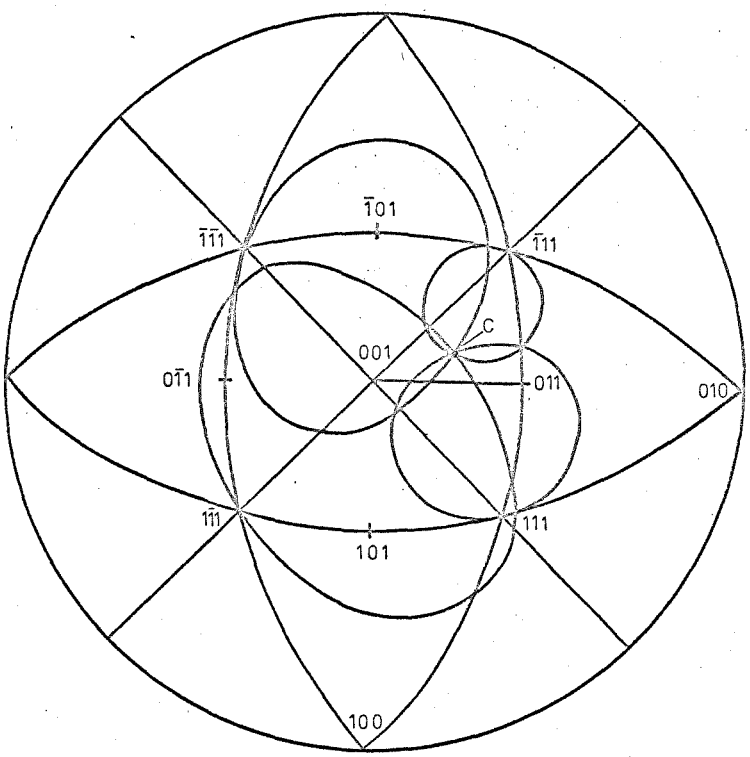
A is any plane tangential to the cylindrical surface of the specimen.

B is that plane which is perpendicular to the chosen tangential plane and which belongs to the zone of the $\underline{b}$.

The model was further refined to accommodate the tendency for slip to occur on $\{110\}$ crystallographic planes and the necessary influence of the Schmid factor in determining the activity of the predicted systems. The activity of a particular slip system is visualised to be partly a function of the surface effect, characterised by the orientation factor, $\sin\beta$ (β is the angle between the $\underline{b}$ and the local surface normal) and partly a function of the Schmid factor. The importance of the surface effect should diminish as the screw mobility increases. So, with increasing stress or temperature a deviation of the observed slip systems from those predicted by the surface orientation effect towards the maximum resolved shear stress plane would be expected. This is consistent with the observed onset of primary slip as the stress rises to the stage I level and the increased strain range over which the characteristic stage 0 slip geometry is observed as the temperature is decreased.

The surface effect model gives qualitative agreement with both Vesely's (1968a,b) observations and the more recent results of Jeffcoat (1975). But it is not fully consistent with the edge exhaustion theories of microstrain (see Section 8.2) which assume that only the motion of non-screw dislocation segments contributes to the deformation in the microstrain region. This may point to deficiencies in both the exhaustion hardening models and the surface

Figure B1 Standard [001] Stereogram Showing 'Vesely' (1968b) Curves for Central Triangle Orientation (C)


$\bar{1}01$
$\bar{1}\bar{1}1$
$\bar{1}11$
C
001
$0\bar{1}1$
011
010
$1\bar{1}1$
111
101
100

model.

There is little doubt that the surface plays a very important role during the initial stages of deformation of metals (Feng and Kramer 1965) including molybdenum (Kramer 1967, Thornley 1968). Also, the relative orientation of the $\underline{b}$ and surface has been shown to exert a strong effect not only on the slip geometry but also on the yield stress (Vesely 1972). It would appear that these two major tenets of the surface model are well founded. But it is very difficult to reconcile the operation of surface sources at small, temperature independent stresses with the large and temperature dependent stress rise to stage I which is attributed to the low mobility of screws. It is also doubtful if the surface slip behaviour is representative of the bulk deformation. Should slip on surface determined systems be propagated into the bulk, problems of geometrical compatability arise where the deformation in different regions of the specimen cross-section is occurring on different slip systems.

At the higher stress and strain levels associated with stage I, a single primary system tends to dominate the slip geometry. The dependence of the primary system on orientation is usually described by means of the $\psi(\chi)$ diagram (Taylor 1928). This method of representation is strictly valid only when the resolved shear stress on a slip system determines its activity. This is confirmed by the validity of the relation $\psi(\chi)_t = -\psi(-\chi)_c$ (t-tension, c-compression) which is obeyed for most metals including molybdenum as shown in Fig.B2. It is not obeyed for some iron-silicon and niobium-molybdenum alloys (Taylor et al. 1973a) which implies that the normal stress or some other factor influences the slip geometry. The $\psi(\chi)$ curves for molybdenum shown in Fig.B2 also indicate an asymmetry about the ψ-axis which is consistent with shear on $\{112\}$ planes being more difficult in the anti-twinning than in the twinning sense. The slip behaviour of most b.c.c. metals is consistent with such an asymmetry which becomes more pronounced as the temperature is decreased. More direct evidence supporting this interpretation has been

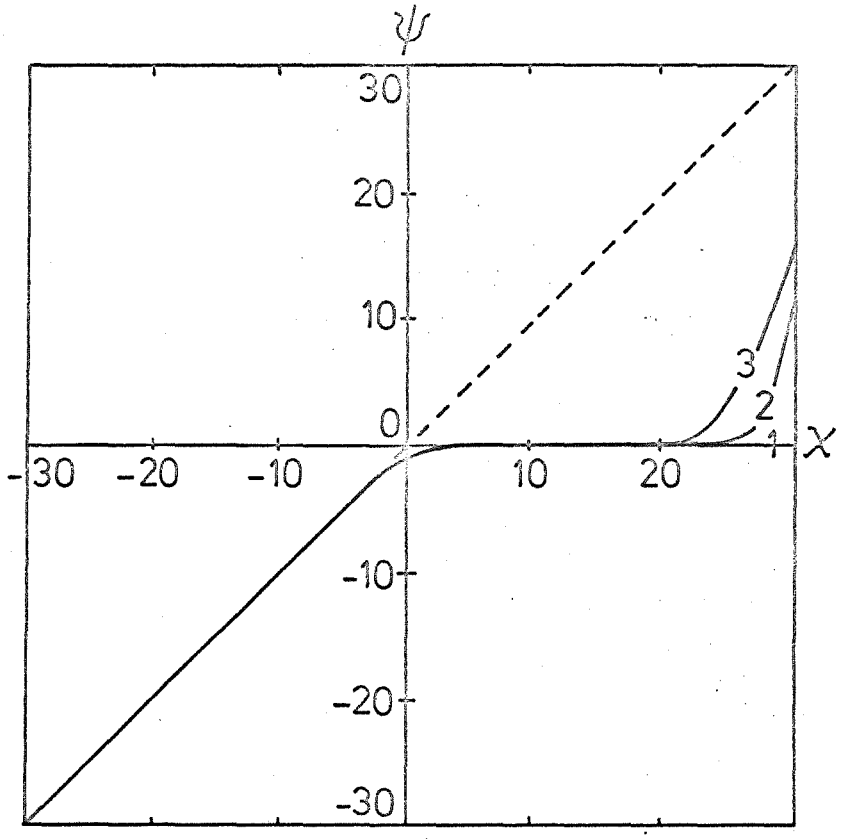
Figure B2 $\psi(\chi)$ Curves for Molybdenum in

(a) Tension

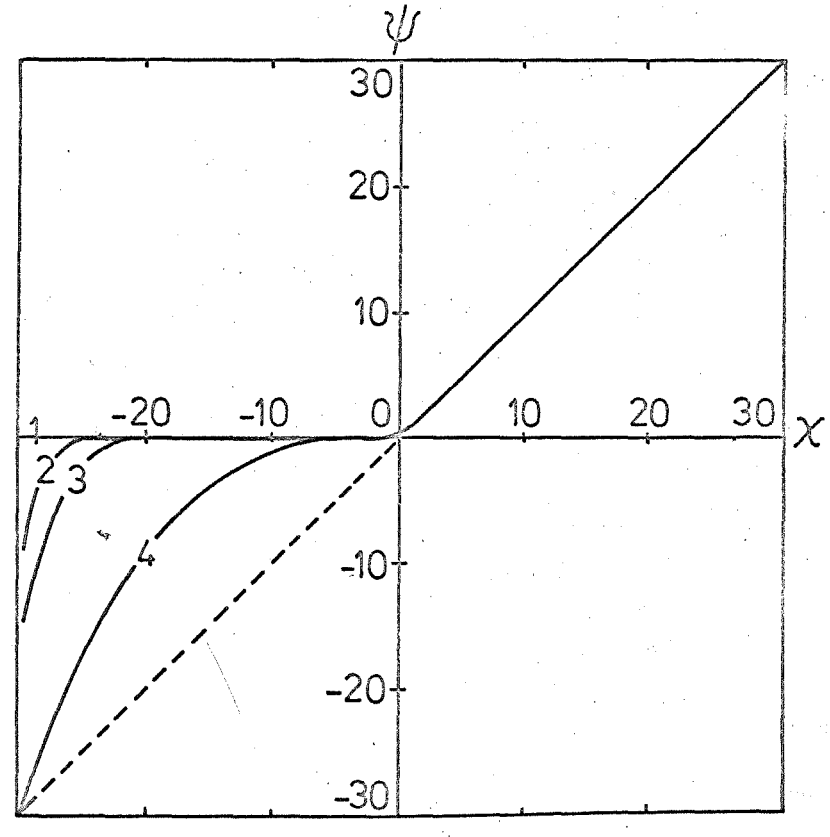
(b) Compression

at 1. $77^{o}K$
2. $298^{o}K$
3. $378^{o}K$
4. $500^{o}K$

after Taylor et al. (1973a)


ψ
30
20
10
0
-10
-20
-30
-30
-20
-10
10
20
χ
1
2
3

(a)


ψ
30
20
10
0
-10
-20
-30
-20
-10
10
20
30
χ
1
2
3
4

(b)

obtained by Guiu (1969) who deformed molybdenum in direct shear on {110} and {112} planes. Microscopic slip was not always observed to occur on the plane on which the macroscopic shear was imposed. However, Guiu (1969) allowed for this in estimating that the ratios of the shear stress in the anti-twinning sense on {112} planes to that in the twinning sense on {112} planes and to that on {110} planes were >1.5 and >2.0 respectively.

The low temperature slip behaviour observed in some metals and alloys cannot be explained by a modified shear stress criterion. This anomalous slip occurs in both tension and compression and predominantly on the $(0\bar{1}1)$ plane which, for central triangle orientations, has a resolved shear stress less than half that of the primary slip system. Slip of this type was first observed in niobium at temperatures below ~150°K and for an increasing range of orientations about the <001> deformation axis as the temperature was decreased (Duesbery and Foxall 1969). Coarse crystallographic $(0\bar{1}1)$ traces were observed around the full circumference of the specimens. The absence of any dead zones implied both [111] and $[\bar{1}11]$ $\underline{b}$'s were operative and this has been confirmed in later transmission electron microscopic studies (Garratt-Read 1973). Bolton and Taylor (1972), using shape change analysis, were able to show that the anomalous slip was not simply a surface phenomenon but that the major part of the bulk deformation was occurring on the anomalous systems.

Strikingly similar observations of anomalous slip have been made in high purity vanadium deformed at 77°K (Taylor, Bajaj and Carlson 1973). There are also indications of this type of anomalous slip occurring in high purity tantalum (Takeuchi et al. 1972, Webb et al. 1973). A distinctive feature of these observations is that the slip behaviour is very sensitive to traces of impurities. Only ultra high vacuum annealed niobium and tantalum, and electrotransport refined vanadium show anomalous slip of this type. Jeffcoat (1975) has observed anomalous slip in molybdenum-niobium and molybdenum-rhenium alloys which shows similar characteristics to that observed in the

Group Va metals. This contradicts the previous conclusion that anomalous slip only occurs in ultra pure metals.

Anomalous $(0\bar{1}1)$ slip traces have also been found in molybdenum (Vesely 1968b) and tungsten (Garlick and Probst 1964), but only over restricted surface ranges. Several other unexpected slip systems were simultaneously active and it would appear that this occurrence of $(0\bar{1}1)$ slip is a manifestation of the unexpected slip, characteristic of stage 0.

Matsui and Kimura (1973) have proposed a model to explain anomalous $(0\bar{1}1)$ slip based on the influence of image forces at the surface on dislocation behaviour. However, the model is deficient in several respects (Taylor 1974, Matsui and Kimura 1974). For example, it is unable to satisfactorily explain the observed orientation range over which anomalous slip is observed. At present there is no satisfactory explanation of anomalous slip but the operation of both $\underline{b}$'s suggests that some type of co-operative motion of dislocations of both $\underline{b}$'s is involved.

8.2 The Theories of the Yield

Both single and polycrystals of iron and other b.c.c. metals are commonly observed to exhibit discontinuous yielding behaviour in the presence of small concentrations of interstitial impurities.

This phenomenon was first explained in terms of the formation of pinning atmospheres on the original dislocations during annealing and the thermally activated unpinning of these dislocations at the upper yield stress (Cottrell and Bilby 1949). This 'static' theory was not able to explain many experimental observations including the temperature insensitivity of k_y, the stress intensity factor in the Hall-Petch equation, and the similar temperature dependence of the yield and flow stress. It now appears unlikely that, except in certain cases where 'weak' pinning occurs (Cottrell 1963), the thermally activated unpinning of dislocations or dislocation sources plays an

important role in the yield process.

An alternative view of the yield point was presented by Johnston and Gilman (1959) to explain the discontinuous yield behaviour of lithium fluoride and this idea was subsequently applied to b.c.c. metals by Hahn (1962) and Cottrell (1963). This interpretation involved the quantitative treatment of the dynamic properties of dislocations and their multiplication rates. It was proposed that during yielding free dislocations must move at a velocity sufficient to match the applied strain rate. It has been shown experimentally for a wide range of materials (e.g. Johnston and Gilman 1959, Stein and Low 1960, Prekel et al. 1968) that the effective stress (τ^*) required to move a dislocation at a velocity (v) may be described by the empirical relation

$$\left(\frac{\tau^*}{\tau_o}\right)^m = v$$

where τ_o is the stress to produce a unit dislocation velocity

m is a dimensionless constant

If initially the number of free dislocations is small, large dislocation velocities will be necessary to produce a significant plastic strain rate and hence, the stress rate will be large. With continued straining dislocation multiplication will occur, a smaller dislocation velocity will be required and the stress rate will be reduced. As m decreases τ^* becomes increasingly sensitive to velocity. So provided m is small and a rapid increase in the number of mobile dislocations occurs, a sharp yield point or drop of load may occur. It should be emphasised that this model is purely phenomenological in that it is based on empirical relations. It therefore gives no insight into the origin of the stress dependence of the dislocation velocity or of the dislocation multiplication rate.

The dynamical theory does not deny the important role sometimes played by interstitial pinning in producing a discontinuous yield by reducing the initial free dislocation density. Nor does it exclude the possibility of

dislocation multiplication occurring by the athermal activation of pinned sources at points of stress concentration. But the theory is not contingent on the pinning of dislocations by interstitials as are the static models and it may be applied to materials where there is no evidence of such pinning effects.

Single crystals of high purity iron and Group Va and VIa metals are observed to yield discontinuously at some, if not all, crystal orientations. In some cases this is associated with trace concentrations of interstitials and other impurities to the extent that their removal reduces the magnitude of the yield stress, though not necessarily eliminating the discontinuity itself. (e.g. Taylor and Christian 1965). In other metals such as molybdenum the yield is far more sensitive to the orientation of the crystal than it is to its purity (Stein 1968). There is no evidence to suggest that the discontinuous yield shown, for example, by molybdenum <011> crystals is a consequence of any impurity pinning effects. The absence of any yield discontinuity at other orientations indicates that intrinsic dislocation processes are determining the yielding behaviour of molybdenum.

There are two types of dynamic descriptions of the general yield behaviour shown by metals in the absence of impurity effects. The first proposes that a single mechanism determines the deformation throughout the whole of the flow curve. The rise in the stress to the macroyield, whether continuous or discontinuous, is then ascribed to the low initial mobile dislocation density and the velocity-stress relation. The second type of model proposes that different mechanisms control the microflow and macroflow. This two mechanism or so-called, 'edge exhaustion' model, is based on the idea that the lattice friction stress for a screw dislocation is much greater than for an edge dislocation. The strongest evidence for this large edge/screw mobility ratio is provided by transmission electron microscopic observations. High densities of long, straight screw dislocations are commonly observed after low temperature deformation. These are argued to be screw dislocation

trails generated by the motion of more mobile edge dislocation segments (e.g. Taylor and Christian 1967, Solomon and McMahon 1968, Luft 1970). There have also been several dynamic straining experiments where direct evidence for a low screw dislocation mobility at low temperatures has been obtained (Saka et al. 1974, Vesely 1973b, 1974).

The edge exhaustion theory attributes the stage 0 microstrain to the motion of edge and other non-screw dislocations. It implies that screw motion, and therefore dislocation source operation, does not occur until the exhaustion of the relatively mobile non-screw dislocations has caused the stress to rise to the macroyield level. The theory also predicts that the temperature dependence of the microyield and macroyield stresses should equal the temperature dependence of the stresses for constant edge and screw dislocation velocities, respectively. A critical comparison of these is difficult to make because of the uncertainties of the yield definition and of the confounding effects of orientation. It is also difficult to obtain experimental data on the mobility of screw dislocations and so, only the temperature dependence of the stress for constant edge velocity has been determined. Most of the results show a stronger temperature dependence of the macroflow stress than the stress for constant edge velocity. For example, Prekel et al. (1968) and Das and Pratt (1970) have found the stress for constant edge dislocation velocity in molybdenum to be less than the temperature dependence of the macroyield stress at all orientations (Stein 1967). These results support an edge exhaustion model of the yield where the screw velocity controls the macroscopic deformation.

The edge exhaustion model is capable of explaining the magnitude of the stage 0 microstrain observed but the discrepancy between the very large screw dislocation densities predicted (Christian 1970) and the significantly lower densities observed experimentally at the macroyield (e.g. Vesely 1973a) implies that some screw annihilation by cross-slip has occurred. The latter necessarily admits the possibility of the operation of double cross-slip or

Frank-Read type dislocation sources during the stage O microflow. This is also implied by the surface source models of the stage O slip geometry (Vesely 1968b).

A major problem with both the edge exhaustion and single mechanism dynamical theories of the yield is their inability to explain the orientation dependence of the yield behaviour. This is particularly pronounced in the Group VIa metals molybdenum and tungsten and will be discussed in the following section.

8.3 The Orientation Dependence of the Yield and Flow Stress

The majority of b.c.c. metals show a variation of the shear yield stress (defined as a proportional limit or proof stress) with the crystallographic orientation of the deformation axis. This orientation dependence generally increases as the temperature is decreased and may be very large at low temperatures. For example, in molybdenum at $77^{\circ}K$ the difference between the yield stress at the <011> and <001> orientations is as much as 150% (Stein 1967). This implies that the orientation dependence is associated with the thermal component of the yield stress.

The results indicating a variation of the yield stress with orientation have been summarised and discussed by Christian (1970) and Stein et al. (1973). They are difficult to classify, particularly when the yield stress is found also to depend upon the sense of deformation. However, almost invariably crystals are harder in both tension and compression when tested along the <011> axis than when tested along the <001> axis. At high temperatures approaching the athermal flow region, the Schmid law is reasonably well obeyed. At lower temperatures most of the results in tension are qualitatively in agreement with the asymmetry of shear on {112} planes implied by the independent evidence of $\psi(\chi)$ curves (see Section 8.1). Many of the results in compression, however, cannot be explained by such a modified Schmid law.

It has been suggested that this anomalous orientation dependence is associated with different impurity levels secured in differently oriented crystals during their preparation (Stein 1967, Stein et al. 1973). Such an effect, if present, is too small to account for the very strong orientation dependence shown, for example, in molybdenum. So it would appear that for most, if not all b.c.c. transition metals,there is a general failure of the Schmid law at low temperatures.

No direct measurements of dislocation mobility to test the validity of this conclusion have been possible. This is unfortunate since the relationship between the variously defined macroyield parameters and the mobility of individual dislocations is not well understood. Certainly, the use of a proportional limit or proof criterion to characterise the dislocation mobility is unsatisfactory when both continuous and discontinuous yielding occur at different orientations. Thus, in the Group VIa metals the orientation dependence of the yield stress is probably as much a consequence of the change in the yield form with orientation as any posited variation in the dislocation mobility or critical resolved shear stress. This conclusion is supported by the general observation that the macroflow stress at large strains is much less sensitive to orientation than is the yield stress. The orientation dependence of the macroflow stress itself, however, is not always consistent with the $\{112\}$ shear asymmetry. This may be related to the uncertainty of the slip geometry or possibly to the influence of non-shear components of the stress tensor.

The variation with orientation of both the form of yielding and the magnitude of the work hardening rates is most marked for the Group VIa metals molybdenum and tungsten (Guiu 1966, Rose et al. 1962). For example, when molybdenum is tested in tension at room temperature the <011> orientation shows a discontinuous yield with $\sim\frac{1}{2}\%$ microstrain and a subsequent low work hardening rate. The <001> orientation yields continuously showing >5% stage 0 microstrain and a quasi-parabolic flow curve.

Neither the single mechanism nor the edge exhaustion yielding theories discussed in Section 8.2 give any insight into the origin of this behaviour. An explanation in terms of either model would seem to require a variation of the effective initial mobile dislocation density or of the dislocation multiplication rate with orientation.

Direct experimental evidence of an orientation dependence of the increase in dislocation density with strain has been obtained in a transmission electron microscopic investigation of deformation structures in <011> and <001> molybdenum crystals. Kopetskii and Pashkovskii (1974) found that after 1% strain at 293°K the predominantly screw, dislocation density was $\sim 5 \times 10^7/cm^2$ for the <011> crystals and $\sim 5 \times 10^9/cm^2$ for the <001> crystals. Argon and Maloof (1966) and Ohba et al. (1971) have also obtained evidence indicating the dislocation density increase for <011> crystals is small compared to that for <001> crystals of tungsten. These observations indicate a strong correlation between the magnitude of the work hardening rate and the increase in dislocation density in the microstrain region. The predominance of screw dislocation trails in the deformation structures also confirms that non-screw motion makes a large contribution to the microstrain. But these results furnish further support for the earlier conclusion that some source operation and screw motion occur prior to the macroscopic yield.

Takeuchi (1969, 1973) has developed a model which predicts an orientation dependence of the rate of dislocation multiplication and annihilation and hence, of the cumulative dislocation density. In crystals with an <001> deformation axis dislocation multiplication is assumed to occur by double cross-slip, induced by the formation of repulsive junctions between dislocations of the four <111>{112} slip systems. The rate of multiplication and annihilation are determined by the ease of cross-slip. The deformation of <011> crystals does not give rise to repulsive junctions between the primary and secondary dislocations on the two <111>{112} systems and so, no significant dislocation multiplication is predicted to occur. It should be noted that the

model assumes microscopic slip on {112} planes which does not appear to occur, at least in the anti-twinning sense, in metals such as molybdenum.

Takeuchi (1969) initially proposed that the rapid work hardening rate displayed by <001> crystals of iron, molybdenum and tungsten was due to glide-forest dislocation cutting but later the model was revised and a jog-drag mechanism substituted (Takeuchi 1973). Neither of these hardening mechanisms seems satisfactory (e.g. Hirsch 1968) and the assumption that the screw dislocation velocity controls the deformation from the outset is not consistent with most experimental observations.

A further set of experimental observations seem relevant to the orientation dependence of the yield and flow behaviour of molybdenum and other metals. These observations provide strong evidence that different mechanisms control the deformation in the microflow and macroflow regions. Guiu (1967) found the activation volume (v^*) during the stage 0 microstrain greatly exceeded that in the macroflow region of continuously yielding molybdenum <001> crystals. v^* was also observed to be a function of both the effective stress and temperature which suggested that more than one mechanism was controlling the deformation. A similar variation of v^* during the initial rapid work hardening of <149> molybdenum crystals was obtained by Pink (1973), who also concluded that this variation could not be reconciled with a single rate controlling mechanism. Prekel et al. (1968) using dislocation velocity measurements found a large variation in v^* in the microflow region and interpreted the stress dependence of v^* in terms of a single deformation mechanism. This interpretation has, however, been disputed because different activation enthalpies were obtained in the microflow and macroflow regions (Vreeland and Turner 1969). Since more than one mechanism appears to be operating, v^* does not have a clearly defined physical significance and it is not possible to give a satisfactory explanation of its detailed variation. But, the variation is generally consistent with an edge exhaustion hardening model where there is a progressive shift in control from edge to screw

dislocations as the stress rises to the macroflow level.

Guiu (1967) concluded that the Peierls stress on screw dislocations did control the macroflow but attributed the rise in stress and decrease in v^* in the microflow region to the jogging and progressive exhaustion of mobile screw dislocation. Guiu and Pratt (1966) also proposed that the orientation dependence of the microstrain was related to a change in the work hardening mechanism. Deformation of <011> crystals was shown to lead to the formation of non-conservatively moving jogs on screw dislocations. A rapid exhaustion of mobile screws and a rapid rise in the stress to the yield point resulted. The conservatively moving jogs, which were formed during the deformation of <001> crystals, were argued to cause a less rapid exhaustion of mobile screws and a lower work hardening rate. The principal difficulty with this model is that improbably large jog densities are required to explain the magnitude of the work hardening rates observed.

There appears to be a close relationship between the work hardening behaviour, the rate of dislocation multiplication, the strain dependence of v^* and the distinctive slip geometry of crystals with symmetry orientations. Both Takeuchi's (1969, 1973) and Guiu's (1966, 1967) theories of the orientation dependence of the yield and work hardening behaviour are unsatisfactory because they make no distinction between edge and screw dislocation mobilities and rely on conventional and inadequate work hardening mechanisms. They are important because they propose dislocation mechanisms which are a direct consequence of the slip geometry and its orientation dependence. It is likely that the modifications to the edge exhaustion models necessary to give an explanation of the orientation dependence of the yield behaviour will involve the superimposition of similar orientation dependent multiplication or work hardening mechanisms.

The recognition of the tenuous relation between the dislocation mobility and conventionally defined yield parameters has led to several attempts to define the yield more satisfactorily. Christian (1970) has defined the

macroyield stress as that at which the plastic strain rate becomes a large fraction of the applied strain rate. This definition circumvents some of the difficulties associated with a comparison of continuous and discontinuous yielding behaviour but no measurements of such a parameter have been reported. Pink (1973) observed that the upper limit of the stress range, over which the dislocation density and stress level rose rapidly in continuously yielding orientations of molybdenum (viz. <149> and <001>), was approximately defined by the stress at which v^* became constant. This stress was said to define the macroyield and found to be approximately equal to the lower yield stress for the discontinuously yielding <011> crystals. Jeffcoat (1975) verified that a macroyield stress so defined was independent of orientation and further interpreted this parameter as that required for long range screw dislocation movement.

8.4 The Temperature Dependence of the Yield and Flow Stress

The models developed to explain the temperature dependence of the yield and flow stress of b.c.c. metals at low temperatures are based on the theory of the thermally activated motion of dislocations. The applied shear stress (τ) is resolved into an effective stress (τ^*) which shows a strong temperature dependence, and an internal stress (τ_i) which shows only a very weak temperature dependence. τ^* is identified as the stress required to move dislocations through short range stress fields where thermal activation may play an important role at temperatures above $0^{\circ}K$. τ_i is equated with the amplitude of the fluctuating long range stress field which shows only the small temperature dependence of the elastic constants. One of the greatest problems in comparing theory with experiment is that of the definition of τ^* and τ_i in terms of measurable quantities. Frequently, they are evaluated by equating τ_i to the stress at high temperatures where athermal flow is assumed to occur. Changes in the flow stress associated with alloying are often ascribed to

changes in τ^* or τ_i on the basis of their sensitivity or insensitivity to temperature.

8.4.1 Recent Experimental Evidence

There has been considerable controversy over the extent to which the strong temperature (and strain rate) dependence of the flow stress of b.c.c. metals is an intrinsic property of the lattice and to what extent a consequence of the extrinsic hardening effects of residual interstitial impurities. Both the magnitude and the mechanism of any interstitial hardening effect are still in doubt but it would now appear that independent of this uncertainty, there is a substantial lattice contribution to the low temperature flow stress.

Much of the experimental evidence concerned with interstitial impurity effects has been conflicting. A major difficulty with the earlier work was associated with the measurement and control of interstitial impurity levels. Improvements in both purification and monitoring techniques have led to a series of investigations in recent years involving the controlled interstitial doping of very pure iron and Group Va metals (e.g. Nakada and Keh 1968, Taylor and Bowen 1970, Lachenmann and Schultz 1973, Bressers et al. 1975). However, the poor agreement between some workers' results may still be a consequence of the problems of impurity control in their material. For example, Loomis and Gerber (1970) and Ravi and Gibala (1970) have observed solution hardening and softening respectively in niobium-oxygen alloys at low temperatures. This is probably related to the different purities of their base materials.

Another major interpretative problem which remains largely unresolved relates to the satisfactory definition of a yield or flow parameter which reflects the frictional stress on dislocations. This is well illustrated by the contradictory results obtained by Stein and Low (1966) and Altshuler and Christian (1967) on the same iron-carbon alloys. The former workers found a strong concentration dependence of the low temperature proportional limit and

0.2% proof stress while the latter, using incremental temperature changes, obtained a very small effect on the macroflow stress. It is likely that this disagreement partly derived from the different yield and flow parameters employed and is consistent with the generally agreed stronger effects of interstitial solutes on the microflow than the macroflow behaviour (Stein 1968).

The well established sensitivity of the proportional limit to test machine characteristics (Bernstein 1969) and the obviously arbitrary nature of a proof stress definition of the yield may account for a further discrepancy between Stein and Low's (1966) results and those of a later study of iron-nitrogen alloys. Nakada and Keh (1968), using the lower yield stress and a 0.5% proof stress to define the macroyield, found nitrogen to cause a strong hardening effect at high temperatures but to cause little change in the macro-yield stress at low temperatures. Differently oriented crystals were also used in the two investigations and both Nakada and Keh (1968) and Stein (1968) recognised the possibility that the orientation dependence of the τ^* versus T relation may explain such contradictory results.

The interpretation of alloying effects in some of the recent investigations where single crystals have been employed may be complicated by the influence of orientation. Both Lachenmann and Schultz (1972) and Webb et al. (1973) have found that the magnitude of the hardening effect of nitrogen on the yield stress of tantalum varies with orientation. A similar orientation dependence of the hardening rate was obtained by Takeuchi et al. (1967) in substitutional iron alloys. However, most of the investigations have used crystals oriented for $[111](\bar{1}01)$ slip and direct comparisons of alloy hardening are not complicated by such orientation effects.

The results of an investigation of niobium-nitrogen <149> crystal alloys by Taylor and Bowen (1970) also point to the importance of the parameters chosen to characterise the friction stress of individual dislocations. Nitrogen alloying was found to increase the yield stress at low temperatures appreciably, but the effective stress obtained by incremental temperature changes in the

macroflow region was relatively insensitive to the nitrogen content. Since the material showed a discontinuous yield and subsequent low work hardening rate (Taylor and Bowen 1975) the discrepancy is unlikely to be a consequence of the yield definition used (viz. 0.3% proof stress). Rather it would appear that the interstitials produced a much stronger effect on the macroflow stress defined by direct deformation than on that defined by differential temperature changes. Taylor and Bowen (1970) considered the latter to be a more reliable index of the friction stress because it avoided the confounding effects of a variable dislocation density which may arise in the case of direct deformation tests.

Smialek and Mitchell (1970a), however, have observed a strong thermal hardening of the macroflow stress (using a 2% proof criterion) in direct deformation tests of tantalum-interstitial alloys and have interpreted this in terms of an increase in the frictional resistance to dislocation motion.

The accumulated evidence of this and other recent investigations is that the temperature dependent component of the yield stress is usually increased by interstitial alloying and that, above concentrations of 200-300 at.ppm., some temperature independent solution hardening also occurs. Given the purity of the base material employed and the interstitial hardening rates observed these measurements also indicate a substantial low temperature frictional stress in interstitial free material.

8.4.2 Theories

There are three types of theoretical models concerned with explaining the temperature dependence of the flow stress, viz. the interstitial atom or cluster hardening models, the Peierls double kink models and the screw sessile - glissile models. The first is concerned with the extrinsic hardening mechanism of interstitial impurities and the latter two with the origin of the intrinsic "strength" of b.c.c. metals. They have been extensively discussed by Christian

(1968, 1970) and only a brief description of the models and their major predictions will be given here.

The Interstitial Hardening Models

An interstitial impurity hardening model was proposed by Fleischer (1962a,b) and further developed by Frank (1966, 1967, 1968). It ascribes the rapid thermal hardening caused by interstitial impurities in many b.c.c. metals to the interaction of their tetragonal elastic strain fields with moving edge and screw dislocations. The existence of such a tetragonal distortion associated with interstitial impurities is indicated by Snoek peaks observed in internal friction measurements (Snoek 1941).

Some of the strongest experimental evidence supporting a Fleischer type model comes from the work of Stein and Low (1966) who obtained both the predicted concentration (C) dependence (viz. $\Delta\tau^* \propto C^{\frac{1}{2}}$) and the predicted temperature (T) dependence of the hardening. However, the disagreement with later work (Altshuler and Christian 1967, Nakada and Keh 1968) places the significance of this result in doubt. Other comparisons of theory and experiment (Frank 1966, Boser 1968) have indicated good agreement for the $\tau^* v.C$ and $\tau^* v.T$ relations. More recently Smialek and Mitchell (1970a) obtained rapid thermal hardening in tantalum-interstitial alloys which conformed to the predicted $\Delta\tau^* \propto C^{\frac{1}{2}}$ relation. But, it has been argued (Christian 1968, 1970) that such comparisons usually do not provide a critical basis for distinguishing between rival theories because they are made over too small a concentration range and/or do not ensure that both the predicted temperature and concentration relations are simultaneously obeyed. Comparisons of the predicted and observed stress dependence of activation volumes and enthalpies are no more satisfactory in this respect.

The general observation that v^* is independent of the solute content (Altshuler and Christian 1967, Nakada and Keh 1968, Bluem 1972), even when there is a large increase in the flow stress temperature dependence (Smialek

and Mitchell 1970b) would argue against a model involving the thermally assisted motion of dislocations past point obstacles. Ravi and Gibala (1972) have reported a change in v^* on alloying niobium with oxygen but their results were complicated by solution softening. There is also an essential difficulty in rationalising such solution softening effects, where gettering and other explanations do not seem applicable, in terms of a dislocation-point obstacle model.

A final major deficiency of the point obstacle theory is its inability to explain the orientation dependence of the macroyield hardening rate suggested by the recent results of Lachenmann and Schultz (1972) and Webb et al. (1973). These results can only be fitted to the model by assuming different obstacles strengths for different orientations.

It would appear that many of the experimental observations of interstitial hardening behaviour are incompatible with any model based on dislocation-point obstacle interactions. These observations suggest that the hardening may be a result of a more indirect mechanism involving a change in the strength of the dislocation interaction with the lattice or, perhaps, a change in other important parameters which determine the nature of the dislocation substructure.

The Double Kink and Sessile-Glissile Models

Both the double kink and sessile-glissile models are primarily concerned with explaining the behaviour of 'pure' metals. The formal theory of both these intrinsic models is similar; they both postulate that the line energy of a dislocation varies periodically with position giving rise to a lattice friction or generalised Peierls stress. The models are essentially descriptive since the energy barrier to dislocation motion is simply a postulated one.

In the double kink model the dislocation surmounts the energy barrier

by the nucleation of a double kink which then grows by the lateral glide of the two kinks. At low temperatures where the stress is large the nucleation of the kink is the critical step. The theories, which were developed by several authors assuming different barrier shapes and critical configurations, have been critically reviewed by Guyot and Dorn (1967). More recently Dorn and Mukherjee (1969) and Kroupa and Hull (1969) have modified the theory to explain the observed asymmetry of slip on {112} planes. These explanations are limited in the sense that there is no basis for the modifications independent of the experimental observations they are intended to 'predict'.

The sessile-glissile theories of the lattice friction stress were developed using dissociated core models. The latter were based on a suggestion of Hirsch (1960) that the screw dislocation core in the b.c.c. lattice is extended in a non-planar, sessile configuration. The resistance to dislocation motion is assumed to arise from the thermally activated transformation of screw dislocations between dissociated sessile and planar glissile configurations. The critical configuration is a function of stress, but as with the double kink models the activation energy at high stresses is associated with the nucleation of a constriction. A number of calculations based on this hypothesis have been made (e.g. Escaig 1966, Kroupa and Vitek 1967, Duesbery 1969) and the predictions and experimental support for the theories recently discussed by Christian and Vitek (1970) and Vitek (1974).

The sessile-glissile models seem to give a more satisfactory explanation of the shear asymmetry on {112} planes than does, for example, the double kink model of Dorn and Mukherjee (1969) where an asymmetric Peierls barrier is quite arbitrarily introduced. The sessile-glissile models (e.g. Kroupa and Vitek 1967, Duesbery 1969), though still phenomenological, show the asymmetry to be a natural consequence of the threefold symmetry of the core, and the slip mechanism itself.

Both the double kink and the sessile-glissile models give good agreement with most of the experimental results on the temperature dependence of the flow

stress (e.g. Wynblatt and Dorn 1966, Escaig 1967). It may be argued, however, that this type of comparison is non-critical and that agreement provides little more than confirmation that a thermally activated mechanism is rate controlling (Christian 1968, 1970).

The Impurity Modified Intrinsic Models

The demonstrated inadequacies of the point obstacle hardening theories have given impetus to the development of several models which describe interstitial alloying effects in terms of lattice-dislocation interactions.

Several modifications to the double kink model have been proposed to explain interstitial effects on the temperature dependence of the flow stress (e.g. Conrad and Hayes 1963, Arsenault 1966, Ono and Sommer 1970). These have considered the possible effects of dislocation pinning by interstitials on the nucleation and growth of a double kink. In the most recent treatment, Ono and Sommer (1970) predicted that at high temperatures interstitial pinning causes an increased friction stress, but at low temperatures there is only a small deviation from the stress given by the unmodified double kink model (Dorn and Rajnak 1964). The model contradicts the general assumption that the high temperature hardening is additive with the low temperature thermal component of the flow stress and could offer an explanation of some apparent solution softening observations at low temperatures (Nakada and Keh 1968).

Frank and Sestak (1970) have proposed a 'unified' impurity, sessile-glissile model where screw dislocations are assumed to be dissociated on $\{112\}$ and $\{110\}$ planes. It is shown how repulsive interactions between impurity atoms and the partial dislocations of the dissociated core can in principle explain the effects of impurities on the flow stress and slip geometry. The theory predicts an enhancement of the yield stress asymmetry by alloying which is in agreement with the behaviour of some substitutional iron alloys (Takeuchi et al. 1967) but directly contradicts the reduction in yield asymmetry observed in nitrogen doped tantalum (Webb et al. 1973, Lachenmann and Schultz 1972).

The Atomistic Models of the Dislocation Core

There is strong evidence that the dominant factor determining the deformation behaviour of b.c.c. metals is the structure of the screw dislocation core. (Christian and Vitek 1970). This includes the transmission electron microscopic observations indicating a low mobility of screw dislocations at low temperatures and the slip geometry evidence for a low temperature asymmetry of the shear stress.

The first models of the screw core structure envisaged the core as several regions of stacking fault bounded by partial dislocations on threefold symmetrically distributed planes of the <111> zone. This description of the dislocation core was employed in the sessile-glissile theories of screw dislocation motion and had considerable success in explaining some of the basic features of b.c.c. deformation behaviour referred to above. However, the splitting models involved several assumptions of doubtful theoretical justification. They postulated the existence of stacking faults based on hard sphere model arguments. These may not be valid for the b.c.c. lattice because they take no account of the second nearest neighbour interactions necessary to render it stable. The splitting models also apply the linear continuum theory of elasticity to partial dislocations with separations of approximately an interatomic spacing. This procedure can only be justified as an extrapolation from much larger separations where the theory is valid. These and other theoretical deficiencies pointed to the need for information about the detailed nature of the dislocation core and led to a series of atomistic calculations of the core structure using computer simulations (e.g. Chang 1967, Gehlen 1970, Vitek et al. 1970, Basinski et al. 1970a).

These atomistic models take account of the discrete nature of the lattice and use central forces which ensure the stability of the b.c.c. lattice. With the exception of the calculations for sodium, where a well established potential is available (Basinski et al. 1970b), the potentials used are

empirical. They are chosen to characterise the b.c.c. lattice rather than represent the properties of any individual metal and so only permit qualitative information about the core structure to be obtained.

The initial calculations confirmed the main assumptions of the dissociated screw models viz. that the screw is sessile and has threefold symmetry. There was not good agreement between the calculations in detail, but these two features emerged as being generally characteristic of the b.c.c. structure. The calculations of Vitek (1968, 1970) and Basinski et al. (1970a) showed that no mechanically stable, single layer stacking fault exists on either the $\{110\}$ or $\{112\}$ planes in the b.c.c. lattice. This result does not preclude the existence of narrow stacking faults in the core since these may be stabilised by repulsive forces between the partials bounding them. But it does indicate that the description of the core splitting in terms of conventional stacking faults bounded by partial dislocations is not appropriate. Vitek and Kroupa (1969) interpreted the core structure in terms of 'generalised' stacking faults and 'fractional' dislocations where the fault vector is treated as a variable and the dislocation $\underline{b}$ is continuously distributed across the fault.

All the calculations referred to above were concerned with the core structure of a screw dislocation in an unstressed condition. However, the changes in the core structure which occur in the presence of an externally applied stress may be of great importance in determining both the stress to move a dislocation at $0^{\circ}K$ and the slip geometry. There have been several calculations concerned with the effect of an applied stress on straight screw (Basinski et al. 1971, Minami et al. 1972, Duesbery et al. 1973) and non-screw (Yamaguchi and Vitek 1973, Vitek and Yamaguchi 1973) dislocations. These calculations indicate that severe changes in the screw core structure do occur under stress before the dislocation moves. The details of these changes are complex but they reaffirm that the screw core is non-planar and sessile and that it exhibits an asymmetry which strongly influences the way it moves.

The magnitude of the asymmetry and of the core width depends upon the particular potential used. The cores of non-screw dislocations are always planar and their Peierls stress is very much less than that for screws. Moreover, Yamaguchi and Vitek's (1973) calculations suggest that the Peierls stress of non-screws may be more sensitive than that of the screws to changes in the interatomic potential. These recent calculations indicate that both the mode of screw motion and the magnitude of the screw/non-screw mobility ratio will depend upon the precise nature of the interatomic forces.

It should be noted that all the atomistic calculations refer to the motion of dislocations at $0^{\circ}K$. At non-zero temperatures movement will probably take place by the formation and growth of double kinks. At very low temperatures the non-screw kinks will be comparatively mobile and it is likely that their nucleation will control the velocity of the screw dislocations. So it is argued (e.g. Duesbery et al. 1973) that in the absence of large thermal activations the screw motion will be governed by the Peierls stress for straight dislocations.

The atomistic models of the dislocation core can, in principle, explain the experimental observations indicative of a low screw mobility and an asymmetry of slip at low temperatures. They also suggest that differences in the deformation behaviour of individual metals are related to differences in the detail of the screw core structure and in the relative mobility of edges and screws. They do not offer any explanation of alloying effects except in the same general terms, i.e. that these may be partly due to changes in the effective interatomic potential and concomitant changes in the screw core structure and mobility. Neither the atomistic models nor the other extrinsic or intrinsic models give a satisfactory theoretical description of a number of features of b.c.c. deformation behaviour. These include anomalous $(0\bar{1}1)$ slip, the stage 0 slip geometry and the very large shear asymmetry sometimes observed in compression at low temperatures.

Chapter 9

EXPERIMENTAL APPARATUS AND PROCEDURE

9.1 Seeding and Orientation Determination

The orientations of the seeds and test specimens were determined by the Laue back reflection X-ray technique with an accuracy of $\pm$ 2-3°.

The crystal growing apparatus and procedure described in PART A was slightly modified to allow the production of crystals of the specific orientations required for the mechanical testing. A zone-melted molybdenum crystal stub was suitably oriented on a twin arc goniometer which could be mounted on the base post in the work chamber in place of the V-notch friction grips. A single pass crystal of uniform cylindrical geometry was readily grown off the goniometer mounted seed. When, after several attempts, a crystal of the required axial orientation was produced, it was sectioned into approximately 4-5 cm. lengths. One of these was mounted in the V-notch grips and used as a seed for the high purity crystals grown for the mechanical test specimens. The V-notch grips required the seed to be of good geometrical quality so that it could be aligned accurately.

The initial orientation of the test specimens was established by determining the orientation of the centreless ground and electropolished single crystal rods before they had been sectioned for doping. The rod was mounted with its axis normal to the incident X-ray beam and both ends of the crystal were Laued to confirm it was a single crystal and to estimate the change in orientation along its length (usually $<3^{\circ}$). All test specimens subsequently cut from the rod were assumed to have this orientation. The

post deformation orientations of at least one H.V.A. and one doped specimen of each orientation employed were determined in a similar fashion.

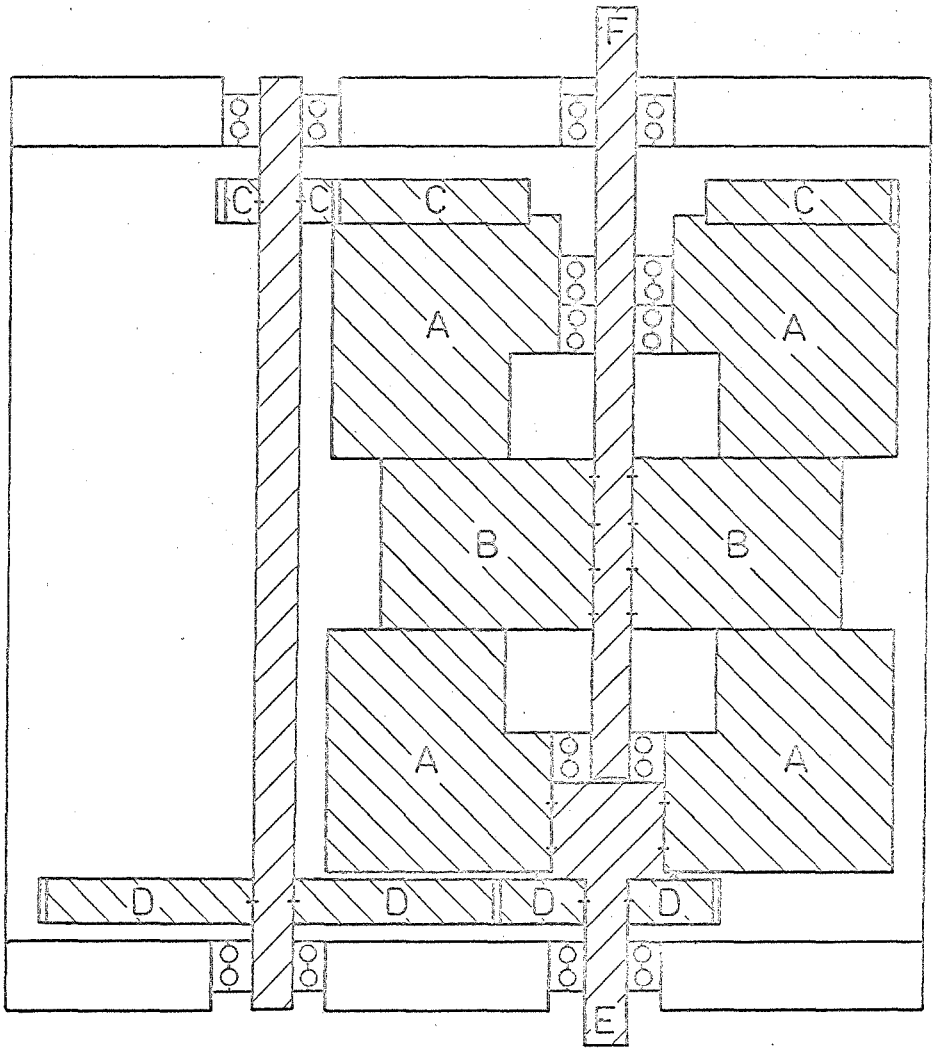
9.2 Compression Testing Machine

The compression machine employed was basically the 'Mark I' machine in the Oxford department described by Taylor (1965) and Bowen (1966). Only modifications made for the purposes of this investigation will be described in detail here.

The compression jig described by Taylor (1965) was made from EN57, unhardened martensitic stainless steel. It was found that some plastic indentation of the polished anvils occurred when preliminary tests on the molybdenum specimens were made. Consequently, highly polished, parallel faced tungsten carbide platens (12 x 12 x 3 mm.) were interposed between the stainless steel anvils and the test specimen in all the subsequent tests. There was no plastic punching of the tungsten carbide anvils at the maximum load (1000 kg.).

A gear box, which could give a step change of 10x, was inserted between the 1/6 hp., 1440 rpm. AC drive motor and the worm and wheel, driving the lead screw connected to the crosshead. A plan view of the gear box which was designed to permit strain rate changes over the full 1000 kg. load range of the rig is given Fig.B3. An Osbourne 'M' type worm reduction gear box with a fixed reduction ratio of 100:1 was also introduced on the input side of the 10x change gear box. In the event, no strain rate change tests were undertaken on the compression specimens and so the only effect of these modifications was to alter the crosshead speed at which the tests were conducted from the previous value of 284μ/min. to 105μ/min. The specification of the differential transformer and load cell employed for displacement and load measurement are given in Table B1. Details of the mounting of the transformer and the load cell on the compression rig are given

Figure B3 Plan View of 10x Change Gear Box



A. WARNER 500 PC CLUTCH ELECTROMAGNETS

B. CLUTCH ARMATURE

C. 100T : 20T MUFFETT GEARS

D. 40T : 80T MUFFETT GEARS

E. INPUT SHAFT

F. OUTPUT SHAFT

CROSS-HEAD SPEED	:	High 105μ/min. Low 10.5μ/min.
MAXIMUM LOAD	:	1000 kg.
MACHINE AND LOAD CELL COMPLIANCE	:	0.25μ/kg. (Linear >150 kg.)
LOAD CELL	:	J.L. Thomson BT2
SENSITIVITY	:	2.992 mV/applied volt.
ACCURACY	:	0.5% (F.R.O.)
MAXIMUM RECORDER SENSITIVITY	:	100 kg. F.S.D.
DIFFERENTIAL TRANSFORMER	:	Sanborn 7DC DT-500
STROKE	:	± 0.5 in.
SCALE FACTOR	:	6.6 V/in. for 6 V excitation
OUTPUT IMPEDANCE	:	5.3 kΩ
MAXIMUM RECORDER SENSITIVITY	:	10μ F.S.D.
RECORDER	:	Leeds-Northrup XL680
FULL SCALE RESPONSE TIME	:	0.5 sec.
LOAD SIGNAL RANGE	:	5.0 mV F.S.D.
DISPLACEMENT SIGNAL RANGE	:	~2.0 mV F.S.D.
CHART SPEED	:	1,3 cm/min.

Table B1 Compression Machine Specification

in Taylor's (1965) and Bowen's (1966) theses.

The load and displacement signals were fed through two redesigned measuring circuits to a Leeds-Northrup XL680 two pen chart recorder.

The load measuring circuit is given in Fig.B4a. It provides for the alternate use during a single test run of either a 1000 kg. or a 100 kg. F.S.D. range with up to nine 100 kg. suppressions. Thus, it permitted the overall flow behaviour to be monitored on the low sensitivity range but, should a region of the flow curve (e.g. a yield point) be of particular interest, it could be examined and recorded with greater accuracy on the high sensitivity range. The balancing and calibration circuit was similar to that of Sharp (1964) and included a throw-off facility for rapid checking of calibration. The load cell was initially calibrated to give 100 kg. F.S.D. on the 5 mV. recorder range using a 50 kg. dead weight. The imbalance voltage generated by the introduction of the approximately 200 k.ohm throw-off resistance was 17.675 mV.

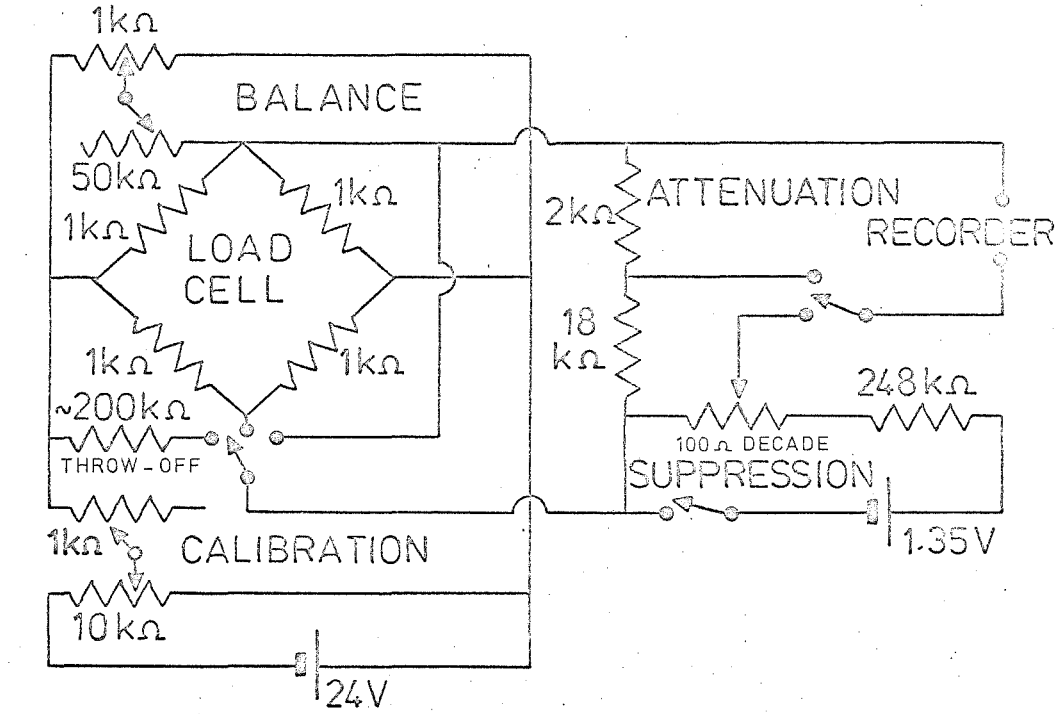
The displacement measuring circuit is shown in Fig.B4b. When the specimen was in position and just beginning to come under load from the anvils, the transducer output could be balanced to give a zero input to the recorder. Four attenuations and a 'recorder short' position were provided giving 10μ, 100μ, 500μ, 1000μ and a variable 10-100μ F.S.D. ranges. Since the output impedance of the attenuation circuit was constant for all except the 10-100μ variable range, switching between all except this range could be effected during a single test run without a shift of zero or the need for recalibration. Up to nine F.S.D. suppressions could also be made on any of these ranges. The displacement was calibrated on the 2 mV. F.S.D. recorder range using a dial gauge mounted between the fixed and moving crossheads. All tests were conducted using the 100μ F.S.D. range for which the displacement sensitivity was approximately 1μ. This corresponds to a strain sensitivity, for a typical specimen height of 6 mm., of $\sim 10^{-4}$.

The error in strain measurement attributed by Taylor (1965) and Bowen

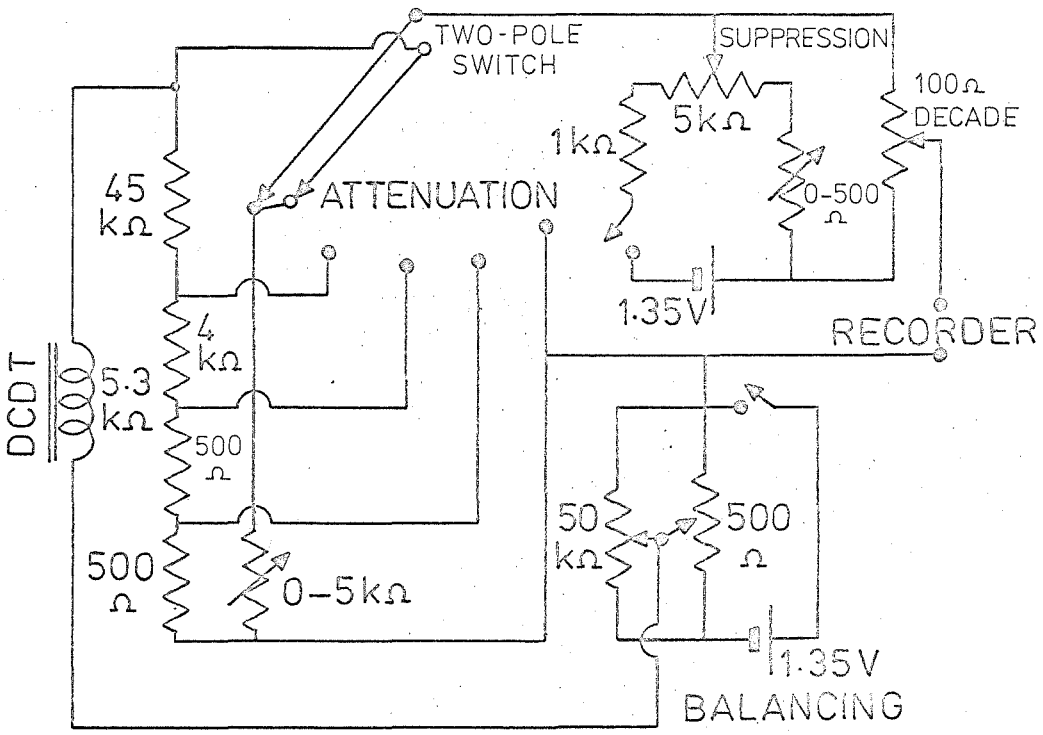
Figure B4 Diagram of

(a) Load Measuring Circuit

(b) Displacement Measuring Circuit


1kΩ
BALANCE
50kΩ
1kΩ
1kΩ
LOAD CELL
1kΩ
1kΩ
1kΩ
~200kΩ
THROW-OFF
1kΩ
CALIBRATION
10kΩ
24V
2kΩ
ATTENUATION
RECORDER
18 kΩ
248kΩ
100Ω DECADE
SUPPRESSION
1.35V

(a)


TWO-POLE SWITCH
SUPPRESSION
100Ω DECADE
5kΩ
1kΩ
0-500 Ω
1.35V
RECORDER
45 kΩ
ATTENUATION
4 kΩ
5.3 kΩ
DCDT
500 Ω
500 Ω
0-5kΩ
50 kΩ
500 Ω
1.35V
BALANCING

(b)

(1966) to elastic indentation of the stainless steel anvils by their niobium test specimens was also observed in this investigation. The reduction in punching expected for the harder tungsten carbide anvils employed here appeared to be more than offset by the much higher Young's modulus of molybdenum compared to niobium. In addition, the difficulty of accurately aligning both the tungsten carbide platens and the test specimen on the axis of the compression rig, had deleterious effects on the reproducibility of the elastic loading line. The methods used to estimate and compensate for these errors are given in Section 9.7.

Fluctuations in the transducer displacement signal were observed when the compression rig was placed in a liquid nitrogen bath to secure a $77^{o}K$ test temperature. This instability was due to the intermittent heating and cooling of the transducer tube by the gas evolved, and was overcome by using the same device as that employed by Bowen (1966). This was a liquid oxygen bath which did not boil and cause fluctuations when enclosed in a liquid nitrogen jacket and cooled to $77^{o}K$.

9.3 Tension Testing Machine

An Instron TT-CM-L machine was used for the tension testing. The test rig, which is shown with ancillary equipment in Fig.B5 was mounted underneath the movable cross-head and the pull-rod connected to the load cell via a universal couple. Although the rig and grips were accurately machined to promote uniaxial loading of the specimen, the bottom pin couples were designed to give some free play and so further reduce the possibility of bending on initial loading.

Special grips were designed to accommodate the 1 mm. diameter tension specimens. A friction gripping system had to be employed because the more attractive shouldered specimens could not be satisfactorily doped by the quenching technique. Friction grips based on collets or plates make the

Figure B5 Tension Testing Rig and Ancillary Apparatus


-0002
BALANCE
INSTRUMENT ZERO
FUNCTION
RANGE
SPAN
P+
P−
S+
S−
DEXT
D120
D350
GND
VISHAY/ELLIS

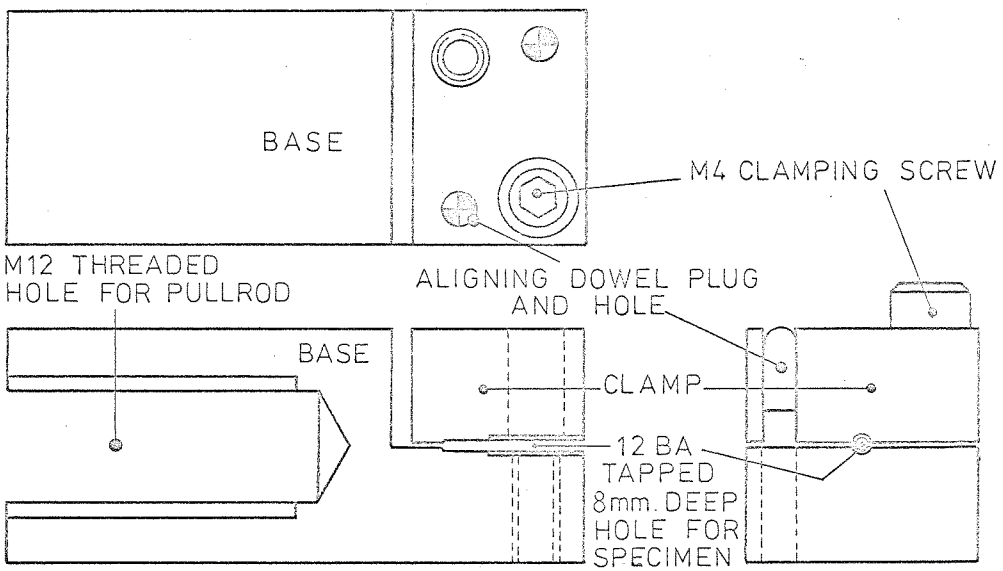
mounting, removal and handling in subsequent examination of soft single crystals difficult. In view of this an attempt was made to adapt the gripping system described by Taylor (1973) where endpieces are swaged onto the cylindrical test specimens and the resultant whole is treated as a shaped specimen. Unfortunately, this gripping system proved unsatisfactory for 1 mm. diameter molybdenum single crystals because of the small radial tolerances necessary on both specimen and endpieces to ensure adequate 'bite'. Conventional block grips, illustrated diagrammatically in Fig.B6, were then designed so as to guarantee a strong grip on specimens with larger tolerance limits on their gauge diameters. The grips were made from a high carbon, manganese oil quenching tool steel (BS4659 Grade B02) and were used in the hardened condition.

A 500 kg. load cell was employed to measure the load. This was calibrated at the commencement of each test series during the course of which the calibration altered by not more than 1%. The load was recorded on the machine chart recorder which had a 1/4 sec. full scale response time.

For the majority of the room temperature tests the strain was monitored using an Instron G51-16M electromechanical strain gauge. This had a 1 cm. gauge length, a 10% extension limit and an accuracy of 0.1% (F.R.O.). The spring-loaded clamps supplied with the gauge were modified to permit attachment to the thin wire specimens without risk of accidental deformation. The gauge itself weighed only ~8 gm. and did not exert a significant bending force on the specimen. The output from the gauge was fed to a Vishay Ellis 20 digital strain indicator. This was calibrated to give a digital displacement output in microns corresponding to a strain sensitivity of $\sim 10^{-4}$.

When the electromechanical gauge was not used, the strain was estimated by deducting the 'machine extension' from the cross-head displacement. By elastically straining polycrystalline molybdenum wires of varying gauge lengths and then extrapolating to zero length, the composite

Figure B6 Block Grips for Tension Specimens


BASE
M4 CLAMPING SCREW
M12 THREADED
HOLE FOR PULLROD
ALIGNING DOWEL PLUG
AND HOLE
BASE
CLAMP
12 BA
TAPPED
8mm. DEEP
HOLE FOR
SPECIMEN

compliance of machine, grips and load cell was estimated to be 2.3μ/kg. This value was checked by comparing the elastic extension of a polycrystalline molybdenum specimen, estimated from the cross-head displacement, with that calculated from its static Young's modulus and also with that measured directly with the strain gauge. The machine extension was approximately linear within the 0-100 kg. load range, provided precautions were taken to minimise take-up effects which inevitably occurred at the pin couples. The composite compliance decreased as the test temperature was lowered but, at least down to 77°K, not to an extent which would have a significant effect on the computed flow curves.

The spring-loaded, knife edge clamps which were used to attach the strain gauge did cause some marking of the single crystals. A series of room temperature tests were conducted to ascertain whether this marking influenced the deformation behaviour. The flow curves obtained in both cases were in excellent agreement and there was no evidence of non-uniform deformation induced by stress concentration at the knife edges. Although the attachment of the strain gauge did not appear to have any deleterious effects on the testing at room temperature, it was not employed in the low temperature tests. The presence of stress concentrating surface markings would be expected to increase the demonstrated susceptibility of the doped specimens to brittle fracture.

9.4 Methods of Obtaining Test Temperatures

The following methods were used to obtain the test temperatures on the 'Mark I' and the Instron machines.

'Hot' water bath	$368 \pm 2^{\circ}K$
Room temperature (compression)	$287 - 293^{\circ}K$
Room temperature (tension)	$296 - 300^{\circ}K$

Solid/liquid methanol bath	$175 \pm 2^{o}K$
Solid/liquid ethanol bath	$158 \pm 2^{o}K$
Solid/liquid 2-methyl butane	$110 \pm 2^{o}K$
Liquid nitrogen	$\sim 77^{o}K$

A mercury thermometer was used to measure room and 'hot' water temperatures. The latter was obtained by using a variable transformer to control the current through a heating coil in a beaker of water. This avoided the agitation of the transducer which would have occurred in a boiling water bath. The remaining test temperatures were measured with a 'Pyrotenax' type chromel-alumel thermocouple. The thermocouple calibration accuracy of $\pm 3^{o}K$ was confirmed by the measured temperature of the methanol, ethanol and liquid nitrogen baths but the 2-methyl butane bath temperature was consistently $5^{o}K$ lower than the literature quoted melting point of $115^{o}K$. The highest purity reagent available (minimum assay 95%, non-volatile matter .005%) was employed but it is probable that sufficient impurity was present or was introduced in handling to depress the melting point by this amount.

In the compression testing, the compression rig was immersed in a dewar containing the liquid baths and temperature equilibration was assumed when the load became constant (after ~30 mins.). Two chromel-alumel thermocouples were attached to the tension rig so that the temperature of the grips and of the bulk bath adjacent to the specimen gauge length could be monitored in each test. It was found that equilibration times could be reduced to as little as five minutes by optimising the bath preparation and introduction procedure.

9.5 Preparation and Testing of Compression Specimens

Doping

The starting point for the preparation of a mechanical test specimen

was a molybdenum single crystal which had been grown and decarburised under the optimum conditions described in PART A. The full length of crystal was then centreless ground to 2.6 mm. diameter and electropolished according to the specification given in PART A. Although the removal of a 25μ surface layer by electropolishing was sufficient to remove the grinding damage indicated by Laue photography, etchpit (Guiu 1966) and transmission electron microscopic studies (Luft and Kaun 1969) have shown that damage, which may influence mechanical properties, extends to greater depths. However, the subsequent annealing treatments given to the specimens here and the ultimate removal of a further 25μ layer prior to testing, ensured that the dislocation density was reduced to the level in the as grown crystals. The orientation of the crystal was determined before it was sectioned into specimens 3.0-3.5 cm. long and 2.55 mm. in diameter. A specimen of each of the orientations used in compression was doped with oxygen or nitrogen as detailed in PART A. Three compression specimens, each ~6 mm. high and 2.5 mm. diameter, were then prepared from each of the doped specimens by the following procedure.

Cutting

The resistivity specimen was wrapped in magnetic tape which was found to provide adequate protection from surface marking when the specimen was mounted for cutting and lapping. It was then secured in a pin chuck and presented to a high speed silicon carbide cutting wheel at the slowest available feed rate (approximately 1 mm./min.) to minimise the damage layer depth. Three $\gtrsim$7 mm. long sections were cut from the resistivity specimen with the spot weld marked material being discarded.

Polishing

No chemical polishing solution could be found which gave a surface polish on molybdenum suitable for slip line analysis studies. A satisfactory electropolished surface was obtained using the solution and polishing

conditions given below.

15 ml. HCl	10 V
25 ml. conc. H_2SO_4	40 $mA/mm.^2$
75 ml. CH_3OH	$<20^{o}C$

The specimen was held in a pair of tantalum tipped tweezers which were designed to hold the specimen in a horizontal position by making point contacts on its end faces. Deep pits developed at the contact points during electropolishing. These could be removed during the lapping operation but made it necessary to grind the specimen after electropolishing rather than vice-versa. During the lapping and all subsequent operations the polished specimen surface had to be carefully protected. It was always handled with P.V.C. tweezers and stored in P.V.C. containers.

Lapping

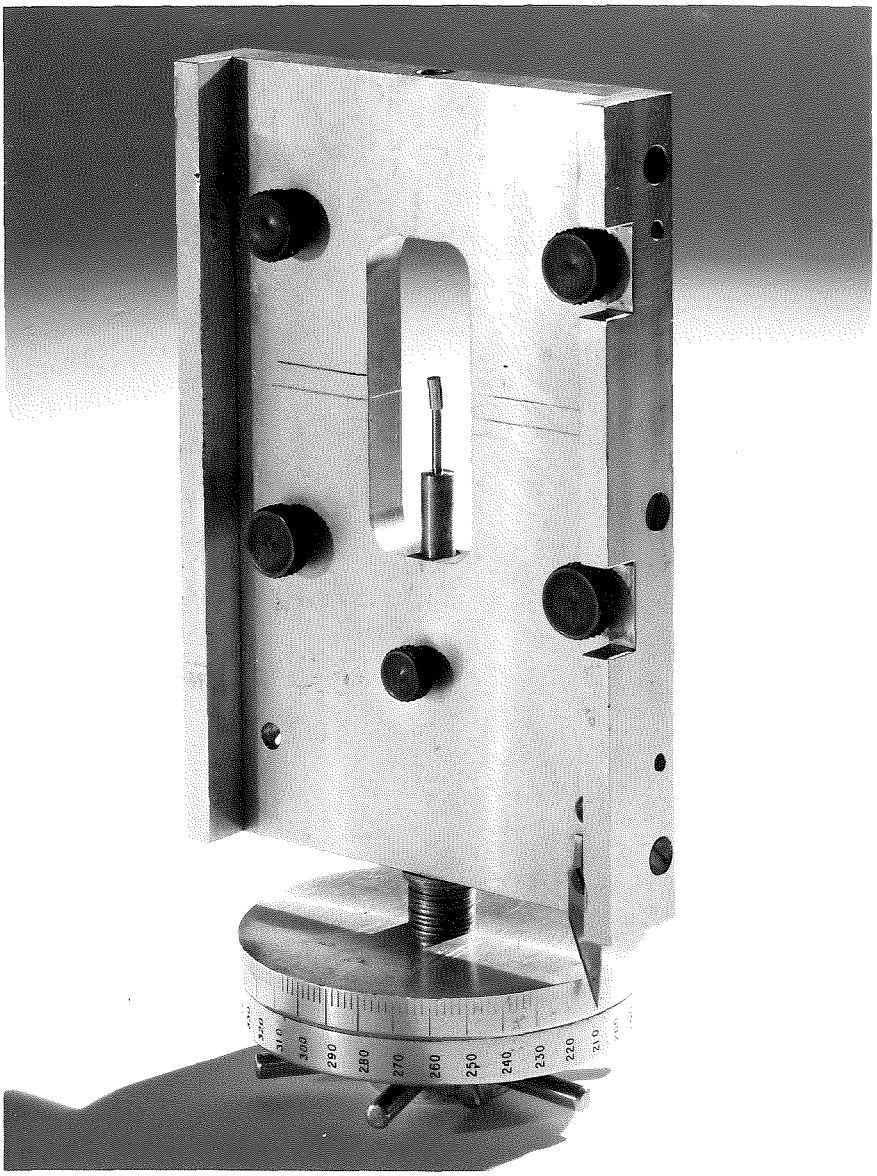
The ends of the polished specimens were ground flat and normal to the specimen axis on 280, 400 and finally 600 mesh silicon carbide paper using the lapping holder shown in Fig.B7b. The holder comprised an 8 mm. thick brass plate with four V-notches machined normal to its faces and two polyethylene clamping strips. The specimen was wrapped in magnetic tape and clamped in a position which ensured that >0.5 mm. would be ground from both its ends. After ultrasonic cleaning the specimen was weighed, its height measured with a micrometer and its mean cross-sectional area calculated using a density value for molybdenum of 10.2 gm/cc.

Testing

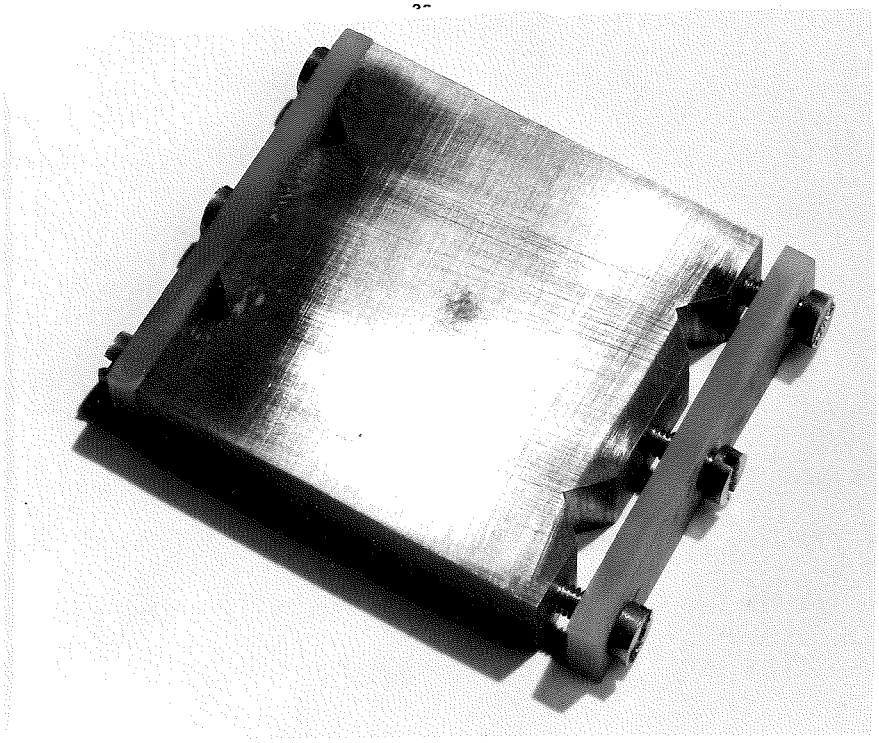
The specimen was mounted in approximately central positions on the tungsten carbide platens which had been coated with a thin but continuous layer of Rocol MoS_2 anti-scuffing lubricant. These in turn were positioned on the stainless steel anvils such that the specimen was accurately aligned

Figure B7 (a) Slip Line Analysis Goniometer

(b) Compression Specimen Lapping Holder



(a)



(b)

with the axis of the compression rig. It was not practical to simultaneously and accurately align the two tungsten carbide platens with respect to the rig axis. The variable position of the platens and hence, variable stress distribution on the rig anvils gave rise to random errors in the measured displacement. The use of an anvil lubricant introduced an additional error into the strain measurement (see Section 9.7) but it was found that reproducible flow curves could only be obtained if lubricant was used and renewed for each test. Specimens were not strained beyond 10%, this being the nominal limit beyond which anvil friction effects significantly modify the deformation behaviour.

9.6 Preparation and Testing of Tension Specimens

Doping

Decarburised, centreless ground and electropolished specimens, 3.0-3.5 cm. long and 1.05 mm. in diameter, were prepared as described in Section 9.5. These were then doped with nitrogen and oxygen as detailed in PART A. Wherever possible specimens of each of the four orientations tested in tensions were doped simultaneously.

Polishing

Only a small amount of tapering of the specimen diameter (<10μ) could be tolerated during the final electropolishing of the tension specimens if the variation of the cross-sectional area along the specimen length was to be kept to less than ± 2%. The solution specified in Section 9.5 was also used to polish the tension specimens but at a much lower current density (5 mA/mm.^{2}). This gave a poorer surface finish but the lower polishing rate (~10μ/min.) permitted finer control of the diameter. The specimen was gripped by a pair of tantalum tipped tweezers at one end and suspended vertically along the axis of a stainless steel beaker. The latter acted as

both the cathode and the container for the polishing solution. The specimen was removed from the solution at one minute intervals, inverted and polished a further minute until the required gauge diameter of approximately 1.0 $\pm$ .01 mm. was reached. The periodic inversion of the specimen served to minimise tapering.

Cutting

The polished specimen was wrapped in magnetic tape, mounted in a pin chuck and cut so as to minimise any bending forces on it. The specimen ends which usually had both spot weld and electropolish contact marks on them were discarded. After lightly deburring the squarely cut ends, the specimen was weighed and its length estimated with a traversing microscope. The mean cross-sectional area was then calculated with an estimated accuracy of $\pm$ 2% and where necessary independently checked by surveying the gauge length with a micrometer screw gauge.

Testing

The tension rig grips were first positioned 20 mm. apart using the cross-head manual control and vernier callipers. The specimen was clamped in position and if required, the strain gauge was attached to the central 10 mm. of the gauge length. The cross-head was then translated to bring the specimen under a prestress of ~1 kg/mm.^{2}, the strain gauge zeroed and the test conducted under the following conditions.

Cross-head speed	200μ/min.
Nominal strain rate	1.7 x 10^{-4}/sec.
Load sensitivity	50 kg. F.S.O.
Strain sensitivity (strain gauge)	10^{-4}

During the room temperature tests, where the strain gauge was employed, it was found useful to monitor both the strain rate measured by the strain gauge and that calculated from the cross-head speed corrected for machine softness. A comparison of the two permitted ready identification of localised yielding or a constriction occurring inside or outside the electromechanical gauge length.

Specimens were not usually strained beyond 10% but some of the H.V.A. <149> specimens were strained further to assess the constricting and embrittling effects of the friction grips. Since the majority of specimen failures at low temperatures occurred by necking and/or fracture, either in or adjacent to the grips, there is little doubt that the stress concentration at the grips was having a detrimental effect on ductility. Many of the doped specimens tested at low temperatures fractured soon after yielding but in any event tests were terminated after a few percent strain to allow subsequent temperature change testing.

The gauge lengths of most of the specimens were examined using oblique illumination on a light microscope to make a qualitative assessment of slip line morphology. The gauge lengths were also surveyed after deformation with a micrometer screw gauge to assess the uniformity of deformation.

9.7 Processing of Mechanical Test Data

The test data recorded autographically during the compression tests required correction for anvil and lubricant punching before stress-strain curves could be computed. The displacement measured by the transducer (X_T) could be resolved into the components given below.

$$X_T = X_P + X_E + X_A + X_L$$

where X_P = Specimen plastic compression

X_E = Specimen elastic compression

X_A = Anvil elastic indentation

X_L = Lubricant punching

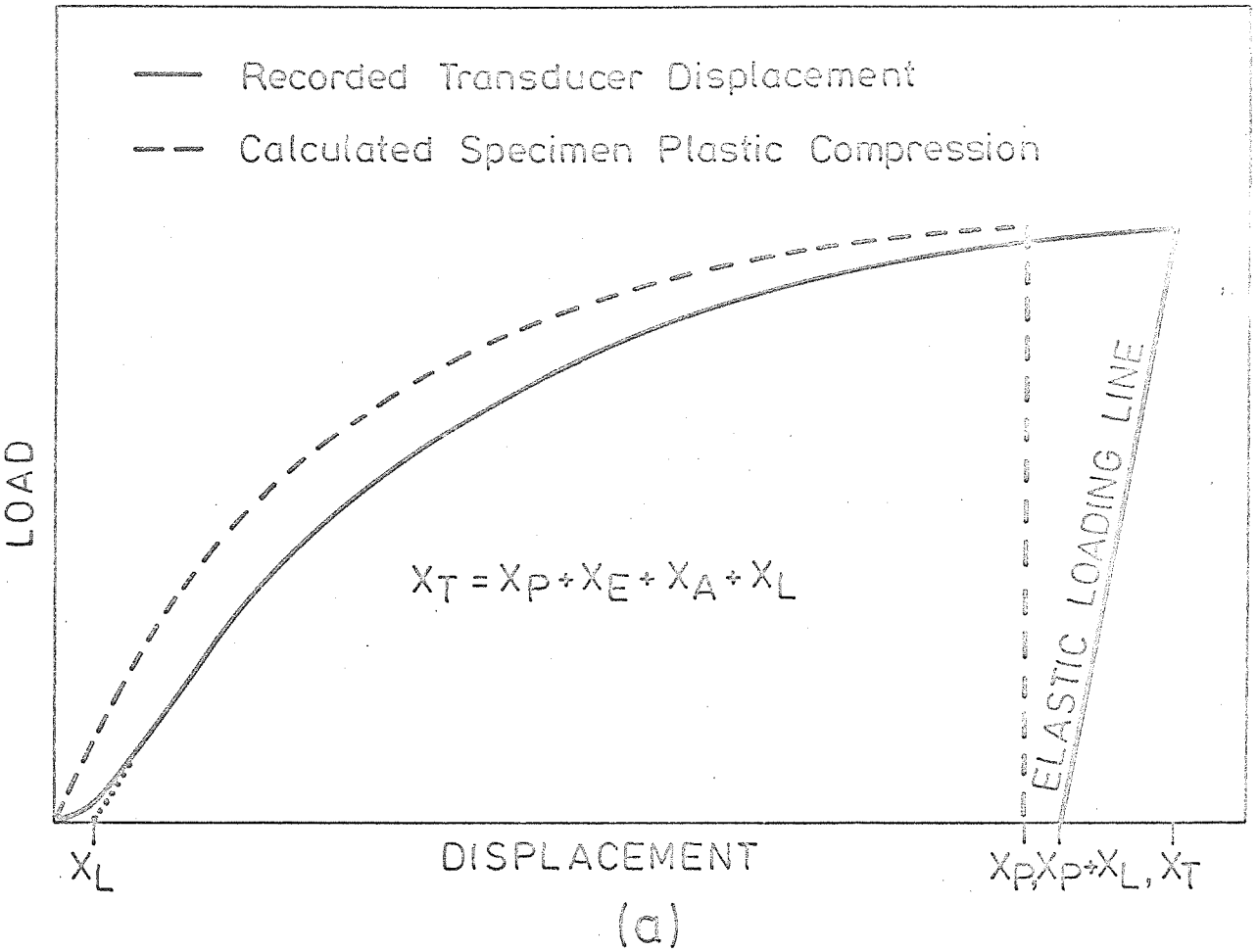
By rapidly unloading the specimen at the end of the test, and recording the recovered elastic displacement ($X_A + X_E$) from the maximum load, the combined specimen plastic compression and lubricant punching ($X_P + X_L$) could be estimated. Progressive compression of the MoS_2 lubricant occurred with increasing load during the test. With discontinuously yielding specimens X_L was estimated by extrapolating the linear elastic loading line to zero stress. With continuously yielding material a more reliable estimate of X_L was obtained by comparing the value of $X_P + X_L$ estimated from the autographic record with that of X_P measured directly with a micrometer after the test. Finally, by assuming the anvil indentation to be proportional to the load, an elastic loading line was constructed and used to compute a load versus specimen plastic compression curve as shown in Fig.B8a. This curve was then converted to a stress-strain curve. The absolute error in the computed plastic strain was of the order of 0.2% strain and was due principally to the uncertainty of the magnitude of X_L.

The displacement measured by the strain gauge in the tension tests was used directly to compute the nominal specimen strain. When the strain gauge was not used, the cross-head displacement (X_C) was corrected for machine hardness as shown diagrammatically in Fig.B8b. The machine extension (X_M) has been subtracted from X_C to give a load versus total specimen extension ($X_P + X_E$) curve. A number of control tests on H.V.A. <149> crystals showed the stress-strain curves computed from the cross-head and strain gauge displacements to be in good agreement. Where disagreement did arise, it was traced to some microscopic inhomogeneity in the specimen deformation. Typically the formation of a neck at the specimen grips would cause the cross-head

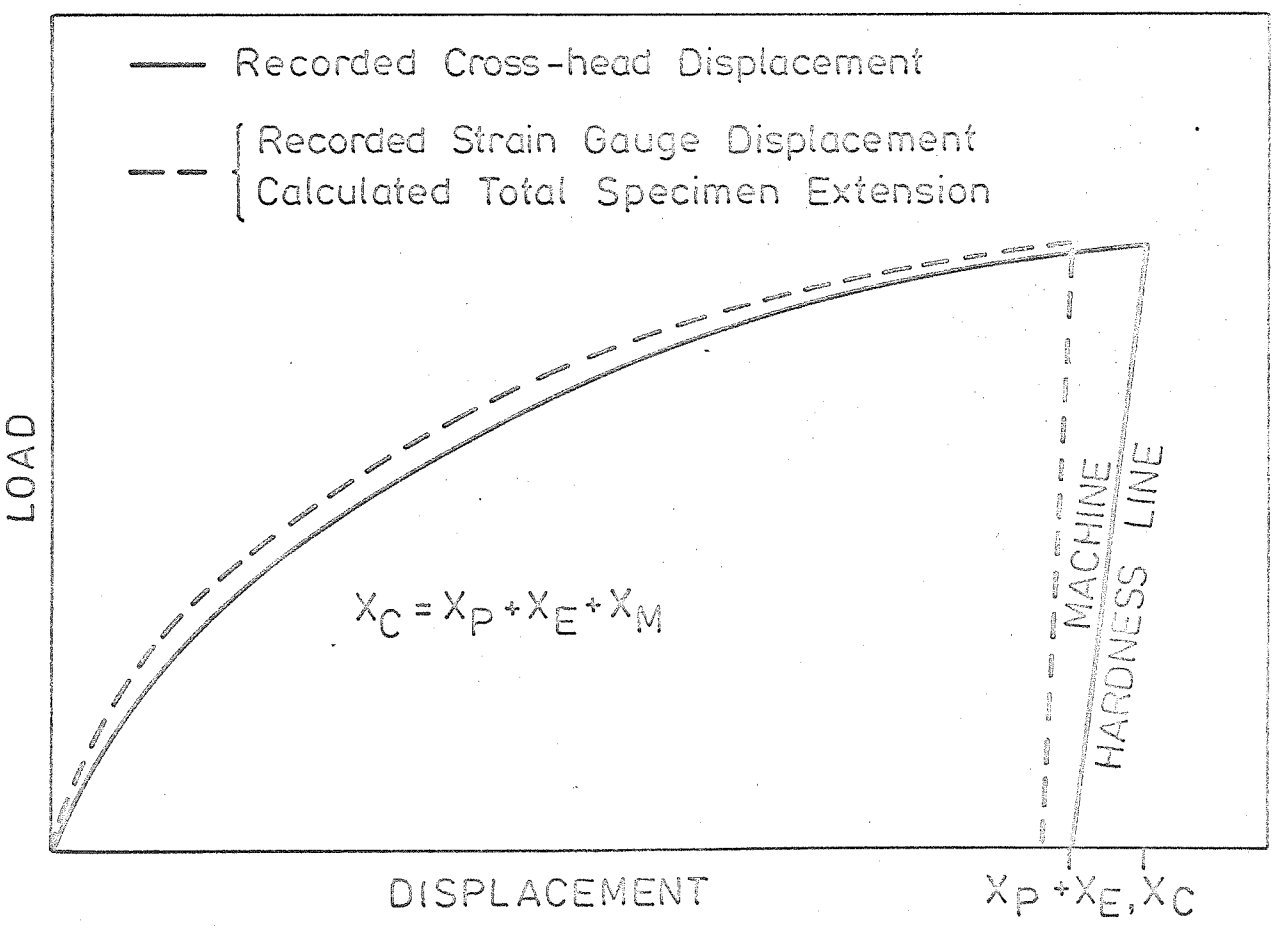
Figure B8 Diagrammatic Representation of Computation Procedure for

(a) Compression Flow Curves

(b) Tension Flow Curves


Recorded Transducer Displacement
Calculated Specimen Plastic Compression
LOAD
$X_T = X_P + X_E + X_A + X_L$
ELASTIC LOADING LINE
X_L
DISPLACEMENT
$X_P, X_P + X_L, X_T$

(a)


Recorded Cross-head Displacement
Recorded Strain Gauge Displacement
Calculated Total Specimen Extension
LOAD
$X_C = X_P + X_E + X_M$
MACHINE HARDNESS LINE
DISPLACEMENT
$X_P + X_E, X_C$

(b)

computed strain to be greater than the strain gauge measured strain because much of the strain occurred outside the strain gauge length.

When comparing flow and, particularly yield behaviour of material tested in tension and compression, consideration should be given to the respective true, as distinct from nominal, specimen strain rates. The relationship between the specimen strain rate, $\dot{\varepsilon}_s$, and the cross-head speed, $\dot{X}_s$, which depends upon both the machine hardness and the specimen geometry is given below.

$$\dot{\varepsilon}_s = \frac{\dot{X}_s}{L_s} - \dot{\sigma}\frac{A_s M}{L_s}$$

where	TENSION	COMPRESSION
L_s, specimen length (mm.)	20	6
A_s, specimen cross-sectional area ($mm.^2$)	1	5
$\dot{\sigma}$, stress rate ($kg./mm.^2 min.$)	-	-
$\dot{X}_s$, cross-head speed (mm./min.)	0.2	0.105
M, machine compliance (mm./kg.)	2.3×10^{-3}	2.5×10^{-4}
$\dot{\varepsilon}_s$, specimen strain rate (min.)	$10^{-2} - 1.2 \times 10^{-4}\dot{\sigma}$	$1.75 \times 10^{-2} - 2.1 \times 10^{-4}\dot{\sigma}$

The difference in the specimen strain rates for tension and compression testing would not change the flow stress level significantly but the greater 'effective hardness' of the tension testing system would promote sharper yielding behaviour.

9.8 Differential Temperature Change Testing

Differential temperature change tests were employed on the tension specimens to determine the reversible flow stress as a function of temperature. In this type of test there is sometimes uncertainty as to whether the

assumptions made when analysing the results are valid in practice. This made it desirable to conduct a number of control experiments to test some of these assumptions and also to assess the general reproducibility of the data.

Probably the most important assumption made is that during the temperature change the dislocation structure (particularly the density of dislocations) is unchanged. It is sometimes found in experiment that the changes in flow stress occurring for downward and upward temperature changes are not the same. This hysteresis behaviour is usually associated with pseudo yield points which suggest some type of structural instability.

Control experiments to test the reversibility of the flow stress were made on <149> H.V.A. specimens prestrained approximately 7% at 298°K. The temperature was cycled between 298°K, 158°K and 77°K in both upwards and downwards directions and for all temperature combinations. The yield points obtained on reloading were usually quite sharp, but only in the case of the temperature changes between 298°K and 77°K were prominent load drops obtained. The stress increments were found to be reversible and reproducible in all cases except for the temperature cycling between 298°K and 77°K where the downward stress increment appeared larger than the upward. The necessity of having to warm specimens, deformed in the solid/liquid ethanol bath, to room temperature for drying before cooling to the next test temperature did not cause any load drops or hysteresis effects. It was concluded that provided no temperature cycling was done directly between 77°K and 298°K, the flow stress was reversible.

This temperature cycling data could be interpreted with even greater confidence if it were further established that the change in the reversible flow stress with temperature is independent of strain. This is of most concern when the material shows a large temperature dependent work hardening rate as does molybdenum at certain orientations. The effect of the prestrain magnitude was only assessed for <149> H.V.A. crystals. The results, which

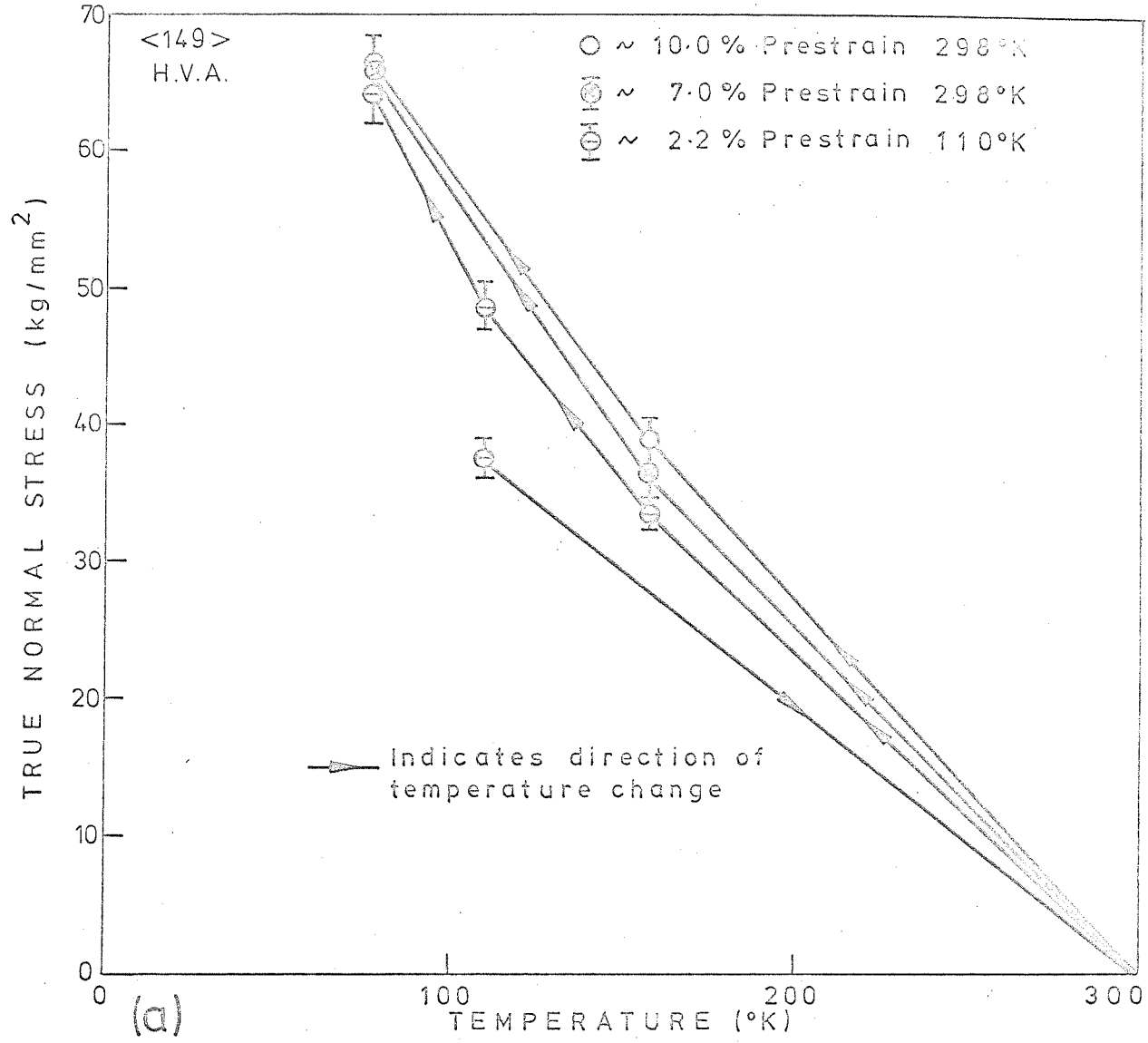
are shown in Fig.B9a for 298°K prestrains of 7.0% and 10.0%,indicate only a small effect. But this cannot be validly generalised to other orientations, temperatures and strain ranges where the work hardening rate is larger.

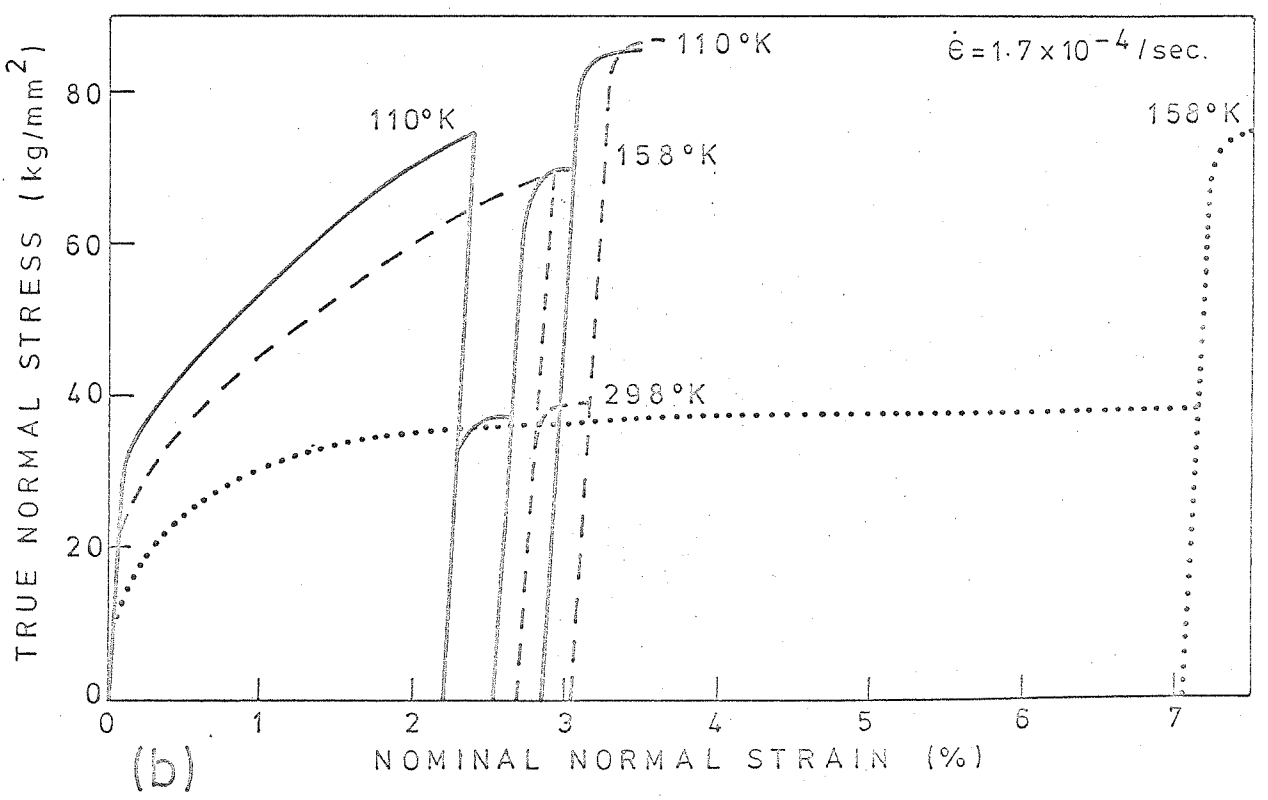
Further tests were conducted which gave some information about the effect of prestrain temperature and/or magnitude on the temperature dependence of the flow stress. <149> H.V.A. crystals were prestrained 2-3% at 110°K and 158°K and then subjected to a number of temperature cycles. The flow curves determined in these tests and the 'effective' stress (flow stress minus the room temperature flow stress) plotted against temperature are shown in Fig.B9 where they are compared with the 298°K, 7.0% and 10.0% prestrained material. It can be seen that a hysteresis of ~10 kg./mm.^{2} or >20% of the stress increment occurred for temperature changes between 110°K and 298°K in the 110°K prestrained material. A similar stress hysteresis of ~5 kg./mm.^{2} or >15% of the stress increment was observed in both H.V.A. and 96 at.ppm. nitrogen doped <001> crystals prestrained 3% at 158°K and subsequently cycled between 298°K and 158°K. No pseudo yield points or load drops were associated with any of these hysteresis effects. When a 34 at.ppm. nitrogen doped <149> specimen was subjected to the same prestrain and temperature cycling sequence as the H.V.A. <149> specimen, no hysteresis was observed. Similarly, both H.V.A. and 96 at.ppm. nitrogen doped <011> crystals, which were prestrained and temperature cycled in an identical fashion to the <001> crystals, showed no hysteresis effects.

These results, which will be further discussed in Chapter 11, appeared to indicate that hysteresis effects would prevent any reliable determination of a reversible flow stress on material subjected to low temperature prestrains. So, all the 'effective' stress versus temperature data reported in Chapter 10 were obtained on material prestrained at room temperature. Only downwards temperature changes were made between 298°K, 158°K and 77°K and the strain administered at each temperature was the minimum consistent with a clear definition of the flow stress level. At the end of each deformation

Figure B9(a) 'Effective' Stress versus Temperature for <149> H.V.A. Crystals with Different Prestrains

(b) Flow Curves for H.V.A. <149> Crystals Subjected to Differential Temperature Changes


<149>
H.V.A.
O ~ 10·0 % Prestrain 298°K
⊖ ~ 7·0 % Prestrain 298°K
⊖ ~ 2·2 % Prestrain 110°K
Indicates direction of temperature change
TRUE NORMAL STRESS (kg/mm²)
TEMPERATURE (°K)
0
10
20
30
40
50
60
70
0
100
200
300
(a)


110°K
158°K
298°K
ė = 1·7 x 10⁻⁴ /sec.
TRUE NORMAL STRESS (kg/mm²)
NOMINAL NORMAL STRAIN (%)
0
20
40
60
80
0
1
2
3
4
5
6
7
(b)

the specimen was rapidly unloaded to prevent plastic relaxation occurring and during all the temperature changes a tensile stress of ~1 kg/mm.^{2} was applied to maintain specimen alignment.

9.9 Reproducibility of Mechanical Test Results

The difficulties of material preparation prevented any repetition of the majority of both the tension and compression tests reported in Chapter 10. Some preliminary testing was undertaken to assess the reproducibility of the results but these were largely confined to the H.V.A. material.

Several <149> H.V.A. crystals were tested in compression at each of the test temperatures. The reproducibility of the flow stress was found to be a function of temperature and varied from approximately $\pm$ 2% at 290^{o}K to $\pm$ 5% at 77^{o}K. The uncertainty of the specimen cross-sectional area was $\pm$ 0.2% so other material and test variables were contributing to this variation. The errors in the strain measurement ($\pm$ 0.2% strain) meant that the reproducibility of the stress level at small strains, where the work hardening rate was high, was poor. Little significance should be given to any 'yield' stress implied by the intercept of the flow curves on the stress axis of stress-strain diagrams presented in Chapter 10. The data scatter for the doped compression specimens would be expected to be greater than the H.V.A. material because of the larger number of variables in the material preparation. The variation in the concentration between the three test specimens cut from a single doped resistivity specimen would probably be the most important of these.

The control experiments for the tension tests were confined to the testing of several H.V.A. <149> specimens at 298^{o}K. These showed a reprodubility of the stress, independent of strain, of $\pm$ 2% which was approximately equal to the uncertainty of the specimen cross-section area. The same trend of increasing scatter with decreasing temperature as shown by

the compression specimens would be expected for the tension specimens. The scatter in the stress-strain data is likely to have been greater for the doped specimens because of the greater sensitivity of discontinuously yielding material to stress concentrating surface imperfections and bending effects. In only one instance, where it was considered important to establish the reliability of a particular test result (see Section 10.3.3), was a test repeated on doped material. In this instance the reproducibility was surprisingly good ($< \pm 4\%$) but is thought to be atypical of the doped specimens in general.

The results given in Fig.B9a provide the only basis for estimating the likely errors of the 'effective' stress determined in the differential temperature change tests. They suggest that the error bars corresponding to the uncertainty of the specimen cross-sectional area ($\pm 2\%$) are realistic estimates of the random errors. These error bars have been used in all 'effective' stress versus temperature plots in Chapter 10 where they are also used to indicate when a specimen failed by brittle fracture before yielding. In such cases the fracture stress defined a lower limit for the flow stress and this is indicated by the absence of an upper error bar.

9.10 Slip Trace Analysis

The cumulative slip traces on a number of deformed compression specimens were analysed using the Nomarski interference contrast technique. The specimen was affixed with 'twin-stick' to the post of the one-circle goniometer shown in Fig.B7a. The specimen was then Laued to determine the rotation of the compression axis which occurred during the deformation and also its radial orientation on the goniometer post. The goniometer was designed to fit a Reichert MeF inverted stage microscope. This was used in conjunction with a protractor eyepiece to determine the slip trace orientations at 10° intervals around the specimen circumference. When these

are plotted on a stereographic projection of the crystal orientation they fall on a great circle corresponding to the trace of their slip plane. In the majority of the analyses where traces were straight and sharp, but only evident over a restricted range of circumference, the orientation of the identified slip plane was accurate to approximately $\pm 4^{\circ}$.

Chapter 10

RESULTS

10.1 Introduction

Table B2 gives the compositions, orientations and test conditions for the molybdenum-nitrogen and molybdenum-oxygen alloy specimens tested in this investigation. Control H.V.A. specimens were also tested for all the orientations and most of the temperatures indicated. Further details concerning the crystal orientations used in the compression and tension tests are given in Fig.B10a.

The two major orientations used in the compression tests were the <149> and <122>, which were chosen to give single slip on the $(\bar{1}01)$ plane and in the twinning sense on the $(\bar{2}11)$ plane respectively. One set of specimens with a <113> easy glide orientation was also tested.

The <149> easy glide orientation was the principal one used in the tension tests but specimens of the three symmetry orientations <001>, <011> and <111> were also tested. The latter were chosen because of their contrasting yield and work hardening behaviour and the consequent interest in any orientation dependence of the alloying effects. Considerable care was taken in seeding these orientations. The <111> and <001> orientations are metastable in tension and if the initial crystal orientation deviates more than a few degrees from this, single glide will occur and the crystal axis will rotate away from the symmetry orientation. The <011> orientation is stable but it is in general undesirable to have crystal axes more than 5° from the poles. Should they be, the resultant single slip which occurs as the

ORIENTATION	TEMPERATURE (^{o}K)	COMPRESSION		TENSION			
		CONC. NITROGEN (at.ppm.)	CONC. OXYGEN (at.ppm.)	CONC. NITROGEN (at.ppm.)			CONC. OXYGEN (at.ppm.)
<149>	290	7	22				
	298			34	93	216	80
	158	7	22	34	93	216	88
	110			34	93	216	100
	77	7	22				
<113>	368	8					
	175	8					
	77	8					
<122>	290	7	22				
	158	7	22				
	77	7	22				
<011>	298				96		93
	158				96		
	110				96*		
<001>	298				96		100
	158				96		
<111>	298				96†		94

*No H.V.A. control

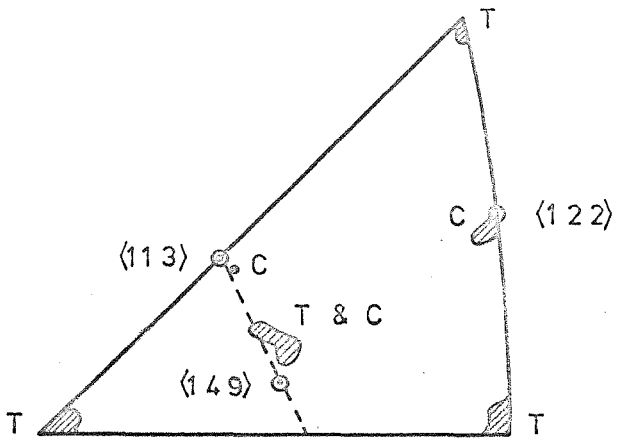
†Test Repeated

Table B2 Details of the Molybdenum-Interstitial Alloy Mechanical Test Specimens

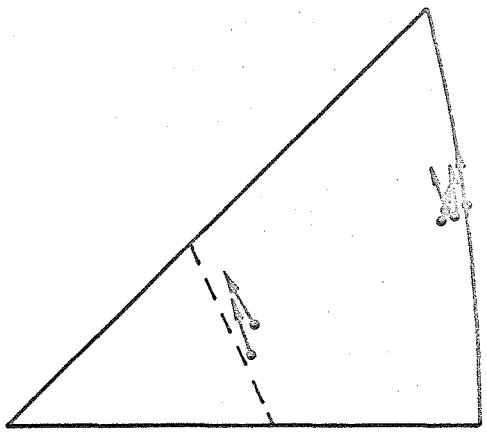
Figure B10 (a) Orientations of Tension (T) and Compression (C) Test Specimens

(b) Axis Rotations of Crystals Tested in Compression

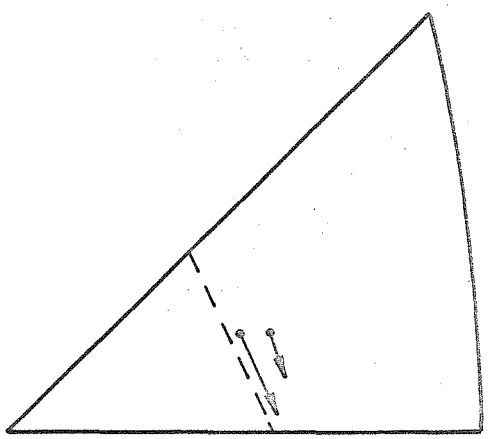
(c) Axis Rotations of <149> Crystals Tested in Tension



(a)



(b)



(c)

crystal rotates back to the symmetry orientation may influence the nature of the multiple slip which follows.

The flow stress curves, and the yield and 'effective' stress versus temperature data presented in this chapter have been plotted as true normal stress rather than the more usual shear stress. There is considerable uncertainty about the primary slip systems for the symmetry orientations and at low temperatures the primary ($\bar{1}01$) plane for the easy glide orientations may not operate till large strains. Thus, the normal stress has been preferred in the initial presentation of results because of the considerable qualification which must accompany the resolution of stresses onto particular slip planes.

The yield stress in the yield stress versus temperature plots for the tension tests has been defined as a 0.2% proof stress which, in the discontinuously yielding material, approximates to a lower yield stress. The 'effective' stress in the 'effective' stress versus temperature plots has been calculated by subtracting the room temperature flow stress from that at the test temperature. In both types of temperature plot the data points have been joined by straight lines for simplicity.

The results of the slip trace analysis reported in Section 10.4 have been presented on standard [001] stereograms where the 'Vesely' curves (see Section 8.1) and the primary maximum resolved shear stress plane are also shown. A data point on the stereogram represents the direction of a slip trace which is necessarily defined by the intersection of the slip plane and a plane tangential to the surface at the point of observation. No distinction has been made between traces observed on diagonally opposed surfaces since in all cases diagonal symmetry was observed. However, a qualitative distinction has been made between clearly defined (full circle) and poorly defined (open circle) traces.

10.2 Crystals Deformed in Compression

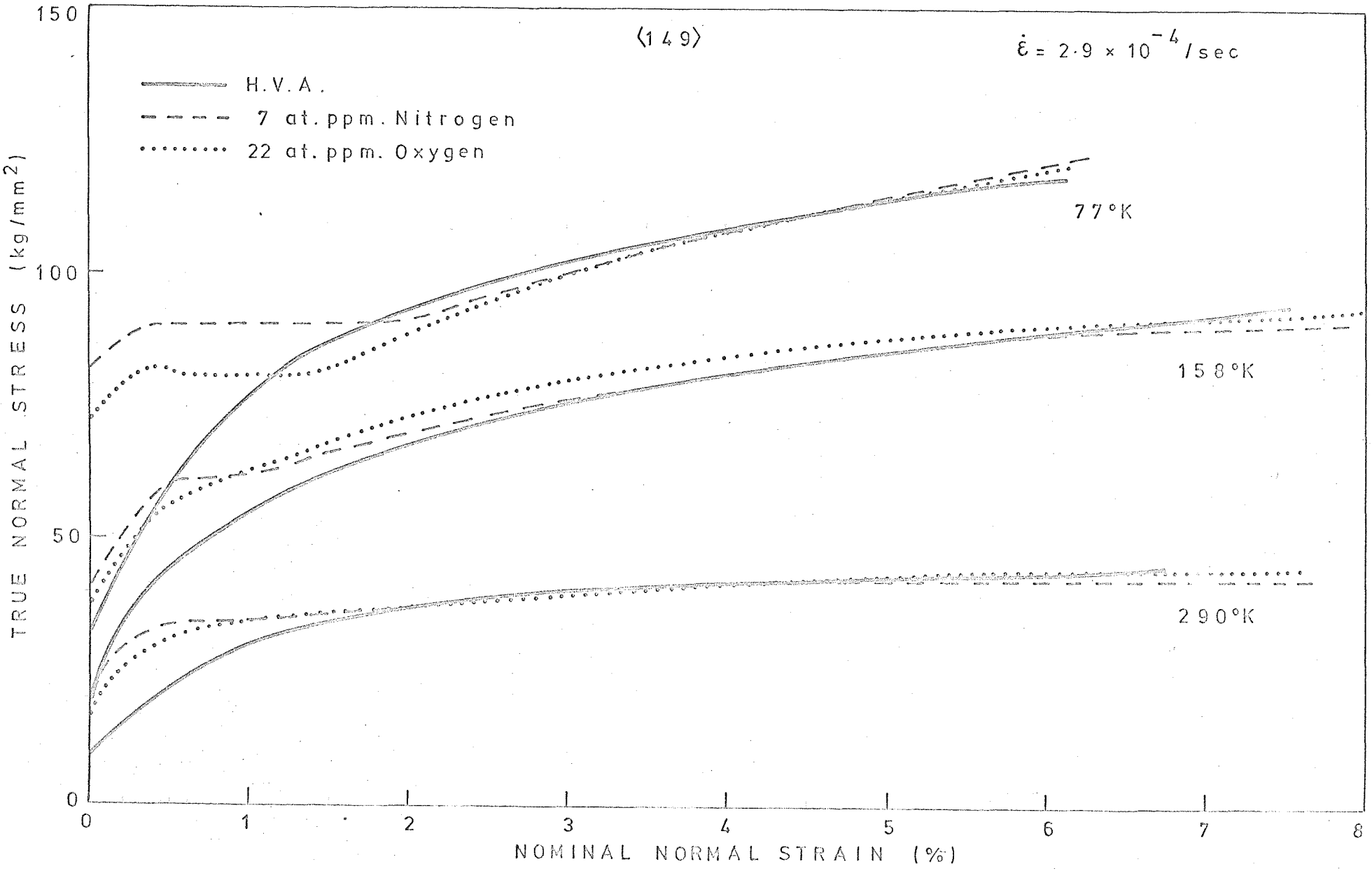
10.2.1 <149> and <113> Crystals

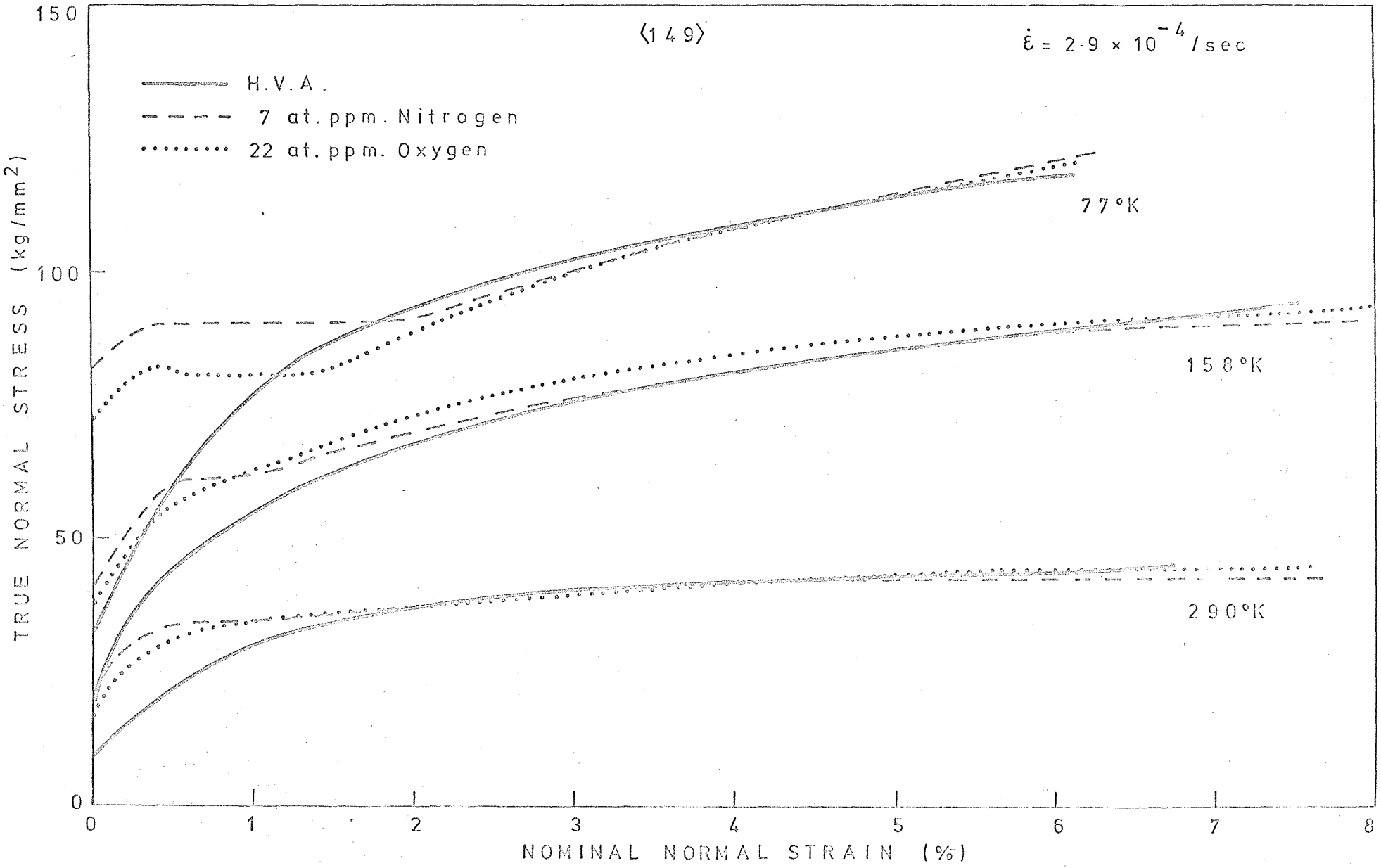
The flow curves for the oxygen and nitrogen doped and the H.V.A. <149> crystals are given in Fig.B11. The H.V.A. specimens yielded continuously showing quasi-parabolic flow curves while all the doped specimens yielded discontinuously. The nitrogen doped material showed a perceptible yield point and constant stress yield elongation at 290°K. The latter increased in magnitude as the test temperature was decreased and at 77°K was >1% strain. The oxygen doped material behaved similarly at low temperatures but at 290°K the yield was more rounded and there was no perceptible yield elongation. In general, where load drops occurred they were small and rounded, and all the discontinuously yielding specimens showed some preyield microstrain ($\geq 10^{-4}$ strain).

The intercept of the flow curves with the stress axis is not a reliable indication of the stress at which the first detectable plastic flow occurred (i.e. the proportional limit). However, it is clear that the macroyield stress defined as a 1% proof stress or 'lower' yield stress is consistently greater for the doped material than for the H.V.A. and, at least at 77°K, nitrogen caused a stronger hardening effect than oxygen. At large strains there was no significant difference between the flow stress levels of the doped and H.V.A. material.

Both the doped and H.V.A. specimens tested at 290°K displayed macroscopically uniform deformation but as the test temperature was decreased there was increasing evidence of non-uniform deformation along their gauge lengths. After deformation at 77°K some barrelling and zonal deformation was in evidence in both the H.V.A. and the doped specimens. There was also a notable absence of twinning in the tests reported here. However, in an earlier exploratory test on a nitrogen doped <149> crystal at 77°K a

Figure B11 Flow Curves of <149> Crystals Tested in Compression


$\dot{\varepsilon} = 2.9 \times 10^{-4}$ /sec
H.V.A.
7 at. ppm. Nitrogen
22 at. ppm. Oxygen
77°K
158°K
290°K
TRUE NORMAL STRESS (kg/mm²)
NOMINAL NORMAL STRAIN (%)
150
100
50
0
0
1
2
3
4
5
6
7
8


$\dot{\varepsilon} = 2.9 \times 10^{-4}$ /sec
H.V.A.
7 at. ppm. Nitrogen
22 at. ppm. Oxygen
77°K
158°K
290°K
TRUE NORMAL STRESS (kg/mm²)
NOMINAL NORMAL STRAIN (%)
150
100
50
0
0
1
2
3
4
5
6
7
8

characteristic click and load drop occurred and a <112> twin trace was later identified on the specimen surface. This proved to be the only incidence of twinning in the whole mechanical test series.

The rotations of the compression axes for <149> H.V.A. and doped specimens tested at 290°K are given in Fig.B10b and are generally those expected for primary ($\bar{1}01$) slip. No significant rotations of the compression axes of crystals deformed up to 6% strain at 77°K were observed.

A further set of stress-strain curves for <113> nitrogen doped and H.V.A. crystals are given in Fig.B12. These were tested over a wider range of temperatures but the effect of doping was observed to be similar to that for the <149> orientation crystals.

10.2.2 <122> Crystals

Fig.B13 gives the stress-strain curves for the <122> crystals. The H.V.A. material of this orientation showed a yield point which was quite distinct at the low test temperatures. No yield elongation was observed although at 77°K the work hardening rate immediately after yield was very low. The doped material showed a much sharper yield point followed by a constant stress yield elongation which increased from a fraction of a percent at 290°K to ~5% at 77°K. The 77°K yield elongation for both the nitrogen and oxygen doped material was noteworthy for both its extent and the large load fluctuations accompanying it. At 290°K the comparative behaviour of oxygen and nitrogen doped material was similar to that for the <149> crystals with only the nitrogen specimen showing a distinct yield elongation.

The discontinuous yielding behaviour of the <122> H.V.A. crystals obviates to some extent the difficulties of comparing the macroyield behaviour of H.V.A. and doped material. Inspection of the flow curves indicates that a 'lower' yield stress defined at 1% plastic strain provides a reasonably satisfactory basis for comparison and this has been plotted against temperature

Figure B12 Flow Curves of <113> Crystals Tested in Compression

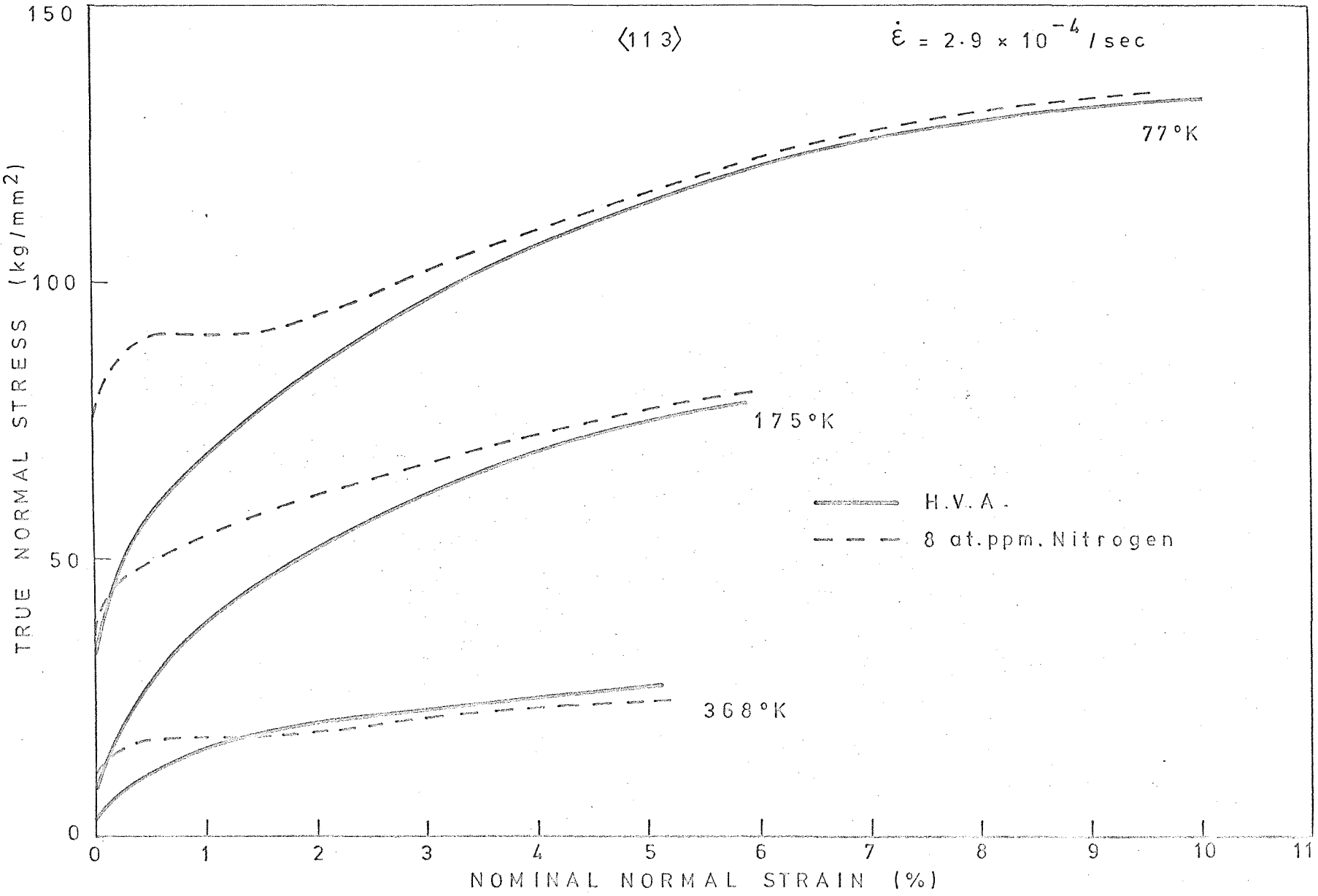
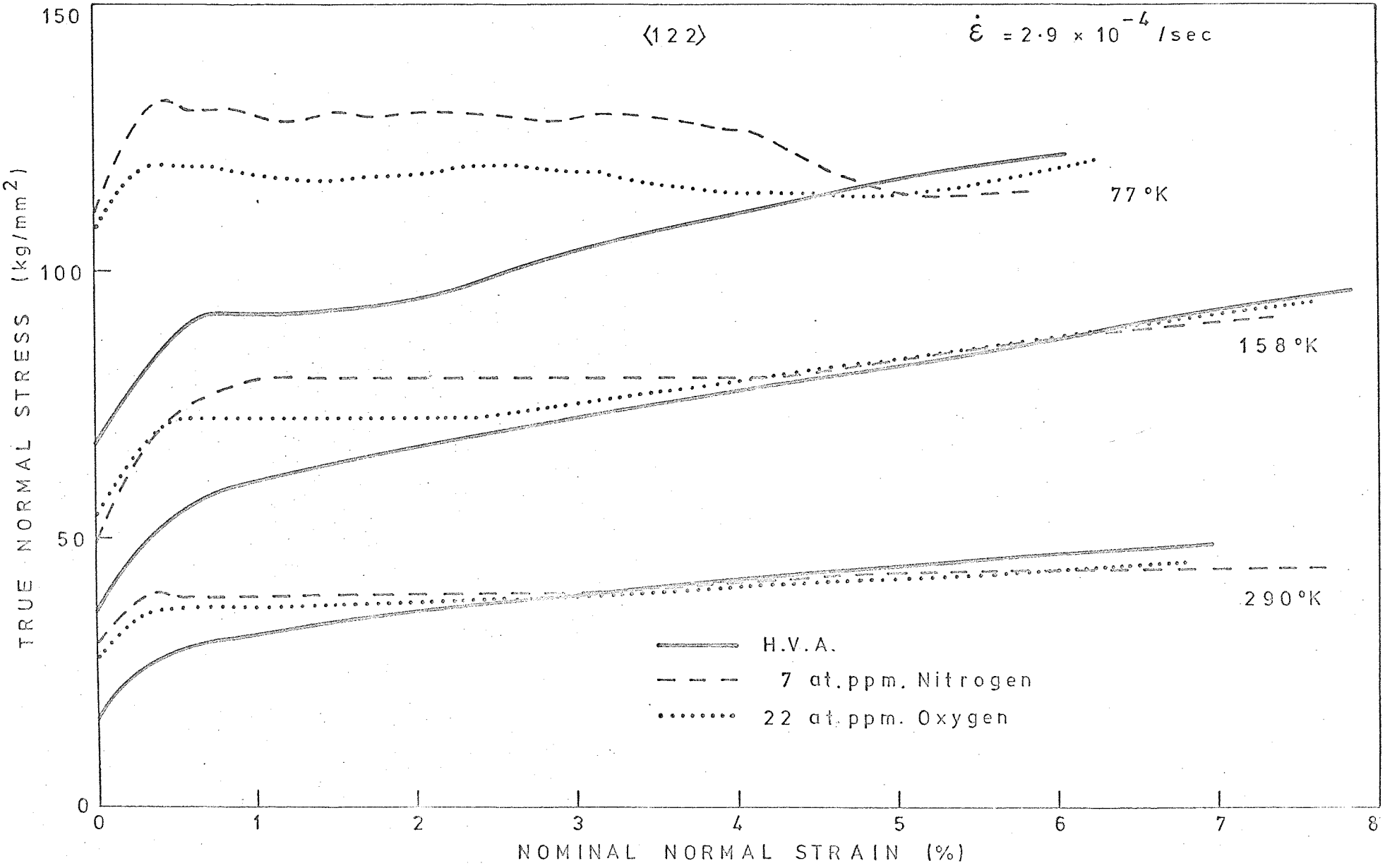

150
100
50
0
TRUE NORMAL STRESS (kg/mm2)
⟨11 3⟩
$\dot{\varepsilon}$ = 2·9 × 10^{-4} / sec
77 °K
175 °K
368 °K
H.V.A.
8 at.ppm. Nitrogen
0
1
2
3
4
5
6
7
8
9
10
11
NOMINAL NORMAL STRAIN (%)

Figure B13 Flow Curves of <122> Crystals Tested in Compression


⟨1 2 2⟩
$\dot{\varepsilon}$ = 2·9 × 10^{-4} /sec
77 °K
158 °K
290 °K
H.V.A.
7 at.ppm. Nitrogen
22 at.ppm. Oxygen
TRUE NORMAL STRESS (kg/mm^2)
NOMINAL NORMAL STRAIN (%)
150
100
50
0
0
1
2
3
4
5
6
7
8

for the H.V.A. and doped material in Fig.B14. It is evident that the doping caused an increase in the temperature dependence of the yield stress and that 7 at.ppm. nitrogen caused a larger increase than 22 at.ppm. oxygen. At large strains there was no significant difference in the flow stress levels between the doped and H.V.A. crystals.

Macroscopic inspection of the specimens after deformation revealed the same general trend found with the <149> crystals. However, the doped specimens after 77°K deformation showed a distinctive 'ripply' surface profile which was not evident in the H.V.A. specimens (see Fig.B15a).

The rotations of the compression axes of some of the doped and H.V.A. <122> crystals deformed at both 290°K and 77°K are given in Fig.B10b.

10.3 Crystals Deformed in Tension

10.3.1 Nitrogen Doped <149> Crystals

The stress-strain curves for the nitrogen doped and control H.V.A. <149> crystals are given in Fig.B16. The H.V.A. specimens tested at room temperature showed quasi-parabolic flow curves in good agreement with that observed in compression. They underwent up to 15% uniform elongation before constriction commenced producing a very localised chisel-shaped neck. After 7% strain they had acquired elliptical cross-sections and optical examination revealed dense, fine slip lines.

All the doped specimens tested at room temperature yielded discontinuously, frequently showing load drops, but the strain gauge gave no evidence of any Lüders band propagation. They also showed very low work hardening rates, and, in the case of the 34 at.ppm. and 93 at.ppm. specimens, a lower flow stress than the H.V.A. material at large strains. Micrometer measurements after 7% strain indicated an elliptical cross-section consistent with single glide, but also several slight tapers (<10μ) along the specimen lengths.

Figure B14 'Lower' Yield Stress versus Temperature for
H.V.A. and Doped <122> Crystals

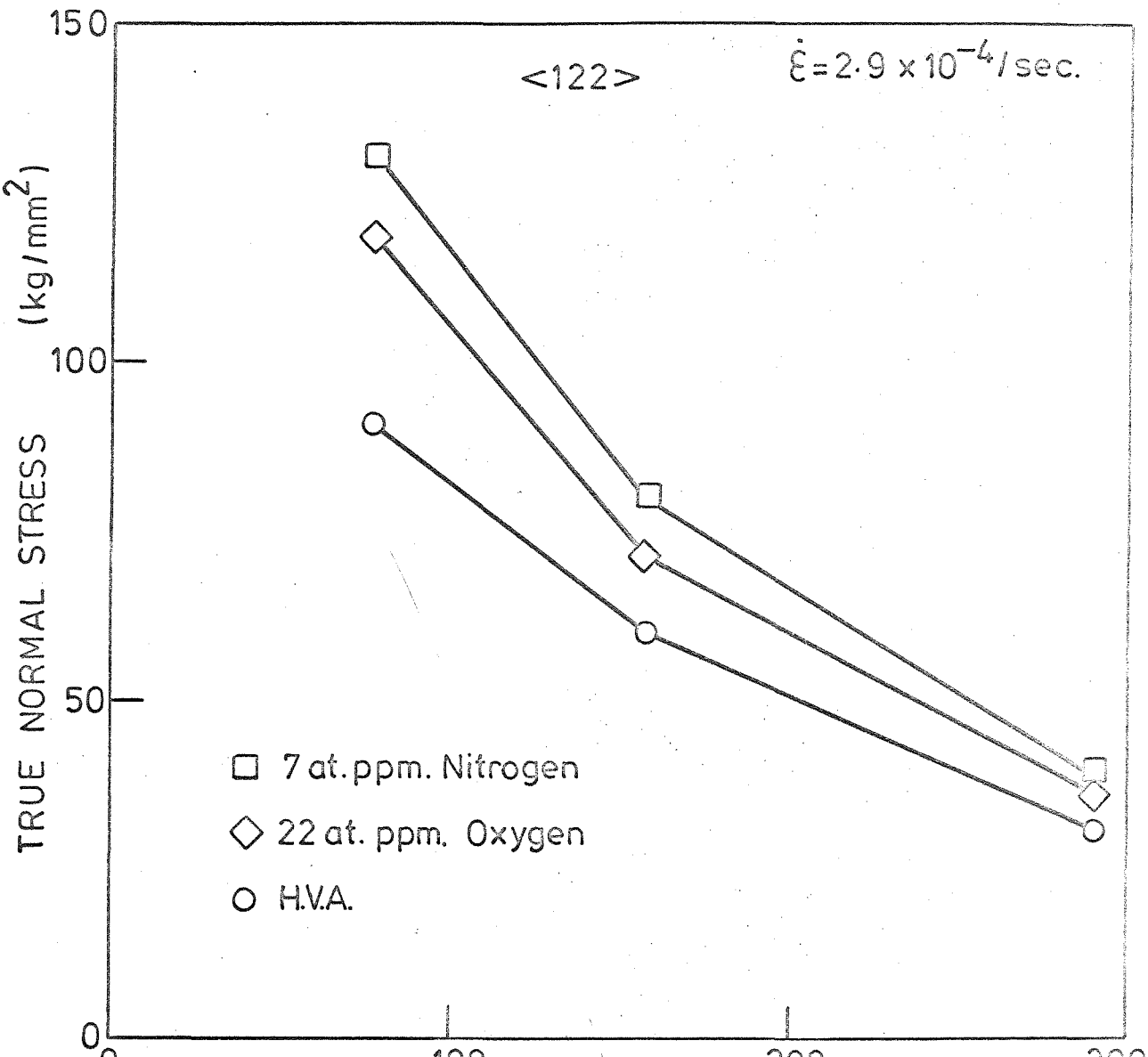
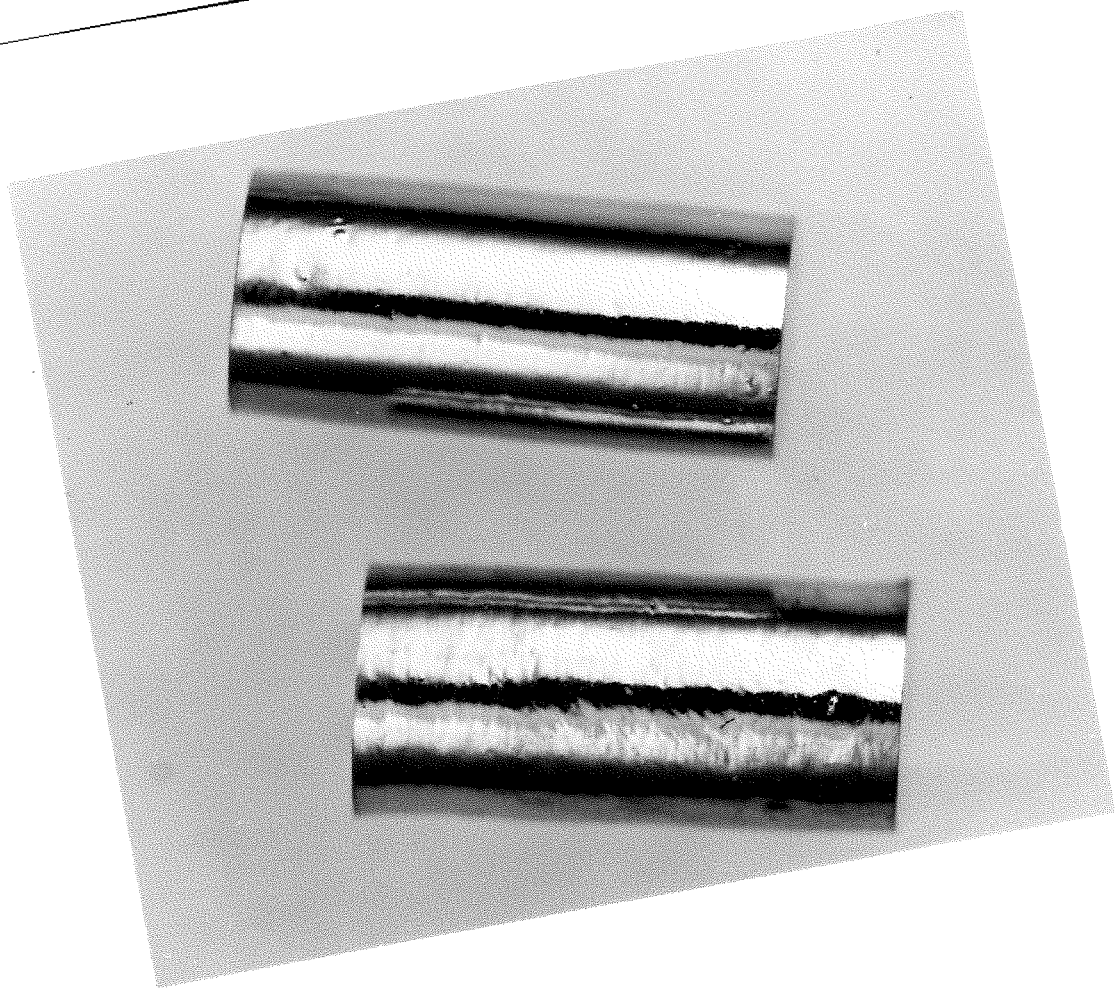
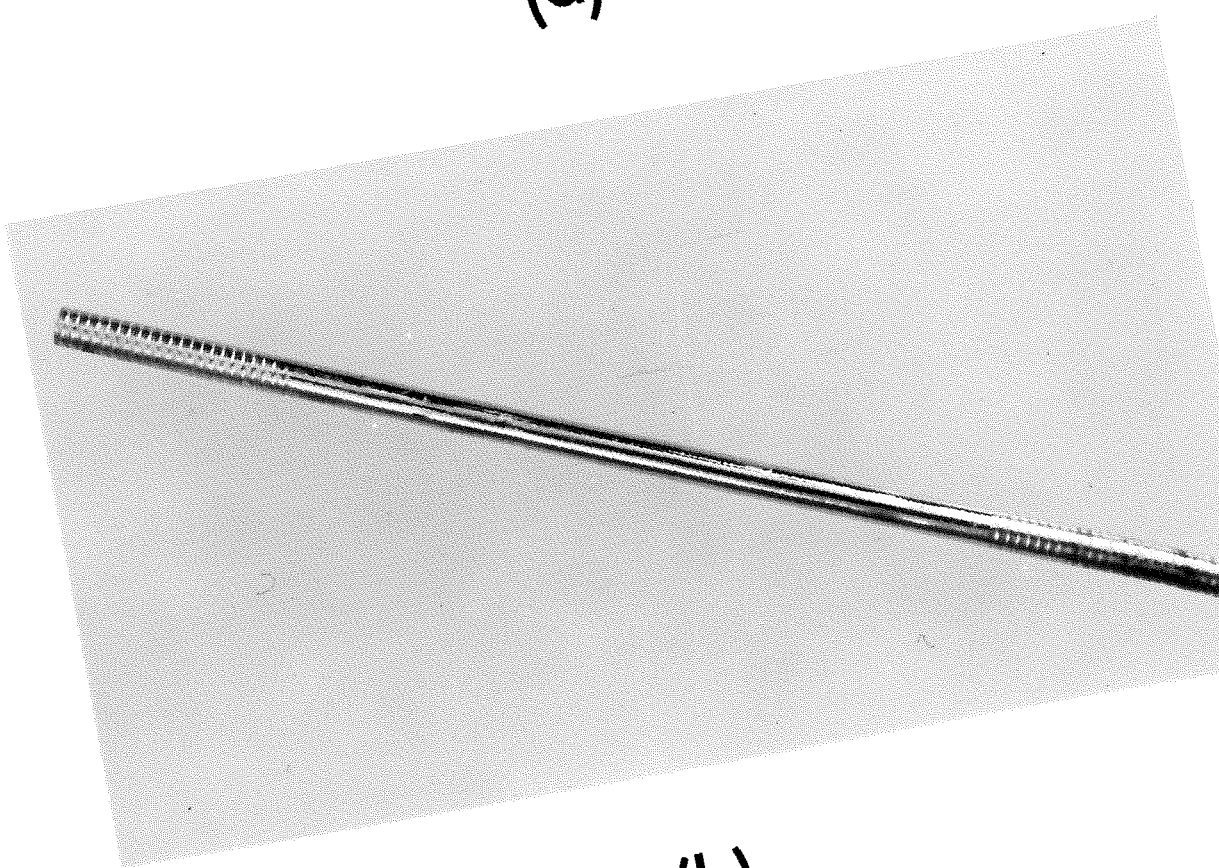

150
100
50
0
0
100
200
300
<122>
$\dot{\varepsilon} = 2.9 \times 10^{-4}$/sec.
TRUE NORMAL STRESS (kg/mm^2)
TEMPERATURE (°K)
7 at. ppm. Nitrogen
22 at. ppm. Oxygen
H.V.A.

Figure B15 (a) Comparison of 'Smooth' Surface of H.V.A. and 'Ripply' Surface of Doped <122> Crystals Tested at 77°K

(b) Diffuse Constrictions in the Gauge Length of a Nitrogen Doped <111> Crystal Tested at 298°K



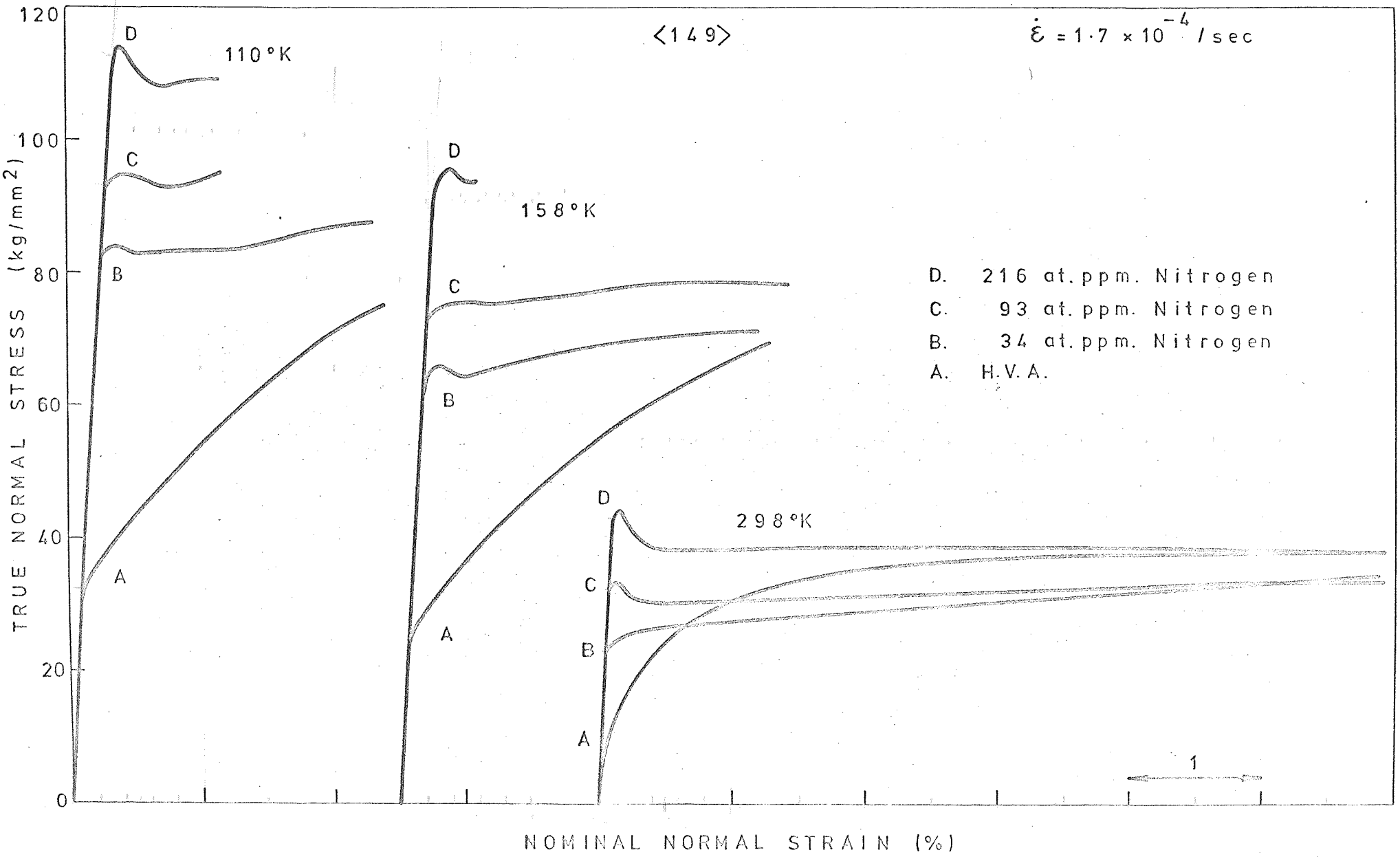
(a)



(b)

POLYTECHNIC SCHOOL
85791
1678

Figure B16 Flow Curves of H.V.A. and Nitrogen Doped <149> Crystals Tested in Tension


$\dot{\varepsilon} = 1{\cdot}7 \times 10^{-4}$ /sec
110°K
158°K
298°K
D
C
B
A
D. 216 at. ppm. Nitrogen
C. 93 at. ppm. Nitrogen
B. 34 at. ppm. Nitrogen
A. H.V.A.
TRUE NORMAL STRESS (kg/mm²)
NOMINAL NORMAL STRAIN (%)
0
20
40
60
80
100
120
1

These were difficult to detect and even more difficult to quantify but it is very unlikely that the tapers were sufficient to account for the marked 'softening' effect observed in the lowest nitrogen content specimens. Optical examination of the doped specimens after 7% strain showed dense, homogeneously distributed slip bands which were obviously coarser than those observed in the H.V.A. specimens.

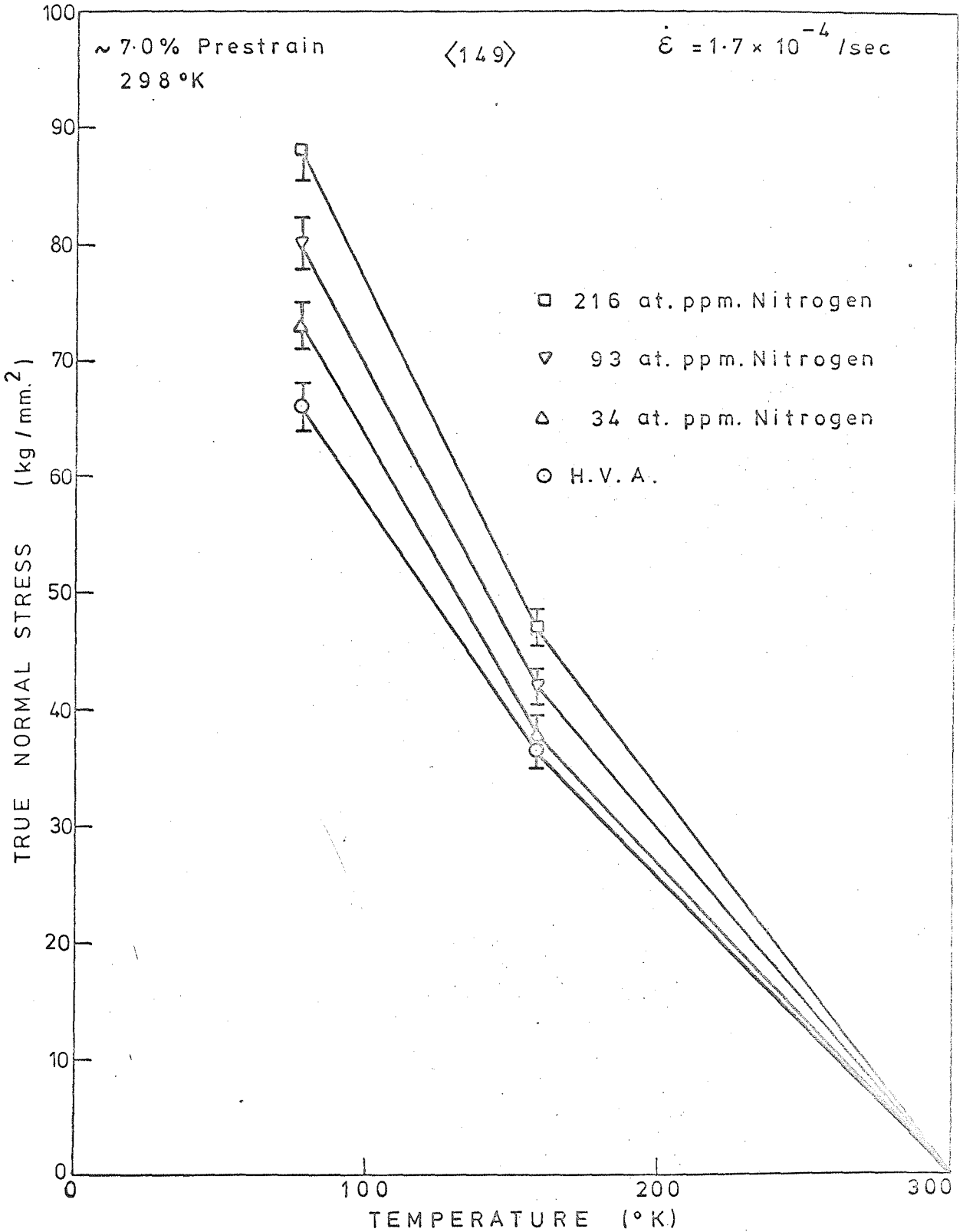
The H.V.A. crystals tested at 158°K and 110°K showed what appeared to be a linear elastic range before the onset of plastic flow. However, machine take-up effects and the absence of any direct strain measurement in these tests rendered any estimate of a proportional limit unreliable. The work hardening behaviour after yield was of the same quasi-parabolic form as at room temperature but occurred at a higher rate and over a larger stress and strain range as the temperature decreased.

The doped specimens deformed at the lower test temperatures showed pronounced yield points and load drops of varying magnitudes. Once again there was no evidence of a yield elongation although the work hardening rate after yield was very low. The higher nitrogen concentration specimens underwent small uniform elongations before necking and fracture. The other more ductile specimens were strained 2-3% before differential temperature changes were made. The limited ductility of the higher nitrogen content material at 110°K argued against attempting any direct deformation at lower test temperatures.

The tension axis rotations observed for a H.V.A. and a nitrogen doped specimen deformed at 298°K are given in Fig.B10c. The small strains applied at the lower test temperatures did not cause any significant rotation of the crystal axes.

The results of the differential temperature change tests on material prestrained approximately 7% at 298°K are presented in Fig.B17. The temperature changes were made to 158°K and then 77°K where only the highest nitrogen concentration specimen fractured without prior yielding. The

Figure B17 'Effective' Stress versus Temperature for H.V.A. and Nitrogen Doped <149> Crystals Tested in Tension


~7·0% Prestrain
298 °K
⟨149⟩
$\dot{\varepsilon}$ = 1·7 × 10^{-4} /sec
216 at. ppm. Nitrogen
93 at. ppm. Nitrogen
34 at. ppm. Nitrogen
H.V.A.
TRUE NORMAL STRESS (kg / mm.^{2})
TEMPERATURE (°K)
0
10
20
30
40
50
60
70
80
90
100
0
100
200
300

remaining specimens underwent from 2-3% plastic deformation before fracturing in or adjacent to the grips. Fig.B18 also gives the temperature dependence of the yield stress for the nitrogen doped and H.V.A. <149> crystals.

10.3.2 Oxygen Doped <149> Crystals

The deformation curves for the oxygen doped and control H.V.A. crystals are shown in Fig.B19. The oxygen doped specimen tested at 298^{o}K displayed a round yield point and low work hardening rate but no non-uniform deformation or 'softening' effects were detected at up to 7% strain. The morphology of the slip bands was qualitatively the same as that observed for the nitrogen doped specimens. The absence of a distinct yield point and drop of load at 158^{o}K may have been a consequence of an initial loading of the specimen where the grips slipped at a stress close to the yield. The 110^{o}K specimen underwent a small amount of localised strain before fracturing in the grips.

Fig.B20 shows the temperature dependence of the 'effective' stress for the oxygen doped and H.V.A. crystals determined after ~7% prestrain at 298^{o}K. After temperature cycling, both specimens underwent 2-3% strain at 77^{o}K before fracturing in the grips. The yield stress of the H.V.A. and oxygen doped molybdenum has also been plotted against temperature in Fig.B21.

The strain rate sensitivities of a <149> H.V.A., 88 at.ppm. oxygen and 93 at.ppm. nitrogen doped specimen were determined at 110^{o}K. These specimens had previously been deformed approximately 2.5-3.0% at 158^{o}K and then subjected to differential temperature change tests. The activation volume was calculated from the average stress changes for three upwards strain rate changes between 1.7×10^{-5}/sec. and 1.7×10^{-4}/sec. Within the limits of the experimental error the stress change, and activation volume, which are given below, were the same for both the doped and H.V.A. specimens.

Figure B18 Yield Stress versus Temperature for H.V.A. and Nitrogen Doped <149> Crystals Tested in Tension

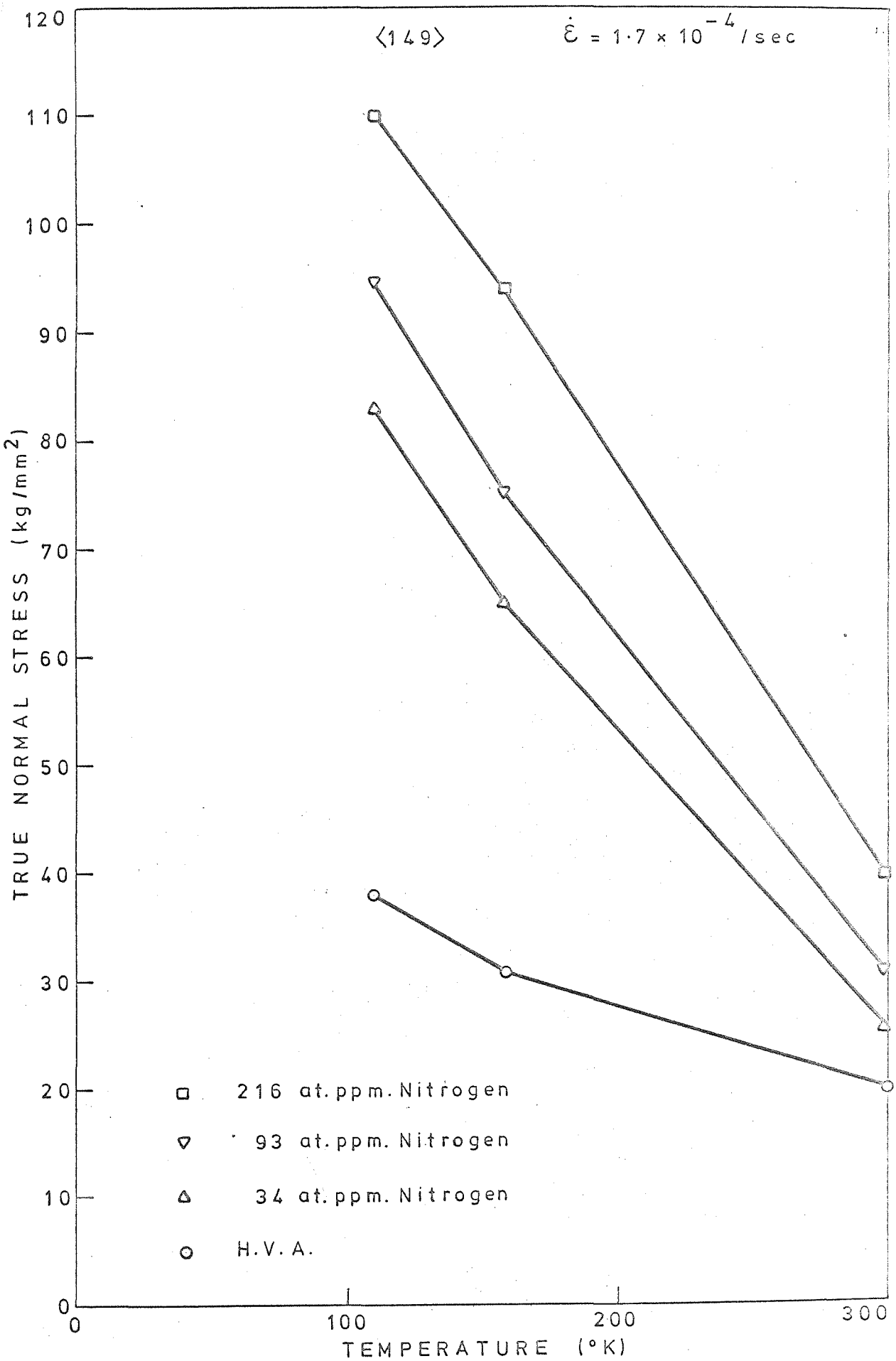

⟨149⟩
$\dot{\varepsilon} = 1{\cdot}7 \times 10^{-4}$ /sec
TRUE NORMAL STRESS (kg/mm^2)
120
110
100
90
80
70
60
50
40
30
20
10
0
0
100
200
300
TEMPERATURE (°K)
216 at.ppm. Nitrogen
93 at.ppm. Nitrogen
34 at.ppm. Nitrogen
H.V.A.

Figure B19 Flow Curves of H.V.A. and Oxygen Doped <149> Crystals Tested in Tension

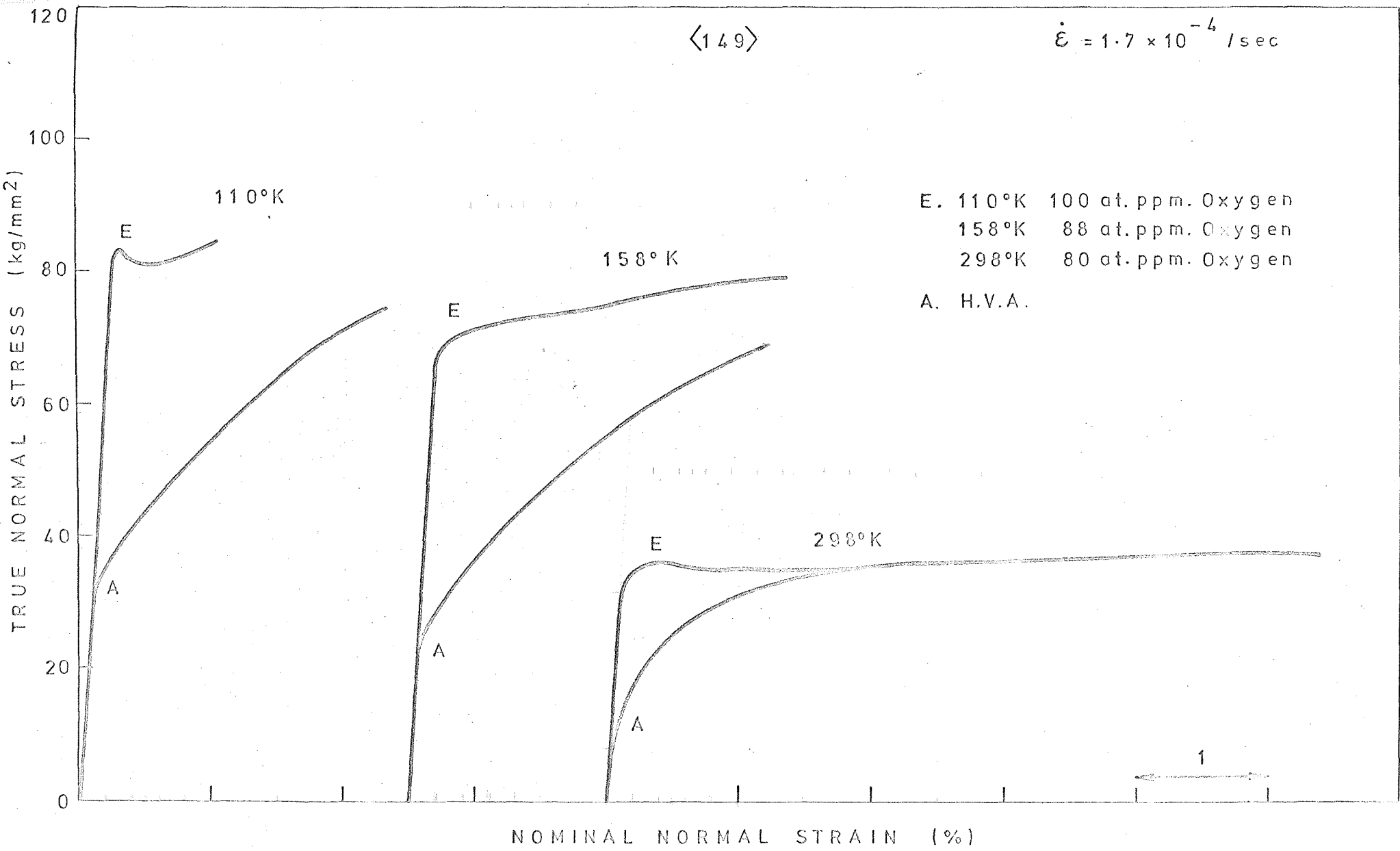

$\dot{\varepsilon} = 1.7 \times 10^{-4}$ /sec
E. 110°K 100 at. ppm. Oxygen
158°K 88 at. ppm. Oxygen
298°K 80 at. ppm. Oxygen
A. H.V.A.
110°K
158°K
298°K
E
A
1
TRUE NORMAL STRESS (kg/mm²)
NOMINAL NORMAL STRAIN (%)
0
20
40
60
80
100
120

Figure B20 'Effective' Stress versus Temperature for H.V.A. and Oxygen Doped <149> Crystals Tested in Tension

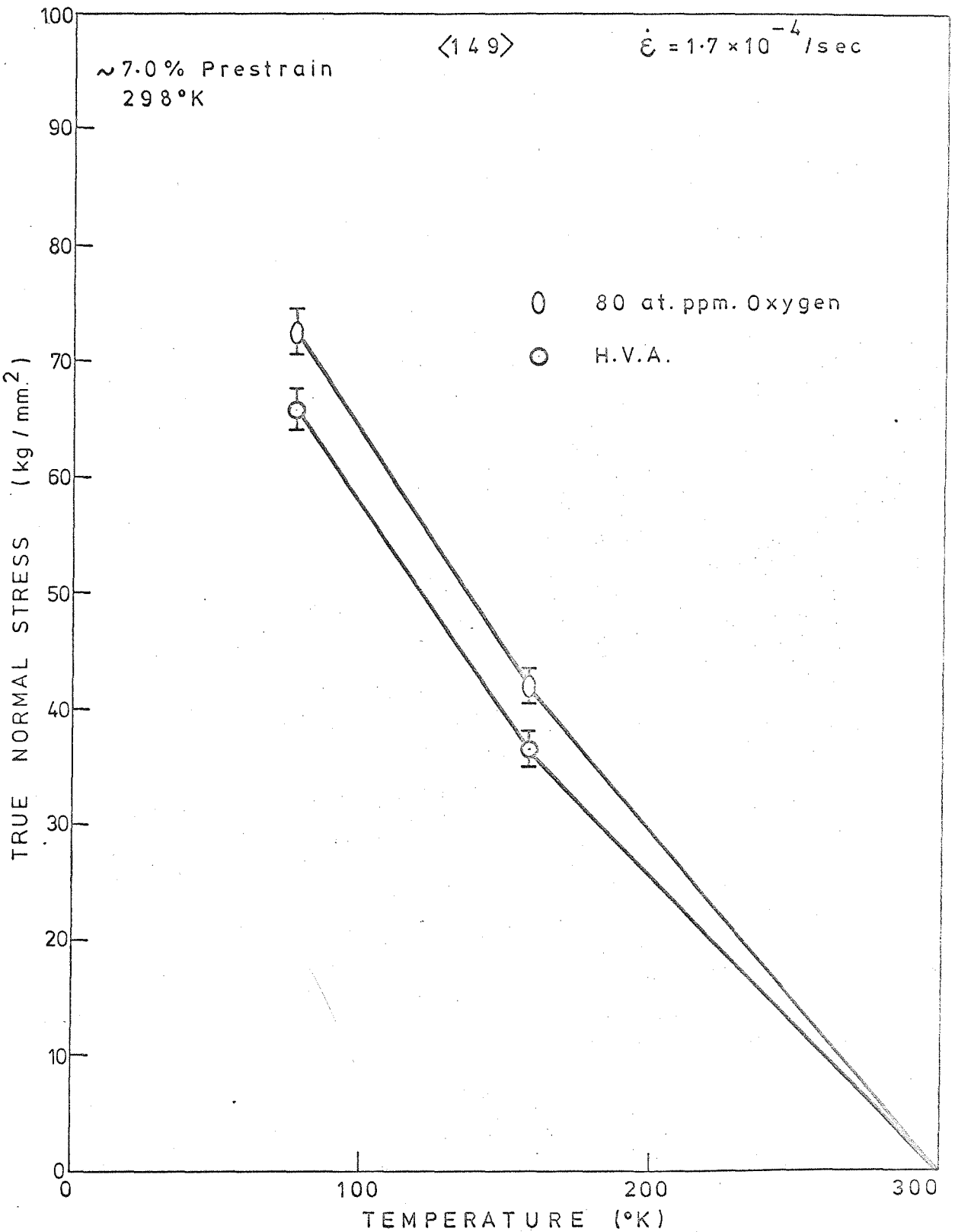
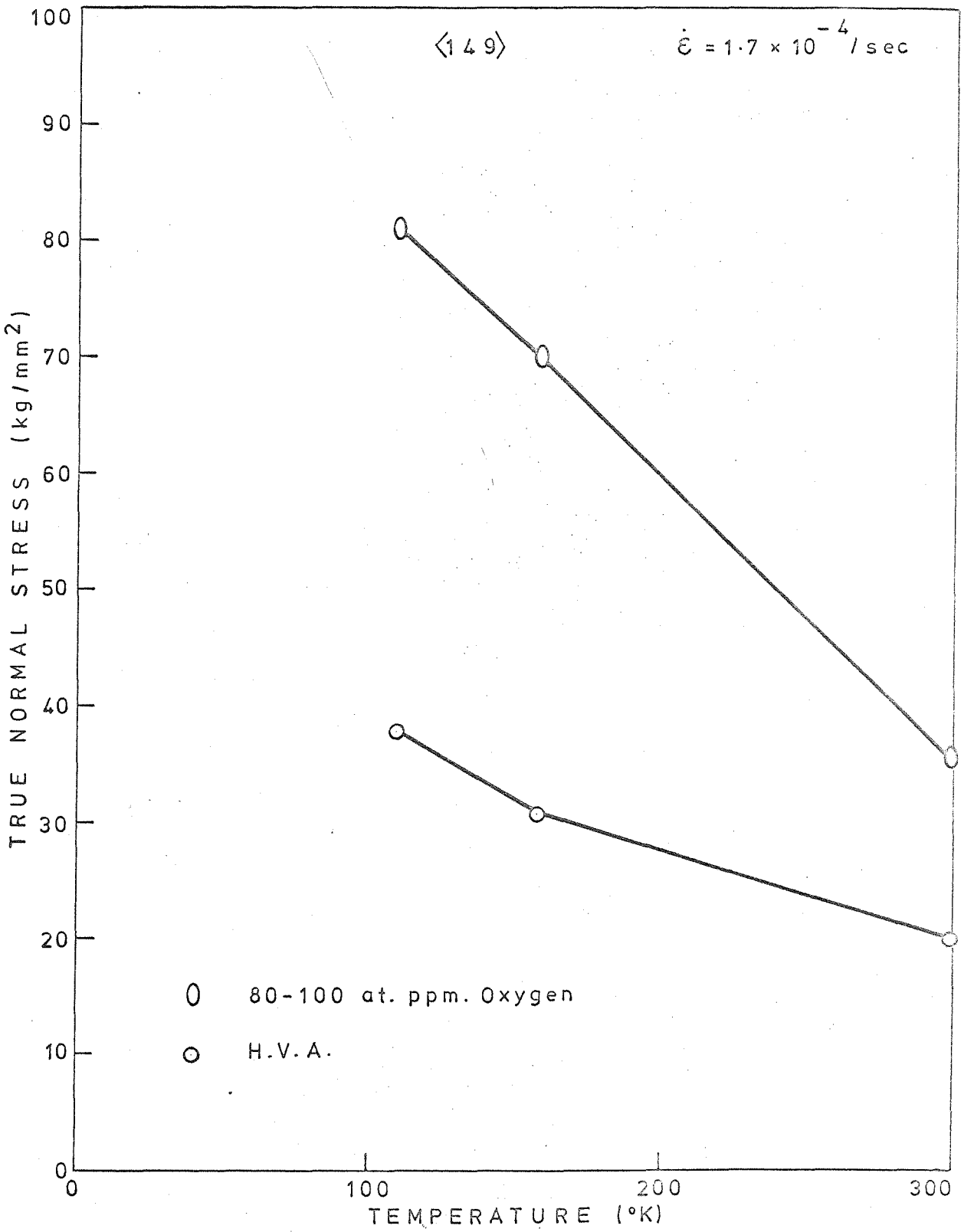

〈149〉
$\dot{\varepsilon} = 1.7 \times 10^{-4}$ /sec
~7.0% Prestrain
298°K
80 at. ppm. Oxygen
H.V.A.
TRUE NORMAL STRESS (kg / mm.^{2})
TEMPERATURE (°K)
0
10
20
30
40
50
60
70
80
90
100
0
100
200
300

Figure B21 Yield Stress versus Temperature for H.V.A. and Oxygen Doped <149> Crystals Tested in Tension


⟨149⟩
$\dot{\varepsilon} = 1{\cdot}7 \times 10^{-4}$ / sec
TRUE NORMAL STRESS (kg/mm²)
TEMPERATURE (°K)
0
10
20
30
40
50
60
70
80
90
100
0
100
200
300
80-100 at. ppm. Oxygen
H.V.A.

Stress change, $\Delta\sigma = 3.3 \pm 0.5$ kg/mm.^{2}

Activation volume, $v^* = 216 \pm 33$ $(\text{Å})^3$

The 'effective' stress at which the activation volume was measured varied from a minimum of 54 kg/mm.^{2} for the H.V.A. molybdenum to a maximum of 64 kg/mm.^{2} for the 93 at.ppm. nitrogen doped molybdenum. Thus, the activation volumes cannot be compared at the same 'effective' stress. The results suggest that only a small, if at all significant, change in the activation volume at constant 'effective' stress would accompany interstitial doping.

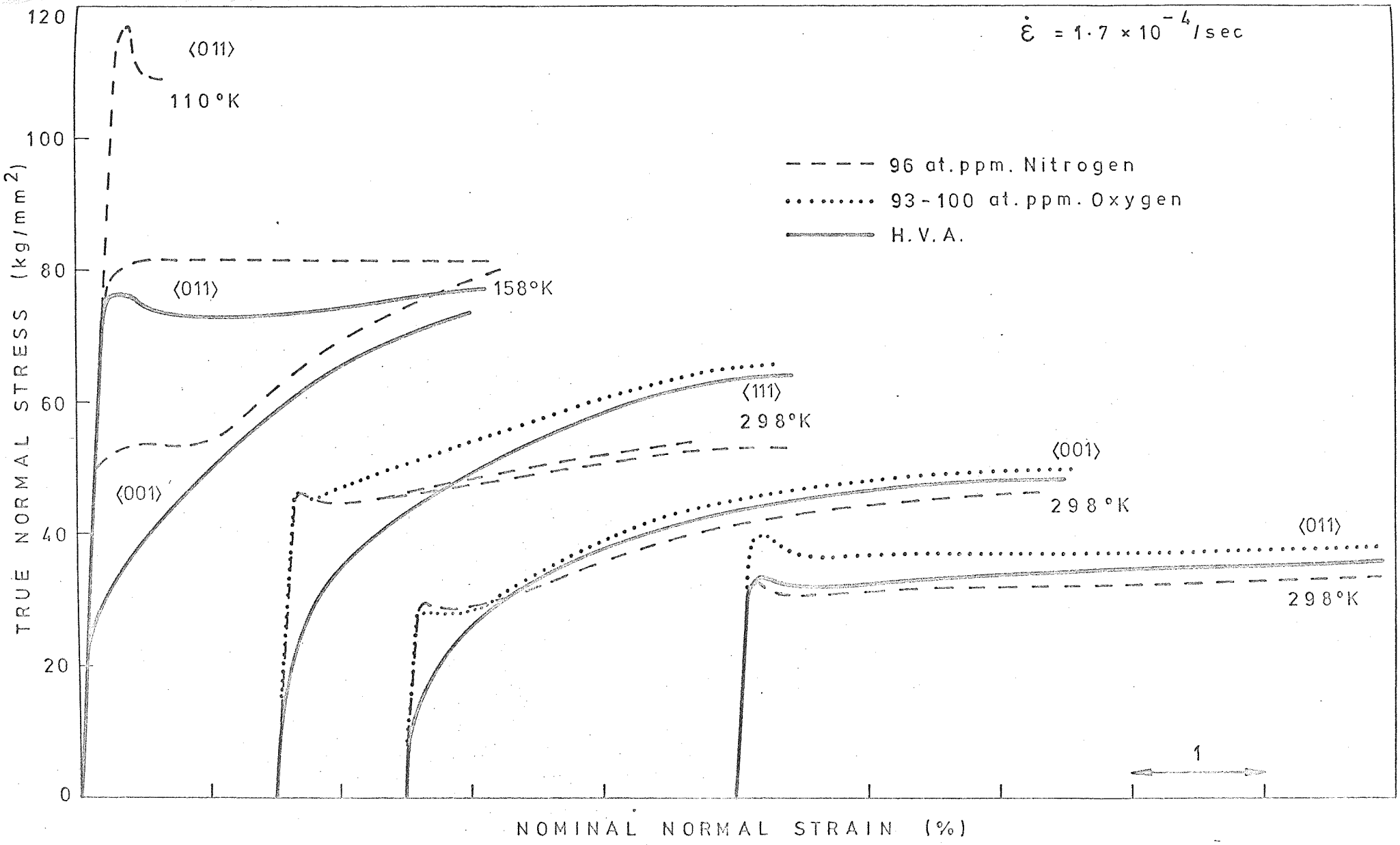
10.3.3 Doped <001>, <011> and <111> Crystals

The flow curves obtained for the corner orientation crystals are given in Fig.B22. The H.V.A. crystals tested at 298°K and 158°K exhibited the strong orientation dependence of the yield and work hardening behaviour which is a well established characteristic of the deformation behaviour of molybdenum.

Doping of the <011> crystals did not modify either the form of yielding or the work hardening rate. However, there were significant increases in the yield and flow stress levels in the oxygen doped specimen tested at 298°K and the nitrogen doped specimen tested at 158°K. With the exception of the 110°K test where necking and fracture occurred immediately after yielding, the doped specimens were strained 3-5% without showing evidence of non-uniform elongation. In the nitrogen doped specimen tested at 298°K the initial yield occurred outside the strain gauge length and in consequence ~0.2-0.3% strain at the yield was not recorded. This gave the yield point a deceptively sharp appearance in comparison with the oxygen doped specimen.

The doping of the <001> crystals introduced a discontinuous yield and a clearly defined constant stress yield elongation at both 298°K and 158°K.

Figure B22 Flow Curves of H.V.A. and Doped Corner Orientation Crystals Tested in Tension


$\dot{\varepsilon} = 1 \cdot 7 \times 10^{-4}$ / sec
96 at. ppm. Nitrogen
93 - 100 at. ppm. Oxygen
H. V. A.
⟨011⟩
110 °K
⟨011⟩
158 °K
⟨111⟩
298 °K
⟨001⟩
⟨001⟩
298 °K
⟨011⟩
298 °K
1
TRUE NORMAL STRESS (kg/mm²)
NOMINAL NORMAL STRAIN (%)
0
20
40
60
80
100
120

After the yield elongation, when presumably deformation had spread throughout the whole specimen, there was a return to the same high work hardening rate shown by the H.V.A. specimens. All specimens underwent 3-5% uniform deformation before temperature cycling was commenced.

The <111> crystals, which were deformed only at 298°K, showed similar behaviour to the <001> crystals. Doping introduced sharp yields and yield elongations into the continuously yielding H.V.A. molybdenum. However, there was a reduction in the work hardening rate with respect to the H.V.A. crystals. In the oxygen doped specimen, where the Lüders nucleus was formed outside the strain gauge length and hence most of the yield elongation was not recorded, the reduction in work hardening rate was small. The nitrogen doped specimen showed a greater reduction in the work hardening rate but optical examination indicated a series of diffuse constrictions along the gauge length (see Fig.B15b). There was some concern that this macroscopically inhomogeneous deformation was responsible for the measured low work hardening rate so the test was repeated. Both the low gradient of the flow curve and the diffuse constrictions were reproduced. It is likely that this macroscopic inhomogeneity did reinforce the low work hardening rate but some reduction in the work hardening rate must have been responsible for the initial incidence of the constrictions.

Micrometer measurements indicated that both the <001> and <111> crystals retained circular cross-sections at large strains but the <011> crystals developed elliptical cross-sections consistent with duplex slip. Post deformation Laues of the doped and H.V.A. corner orientation crystals confirmed that no rotation of the tension axes occurred.

Temperature change tests were conducted on the nitrogen doped and H.V.A. specimens after 4-5% prestrain at 298°K. The temperature dependence of the 'effective' stress is shown in Fig.B23. All specimens, except the nitrogen doped <001>, yielded before fracturing at 77°K. The temperature dependence of the yield stress for the <001> and <011> orientations are also plotted in

Figure B23 'Effective' Stress versus Temperature for H.V.A. and Doped Corner Orientation Crystals Tested in Tension

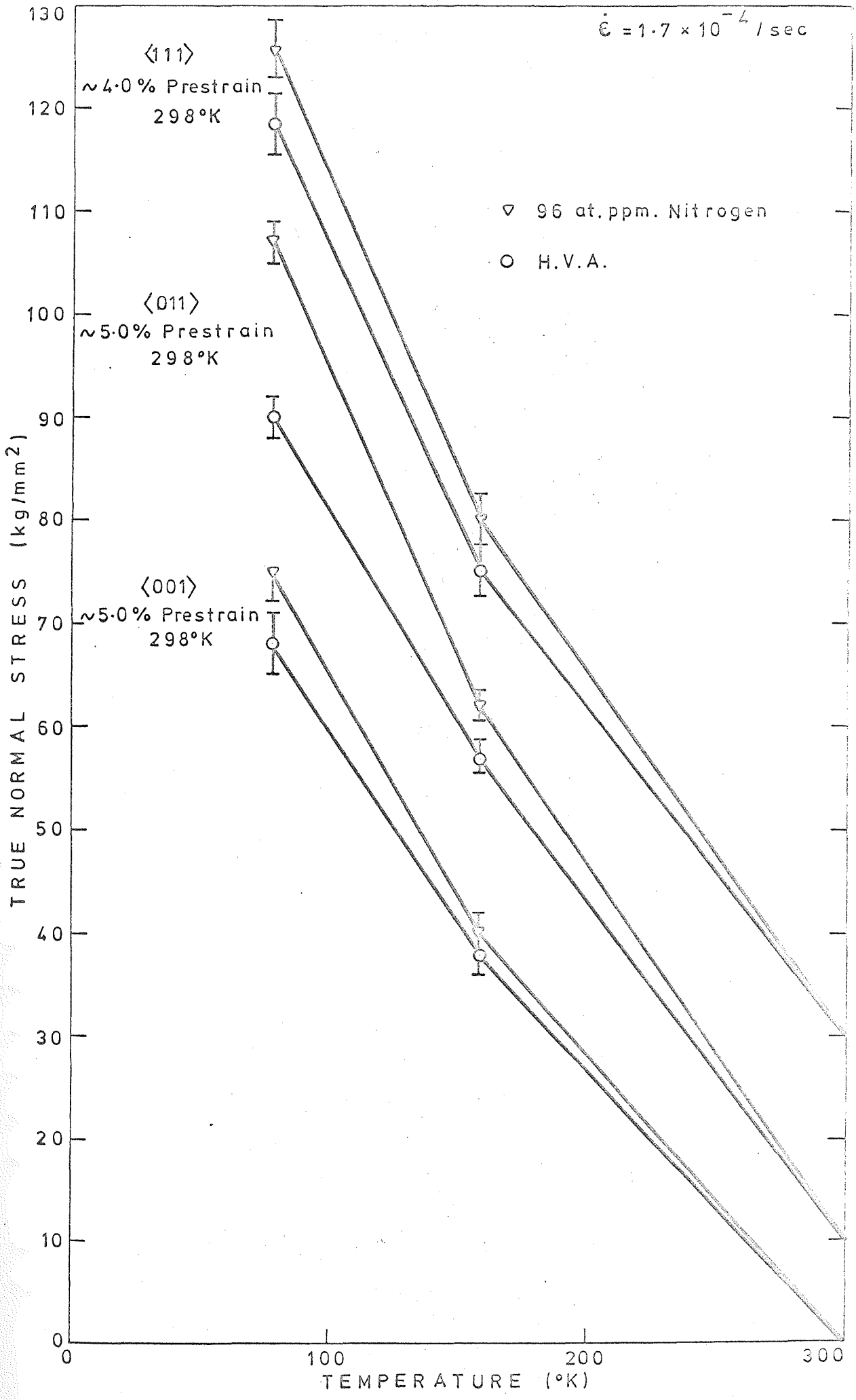

$\dot{\epsilon} = 1.7 \times 10^{-4}$ / sec
⟨111⟩
~4.0% Prestrain
298°K
⟨011⟩
~5.0% Prestrain
298°K
⟨001⟩
~5.0% Prestrain
298°K
▽ 96 at. ppm. Nitrogen
○ H.V.A.
TRUE NORMAL STRESS (kg/mm²)
TEMPERATURE (°K)
0
10
20
30
40
50
60
70
80
90
100
110
120
130
0
100
200
300

Fig.B24.

10.4 Slip Geometry and Morphology

The surface slip traces of 7 at.ppm. nitrogen and 22 at.ppm. oxygen doped <149> crystals deformed in compression at both 290°K and 77°K were analysed. In view of the anomalous yield behaviour and the distinctive 'ripply' surface profile of the doped <122> crystals deformed at 77°K, the slip traces on an oxygen doped <122> crystal after 6% strain at 77°K, were also examined. No full analysis of the slip traces of the H.V.A. material, whose slip geometry has been previously established in a number of investigations (e.g. Vesely 1968b, Jeffcoat 1975) was attempted.

10.4.1 <149> Crystals Deformed at 290°K

A H.V.A. crystal was initially deformed ~1% at 290°K but only very faint slip traces were detected. It was further deformed to a total of 7% strain where the slip traces were sufficiently distinct to permit the primary slip traces to be identified (see Fig.B25a).

The slip traces observed on the doped specimens after small strains at 290°K were straight, coarse and widely spaced (see Fig.B26) which made the analysis much easier than for the H.V.A. molybdenum. They were also non-uniformly distributed along the specimen length although there was no indication of slip being concentrated in pseudo Lüders bands. Both at this temperature and 77°K the slip traces for the nitrogen doped molybdenum were noticeably stronger than for the oxygen doped material.

Fig.B27 shows the results of the slip trace analysis of the doped specimens where very little evidence of non-crystallographic slip was found. The oxygen doped specimen, which was strained 0.7% to the vicinity of yield

Figure B24 Yield Stress versus Temperature for H.V.A. and Doped Corner Orientation Crystals Tested in Tension

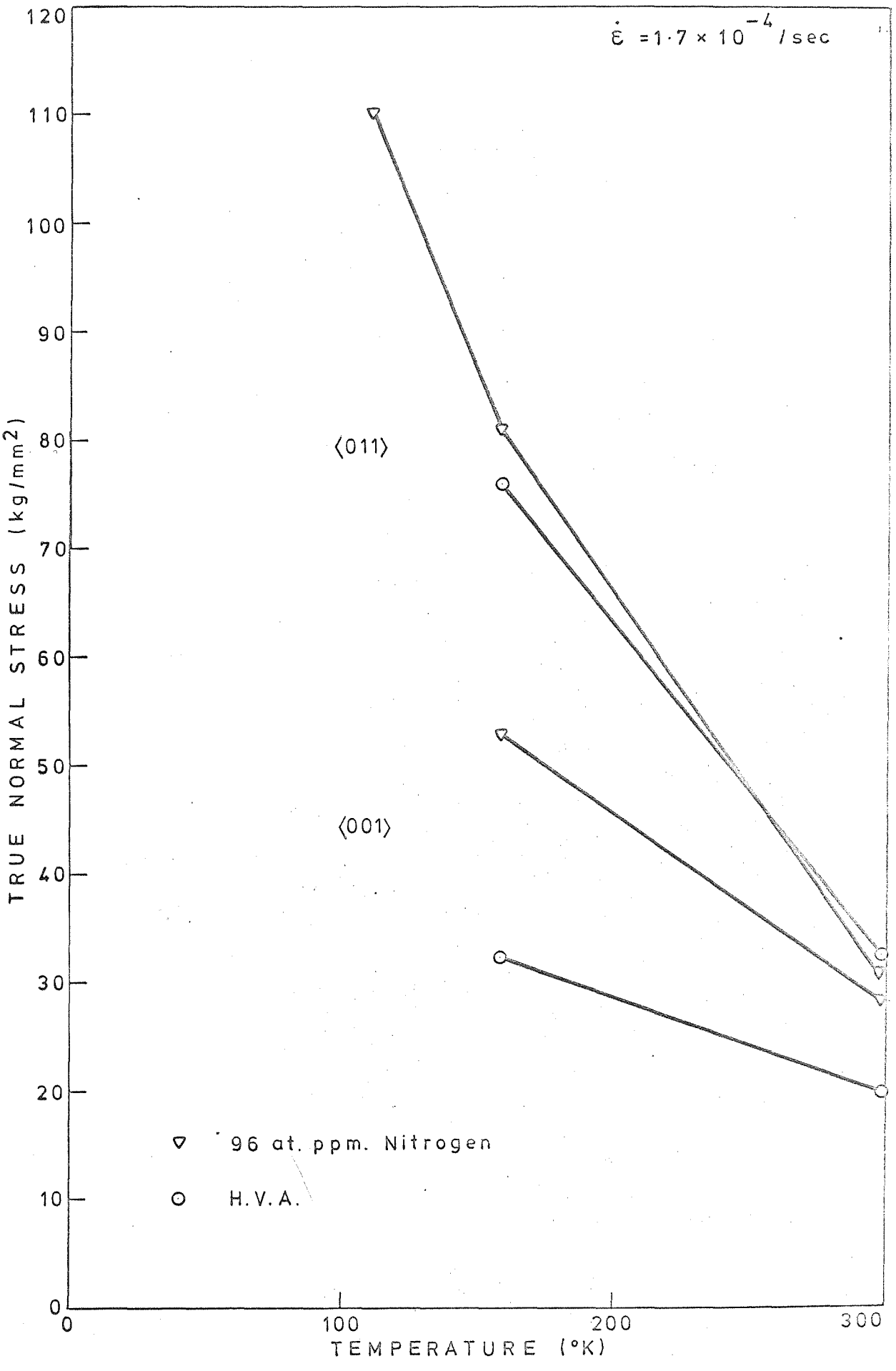
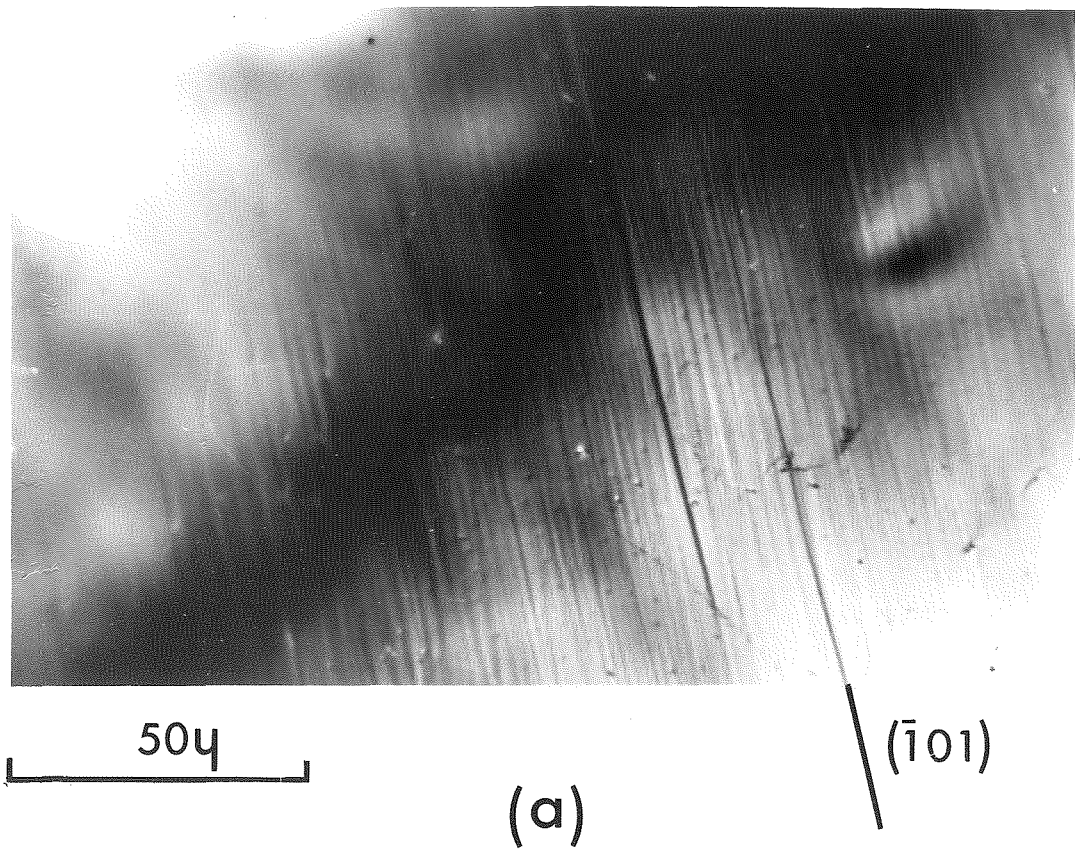

$\dot{\varepsilon} = 1{\cdot}7 \times 10^{-4}$ /sec
TRUE NORMAL STRESS (kg/mm²)
TEMPERATURE (°K)
⟨011⟩
⟨001⟩
96 at. ppm. Nitrogen
H.V.A.
0
10
20
30
40
50
60
70
80
90
100
110
120
0
100
200
300

Figure B25 (a) ($\bar{1}01$) Slip Traces on H.V.A. <149> Crystal Strained 7% at 290°K

(b) Slip Traces on H.V.A. <149> Crystal Strained 5.5% at 77°K


50μ
(a)
(1̄01)

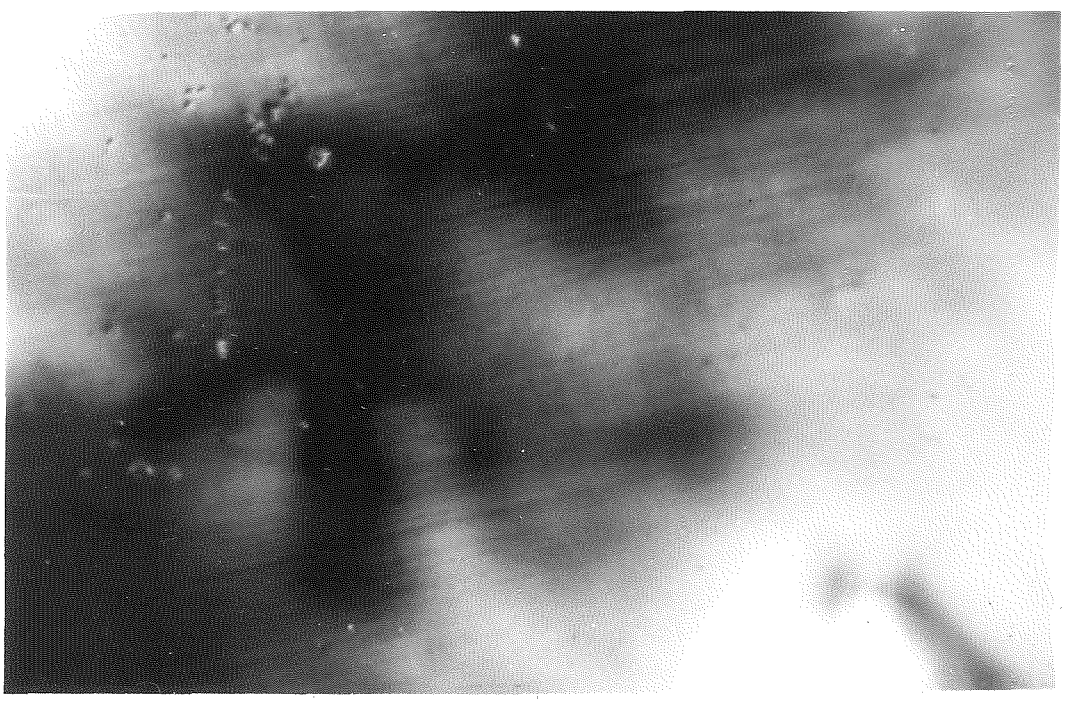
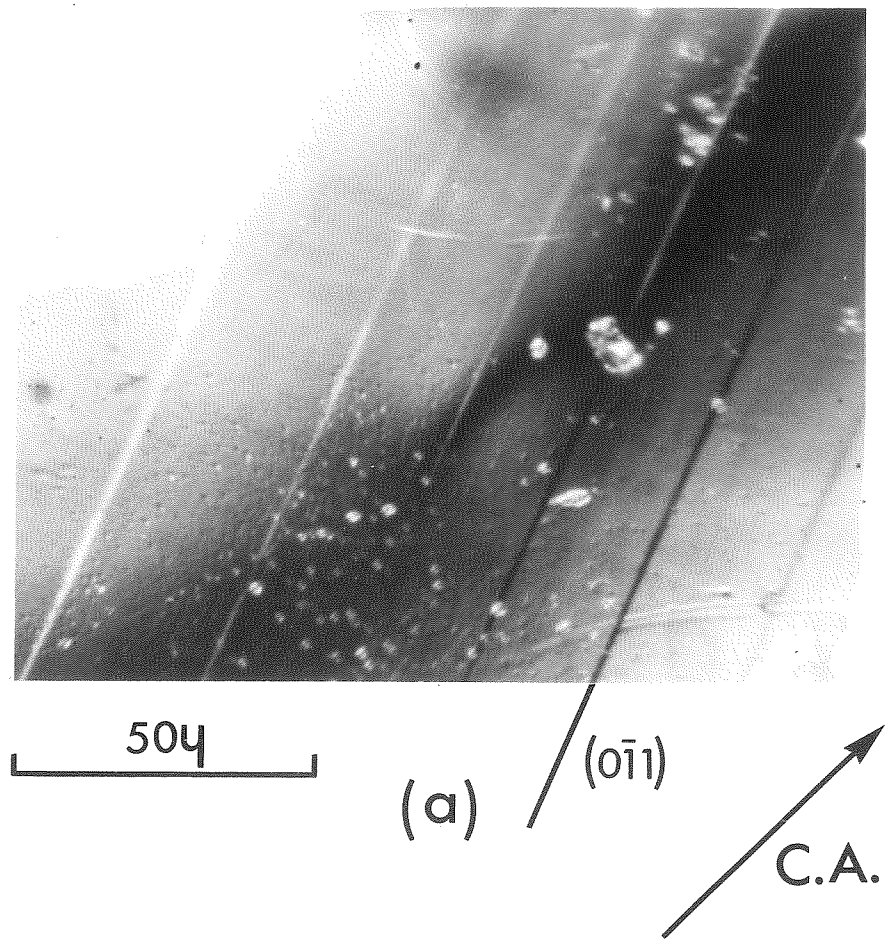

50μ
(b)

Figure B26 (a) $(0\bar{1}1)$ Slip Traces on 7 at.ppm. Nitrogen Doped <149> Crystals Strained 1.0% at 290°K

(b) $(0\bar{1}1)$ Slip Traces on 22 at.ppm. Oxygen Doped <149> Crystal Strained 0.7% at 290°K

C.A. = Compression Axis


50μ
(a)
(0$\bar{1}$1)
C.A.

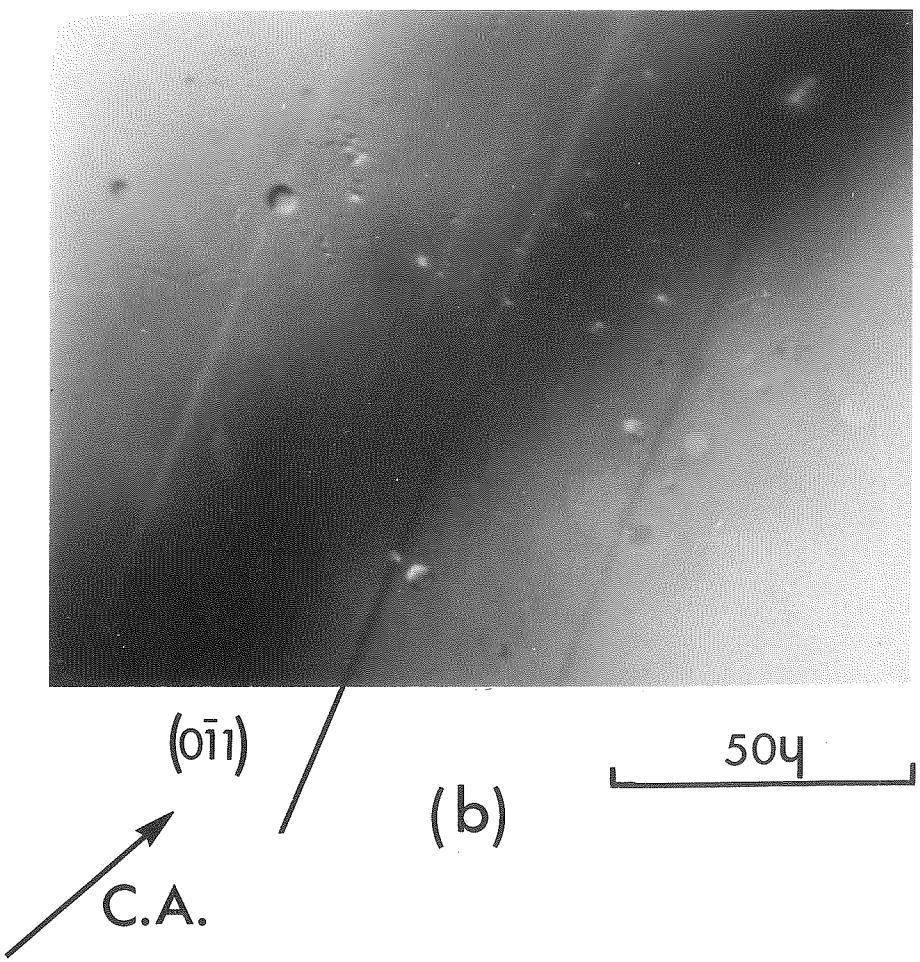
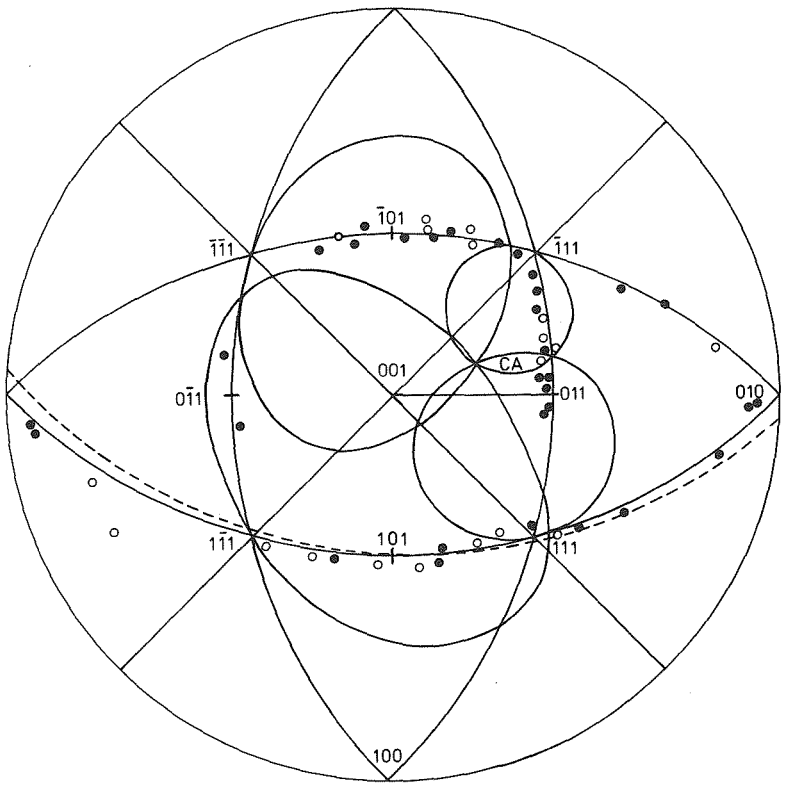

(0$\bar{1}$1)
C.A.
(b)
50μ

Figure B27 Slip Geometry of

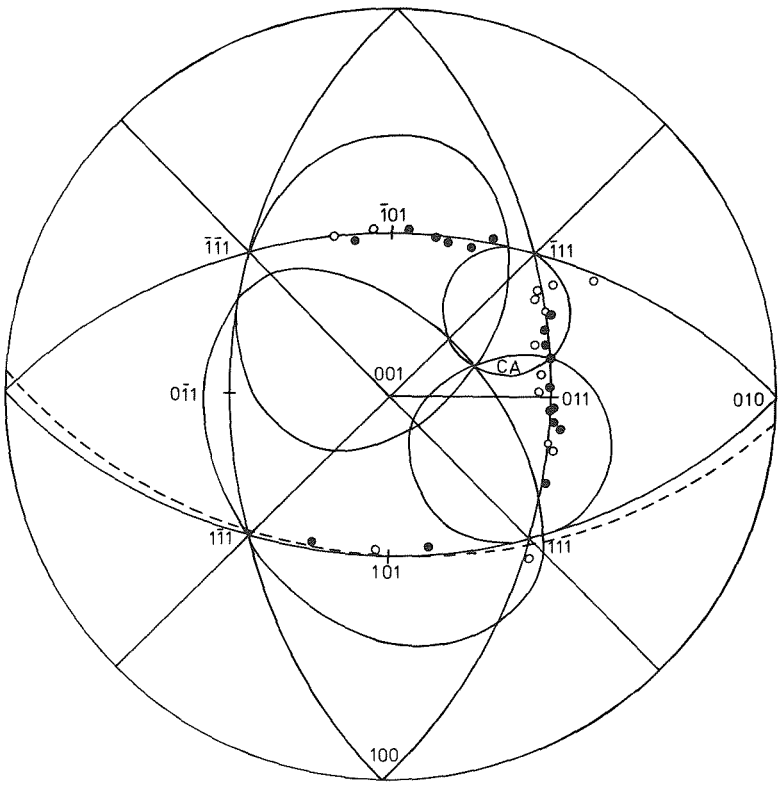
(a) 7 at.ppm. Nitrogen Doped <149> Crystal Strained 1.0% at 290°K

(b) 22 at.ppm. Oxygen Doped <149> Crystal Strained 0.7% at 290°K

C.A. Compression Axis
--- Maximum Resolved Shear Stress Plane


$\bar{1}01$
$\bar{1}\bar{1}1$
$\bar{1}11$
001
CA
$0\bar{1}1$
011
010
$1\bar{1}1$
101
$\bar{1}\bar{1}1$
100

(a)


$\bar{1}01$
$\bar{1}\bar{1}1$
$\bar{1}11$
001
CA
$0\bar{1}1$
011
010
$1\bar{1}1$
101
$\bar{1}\bar{1}1$
100

(b)

initiation, showed both $(0\bar{1}1)$ and (101) slip traces over restricted and well defined ranges of the radial surface orientation. Only a few $(\bar{1}01)$ primary traces were observed. The nitrogen doped specimen was strained 1.0%, approximately to the end of the yield elongation. Primary $(\bar{1}01)$ traces were the most general observed, extending over the full circumference of the specimen. $(0\bar{1}1)$ and (101) slip traces were also in evidence over restricted surface orientation ranges. The (101) traces were observed over a larger range of circumference than in the oxygen doped specimens. A few (011) traces were also observed but only near the specimen ends where the frictional constraint may have influenced the slip behaviour.

10.4.2 <149> Crystals Deformed at 77°K

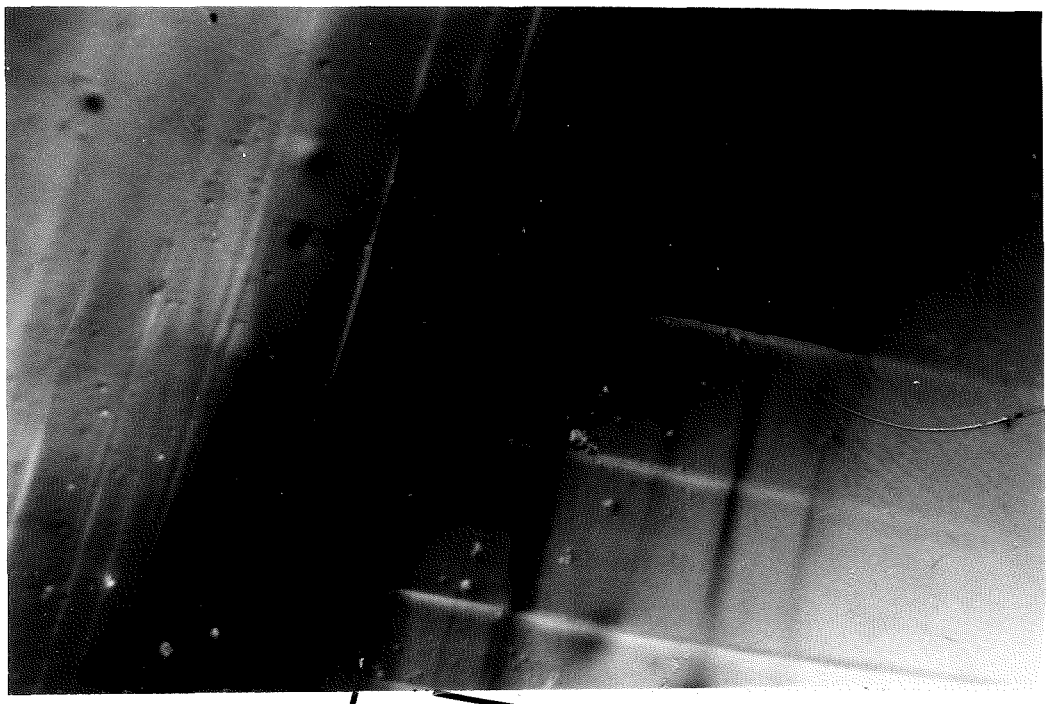
A H.V.A. specimen was first strained ~2% but showed negligible evidence of slip. It was further deformed to a total of ~5.5% strain where much finer and fainter traces were evident than had been detected in H.V.A. crystals at 290°K (see Fig.B25b). Several sets of slip traces could be seen but no analysis was attempted.

The doped specimens again displayed coarse, straight slip traces (see Fig.B28) corresponding, within the limits of the experimental error, to crystallographic slip on {110} planes. Oxygen and nitrogen doped specimens were strained ~0.3% corresponding to incipient yielding. No slip traces were detected on the oxygen doped specimen. A few, fine, sharp lines appeared on the nitrogen doped specimen but their density did not justify any attempt at analysis. The oxygen and nitrogen doped specimens were further strained to~1.2% and ~1.7% respectively, corresponding to the end of the yield elongations. The geometry of the traces observed on both the doped specimens (see Fig.B29) was very similar to that observed for the oxygen doped material at 290°K (see Fig.B27b). $(0\bar{1}1)$ and (101) slip traces were the most prominent

Figure B28 $(0\bar{1}1)$ and (101) Slip Traces on

(a) 7 at.ppm. Nitrogen Doped <149> Crystal Strained 1.7% at 77°K

(b) 22 at.ppm. Oxygen Doped <149> Crystal Strained 1.2% at 77°K


50μ
(0$\bar{1}$1)
(101)
(a)
C.A.

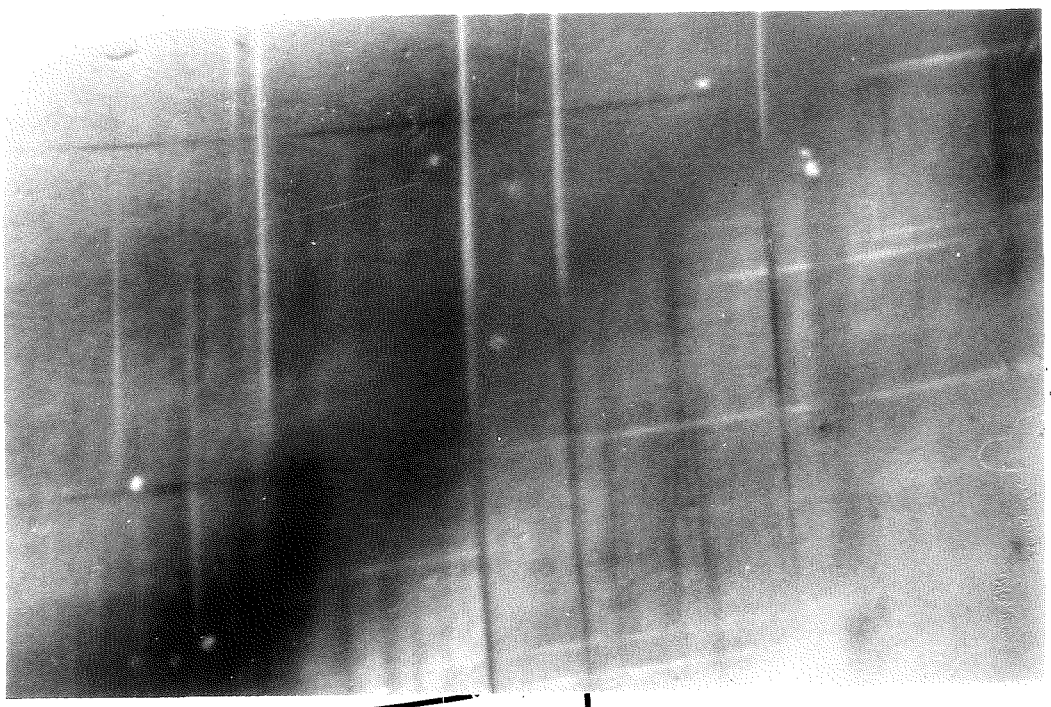
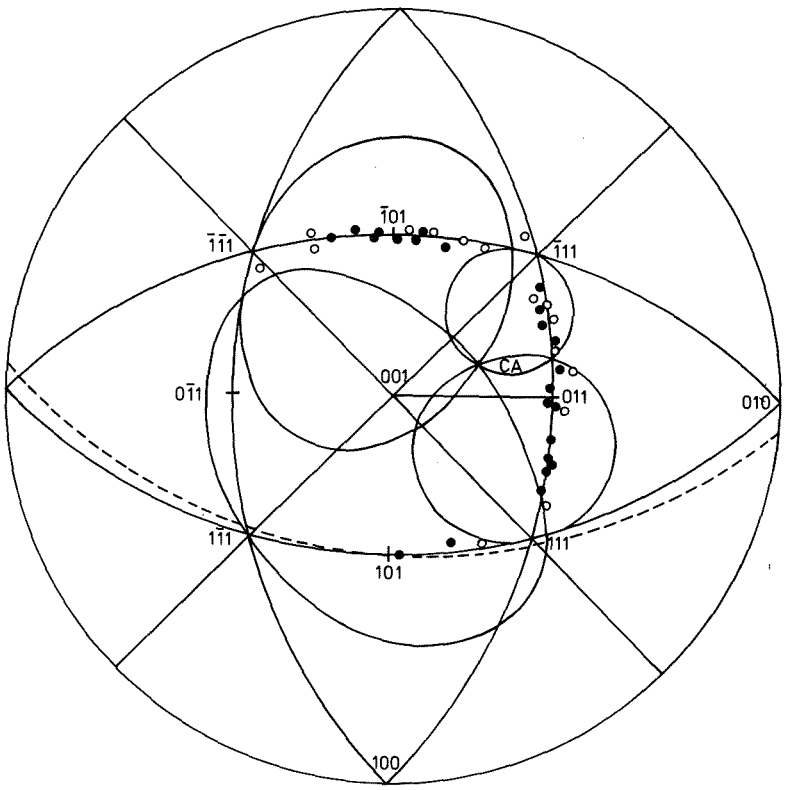

(101)
(0$\bar{1}$1)
50μ
(b)
C.A.

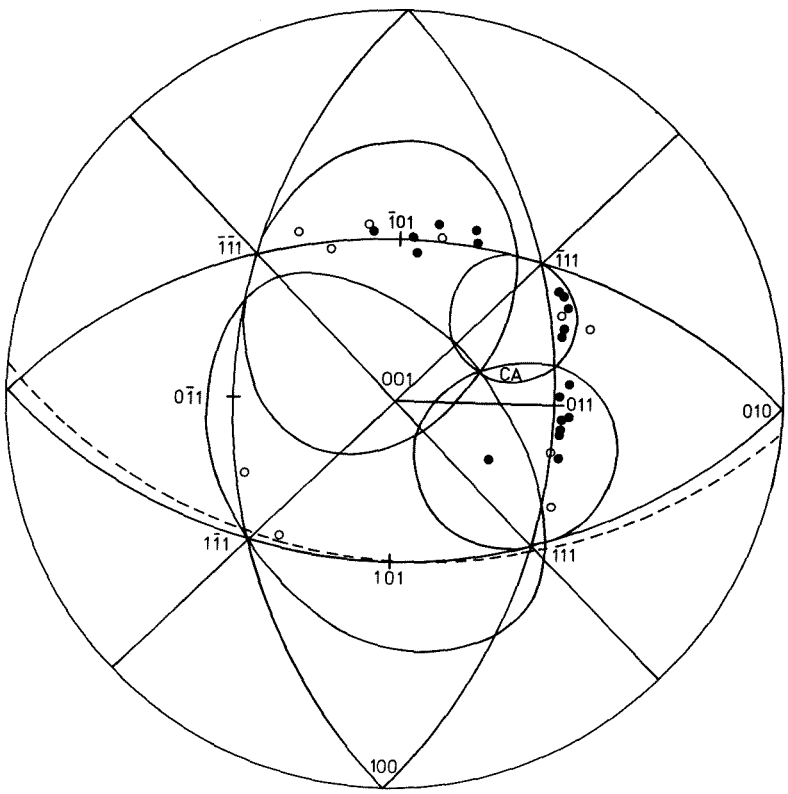
Figure B29 Slip Geometry of

(a) 7 at.ppm. Nitrogen Doped <149> Crystal Strained 1.7% at 77°K

(b) 22 at.ppm. Oxygen Doped <149> Crystal Strained 1.2% at 77°K


$\bar{1}01$
$\bar{1}\bar{1}1$
$\bar{1}11$
CA
001
$0\bar{1}1$
011
010
$1\bar{1}1$
111
101
100

(a)


$\bar{1}01$
$\bar{1}\bar{1}1$
$\bar{1}11$
CA
001
$0\bar{1}1$
011
010
$1\bar{1}1$
111
101
100

(b)

with only an odd (101) or (011) trace being detected.

The oxygen doped specimen was further strained to ~5% and the slip traces analysed to ascertain if primary $(\bar{1}01)$ slip was initiated after straining beyond the yield. The results shown in Fig.B30a indicate that the larger deformation produced no change in geometry. Both $(0\bar{1}1)$ and (101) slip persisted at large strains and over a restricted range of surface orientations. There was no appreciable coarsening of slip traces with increasing strain but the density of the traces did increase (see Fig.B31).

10.4.3 <122> Crystals Deformed at 77°K

Microscopic examination of an oxygen doped <122> crystal after 6% strain at 77°K revealed exceptionally coarse, straight {110} slip traces (see Fig.B32). In addition a series of sharp, lateral traces continuous around the full specimen circumference were evident (see Fig.B32a). The lateral traces occurred at intervals of several hundreds of microns along the specimen length and appeared to be sympathetically related to the 'ripply' surface profile which was observed macroscopically (see Fig.B15a). The directions of these traces in regions of the circumference where they were comparatively straight have been plotted in Fig.B30b. They are seen to lie approximately in the $(\bar{2}11)$ plane. These straight regions were not typical of all the traces, many of which took quite an irregular course around the specimen circumference.

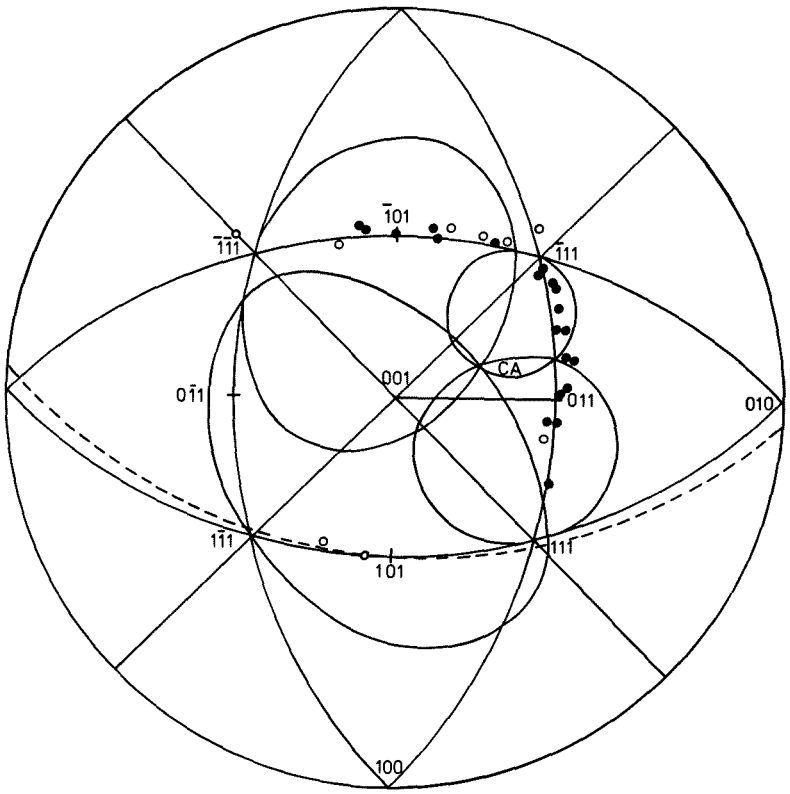
The very coarse, straight crystallographic traces which were also apparent on the doped specimen were analysed and the results are plotted in Fig.B30b. $(1\bar{1}0)$ and $(\bar{1}01)$ traces were most prominent but other faint traces were also observed (see Fig.B32b). The {110} traces were invariant along the specimen length and did not bear any consistent relation to the lateral traces. In some instances the {110} slip traces clearly propagated through the lateral traces as shown in Fig.B32a and Fig.B33a. However, as shown in Fig.B33b, in

Figure B30 Slip Geometry of

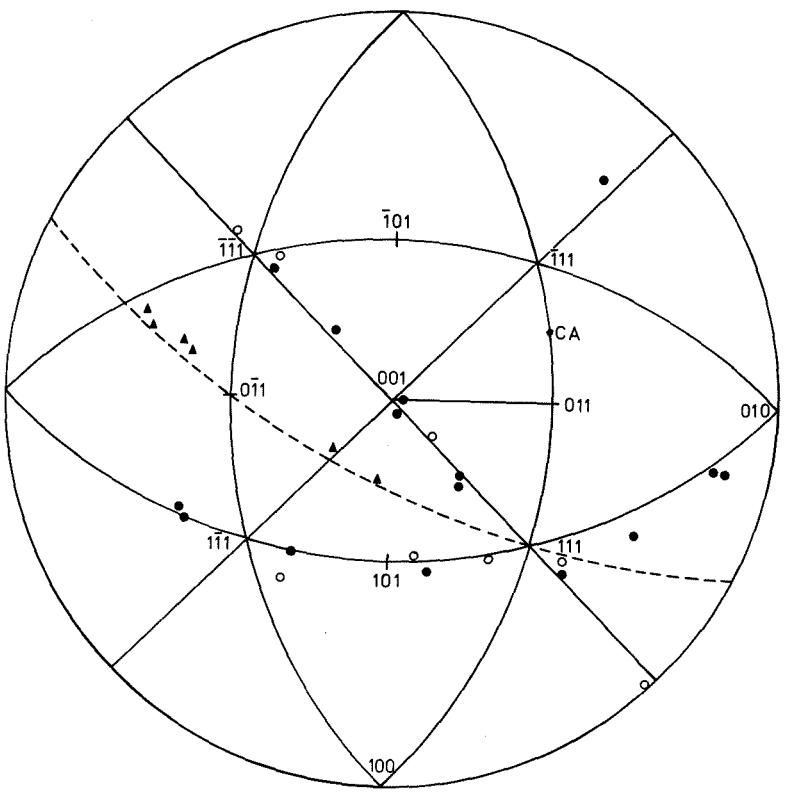
(a) 22 at.ppm. Oxygen Doped <149> Crystal Strained 5% at 77°K

(b) 22 at.ppm. Oxygen Doped <122> Crystal Strained 6% at 77°K

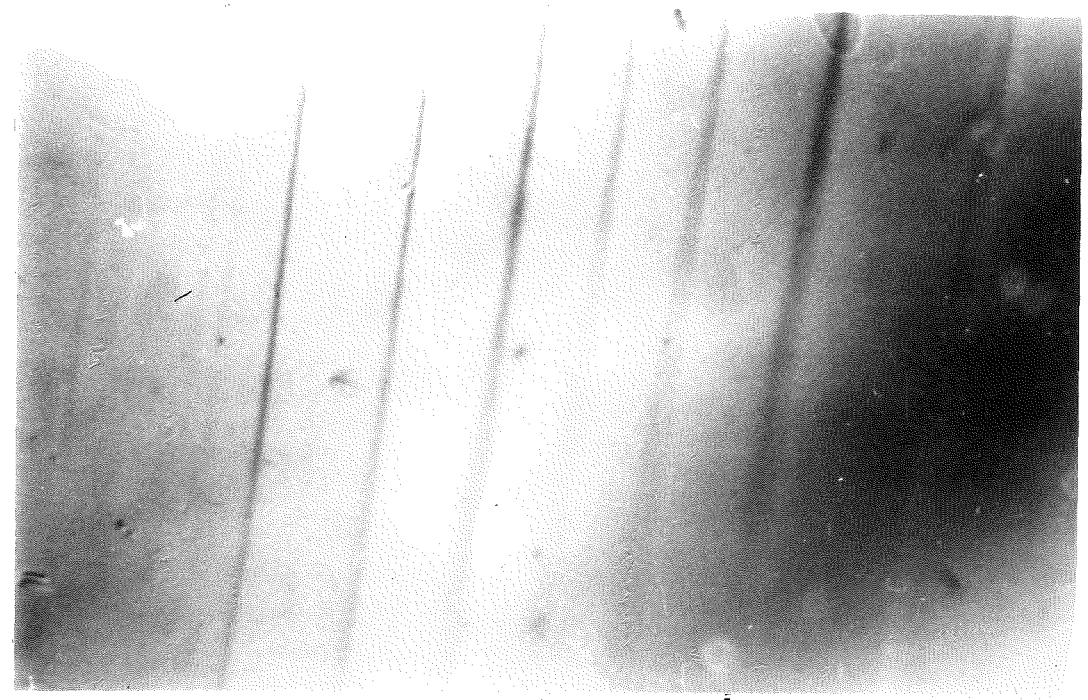
--- Maximum Resolved Shear Stress Plane
▲ Lateral Traces


$\bar{1}01$
$\bar{1}\bar{1}1$
$\bar{1}11$
CA
001
$0\bar{1}1$
011
010
$1\bar{1}1$
111
$\bar{1}01$
100

(a)


$\bar{1}01$
$\bar{1}\bar{1}1$
$\bar{1}11$
CA
001
$0\bar{1}1$
011
010
$1\bar{1}1$
111
$\bar{1}01$
100

(b)

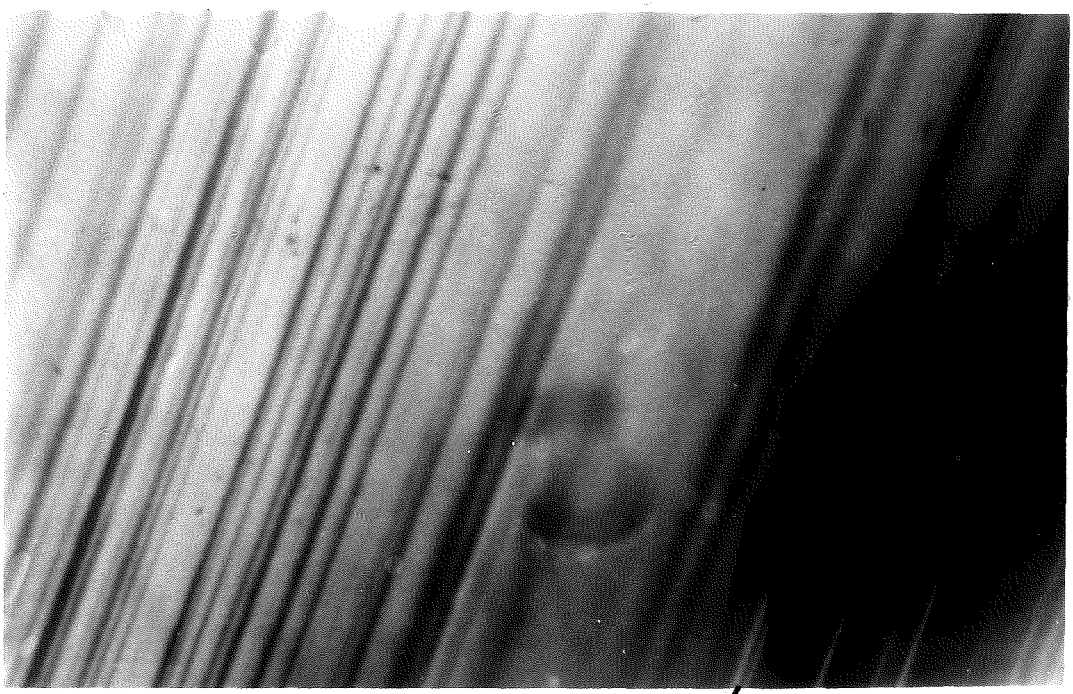


50μ

(a)

(101)

C.A.



50μ

(b)

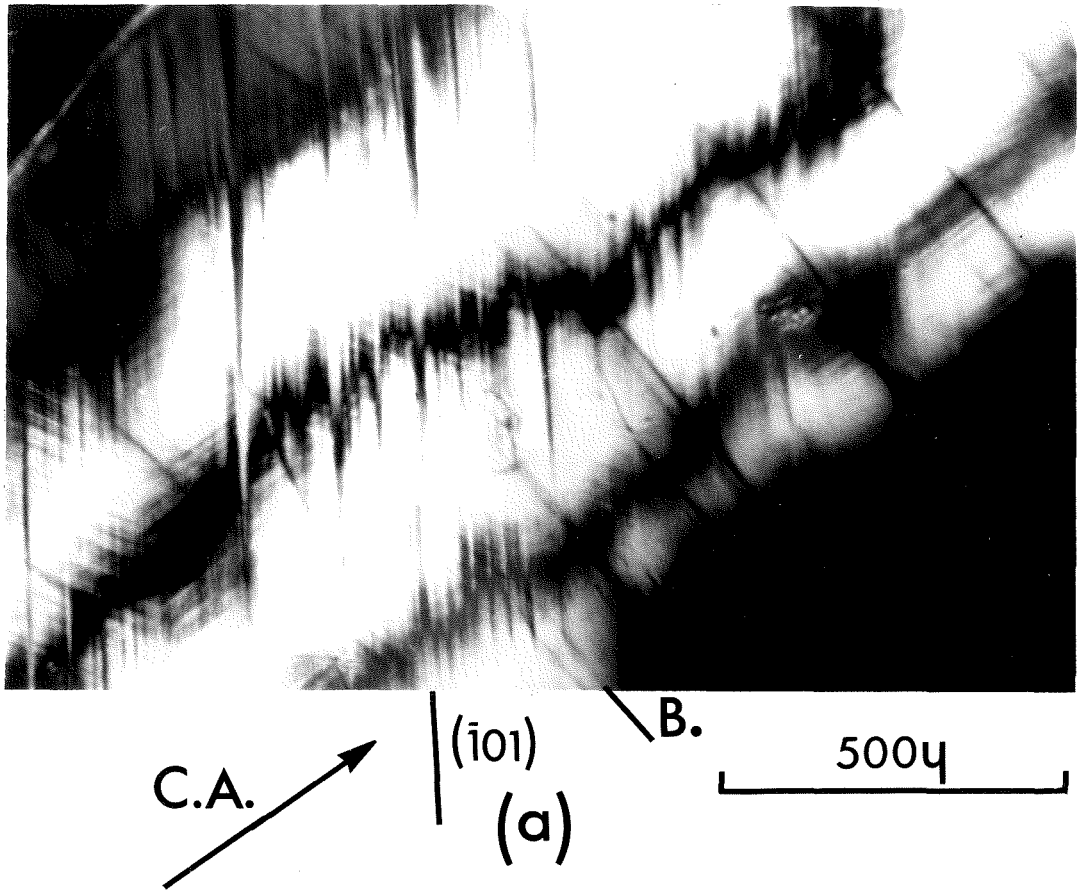
(0$\bar{1}$1)

C.A.

Figure B32 (a) $(\bar{1}01)$ Slip Traces and Lateral Traces (B)

(b) $(1\bar{1}0)$ and $(\bar{1}01)$ Slip Traces

on 22 at.ppm. Oxygen Doped <122>
Crystal Strained 6% at 77°K


C.A.
(ī01)
B.
500μ
(a)

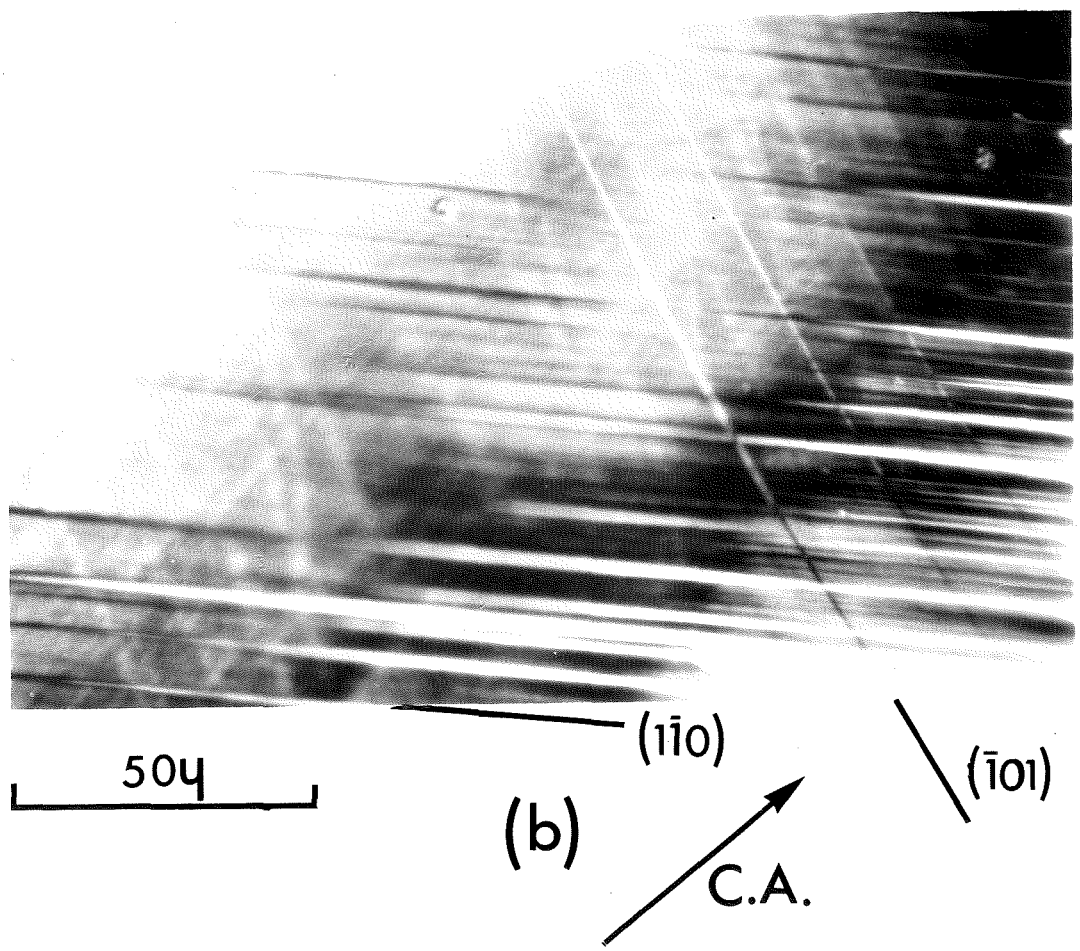
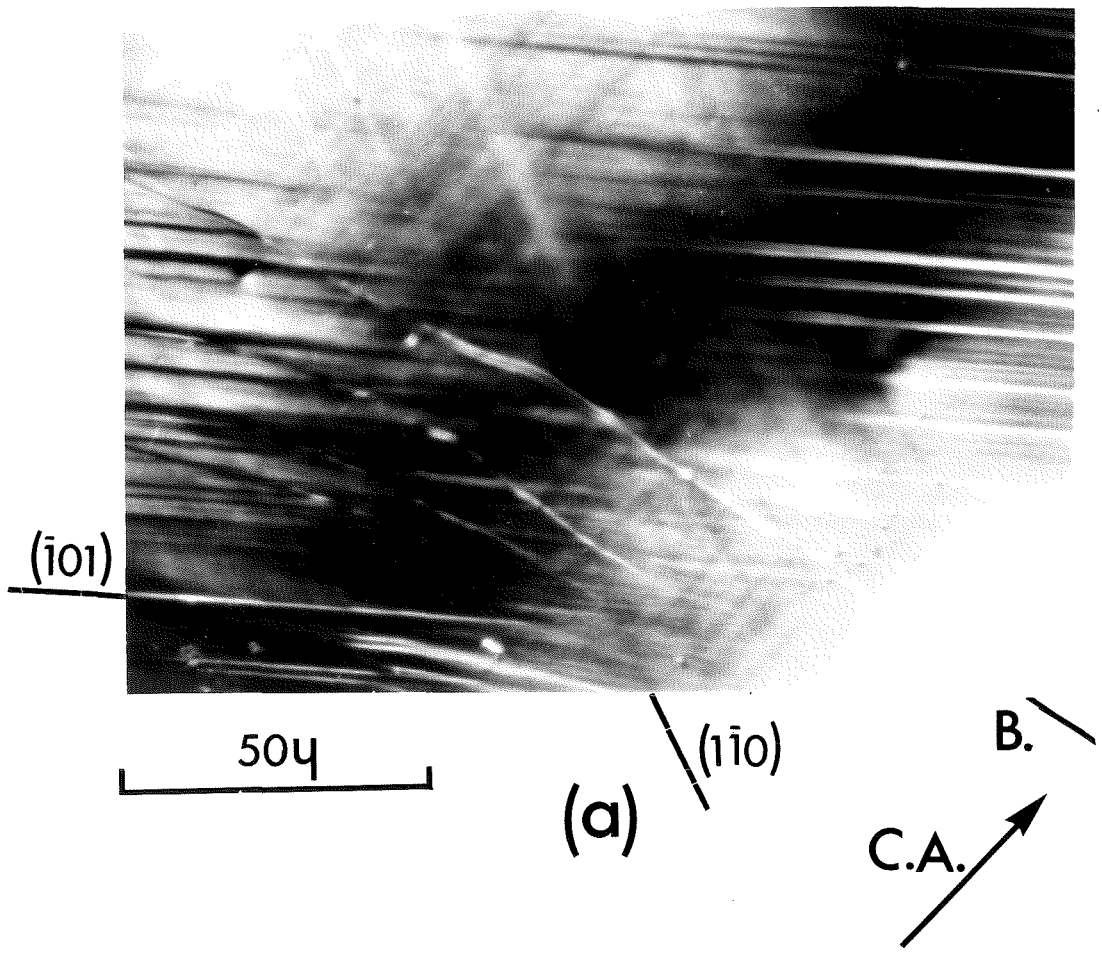
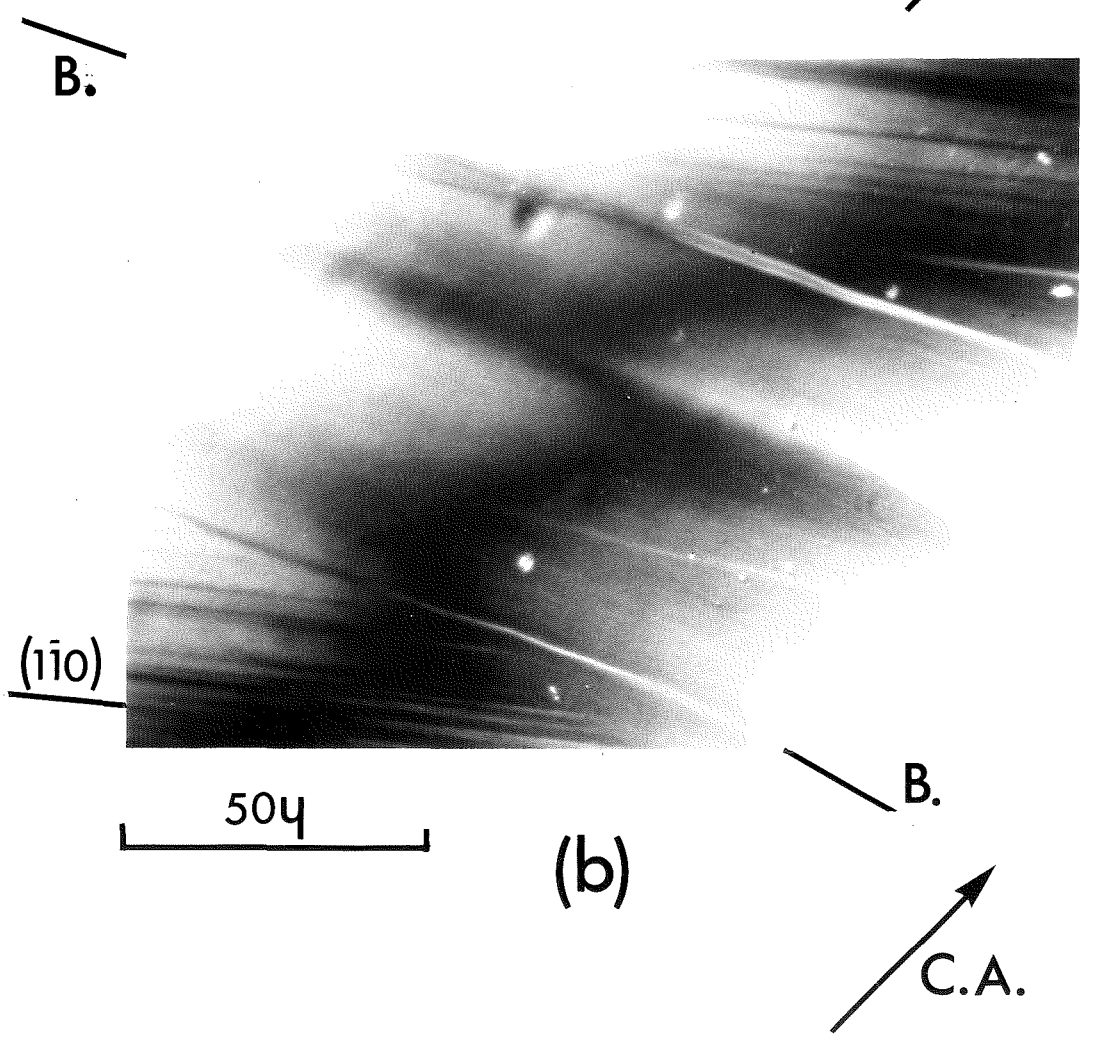

50μ
(1ī0)
(ī01)
(b)
C.A.

Figure B33 Surface of 22 at.ppm. Oxygen Doped <122> Crystals Strained 6% at 77°K showing

(a) $(\bar{1}01)$ Slip Traces Traversing Lateral Trace (B)

(b) $(1\bar{1}0)$ Slip Traces Excluded from Zone Bounded by Lateral Traces (B)


(ī01)
50μ
(1ī0)
B.
(a)
C.A.


B.
(1ī0)
50μ
B.
(b)
C.A.

other cases they appeared to be excluded from or confined within zones bounded by the lateral traces.

Chapter 11

DISCUSSION

The central triangle, easy-glide orientation has been the most frequently employed in investigations of the deformation behaviour of single crystals. Both compression and tension tests were conducted on crystals of this orientation in the present study of molybdenum-interstitial alloys. The introductory discussion in Section 11.1 is concerned with the general features of the deformation behaviour observed in these tests. The bulk of the mechanical properties data relating to the variation of temperature, concentration and orientation was obtained on nitrogen doped crystals tested in tension and these are discussed in the following three Sections 11.2 - 11.4. The less comprehensive set of results for the molybdenum-oxygen alloys are compared with that for the molybdenum-nitrogen alloys in Section 11.5. The slip geometry observations for the compression test specimens are treated in Section 11.6. In the final section, the effects of alloying on the mechanical properties are compared with those observed in other investigations and also with the physical property measurements reported in PART A.

11.1 The General Effects of Interstitials on the Deformation Behaviour

The most prominent feature of the deformation behaviour of the interstitials alloys was the discontinuous yield which was observed at all concentrations, temperatures and orientations. The yield point and constant stress yield elongation shown by the low interstitial content (viz. 7-8 at.ppm. nitrogen, 22 at.ppm. oxygen)<149> crystals tested in compression is typical of

the discontinuous yield behaviour of iron and other b.c.c. metals known to contain traces of interstitial impurities. This behaviour is a consequence of the pinning of the initial dislocations by atmospheres of interstitial atoms (Cottrell atmospheres) or precipitates. It may be regarded as a dynamic phenomenon where the rapid rise in the stress to the yield point is a consequence of the low initial mobile dislocation density and the stress dependence of the dislocation velocity.

Some segregation of interstitial atoms to dislocations would be expected during the preparation of the molybdenum-interstitial alloys. The very low terminal solid solubilities of interstitials in molybdenum at low temperatures would promote prenucleation clustering at preferential sites such as dislocations during the quench. The characterisation studies reported in PART A clearly indicated that when the quenching rate was insufficient to secure all the interstitials in solid solution, precipitation first occurred on dislocations. In addition, there may have been segregation of interstitials to form Cottrell atmospheres at the solution treatment temperature but there is evidence to suggest this effect was comparatively minor. For example the H.V.A. material, which was believed to have a total interstitial content of up to 10 at.ppm., showed no effect of dislocation pinning by interstitial atmospheres. The formation of atmospheres would have been favoured by the slow cooling rates from the annealing temperatures.

In the low interstitial content molybdenum tested in compression, it would appear that dislocation pinning alone was responsible for the changes in the stress-strain behaviour. No change in the stress level or work hardening rate at large strains was observed in this material. This indicates that the low interstitial concentrations in solid solution had a negligible effect on the dynamic properties of the dislocations. The yield discontinuity may then be ascribed to a reduction in the initial mobile dislocation density and is unlikely to be associated with other dislocation parameters such as the friction stress on individual dislocations. Although it has been shown

that thermal activation usually plays no role in source activation during discontinuous yielding, there is no evidence in this particular case to indicate it does not. So the possibility of the thermally activated unpinning of 'weakly' pinned dislocations should not be discounted.

The introduction of a yield discontinuity is also commonly associated with substitutional alloying where there is no evidence of dislocation pinning occurring. For example, the addition of 2 at.% niobium to continuously yielding <149> molybdenum crystals reduces the stage 0 microstrain and causes the stress to rise rapidly to a rounded yield point (Taylor et al. 1973a). The edge exhaustion hardening models of the yield attribute this stage 0 alloy hardening to an increase in the friction stress for edge dislocations relative to screw dislocations. It is probable that in molybdenum doped with larger concentrations of interstitials (viz. >34 at.ppm. nitrogen, >80 at.ppm. oxygen) this type of edge hardening mechanism was also operative and was responsible for reinforcing or modifying the discontinuous yield associated with dislocation pinning.

The marked reduction in the work hardening rate at large strains which occurred in the higher interstitial content tension specimens indicates that interstitial atoms in bulk solid solution, as distinct from those segregated to dislocations, were influencing the deformation behaviour. Changes in dislocation parameters, including the friction stress and/or dislocation multiplication rate, caused by interstitial atoms in solid solution may therefore account for some of the qualitative changes in the form of the yield which occurred at the higher interstitial concentrations. The most notable of these was the usual absence of a yield elongation. The constant stress yield elongation, which was very pronounced in the low interstitial content <149> compression specimens at low temperatures, is normally associated with the propagation of macroscopic bands of deformations (Lüders bands) along the specimen length after localised yielding has occurred. This behaviour is particularly characteristic of the heterogeneous deformation induced by

dislocation pinning in both polycrystals and single crystals. Although the molybdenum <149> crystals containing higher interstitial concentrations showed an initial low work hardening rate this was not associated with any obvious deformation bands. This more homogeneous yield behaviour is consistent with an influence of unsegregated interstitials in solid solution on the dynamic behaviour of dislocations.

The reduction in the work hardening rate after the yield, which occurred in the molybdenum <149> crystals doped to high interstitial concentrations, is typical of the effects of alloying. Slip band coarsening is also generally observed when pure b.c.c. metals are alloyed with both interstitial and substitutional solutes. Coarse slip traces were observed in all the interstitially doped molybdenum crystals. It would seem that there is a close relationship between a coarse, inhomogeneous slip morphology and a low work hardening rate.

Coarse slip reflects a low work hardening rate within slip bands such that slip does not spread to the surrounding undeformed material. In turn, a low macroscopic work hardening rate may be in part a consequence of the concentration of deformation into coarse slip bands. This type of heterogeneous slip behaviour tends to stabilise slip bands, corresponding to a particular slip system, in localised regions of material and inhibits the formation of slip bands of other slip systems. In so far as a high work hardening rate is associated with the interaction of dislocations on intersecting slip systems, the greatly reduced volume of crystal in which such intersections can occur will promote a low work hardening rate. Although the microscopic inhomogeneity of slip caused by alloying may reinforce a reduction in the work hardening rate, it is probably only a second order effect. This conclusion is supported by the occurrence of coarse slip traces in the low nitrogen and oxygen content molybdenum alloys where the work hardening rate was not reduced.

A coarse, inhomogeneous slip morphology is generally caused by the difficult nucleation and easy propagation of slip. At low oxygen and nitrogen

concentrations the slip band coarsening observed may be rationalised in terms of interstitial pinning directly inhibiting the nucleation of slip. The formation of a slip band would then be associated with the activation of dislocation sources at some critical stress and the subsequent propagation of an avalanche of dislocations at high velocity into undeformed material. This behaviour is not contingent on any changes in the dynamic properties of dislocations but simply on the heterogeneous and catastrophic activation of slip. At higher concentrations interstitial atoms in bulk solid solution are likely to influence mobile dislocation parameters. For example, the inhibited operation of dislocation sources may, additionally or alternatively, be due to more difficult cross-slip. This is generally held to be the case in substitutional alloys where no direct pinning occurs. An increase in the stress dependence of the velocity or density of mobile dislocations which facilitates easy slip propagation will also favour a coarse slip morphology. The simultaneous reduction in the work hardening rate which occurred in the higher interstitial content molybdenum is also probably a consequence of such changes, since a large stress sensitivity of the dislocation velocity or multiplication rate promotes a low work hardening rate.

11.2 The Temperature Dependence of the Yield and Flow Stress

The relation between yield and flow stress parameters and the frictional resistance to dislocation motion is not well understood. The most commonly used parameters are defined with respect to the stress-strain curve obtained in direct deformation tests. As the discussion in Section 8.4.1 has shown, conclusions about the friction stress on dislocations based on this type of data alone may be misleading. The author believes that differential temperature change tests provide a more satisfactory means of establishing the temperature dependence of the friction stress on individual dislocations.

This method avoids the confounding effects of dislocation pinning which may be associated with the yield stress and should minimise any variation in the dislocation structure and, in particular in the mobile dislocation density, with temperature.

The control, temperature change experiments reported in Section 9.8 indicated stress increment hysteresis effects which may influence the interpretation of some of the effective stress data. This general type of hysteresis effect was first noted by Stokes and Cottrell (1954) who observed that in aluminium the stress increment for downward temperature changes between $0^{o}C$ and $-185^{o}C$ was significantly greater than for upwards temperature changes. This behaviour was closely associated with a pseudo yield and load drop which occurred on reloading at $0^{o}C$ after the low temperature prestrain. It was suggested that the deformation structure introduced at the low temperature was unstable, at least under load, at the high temperature causing a relaxation of the load and a 'work softening' effect.

A similar type of phenomenon, usually involving both a hysteresis of the stress increment and pseudo yield points, has also been observed in temperature change tests in b.c.c. metals (e.g. Statham 1968). However, the effect is observed at much lower homologous temperatures and it is not certain that the same relaxation explanation is always appropriate.

The temperature change hysteresis observed in this investigation does not appear to conform with the usual work softening observations or explanations. There was a notable absence of any pseudo yield points or load drops indicative of a breakdown of the deformation structure. Further, the discrepancy in the stress level responsible for the hysteresis occurred at the lower temperature before and after room temperature deformation. Usually, the hysteresis derives from the uncertain definition of the flow stress at the higher temperature due to the occurrence of a pseudo yield point.

A distinguishing feature of the <149> and <001> crystals which showed temperature change hysteresis effects was that, at the strains and temperatures

concerned, high work hardening rates characteristic of the stage 0 microstrain region of the flow curves occurred. Those other specimens which did not exhibit hysteresis effects were all subjected to the same prestrain and temperature cycling sequence but, in stage I, where the work hardening rate was low at all temperatures. These included both doped and H.V.A. crystals of the same and different orientations to those showing the anomalous behaviour. This strongly suggests that the hysteresis effect is related to the high stage 0 work hardening rate rather than the crystal orientation or interstitial content.

It is generally recognised that in stage I deformation in b.c.c. metals the work hardening is associated with a rise in the long range internal stress and that there is no appreciable strain dependence of the density of thermal obstacles (Sestak and Seeger 1973). Hence, both the strain rate sensitivity and the stress increments associated with differential temperature changes are largely independent of strain.

The work hardening mechanism in the stage 0 microstrain region which is most prominent at certain orientations in molybdenum, is not well understood. The strain dependence of the activation volume (v^*) in this region (Guiu 1967, Pink 1973) implies that the work hardening is due to an increase in the effective stress. So the stress increment ($\Delta\tau$) associated with a temperature change would also be expected to be stress and hence, strain dependent. Guiu (1967) has in fact found that a generalised Cottrell-Stokes law of the type, $\frac{\Delta\tau}{\tau}$ = constant, is obeyed in the rapid work hardening stage 0 region for <001> molybdenum crystals. This does not necessarily signify an increase in the density of thermal obstacles with strain, since the probable change in the mobile dislocation density and the operation of more than one rate controlling mechanism precludes any simple interpretation of the relation.

In any event, the increase in the temperature change stress increment with strain is consistent with the hysteresis shown by the <001> crystals in this investigation. Pink's (1973) observation of a decrease in v^* with strain

in the stage O region for <149> molybdenum crystals suggests a similar thermal work hardening explanation for the hysteresis shown in Fig.B9b. If the relatively small amount of work hardening which occurred at 298°K and 158°K, after the 110°K prestrain of the <149> H.V.A. specimen, were due to an increase in the effective stress, a flow stress similar to that observed on recycling to 110°K would be predicted. Pink (1973) has also found that v^* is relatively constant at strains > 5% and temperatures between 77°K and 300°K, indicating that no appreciable thermal hardening is occurring at these strains. This observation is consistent with the absence of any hysteresis effects at large strains (>7%) in the H.V.A. <149> crystals tested in this investigation (see Section 9.8). It also implies that the work hardening is athermal at these strains. It may thus be concluded that the 'effective' stress versus temperature data for <149> crystals reported in Chapter 10 is likely to represent the temperature dependence of the friction stress on screw dislocations moving on the primary slip system in stage I.

The 'effective' stress data for the H.V.A. and nitrogen doped <149> crystals presented in Fig.B17, shows that nitrogen causes an increase in the temperature dependence of the 'effective' stress between 300 and 77°K. The magnitude of this increase is a monotonic increasing function of the nitrogen concentration and for 100 at.ppm. nitrogen is ~20% of the 'effective' stress at 77°K. In contrast, the concentration of residual interstitials in solid solution in the H.V.A. material (1-2 at.ppm.) would make a very small contribution to the 'effective' stress at 77°K.

The 'effective' stress is referred to the flow stress at room temperature which is well below the athermal flow temperatures for molybdenum (>450°K). The nitrogen doped specimens could not be tested above ~370°K because ageing could have occurred during testing. Extrapolation of the 'effective' stress from room temperature to the athermal flow temperatures may not provide a reliable basis for estimating the contribution of nitrogen to the thermal component of the flow stress above room temperature. At best, the thermal

contribution of nitrogen determined in the 300-77°K temperature range defines a minimum value for the total thermal contribution. This may be invalidated by such effects as the apparent 'softening' of the doped material with respect to the H.V.A. material, which was observed at room temperature. The significance of this behaviour will be discussed in Section 11.3. There is also little justification for extrapolating the 'effective' stress to the 0-77°K temperature range where as much as half of the total increase in the stress level may occur. There have been frequent observations of solution softening (e.g. Nakada and Keh 1968) where the hardening effect of interstitials at high temperatures has been reversed at lower temperatures.

The temperature dependence of the yield stress shown in Fig.B18 is also seen to increase with increasing nitrogen content. The large difference between the temperature dependence of the doped and undoped material is a direct consequence of their different forms of yielding and has no other significance. The 0.2% proof stress used to define the yield, generally corresponded to the lower yield stress of the discontinuously yielding doped material. This is more a material constant than the upper yield stress or proportional limit and so comparisons between the yield stress of material doped to different nitrogen levels should be reliable. The same comments apply to the extrapolation of the yield stress data as have been made above with respect to the 'effective' stress data.

The temperature dependence of the yield stress of the doped material does not differ significantly from that of the 'effective' stress except perhaps, at the lowest temperatures, where the yield stress does not rise as rapidly as the 'effective' stress. Given the likely scatter of the data (larger for the yield than for the 'effective' stress) this difference may not be significant. It would appear that, at least at the concentrations considered here (34-216 at.ppm.) similar thermally activated processes control the yield behaviour and the flow behaviour at large strains.

11.3 The Concentration Dependence of the Yield and Flow Stress

To permit any useful comparison of the hardening effect of nitrogen in molybdenum with theoretical predictions and other experimental data, it is necessary to separate the thermal and athermal hardening components.

Since no yield or flow stress data was obtained at temperatures in the athermal flow region (>450°K) in this investigation, no reliable estimate of the magnitude of any athermal hardening which may have occurred can be made. However, the accumulated results of comparable Group Va metal-interstitial alloy studies (Smialek and Mitchell 1970a, Loomis and Gerber 1970, Taylor and Bowen 1970) indicate that the athermal hardening effects are very small at concentrations less than 200-300 at.ppm.

Somewhat less than 15% of the total rise in the macroflow stress between temperatures >450°K and 77°K for molybdenum <149> crystals, occurs above room temperature (Guiu 1966). Assuming a simple extrapolation from room temperature to athermal flow temperature is valid, a conservative upper limit can be placed on the thermal hardening by subtracting the room temperature flow or yield stresses from the low temperature values.

The temperature dependence of the 'effective' stress shown in Fig.B17 indicates that nitrogen causes thermal hardening in the temperature range 77°K to 300°K. But, at room temperature, where all the specimens were prestrained before commencing temperature cycling, the flow stress of some of the doped crystals was less than that of the H.V.A. crystal. This apparent solution softening may complicate the interpretation of the 'effective' stress versus temperature data.

Reference to Fig.B16 indicates that the 34 and 93 at.ppm. nitrogen doped molybdenum tested at room temperature, showed flow stress levels at large strains ~5 kg/mm.^{2} less than that of the H.V.A. and 216 at.ppm. nitrogen doped material. This is in part a consequence of the comparatively low work

hardening rates shown by the doped material after yielding. The magnitude of the softening is a function of strain and it is probable that at sufficiently large strains, corresponding to stage I for both the H.V.A. and doped molybdenum, softening effects would also occur at lower temperatures. In so far as this softening behaviour does not exhibit many of those characteristics normally associated with solution softening phenomena, none of the conventional explanations seem applicable.

Solution softening is generally observed over a restricted temperature range and at low temperatures. It is frequently rationalised in terms of a reduction in the thermal component of the flow stress. The softening observed in the molybdenum-nitrogen alloys probably extends over the full temperature range and is quite obtrusive at high temperatures. It would be difficult to reconcile these observations with a reduction in the thermal component of the lattice frictional stress on alloying molybdenum with nitrogen. Furthermore, although the magnitude of the thermal hardening effect of nitrogen deduced from the yield stress or 'effective' stress versus temperature data is in doubt, there is no doubt that thermal hardening rather than softening occurs in the 77-300^{o}K temperature range.

Scavenging explanations of the type used by Ulitchny et al. (1972) to rationalise solution softening in many Group Va-interstitial systems, do not necessarily predict softening which is confined to low temperatures. The concentration of interstitial atoms in solid solution in the H.V.A. molybdenum is very small (1-2 at.ppm.) and has been shown to cause a negligible hardening effect. Thus, the association of these residual interstitial atoms with the doped nitrogen atoms is unlikely to cause solution softening at the comparatively large concentrations observed ($\geq$34 at.ppm.).

Since the apparent solution softening observed in these alloys is accompanied by, and in some sense is a direct consequence of, a reduction in the work hardening rate, a satisfactory explanation of the phenomenon should also account for the change in the work hardening behaviour. The possible

mechanisms responsible for the alloying effects on the work hardening behaviour and the parallel effects on the slip morphology have been discussed in Section 11.1. Both a low work hardening rate and a coarse slip morphology are favoured by a strong stress dependence of the dislocation velocity and multiplication rate. The objections to any explanation of the apparent softening involving an increase in the stress dependence of the dislocation velocity (or a reduction in the lattice friction stress) have been stated above. A suggestion based on a change in the stress sensitivity of the dislocation multiplication rate after the initial activation of sources, would seem more attractive.

Both the reduction in the work hardening rate and in the flow stress level at room temperature on doping molybdenum with 34 at.ppm. nitrogen may be explained by an increase in the dislocation multiplication rate and a concomitant increase in the mobile dislocation density. Provided such an interstitially induced increase in the stress dependence of the dislocation multiplication rate is relatively insensitive to temperature and to increases in the interstitial concentration above some critical level required to produce it, both the concentration and temperature dependence of the softening effect can be explained. After the initial reduction in the flow stress at room temperature, on doping with 34 at.ppm. nitrogen, the subsequent increase in the flow stress as the nitrogen content is further increased is a consequence of the increasing frictional hardening effect of the nitrogen. At lower temperatures the larger thermal hardening contribution of nitrogen to the friction stress, which is indicated by the 'effective' stress versus temperature data, should reduce the magnitude of the softening. Also, if the apparent solution softening is a consequence of a temperature independent change in the mobile dislocation density, the 'effective' stress versus temperature data may then be validly employed to estimate the thermal hardening rate for nitrogen.

The 'effective' stress of the H.V.A. <149> molybdenum crystal given in

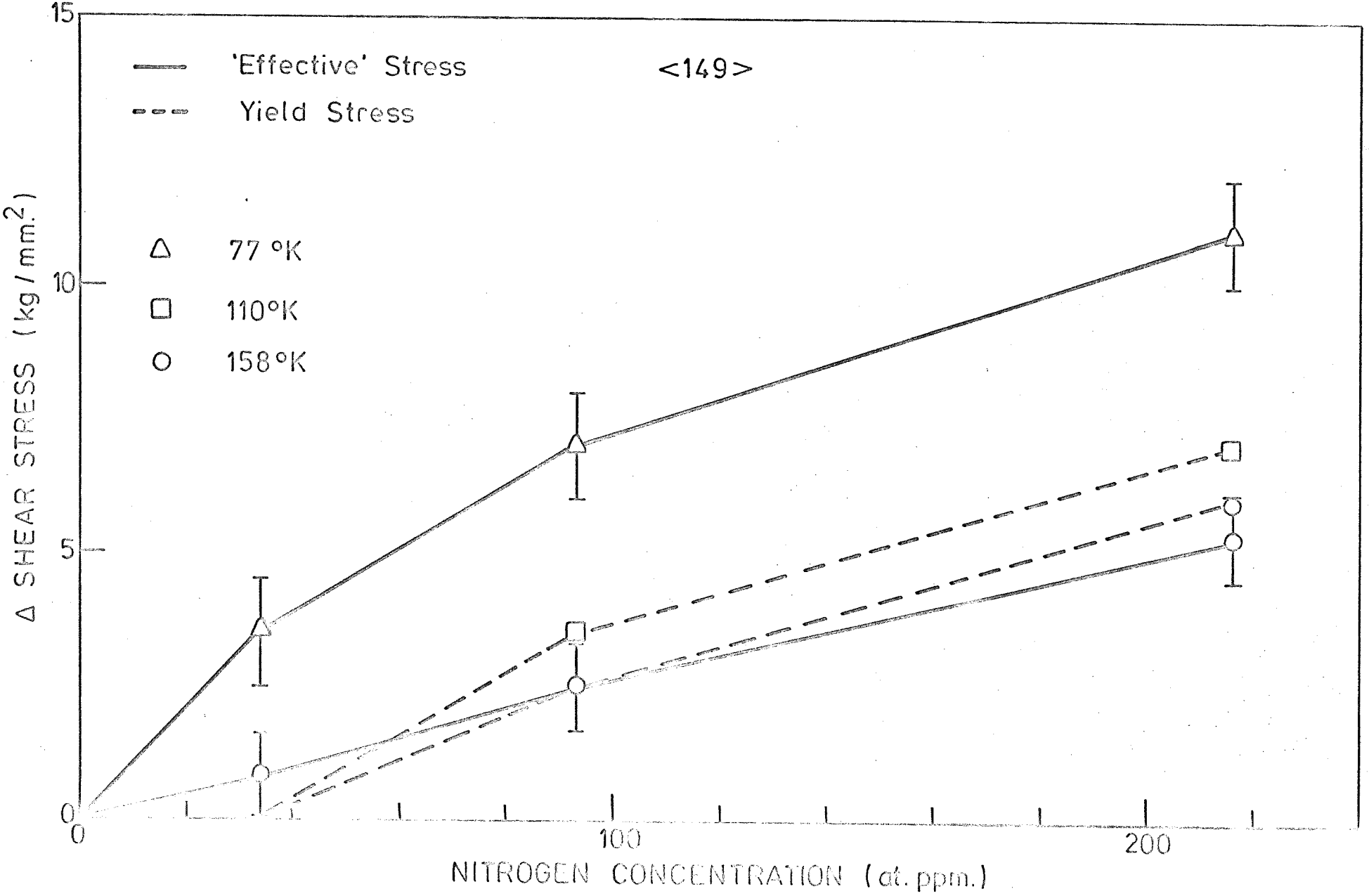
Fig.B17 has been subtracted from the 'effective' stress of the nitrogen doped molybdenum and plotted against concentration in Fig.B34. The consistent trends shown by the 'effective' stress data as presented in both Fig.B17 and Fig.B34 suggest that the error bars based on the uncertainty of the specimen cross-sectional areas are realistic estimates of the random errors. So both the increase in the magnitude of the hardening with decreasing temperature at a given concentration, and the decreasing hardening rate with increasing concentration shown at 77°K, are significant trends.

The yield stress versus temperature plots given in Fig.B18 also indicate some thermal hardening due to nitrogen. No meaningful comparison of the yield stress of the doped and H.V.A. molybdenum can be made because of their different yield forms. So, any estimate of the thermal hardening rate for the yield must be confined to a comparison of the yield stress of molybdenum doped to different nitrogen levels. This means that the hardening rate can only be estimated in the concentration range 34-216 at.ppm. nitrogen.

The thermal component of the yield stress, referred to that of the 34 at.ppm. nitrogen crystals, has also been plotted against concentration in Fig.B34. The magnitude of the thermal hardening has been calculated from the yield stress data in Fig.B18 by first subtracting the room temperature yield stress values to give the 'thermal' component of the yield stress, and then subtracting the thermal component of the yield stress of the 34 at.ppm. nitrogen specimens from those of the 93 and 216 at.ppm. specimens. There is a significant increase in the thermal hardening of the yield stress between 298°K and 158°K. The data scatter for the yield stress is probably greater than that indicated for the 'effective' stress. Thus, the unexpectedly small difference between the 158°K and 110°K hardening rates is probably within the experimental error (say $\pm$ 2 kg/mm.^{2}).

A comparison of the concentration dependence of the yield and 'effective' stress is only possible at 158°K and over the concentration range 34-216 at.ppm. The larger hardening rate of the yield stress at this temperature may not be

Figure B34 Thermal Hardening of 'Effective' and Yield Stress versus Nitrogen Concentration for <149> Crystals


'Effective' Stress
Yield Stress
77 °K
110°K
158°K
Δ SHEAR STRESS (kg/mm.2)
15
10
5
0
0
100
200
NITROGEN CONCENTRATION (at. ppm.)

significant given the probable errors mentioned above. Should it be, the result is consistent with those obtained by Taylor and Bowen (1970) on niobium <149> crystals. They found that the yield stress was far more sensitive to the nitrogen content than was the 'effective' stress. Although there is a general indication that in the molybdenum-nitrogen alloys both the yield and 'effective' stress are equally valid indices of dislocation mobility, the better quality of the 'effective' stress data would recommend its use, wherever possible, in comparisons with theory or other experimental results.

The 77°K 'effective' stress data may be fitted to a $\Delta\tau^* \propto C^{\frac{1}{2}}$ obstacle hardening type relation but the 158°K 'effective' stress does not deviate significantly from a linear concentration dependence. Some of the unsatisfactory aspects of comparisons of the observed concentration dependence with those predicted by the point obstacle hardening models have been discussed in Section 8.4. There are further difficulties in this instance. Both the characterisation studies reported in PART A and the results of Evans et al. (1970) indicate that an increasing proportion of the nitrogen is aggregated into nitrogen pairs and larger clusters as the total nitrogen content of the alloys is increased. Therefore, the concentration dependence of the 'effective' stress will reflect not only a change in the density of solute obstacles but also a change in the magnitude of the obstacles. Frank (1968) has developed a hardening theory treating a multiple spectrum of dislocation obstacles. However, the model does not consider a concentration dependence of the spectrum and so a comparison of these experimental observations with its predictions is invalidated.

Any comparison of the thermal hardening rates observed in the molybdenum-nitrogen alloys with those observed in other investigations must be carefully made because of the large influence different yield and flow definitions may have on the apparent hardening rates. The frequently non-linear concentration dependence of the hardening rate in the thermal region also means that the concentration range over which the comparison is made is important.

The only recent investigation of a b.c.c. metal-interstitial alloy which has employed differential temperature change tests to define the effective stress was conducted by Taylor and Bowen (1970) on <149> niobium-nitrogen alloy crystals in the concentration range 0-150 at.ppm. A small hardening effect relative to the total flow stress was observed, but at 77°K the hardening rate of the shear stress averaged over the concentration range 0-150 at.ppm. may be calculated from their data to be 200 ± 100 kg/mm.^{2} at.%. The hardening rate of nitrogen in the molybdenum averaged over the same concentration range is ≥ 600 kg/mm.^{2} at.%. So the hardening rate of nitrogen in molybdenum is at least a factor of two greater than in niobium.

Both Smialek and Mitchell (1970a) and Taylor and Bowen (1970) have also obtained reliable data for the thermal hardening of the yield stress in tantalum-nitrogen and niobium-nitrogen alloys respectively. The hardening rates for these and the molybdenum-nitrogen alloys at 110-115°K have been averaged over their common concentration range (viz. 30-150 at.ppm.) and are presented in Table B3. The quoted errors of the hardening values represent

	Mo	Nb	Ta
$\Delta\tau^*$ (kg/mm.^{2} at.% Nitrogen) 110-115°K 30-150 at.ppm.	≥ 400	330 ± 70	300 ± 150
YIELD DEFINITION	0.2%ε Proof Stress	0.3%γ Proof Stress	2%γ Proof Stress
$\dot{\varepsilon}$ (sec.$^{-1}$)	1.7×10^{-4}	1.3×10^{-4}	3.5×10^{-4}
REFERENCE	This work	Taylor and Bowen (1970)	Smialek and Mitchell (1970a)

Table B3 Thermal Hardening Rates for the Yield Stress of <149> Crystals

the observed scatter of data but neither the different yield definitions nor the averaging of the hardening rates would give rise to larger errors. The

absolute magnitude of the thermal hardening rates are similar in all three alloys. However, it should be appreciated that the hardening effect of nitrogen relative to the total flow stress is much larger in the Group Va metals, where the base level flow stress of the pure metals is comparatively small, than it is in molybdenum.

11.4 The Orientation Dependence of the Deformation Behaviour

11.4.1 The Yield and Flow Behaviour

There is no satisfactory explanation of the orientation dependence of the yield and flow behaviour of pure molybdenum and this must necessarily limit any interpretation of the effects of interstitial alloying. The discussion in Section 8.3 has shown that an edge exhaustion model should provide the basis for an explanation of the yield but it must be modified to account for the variation in both the yield form and work hardening rate with deformation orientation. The modification would involve some unknown dislocation multiplication or work hardening mechanism, probably requiring screw dislocation motion at stresses below the stage I stress plateau. Furthermore, its operation would depend on crystal orientation and could be related to the orientation dependence of the slip geometry.

The qualitative changes which occur in the deformation behaviour of molybdenum <149> crystals, when doped with low concentrations of interstitials and tested in compression, have been discussed in Section 11.1. The <113> crystals, which also have an easy glide orientation, showed very similar deformation behaviour. The almost immediate onset of duplex glide in the <113> crystals would readily account for the larger flow stress at large strains shown by the <113> crystals at 77^{o}K in comparison with the <149>.

The <122> doped crystals did exhibit more pronounced yield points and

yield elongations than the <149> crystals and at 77°K showed an anomalous, extended yield elongation which will be discussed in more detail in Section 11.6.2. Also, the magnitude of the yield hardening effect appeared far greater for the <122> than the <149> crystals. The continuous yielding behaviour of the H.V.A. <149> specimens prevents any meaningful estimation of the increase in yield stress for this orientation but certainly, in qualitative terms, the hardening effect for the <122> crystals was more dramatic. These differences are probably related to the contrasting yield behaviour of the H.V.A. material at these two orientations. The <149> crystals show a continuous yield and quasi-parabolic flow curve while the <122> crystals show a rounded yield point and then work harden to stress levels at large strains similar to the <149> crystals.

There have been a number of observations of the comparative hardening effects of interstitials for these and similar orientations. (Taylor and Bowen 1970, Lachenmann and Schultz 1972, Webb et al. 1973). Lachenmann and Schultz (1972) found the magnitude of the thermal hardening of the yield stress for nitrogen in tantalum crystals to be strongly dependent on orientation. They interpreted this is terms of an orientation dependence of the thermal component of the friction stress. The difference in the yield stress levels for the doped <122> and <149> crystals tested in the present investigation, represents an orientation dependence of the effect of dislocation pinning on the yield behaviour and should not be interpreted in this way. Only the 'effective' stress data discussed in Section 11.4.2 can be reliably interpreted as indicating any friction stress dependence on orientation.

The general changes in the deformation behaviour of the corner orientation (<001>, <111> and <011>) tension specimens caused by interstitial doping were similar to those of the <149> crystals discussed in Section 11.1 viz. the introduction or reinforcement of a discontinuous yield, the coarsening of the slip morphology, and a tendency to reduce the work hardening rate.

The flow curves of the nitrogen doped and H.V.A. corner orientations crystals have been compared with those of the <149> crystals at 298°K and 158°K in Figs.B35 and B36 respectively. The stress has been resolved on the primary slip systems indicated by the $\psi(\chi)$ curves for molybdenum in Section 8.1 (i.e. the $[111](\bar{1}01)$ system for the <149> crystals, the maximum resolved shear stress $\langle 111 \rangle \{122\}$ for the corner orientation crystals). There is some doubt, however, whether microscopic slip occurs on $\{112\}$ planes, particularly in the anti-twinning sense. Slip on $\{110\}$ planes may be preferred for the corner orientations which would mean an ~14% reduction in the shear stress levels. In general, comparisons of yield and flow stress values between the corner orientations should consider this $\pm$ 14% uncertainty in their magnitudes.

The failure of doping to effect any qualitative changes in the yield and flow behaviour of the <011> crystals is hardly surprising since the H.V.A. crystals exhibited the two main features, i.e. a discontinuous yield and low subsequent work hardening rate, generally favoured by the interstitial alloying. If the occurrence of a discontinuous yield in the H.V.A. material signifies a rapid exhaustion of edge dislocations then a reduction in non-screw dislocation mobility, or changes in other dynamic dislocation properties, would not be expected to do more than reinforce the discontinuous yield behaviour.

The significant increase in the yield stress at room temperature on doping with oxygen (see Fig.B22) suggests direct pinning of the dislocation sources is occurring, where a critical stress greater than the friction stress on mobile screw dislocations is required to activate slip. But the increased yield stress of the nitrogen doped <011> crystals at 158°K shown in Fig.B36 is probably a consequence of an increased friction stress on dislocations. Since the temperature dependence of the yield and 'effective' stress of both the H.V.A. and nitrogen doped <011> molybdenum crystals are the same, within the limits of the experimental error (see Figs.B23 and B24), it is likely that the frictional resistance to dislocation motion determines the magnitude of the yield stress. So the yield hardening observed at low temperatures would

Figure B35 Flow Curves for H.V.A. and Nitrogen Doped Crystals at 298°K

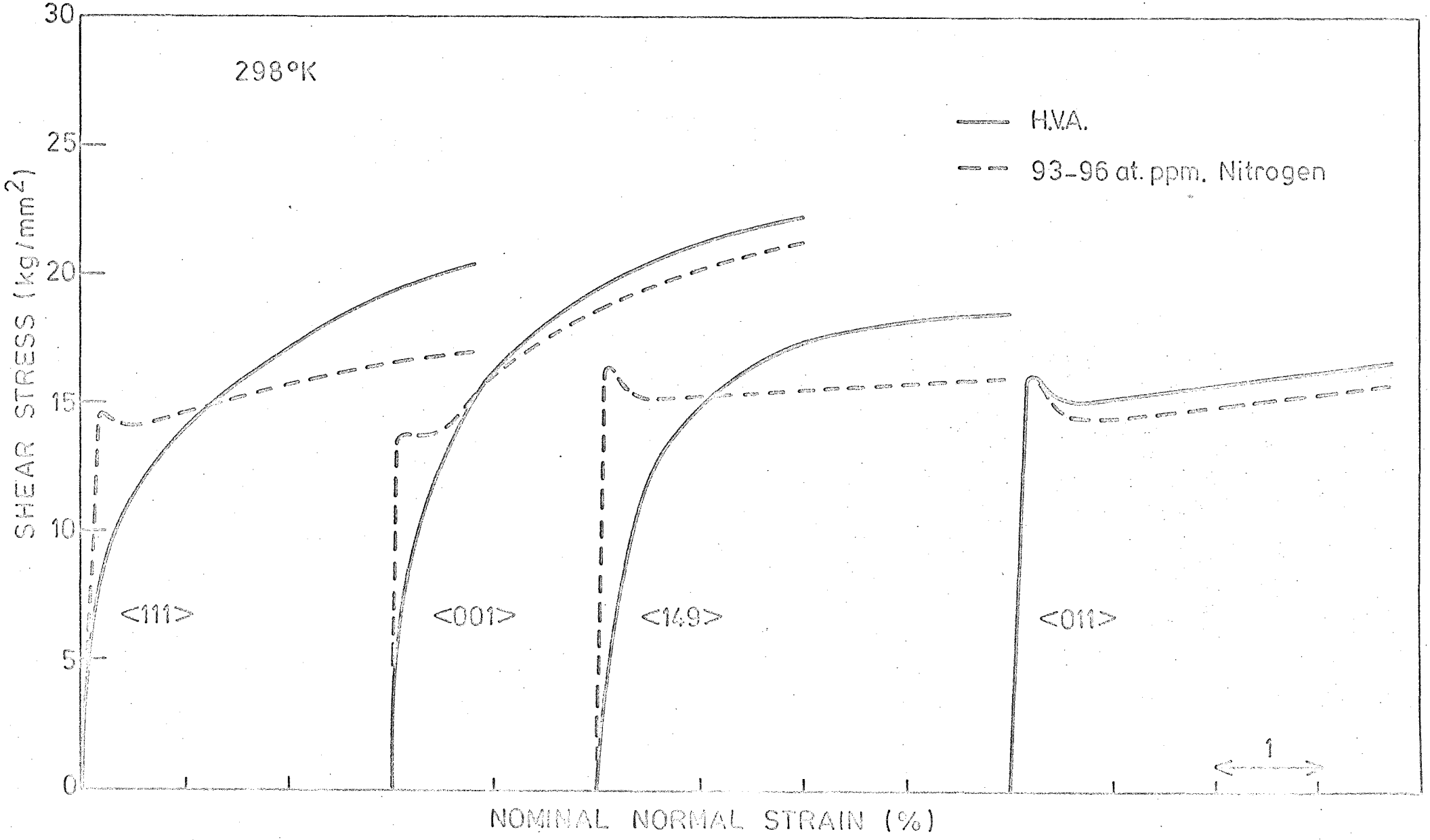
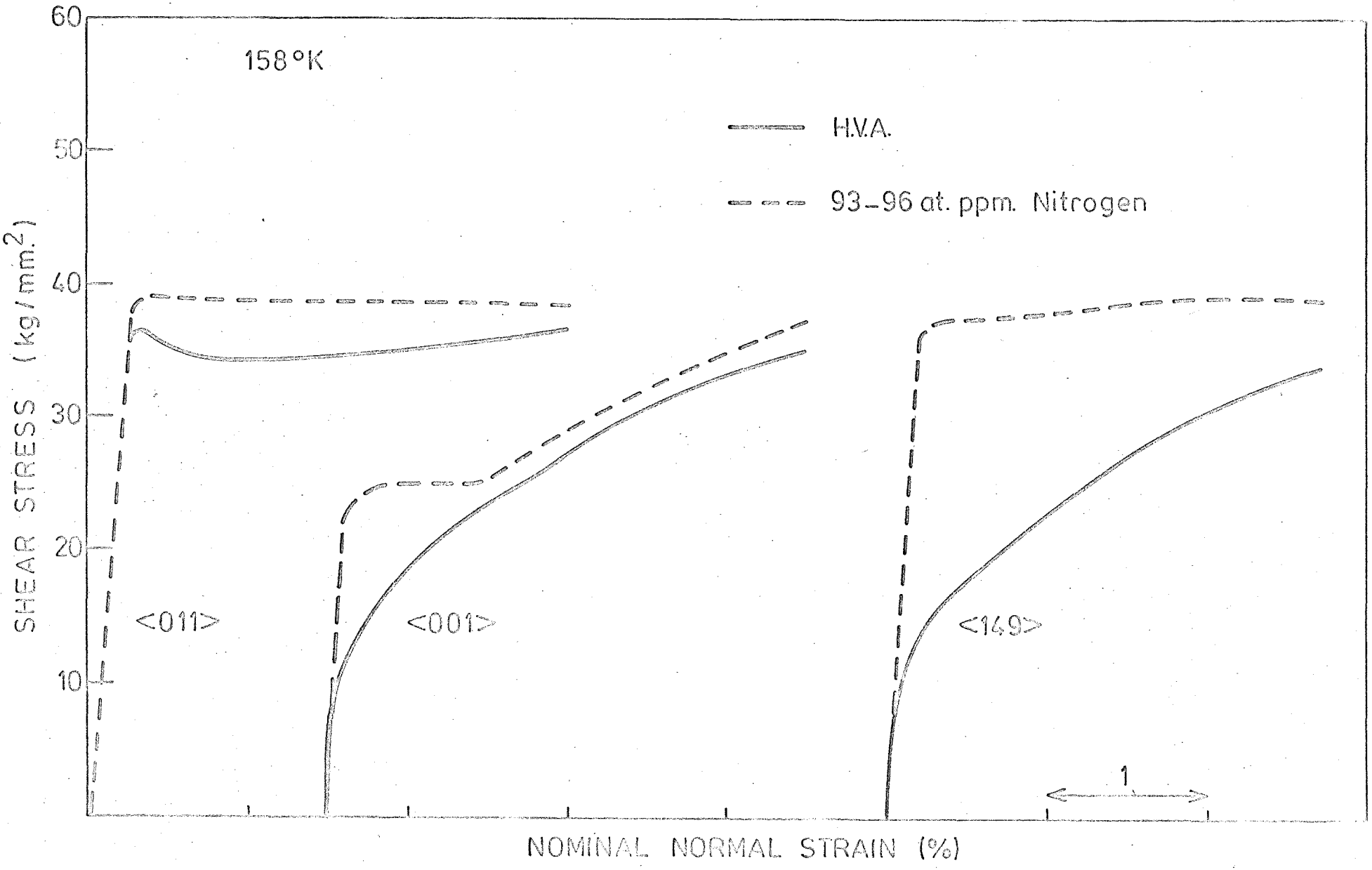

298°K
H.V.A.
93-96 at. ppm. Nitrogen
SHEAR STRESS (kg/mm²)
30
25
20
15
10
5
0
<111>
<001>
<149>
<011>
1
NOMINAL NORMAL STRAIN (%)

Figure B36 Flow Curves for H.V.A. and Nitrogen Doped Crystals at 158^{o}K


158°K
H.V.A.
93–96 at. ppm. Nitrogen
SHEAR STRESS (kg/mm.²)
60
50
40
30
20
10
<011>
<001>
<149>
1
NOMINAL NORMAL STRAIN (%)

represent an increase in the thermal component of the friction stress.

The quasi-parabolic flow curves of the <001> crystals were only modified by doping to the extent that a yield point/constant yield stress elongation occurred at a comparatively low stress level. Should the introduction of the yield be associated with a decrease in the mobility of edge dislocations relative to screws, it is difficult to reconcile the low value of the yield stress with the much higher stress of the stage I stress plateau. This discrepancy suggests that much of the rise in the stress to stage I may not be associated with the exhaustion of non-screw dislocations, but with some other work hardening mechanism not contingent on a large edge to screw mobility ratio. Alternatively, the operation of dislocation sources prior to stage I may ameliorate the effect of a reduction in edge mobility on doping. This proposition would also imply that the orientation dependence of the yield and flow behaviour of pure molybdenum is associated with a dislocation multiplication mechanism whose operation depends on orientation. If dislocation sources should operate in the H.V.A. material at low stresses, the introduction of a yield stress by doping may be partly a consequence of source pinning due, for example, to inhibited cross-slip. This explanation is in good agreement with the inhomogeneous yield/yield elongation observed which is not typical of a stage 0 edge hardening yield mechanism. It may also offer an explanation of the much lower temperature dependence of the yield stress for <001> nitrogen doped crystals in comparison with <011> (see Fig.B24) and <149> (see Fig.B18) nitrogen doped crystals, where the yield stress is more obviously associated with stage I screw dislocation motion. The perseverance of a high work hardening rate after the yield in the <001> doped crystals implies that the mechanism responsible for the discrepancy between the yield and stage I stress level is insensitive to changes in mobile dislocation parameters (e.g. the mobility of edge dislocations).

The <111> doped molybdenum crystals showed a low, discontinuous yield stress similar to the <001> doped crystals and this is also probably indicative

of edge hardening and/or source pinning. But the mechanism responsible for the subsequent rise in stress to the stage I level showed some sensitivity to interstitially induced changes in the dynamic behaviour of dislocations. A reduction in the work hardening rate and stage I stress level occurred. This is possibly due to an increase in the stress sensitivity of the dislocation multiplication rate and mobile dislocation density, as has been suggested for the <149> doped crystals in Section 11.3. The stronger effect of nitrogen than oxygen on the work hardening behaviour (see Fig.B22) is generally consistent with the stronger influence of nitrogen on mobile dislocation parameters such as the friction stress. The comparative behaviour of oxygen and nitrogen doped corner orientation crystals will be further discussed in Section 11.5.

To conclude, it is apparent that the strong orientation dependence of the yield and flow behaviour of the interstitial alloys is sympathetic with that of pure molybdenum. However, a satisfactory explanation of the effects of alloying will necessarily require a better understanding of the mechanism which, in conjunction with the exhaustion hardening of non-screw dislocations, is responsible for the orientation dependence of the deformation behaviour of molybdenum.

11.4.2 The Temperature Dependence of the Yield and Flow Stress

The control, differential temperature change experiments discussed in Section 11.2, have indicated that the stress increments associated with temperature changes are a function of strain in the high work hardening stage 0 microstrain region of <149>, <001> and by implication <111> crystals. The work hardening in the stage 0 region is clearly associated with an increase in the effective stress. So the temperature dependence of the flow stress, determined by temperature change tests, should increase with increasing strain

until stage I is reached. It is important to confirm that the prestrains given to the corner orientation crystals before temperature cycling, were sufficient to ensure that the 'effective' stress versus temperature (τ^*v.T) relation (see Fig.B23) was characteristic of the long range motion of screws in stage I.

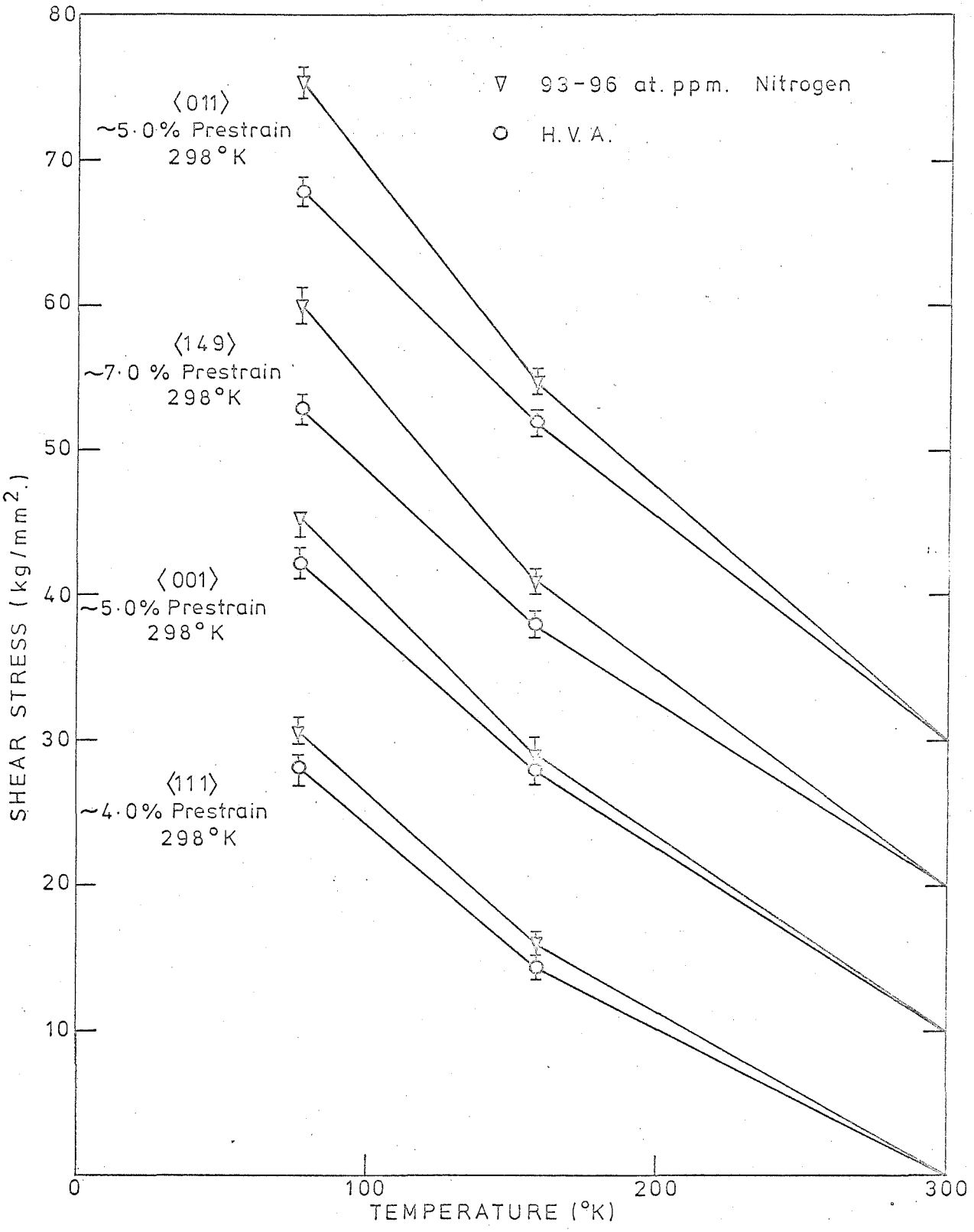
At the ~5% room temperature prestrain employed for the <011> crystals, no strain dependence of the temperature change stress increment was found. This is in agreement with the strain independence of v^* after the macroyield, found by Guiu (1967) for <011> crystals. This firmly establishes that the τ^*v.T relation obtained relates to stage I macroflow. The 4% and 5% room temperature prestrains given to the <111> and <001> crystals respectively, may not have been sufficient to reach the stage I macroflow region. There is no v^* data available for <111> molybdenum crystals. But the prestrain of 4% is only a little greater than the 3% 158^{o}K prestrain at which a hysteresis of the stress increment was observed in <001> crystals. The latter show a similar high work hardening rate to the <111> crystals and it is likely that, at 4% strain, thermal hardening is still occurring in the <111> crystals. Thus the temperature dependence of τ^* given in Fig.B23 is probably smaller than that for stage I deformation. Guiu (1966) has determined v^* for <001> crystals as a function of strain. At the lowest temperature investigated (viz. 195^{o}K) v^* did not saturate until ~7% strain, though the variation between 5% and 7% strain was small (<5% of the total change in v^* in the stage 0 microstrain region). So the τ^*v.T relation determined for <001> crystals after 5% prestrain should be a good estimate of the temperature dependence of the friction stress on screw dislocations in stage I.

The 'effective' stress data plotted in Fig.B23 indicates that 96 at.ppm. nitrogen increases the temperature dependence of the 'effective' stress at all three corner orientations. To make any quantitative comparison of the magnitude of this increase between the different orientations, the 'effective' stress must be resolved onto the operative slip planes. This has been done

in Fig.B37 assuming the operative slip planes for both the H.V.A. and doped material to be those indicated by Taylor et al.'s (1973a) $\psi(\chi)$ data for molybdenum (see Section 8.1). The <149> 'effective' stress data from Fig.B17 has also been presented in Fig.B37. There is the same $\pm$ 14% uncertainty in the magnitude of the shear stress as was specified for the stress-strain curves in Figs.B35 and B36.

To first consider the temperature dependence of the 'effective' stress for the H.V.A. molybdenum, there is a strong indication, but no unambiguous evidence, that the lattice friction stress at low temperatures depends on the operative slip plane. A comparison of the <149> and <011> τ^*v.T data shows the 'effective' stress of the <011> crystal at 77°K to be ~16% greater than that for the <149>. The difference is consistent with the friction stress on {112} planes in the anti-twinning sense being greater than the friction stress on {110} planes. It does not imply that {112} slip is actually occurring in the <011> crystals since a reduction of ~14% in the <011> stress values would also be consistent with {110} slip occurring for both orientations and at approximately the same critical resolved shear stress.

Any comparison of the apparently much larger 'effective' stresses for the <011> and <149> orientations with that for the <111> orientation are not reliable because the latter probably does not relate to the stage I deformation. The <011> and <149> 'effective' stress values at 77°K are at least 3 kg/mm.^{2} greater than the 'effective' stress for the <001>, independent of whether {112} or {110} slip occurs. These differences are approximately equal to the experimental error associated with the uncertainty of specimen cross-sectional areas. They are consistent with the friction stress on {112} planes in the anti-twinning sense and, on the {110} planes, being larger than on the {112} planes in the twinning sense. These observations cannot be regarded as providing evidence for a slip asymmetry themselves but they do agree with the general conclusions reached by Guiu (1969) using direct shear tests on molybdenum (see Section 8.1).


80
70
60
50
40
30
20
10
0
100
200
300
SHEAR STRESS (kg/mm2)
TEMPERATURE (°K)
⟨011⟩
~5·0% Prestrain
298°K
⟨149⟩
~7·0 % Prestrain
298°K
⟨001⟩
~5·0% Prestrain
298°K
⟨111⟩
~4·0% Prestrain
298°K
93-96 at. ppm. Nitrogen
H.V.A.

The evidence for an orientation dependence of the thermal hardening due to the addition of ~100 at.ppm. nitrogen to molybdenum is more impressive. Once again the difference in the magnitude of the thermal hardening for the <011> and <149> orientations is within the ± 14% error defined by the uncertainty of the operative slip plane for the <011> crystals. Both the <011> and <149> orientations show thermal hardening magnitudes more than 100% greater than those for the <111> and <001> crystals. This difference is well outside the limits of the error associated with either the uncertainty of the operative slip system or the specimen cross-sectional area.

The hardening rate for the <111> crystals is unlikely to be such a strong function of the effective stress of the pure molybdenum that a 100% increase in its magnitude could result from the rise in effective stress from the 4% strain level to that of stage I. This possibility cannot be totally excluded because of the uncertainty about the mechanisms responsible for the stage 0 work hardening and the interstitial thermal hardening. The elastic fracture stress of the nitrogen doped <001> crystal at 77°K only defines a lower limit for the nitrogen hardening but a comparison with magnitude of the 158°K hardening indicates it is unlikely to be 100% in error.

11.5 The Comparative Effects of Oxygen and Nitrogen

Although many of the mechanical property changes discussed above are typical of interstitial alloying in general, differences might be expected between the effects of specific atom species. The physical property measurements reported in PART A indicated differences in the behaviour of oxygen and nitrogen in molybdenum which were reflected in their effects on mechanical properties. Any discussion of these should be preceded by a number of qualifying remarks which relate to the preparation and testing of the oxygen and nitrogen doped mechanical test specimens.

Firstly, any comparison of the compression and tension specimens' deformation behaviour should take account of the different precision of characterisation of the alloys prepared in each case. The results reported in PART A have indicated that the certainty of securing all the interstitial atoms in solid solution was greater for the tension specimens than for the compression specimens. Some of the differences in the deformation behaviour of alloys tested in tension and compression may be associated with the greater probability of segregation and clustering occurring in the compression specimens.

Secondly, the uncertainty of the kinetic and thermodynamic data for oxygen in molybdenum leads to some doubt as to both the form and distribution of the oxygen secured in the mechanical test specimens. This may be responsible for some of the features of the deformation behaviour of the oxygen doped specimens which differ from those of the more thoroughly characterised nitrogen doped specimens.

In the low interstitial concentration alloys deformed in compression, nitrogen was observed to exert a much stronger influence on the deformation behaviour than oxygen. For both the <149> and <122> orientations, the 7 at.ppm. nitrogen doped crystals showed a greater yield stress than the 22 at.ppm. oxygen doped crystals. This suggests that the initial dislocations were more strongly pinned by the nitrogen than by the oxygen atoms. The more distinct constant stress yield elongations and the coarser slip bands shown by the nitrogen doped specimens support this conclusion. It has been argued that the dislocation pinning is caused by the preferential clustering of interstitials on dislocations during quenching, rather than the formation of Cottrell atmospheres at the solution treatment temperature. The difference in the pinning strengths of the oxygen and nitrogen atoms would then be a complex function of their relative diffusivities at the solidus temperatures and of other factors such as the volume changes for the respective precipitation reactions.

The flow curves and the temperature dependence of the yield and 'effective' stress for the higher oxygen and nitrogen concentration alloys are compared in Figs.B38 and B39. In calculating the shear stress values it has been assumed that the primary $[111](\bar{1}01)$ system observed to operate in pure molybdenum also operates in the doped material. Reference to Fig.B39 shows that the temperature dependence of the yield stress of the 93 at.ppm. nitrogen material is significantly greater than that for the 70-100 at.ppm. oxygen material. But the absence of any satisfactory yield stress to characterise the strength of the continuously yielding H.V.A. material prevents any quantitative comparison of the thermal hardening of the yield stress by oxygen and nitrogen being made. A comparison of the temperature dependence of the 'effective' stress for the 80 at.ppm. oxygen doped and the 93 at.ppm. nitrogen doped molybdenum indicates that the thermal hardening rate for nitrogen at $77^{\circ}K$ is approximately twice that for oxygen. This may be interpreted as indicating a stronger increase in the frictional resistance to dislocation motion for nitrogen than for oxygen atoms. Smialek and Mitchell (1970a) have also investigated the comparative hardening effects of nitrogen and oxygen on the yield stress of <149> tantalum crystals. At low concentrations (<300 at.ppm.), where rapid thermal hardening occurred, the nitrogen hardening rate was also approximately twice that for oxygen. But at larger concentrations where linear athermal hardening was observed both showed similar hardening rates.

The weak frictional hardening effect of oxygen is consistent with other observations of the macroflow behaviour, which indicate a comparatively weak effect of oxygen on mobile dislocation parameters. For example, 94 at.ppm. oxygen caused a smaller reduction in the work hardening rate of <111> crystals than did 96 at.ppm. nitrogen (see Fig.B22). There is also evidence which suggests that oxygen, through its effect on dynamic dislocation properties, exerts a smaller influence on the yield behaviour than does nitrogen at these concentrations. As shown in Fig.B39, the temperature dependence of the yield

Figure B38 Flow Curves for Nitrogen and Oxygen Doped <149> Crystals

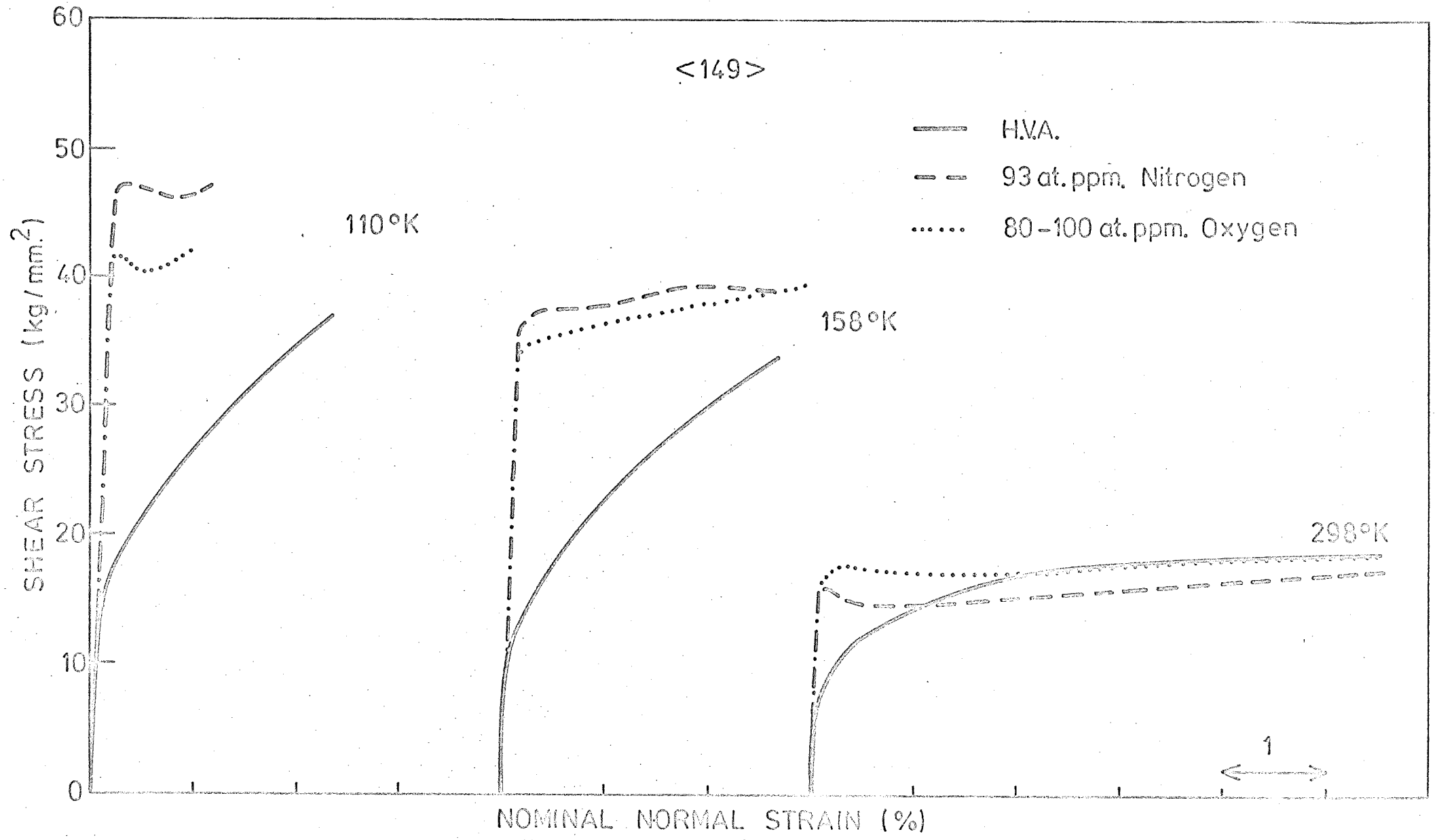
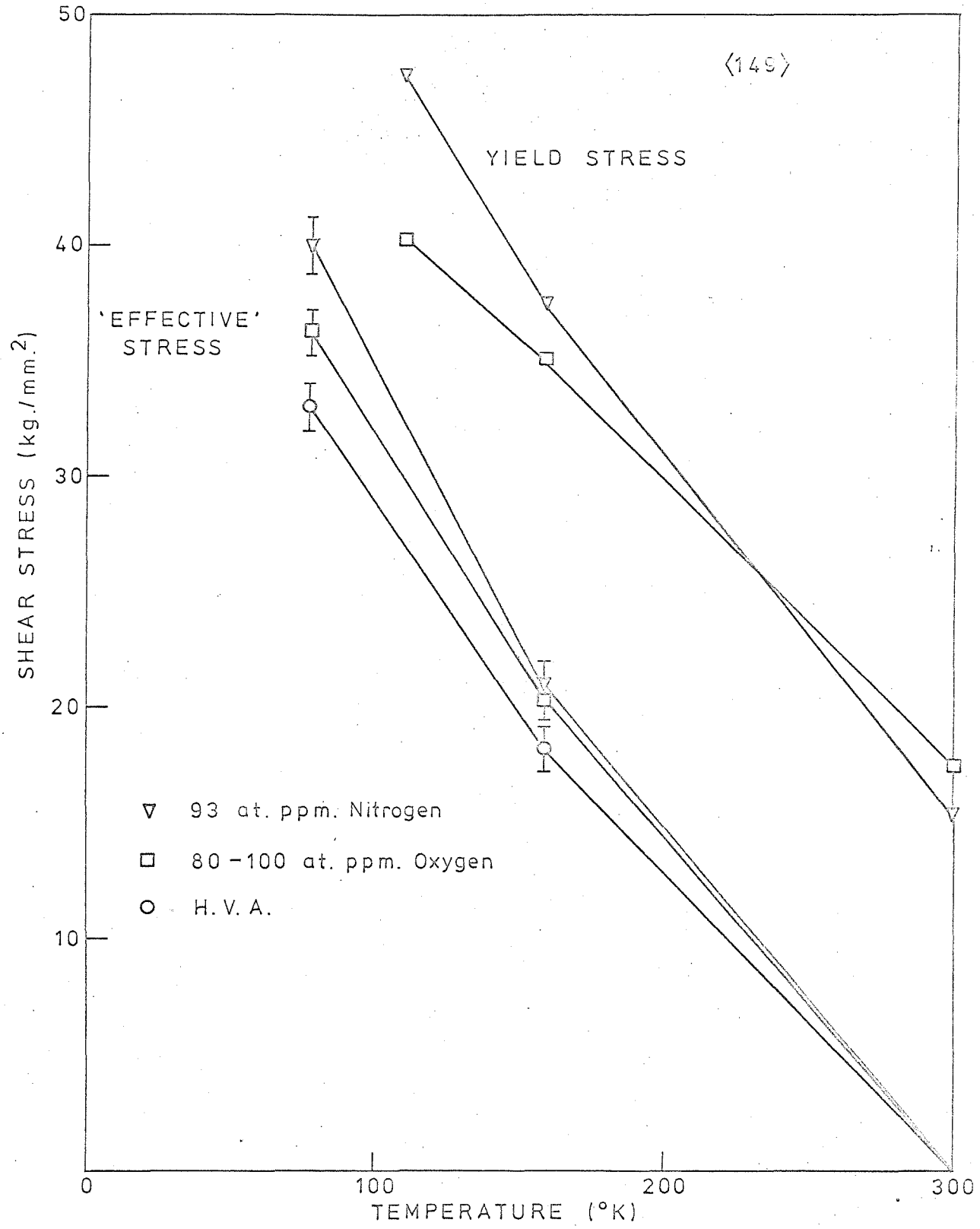

H.V.A.
93 at. ppm. Nitrogen
80-100 at. ppm. Oxygen
110°K
158°K
298°K
SHEAR STRESS (kg/mm²)
NOMINAL NORMAL STRAIN (%)
0
10
20
30
40
50
60
1

Figure B39 'Effective' and Yield Stress versus Temperature
for Nitrogen and Oxygen Doped <149> Crystals


YIELD STRESS
'EFFECTIVE' STRESS
SHEAR STRESS (kg./mm.2)
TEMPERATURE (°K)
50
40
30
20
10
0
100
200
300
93 at. ppm. Nitrogen
80 – 100 at. ppm. Oxygen
H. V. A.

stress is significantly smaller than that of the 'effective' stress in the oxygen doped material. This indicates that the frictional resistance to dislocation motion does not determine the yield stress in this instance. The comparatively weak effect of oxygen on the dynamic behaviour of dislocations may mean that dislocation pinning continues to partly or wholly determine the yield behaviour, as was the case at lower oxygen concentrations.

This would also imply that at low concentrations dislocation pinning effects control the yield in both oxygen and nitrogen doped material but at high concentrations different processes determine the yield behaviour of molybdenum doped with the two respective interstitials. The pinning of dislocations by segregated oxygen atoms may still determine the magnitude of the yield stress at concentrations of ~100 at.ppm. but in molybdenum containing similar concentrations of nitrogen, the yield stress has been shown to be determined by the friction stress on dislocations.

A consideration of the relative importance of the static and dynamic interaction of dislocations with interstitials, in determining the yield behaviour, permits the rationalisation of some apparently contradictory results. For example, the <149> and <011> crystals tested at room temperature showed larger yield stress values after doping with ~100 at.ppm. oxygen than after doping with similar concentrations of nitrogen (see Figs.B22 and B38). This does not contradict the stronger friction hardening effect of nitrogen, established by the differential temperature change results, since the yield of the oxygen doped material is not controlled by the friction stress. Similarly, a comparison of Figs.B11 and B16 indicates much larger yield stress hardening rates for the low nitrogen content material, tested in compression, than for the high nitrogen content material tested in tension. In fact, at room temperature the 'lower' yield stress of the 7 at.ppm. nitrogen doped specimen (~35 kg/mm.^{2}) is greater than that for the 34 and 93 at.ppm. nitrogen doped specimens (~25 and 30 kg/mm.^{2} respectively). This apparent 'softening' may be a consequence of the shift in control of the yield behaviour with

increasing concentration from the static interaction of dislocations and segregated interstitial atoms to the dynamic interaction of dislocations and atoms in bulk solid solution.

11.6 The Effects of Interstitials on the Slip Geometry

The absence of adequate information about the operative slip systems in previous investigations of interstitial alloys has necessarily prejudiced the interpretation of their macroscopic properties. The primary aim of the slip line studies reported in Section 10.4 was to establish what changes in slip behaviour accompanied those changes in the stress-strain curves produced by nitrogen and oxygen doping.

11.6.1 <149> Crystals

The doping of <149> molybdenum crystals with small concentrations of interstitials produced a marked coarsening of slip traces. The origin of this behaviour, which was typical of all the doped material, has been discussed in Section 11.1. The changes in slip geometry which accompanied the coarsening of the slip morphology were far less dramatic.

The <149> doped specimens deformed to small strains (~1%) at 298°K and larger strains (1-5%) at 77°K showed unexpected slip systems characteristic of stage 0 slip behaviour. Slip traces corresponding to $(0\bar{1}1)$ and (101) planes, which have Schmid factors less than the primary $[111](\bar{1}01)$ system (see Table B4), were evident over similar ranges of circumference in all the specimens. Given the demonstrated preference for $\{110\}$ crystallographic slip, both the occurrence of $(0\bar{1}1)$ and (101) slip and the surface ranges over which they were observed are in good agreement with the predictions of Vesely's (1968a,b) surface model (see Section 8.1).

The density of slip traces was not sufficient to permit the presence or absence of dead bands at the side faces for the Burger's vectors ($\underline{b}$) to be established. So it is not certain that the lower Schmid factor $[111]\,\underline{b}$ in the $(0\bar{1}1)$ plane was operative. However, the higher Schmid factor $[\bar{1}11]\,\underline{b}$, which is common to both observed slip planes, is that with the largest surface orientation factor ($\sin\beta$) of all possible $\underline{b}$'s and hence should be preferred over the widest range of surface orientations. In addition, the surface ranges over which the $(0\bar{1}1)$ and (101) traces were observed include the region adjacent to the $[\bar{1}11]$ side face where the slip distance of a screw dislocation to the surface is small, and the surface model predicts slip will be most favoured. Reference to the stereograms in Section 10.4 shows that where the Vesely curve corresponding to the $[\bar{1}11]\,\underline{b}$ most closely approaches the $(0\bar{1}1)$ and (101) great circles, slip traces were observed. This indicates that slip occurred at those surface orientations where the $(0\bar{1}1)$ and (101) planes were most nearly normal to surface and so, allowed the easy escape of screws.

SLIP SYSTEM	SCHMID FACTOR
$[111](\bar{1}01)$	0.50
$[\bar{1}11](101)$	0.45
$[\bar{1}\bar{1}1](011)$	0.32
$[\bar{1}11](0\bar{1}1)$	0.30
$[111](\bar{1}10)$	0.30
$[111](0\bar{1}1)$	0.23
$[\bar{1}\bar{1}1](101)$	0.20
$[1\bar{1}1](011)$	0.18
$[1\bar{1}1](\bar{1}01)$	0.16
$[\bar{1}\bar{1}1](\bar{1}10)$	0.15

Table B4 Schmid Factors for $\langle 111\rangle\{110\}$ Slip Systems at Central Triangle Orientation (see Fig.B10a)

The slip geometry observed for the interstitially doped molybdenum after deformation at 77°K (see Fig.B29).is very similar to that determined for pure molybdenum by Jeffcoat (1975). For example, after both 3% and 6% deformation at 77°K Jeffcoat (1975) found slip to be confined to the same $(0\bar{1}1)$ and (101) planes, although traces were observed over a wider range of surface orientations.

The absence of any significant change in the slip geometry, in spite of the large effects of interstitial doping on the macroyield behaviour at 77°K, is not unexpected. It has been concluded that the discontinuous yield in the low interstitial content material is due to the pinning of dislocations by segregated interstitials, and not edge hardening associated with interstitials in bulk solid solution. Yielding occurs when the stress is sufficient to activate pinned non-screw dislocations and need not lead to the immediate propagation of screw dislocations in the bulk. Instead, work hardening involving the further exhaustion of less favourably oriented non-screw segments must continue until the stress has risen to those levels associated with primary slip in pure molybdenum. Jeffcoat's (1975) results indicate that primary slip does not commence until strains ~6%, which implies that a stress level ~25% greater than the yield stress observed in the doped molybdenum is required to move primary screw dislocations in the bulk. There may also be a critical strain level, in addition to a critical stress level, necessary to initiate primary slip. When primary sources do operate in the bulk, the necessity to eliminate screws previously generated by surface sources during stage 0 may initially inhibit the motion of primary screw dislocations.

Thus, the usual association of the rapid hardening, preyield microstrain region of the stress-strain curve with a stage 0 slip geometry is not valid in the low interstitial content alloys. There are no grounds for equating the anomalous $(0\bar{1}1)$ slip observed here at strains well beyond the yield point with the type observed in stage I in the Group Va metals or in molybdenum-rhenium and molybdenum-niobium alloys (Jeffcoat 1975). The $(0\bar{1}1)$ slip traces

observed in ultra high purity niobium for example, (Duesbery and Foxall 1969) are continuous around the full specimen circumference and are clearly associated with bulk deformation (Bolton and Taylor 1972). In contrast, the $(0\bar{1}1)$ traces in the interstitially doped molybdenum show strong evidence of a surface orientation effect characteristic of stage 0 slip.

The slip geometry observed in the interstitial alloys after 290°K deformation are consistent with a dislocation pinning explanation of the yield. Both the nitrogen and oxygen doped specimens showed $(0\bar{1}1)$ and (101) traces which may be reconciled with deformation in the stage 0 microstrain region. The additional $(\bar{1}01)$ traces shown by the nitrogen doped specimen is probably associated with stage I deformation; a consequence of the larger strain it received. The stage 0 geometry shown by both the nitrogen and oxygen doped material (see Fig.B27) does not, however, agree in detail with previous observations on pure molybdenum at room temperature. For example, after 3% deformation Jeffcoat (1975) observed $(0\bar{1}1)$ traces over a restricted range of surface orientations and also primary $(\bar{1}01)$ traces over the full circumference. Vesely (1968b) also found (011), $(0\bar{1}1)$ and (101) slip after 0.5% strain at room temperature but with many additional non-crystallographic traces. These approximated to planes with the locally shortest slip distance of screws to the surface. All these observations are in reasonable agreement with the general, though not necessarily detailed, predictions of Vesely's (1968b) model. The discrepancy between the individual results may simply reflect the influence of the differing central triangle orientations and strain magnitudes employed.

Thus, low concentrations of interstitials do not appear to cause any significant changes in the slip geometry of molybdenum at 290°K and 77°K. Nevertheless it should be recognised that changes may occur at the much larger interstitial concentrations introduced into the tension specimens.

A reduction in the interstitial impurity content of b.c.c. metals is generally recognised to favour the operation of unexpected or anomalous slip.

The most notable instance of this occurs in the Group Va metals where anomalous $(0\bar{1}1)$ slip only occurs, for example, in niobium and vanadium with very low interstitial impurity contents (Taylor et al. 1973a). There is also evidence that the removal of interstitial impurities from molybdenum modifies the slip geometry. Jeffcoat (1975) compared the slip geometry of 2 and 8 pass zone-melted molybdenum after deformation at 77°K and found that a reduction in the total interstitial content from $\gtrsim$100 at.ppm. to $\lesssim$10 at.ppm. greatly increased the incidence of $(0\bar{1}1)$ anomalous slip. It also promoted the earlier onset of $(\bar{1}01)$ primary slip. The change in the interstitial concentration in solid solution would be very much smaller than the quoted change in total concentration because of the low solid solubility of interstitial elements in molybdenum. Although the magnitude of the change cannot be reliably estimated, these results do suggest a greater sensitivity of the slip geometry to interstitial impurities than was found in the present investigation. A similar discrepancy has been observed in niobium where anomalous $(0\bar{1}1)$ slip is induced by a reduction in interstitial content from $\gtrsim$10 at.ppm. to $\lesssim$1 at.ppm. by ultra high vacuum annealing, zone-melted material (Bolton and Taylor 1972). But Taylor and Bowen (1970) have found that redoping ultra high purity niobium with ~30 at.ppm. nitrogen does not fully suppress $(0\bar{1}1)$ slip.

These results imply that there is some essential difference between observations associated with the controlled introduction of interstitial impurities into high purity metals and those associated with the removal of interstitial impurities by zone-melting, ultra high vacuum annealing and other techniques. It is possible that changes in substitutional impurity concentrations which also occur during purification may account for this difference.

11.6.2 <122> Crystals

Both the unstable yield elongation and the 'ripply' surface profile shown by the interstitially doped <122> crystals which were deformed at 77°K, indicate the occurrence of some type of macroscopically inhomogeneous deformation. The lateral slip traces observed along the specimen length are also probably related to this inhomogeneous deformation. Although twinning frequently occurs in molybdenum at these orientations, the absence of any characteristic load drops and the removal of these traces by electropolishing clearly show that the lateral traces were not twin boundaries. The significance of the $(\bar{2}11)$ plane, which is defined by the more regular traces, is not clear, but it may be important because it is the maximum resolved shear stress plane.

Unstable yield behaviour of the type observed here is frequently associated with the propagation of Lüders bands along the specimen gauge length. No direct evidence of such bands was obtained but the uneven surface profile and lateral traces are generally consistent with the alternate concentration of deformation in macroscopic zones of material. The experimental observations do not offer any explanation as to why interstitials should have such a dramatic effect on the homogeneity of deformation of crystals of this orientation. It is possibly related to the exceptionally coarse slip morphology observed in pure molybdenum at similar orientations (Taylor et al. 1973a).

The dominance of $(\bar{1}01)$ and $(1\bar{1}0)$ crystallographic slip traces at large strains (~6%) in the oxygen doped <122> crystals underlines the general uncertainty about the primary slip system at these symmetry orientations ($\chi = \pm 30^{\circ}$). Jeffcoat (1975) has made similar observations on pure molybdenum which indicate slip on the $(1\bar{1}0)$ and $(\bar{1}01)$ planes (Schmid factors $\simeq 0.41$) is preferred to slip on the $(\bar{2}11)$ plane in the twinning sense (Schmid factor = 0.47) in the macroyield region. These observations imply that the critical resolved

shear stress on the {112} planes in the twinning sense is greater than that on {110} planes which is consistent with Guiu's (1969) conclusions based on direct shear tests. They also confirm that the justification for resolving normal stresses on {112} planes for the corner orientations is in doubt and vindicate the qualifications made in Section 11.4 in this respect.

11.7 General Discussion

There have been numerous investigations of the low temperature deformation behaviour of molybdenum single crystals (e.g. Guiu 1966, Stein 1967, Lau and Dorn 1968, Richter 1971, Vesely 1973a, Kopetskii and Pashkovskii 1974) but few of these have been explicitly concerned with the effects of interstitial impurities. The interstitial impurity, and in particular carbon, content of the material employed in these investigations has varied widely. For example, the carbon content of the zone-melted molybdenum employed by Vesely (1973a) was <4 at.ppm. while that used by Kopetskii and Pashkovskii (1974) was ~250 at.ppm.

The most comprehensive study with respect to the variation of temperature, strain rate and orientation was conducted by Guiu (1966) on molybdenum containing 16-24 at.ppm. carbon, <70 at.ppm. nitrogen and <6 at.ppm. oxygen. The present results obtained on H.V.A. molybdenum containing <4 at.ppm. carbon, <1 at.ppm. nitrogen and <10 at.ppm. oxygen are in good agreement with the temperature and orientation dependence of the flow curves obtained by Guiu (1966) in spite of the apparent difference in material purity. The results reported in PART A have shown that at these generally low impurity levels most of the interstitials are in precipitate form and might not be expected to have a great effect on the deformation behaviour.

At high impurity levels, where larger amounts of interstitials are both precipitated and in supersaturated solid solution, significant changes in the mechanical properties occur. Stein (1967), who reduced the total carbon

concentration in molybdenum from ~100-500 at.ppm. to $\lesssim$80 at.ppm. using a hydrogen annealing treatment, obtained an appreciable reduction in both the proportional limit and the flow stress at large strains. Evidence was also obtained which indicated that interstitials were influencing the low temperature fracture behaviour of molybdenum. When brittle fracture occurred it was frequently found to be associated with precipitates which, although not identified, were probably carbides. But no evidence has been provided by this or other work on molybdenum, concerning the embrittling effects of interstitials when in solid solution. The tension test results obtained in the present investigation demonstrate that nitrogen and oxygen in solid solution increase the susceptibility of molybdenum to brittle fracture. The frequent fracture of the doped specimens after only small elongations at 110°K and 158°K and the occasional elastic fracture of nitrogen doped specimens deformed at 77°K after high temperature prestrain, indicate that both nitrogen and oxygen have a deleterious effect on ductility at low temperatures.

Lau and Dorn (1968) also achieved variable carbon levels in molybdenum by using a number of different post zone-melting annealing treatments. No change in the temperature dependence of the yield stress (0.2% proof) and the activation volume in the concentration range 160-1600 at.ppm. was observed. Since the material was not quenched from the annealing temperature, the concentration of carbon secured in solid solution cannot be determined. It is very likely that precipitated and clustered carbon was responsible for the athermal hardening that was observed and a comparatively small variation in carbon concentration in solid solution accounted for the absence of a detectable thermal hardening effect. So the strong thermal hardening observed in the present investigations, where nitrogen and oxygen were quenched into solid solution, can be readily reconciled with these earlier results.

The much higher terminal solid solubilities of interstitials in Group Va metals allows the experimental and interpretative difficulties associated with precipitation to be avoided. Several investigations of Group Va metal-

interstitial solid solution alloys have been undertaken which allow direct comparisons to be made with the results obtained here for molybdenum-nitrogen and molybdenum-oxygen alloys.

The thermal hardening rates of the yield stress for nitrogen in molybdenum, niobium and tantalum have been shown to be similar (see Table B3). However, this result may not be confidentally held to represent a similar increase in the thermal component of the friction stress on dislocations in the three metals. Certainly, the yield stress in molybdenum at large nitrogen concentrations has been shown to constitute a reasonable index of the friction stress but in Taylor and Bowen's (1970) investigation of niobium-nitrogen alloys the yield stress appears to reflect other parameters (see Section 8.4.1).

The larger thermal hardening rate of the 'effective' stress due to nitrogen in molybdenum in comparison with nitrogen in niobium, which has been estimated in Section 11.3, is a more reliable indication of the comparative frictional resistances to dislocation motion. This result suggests that, in terms of a specific elastic or more general chemical interaction with the lattice, nitrogen atoms have a stronger effect on molybdenum than niobium. But, consideration should be given to the atom clustering which occurs in the supersaturated molybdenum-nitrogen solid solutions. There is no evidence of comparable clustering occurring in Group Va metal-interstitial solid solutions at concentrations $\lesssim$5,000 at.ppm. (Fast 1971). So the difference in the magnitude of the lattice hardening between niobium and molybdenum may reflect the different degrees of aggregation of the nitrogen atoms in addition to any difference in the specific hardenings effects of individual nitrogen atoms. Neither the obstacle hardening nor screw dislocation core models give any clear indication of whether a small density of large atom clusters should cause a stronger or weaker hardening effect than a larger density of unclustered atoms. The experimental evidence from some substitutional alloy hardening systems (e.g. aluminium-copper) is that the maximum frictional hardening occurs when the solute atoms are clustered.

The lattice parameter and residual resistivity measurements reported in PART A may provide supporting evidence for the relative hardening effects of nitrogen in molybdenum and niobium. The specific lattice parameter change for unclustered nitrogen atoms in molybdenum is very much greater than that in niobium (see Table A12). This, to the extent that the increase in the thermal component of the lattice friction stress can be correlated with the mean elastic distortion of the lattice, is consistent with the stronger thermal hardening effect of nitrogen in molybdenum than niobium. The specific residual resistivity of nitrogen in molybdenum and niobium are approximately equal (3.5×10^{-10} and 3.8×10^{-10} ohm cm./at.ppm. respectively) which is not in agreement with their relative hardening rates. But if the resistivity values are normalised with respect to the thermal resistivity components of molybdenum and niobium (5.0 and 12.0μ ohm cm. at 273°K respectively) nitrogen in molybdenum does give a larger value (0.7) than nitrogen in niobium (0.3).

11.8 Summary

(i) Interstitial alloying has been shown to have a strong effect on the deformation behaviour of molybdenum throughout the concentration range investigated (<10 - >100 at.ppm.). The effects are complex and appear to be associated with both the static and dynamic interaction of dislocations with interstitial atoms.

(ii) The doping of molybdenum with low concentrations of nitrogen and oxygen atoms causes a dramatic coarsening of the surface slip traces but no significant change in the slip geometry.

(iii) The principal effect on the stress-strain behaviour at low concentrations is the introduction of a discontinuous yield. This is believed to be a consequence of the pinning of the grown-in dislocations by interstitial atoms.

(iv) At higher concentrations of interstitials changes in the flow

behaviour at large strains occur. The most notable of these is a reduction in the work hardening rate which indicates that unsegregated interstitial atoms in bulk solid solution are influencing the dynamic behaviour of dislocations.

(v) Nitrogen causes an increase in both the temperature dependence of the yield stress defined by direct deformation tests, and the temperature dependence of the flow stress defined by differential temperature change tests. The magnitude of the increase in both cases is dependent on the orientation of the deformation axis.

(vi) There is good evidence to indicate that the thermal hardening rate of the friction stress for nitrogen in molybdenum is more than twice that for nitrogen in niobium. This is consistent with the comparatively large lattice parameter changes and the clustering of the solute atoms which occur in the supersaturated molybdenum-nitrogen solid solutions.

(vii) Nitrogen has a stronger effect than oxygen on the general deformation behaviour of molybdenum. This is in agreement with similar comparative observations made on Group Va metals. However, the influence of each interstitial species on both static and dynamic dislocation processes must be considered in any detailed interpretation of their comparative effects.

Chapter 12

GENERAL CONCLUSIONS

An investigation of the deformation behaviour of molybdenum-nitrogen and molybdenum-oxygen alloys has been conducted which is believed to be the first involving the controlled addition of interstitial solutes to a Group VIa metal.

The molybdenum-interstitial alloys show many properties which are similar to those observed in other b.c.c. metal-interstitial systems. For example, the interstitial doping of molybdenum introduces a yield point, coarsens the slip morphology and usually causes a reduction in the work hardening rate. There is also a large lattice contribution to the low temperature flow stress of molybdenum which is consistent with the results obtained in recent investigations of dilute interstitial alloys of iron and Group Va metals.

However, there are several prominent features of the deformation behaviour of the molybdenum-interstitial alloys which imply significant differences exist between the behaviour of interstitials in solid solution in Group Va and Group VIa metals. There is a strong indication that nitrogen causes a larger increase in the thermal component of the friction stress on dislocations in molybdenum than in niobium. The larger frictional hardening effect of the atom clusters which are present in the supersaturated molybdenum-nitrogen solid solutions may be partly responsible for this difference. But lattice parameter measurements indicate that the mean elastic dilatation of the lattice caused by individual nitrogen atoms is much greater in molybdenum than in Group Va metals. This might also be expected to produce a larger increase in the lattice friction stress of molybdenum than of Group Va metals.

Similar physical and mechanical property measurements for other Group VIa metal-interstitial alloys are necessary to verify the generality of these conclusions about the comparative behaviour of interstitials in metals of the two Groups.

Both the thermal hardening of the yield and of the flow stress caused by nitrogen and oxygen atoms in solid solution would be expected to have a detrimental effect on ductility. Direct experimental evidence confirming this expectation is provided by the occasional elastic fracture, and the usually smaller uniform elongations, of the doped molybdenum in comparison with the H.V.A. molybdenum single crystals. In polycrystalline, commercial purity molybdenum where many of the interstitial impurities are precipitated or segregated to grain boundaries, other embrittling mechanisms may be more important.

An investigation of the deformation and fracture behaviour of polycrystalline molybdenum-interstitial alloys would seem a natural progression from the present work. This would provide information concerning the relative importance of interstitials in bulk solid solution, and those segregated to or precipitated at grain boundaries, in determining the mechanical properties of molybdenum. The now well established techniques for quenching nitrogen into solid solution in mechanical test specimens would recommend an initial examination of molybdenum-nitrogen alloys. An investigation of molybdenum-oxygen alloys might appear more attractive in view of the dramatic embrittling effect of oxygen in polycrystalline molybdenum (Touboul et al. 1971). But more kinetic and thermodynamic data is required to allow the preparation of better characterised molybdenum-oxygen alloys. The use of hydrogen/water vapour, instead of oxygen, annealing atmospheres may avert many of the experimental difficulties caused by the high oxidation rate of molybdenum in the oxygen doping treatments.

An extended study of the deformation behaviour of molybdenum-interstitial single crystals using, in particular, transmission electron microscopy is not

recommended. Recently reported results for tantalum-nitrogen alloys (Welsch et al. 1975) suggest that little useful information concerning the dislocation mechanisms responsible for the effects of alloying on the macroscopic properties would be obtained from such an investigation. However, the well characterised ageing behaviour of molybdenum-nitrogen solid solutions (Eyre and Evans 1972) would provide a suitable basis for a transmission electron microscopic investigation of the deformation behaviour of quenched and aged nitrogen alloys. This may give some insight into the role of precipitates in determining the mechanical behaviour of furnace cooled, commercial molybdenum and molybdenum alloys, where most of the interstitials are present in precipitate form.

ACKNOWLEDGEMENTS

The author would like to thank all those at Harwell and in the Oxford Department who have aided and abetted this research project. He would especially like to thank -

Professor J.W. Christian and Mr. B.L. Eyre for their patient supervision and persevering interest.

Dr. G. Taylor for his invaluable advice and many stimulating discussions.

Hugh Evans for his constant companionship and unfailing assistance in the laboratory.

Professor Sir P.B. Hirsch for the use of laboratory facilities and A.E.R.E. Harwell for financial support.

REFERENCES

Altschuler T.L. and Christian J.W. 1967, Phil. Trans. Roy. Soc. A261, 253.

Argon A.S. and Maloof S.R. 1966, Acta Metall. 14, 1449.

Arsenault R.J. 1966, Acta Metall. 14, 831.

Baker C.A. and Williams D.R. 1968, Talanta 15, 1143.

Baker T.W., George J.D., Bellamy B.A. and Causer R. 1968, Advances in X-ray Analysis 11, 359.

Barthel J. and Eichler K. 1967, Kristall. und Tecknik 2, 205.

Basinski Z.S., Duesbery M.S. and Taylor R. 1970a, Phil. Mag. 21, 1201.

Basinski Z.S., Duesbery M.S., Pogany A., Taylor R. and Varshni Y.P. 1970b, Can. J. Phys. 48, 1480.

Basinski Z.S., Duesbery M.S. and Taylor R. 1971, Can. J. Phys. 49, 2160.

Belk J.A. 1959a, Services Electronics Research Laboratory Technical Report (80), 9.

Belk J.A. 1959b, J. Less-Com. Metals 1, 50.

Bernstein I.M. 1969, Acta Metall. 17, 249.

Birbeck F.E. and Calverley A. 1959, J. Sci. Instr. 36, 460.

Bluem M.F. 1972, Ph.D. Thesis, University of Illinois.

Bolton C.J. and Taylor G. 1972, Phil. Mag. 26, 1359.

Boser O. 1968, Interaction between Dislocations and Point Defects, HMSO, London, p.693.

Bowen D.K. 1966, D. Phil. Thesis, Oxford University.

Bressers J., Creten R. and Van Holsbeke G. 1975, J. Less-Com. Metals 39, 7.

Burck P., Kötthe A. and Werth F.R. 1969, Phys. Stat. Sol. 36, K171.

Calverley A., Davis M. and Lever R.L. 1957, J. Sci. Instr. 34, 142.

Chang R. 1967, Phil. Mag. 16, 1021.

Christian J.W. 1968, Interaction between Dislocations and Point Defects, HMSO, London, p.604.

Christian J.W. 1970, Proc. 2nd Int. Conf. on Strength of Metals and Alloys, Asilomar, ASM, p.31.

Christian J.W. and Vitek V. 1970, Rep. Prog. Phys. 33, 307.

Conrad H. and Hayes W. 1963, Trans. ASM 56, 939.

Cottrell A.H. and Bilby B.A. 1949, Proc. Phys. Soc. A62, 49.

Cottrell A.H. 1963, Relation between Structure and Mechanical Properties of Metals, HMSO, London, p.456.

Damask A.C. and Dienes G.J. 1963, Point Defects in Metals, Gordon and Breach, p.81.

Das G.C. and Pratt P.L. 1970, Proc. 2nd Int. Conf. on Strength of Metals and Alloys, Asilomar, ASM, p.103.

Dorn J.E. and Mukherjee A.K. 1969, Trans. AIME 245, 1493.

Dorn J.E. and Rajnak S. 1964, Trans. AIME 230, 1052.

Duesbery M.S. 1969, Phil. Mag. 19, 501.

Duesbery M.S. and Foxall B.A. 1969, Phil. Mag. 20, 719.

Duesbery M.S., Vitek V. and Bowen D.K. 1973, Proc. Roy. Soc. A332, 85.

Dürrschnabel W. and Hörz G. 1963, Naturwissenschaften 22, 687.

Elefant D. 1971, Thesis, Deutsche Akademie der Wissenschaften zu Berlin.

Escaig B. 1966, J. Phys. 27 (C-3), 205.

Escaig B. 1967, J. Phys. 28, 171.

Evans J.H. 1967, Private communication.

Evans J.H. and Eyre B.L. 1968a, J. Sci. Instr. 1, 578.

Evans J.H. and Eyre B.L. 1968b, Phys. Stat. Sol. 25, K39.

Evans J.H. and Eyre B.L. 1969, Acta Metall. 17, 1109.

Evans J.H., Eyre B.L. and Birnbaum H.K. 1970, Acta Metall. 18, 835.

Eyre B.L. and Evans J.H. 1972, Acta Metall. 20, 267.

Eyre B.L., Maher D.M. and Bartlett A.F. 1970, Phil. Mag. 23, 439.

Fast J.D. 1950, Rev. Met. 47, 779.

Fast J.D. 1971, Interaction of Metals and Gases Vol. 2, Macmillan, London p.246.

Feng C. and Kramer I.R. 1965, Trans. AIME 233, 1467.

Few W.E. and Manning G.K. 1952, J. of Metals 4, 271.

Fleischer R.L. 1962a, Acta Metall. 10, 835.

Fleischer R.L. 1962b, J. Appl. Phys. 33, 3504.

Flinn P.A. 1962, Strengthening Mechanisms in Solids, ASM, p.17.

Foxall R.A., Duesbery M.S. and Hirsch P.B. 1967, Can. J. Phys. 45, 903.

Frank W. 1966, Phys. Stat. Sol. 18, 459.

Frank W. 1967, Phys. Stat. Sol. 19, 239.

Frank W. 1968, Phys. Stat. Sol. 26, 197.

Frank W. and Sestak B. 1970, Scripta Metall. 4, 451.

Frauenfelder R. 1968, J. Chem. Phys. 48, 3966.

Friedrich K., Barthel J. and Kunze J. 1968, J. Less-Com. Metals 14, 55.

Fromm E. and Jehn H. 1967, Z. Metallk. 58, 61.

Fromm E. and Jehn H. 1970, J. Less-Com. Metals 21, 331.

Fromm E. and Jehn H. 1971, Z. Metallk. 62, 372, 378.

Fromm E. and Jehn H. 1972, Met. Trans. 3, 1685.

Garlick R.G. and Probst H.B. 1964, Trans. AIME 230, 1120.

Garratt-Reid A. 1973, D. Phil. Thesis, Oxford University.

Gebhardt E., Seghezzi H.D. and Dürrschnabel W. 1958, Z. Metallk. 58, 61.

Gebhardt E., Fromm E. and Roy U. 1966, Z. Metallk. 57, 732.

Gehlen P.C. 1970, J. Appl. Phys. 41, 5165.

Guiu F. 1966, Ph.D. Thesis, London University.

Guiu F. 1967, Phys. Stat. Sol. 19, 339.

Guiu F. 1969, Scripta Metall. 3, 449.

Guiu F. and Pratt P.L. 1966, Phys. Stat. Sol. 15, 539.

Guyot P. and Dorn J.E. 1967, Can. J. Phys. 45, 983.

Hahn G.T. 1962, Acta Metall. 10, 727.

Hall M.M. 1974, Met. Trans. 5, 955.

Hirsch P.B. 1960, 5th Int. Conf. on Crystallography, Cambridge (Oral communication).

Hirsch P.B. 1968, Trans. Jap. Inst. Metals, Suppl. 9, XXX.

Hislop J.S. and Williams D.R. 1971, Radiochem. and Radioanal. 7, 129.

Holmwood R.A. and Glang R. 1965, J. Chem. Eng. Data 10, 162.

Hörz G. 1968, Z. Metallk. 59, 283.

Hörz G. 1969, Z. Metallk. 60, 50.

Hörz G. 1972, Met. Trans. 3, 3069.

Hörz G., Gebhardt E. and Dürrschnabel W. 1965, Z. Metallk. 56, 554.

Hörz G., Lindenmaier K. and Klaiss R. 1974, J. Less-Com. Metals 35, 77.

Jeffcoat P. 1975, Ph.D. Thesis, University of Liverpool.

Johnston W.G. and Gilman J.J. 1959, J. Appl. Phys. 30, 129.

Jung P. and Trenzinger K. 1974, Acta Metall. 22, 123.

Kopetskii Ch.V. and Pashkovskii A.I. 1974, Phys. Stat. Sol. 21, 741.

Korenko M.K., Mitchell T.E. and Gibala R. 1974, Acta Metall. 22, 649.

Köthe A. 1972, Proc. Int. Discussion Meeting on Defects in Refractory Metals, Mol, SCK/CEN, p.125.

Kovtun G.P., Kruglykh A.D. and D'Yakov I.G. 1966, Rus. Met. 1, 21.

Kramer I.R. 1967, Trans. AIME 239, 520.

Krautz E., Kuhlmann H. and Schultz H. 1968, Z. Metallk. 59, 133.

Kroupa F. and Vitek V. 1967, Can. J. Phys. 45, 945.

Kroupa F. and Hull D. 1969, Czech. J. Phys. 319, 763.

Kunze J. and Reichelt W. 1970, J. Less-Com. Metals 20, 327.

Lachenmann R. and Schultz H. 1972, Scripta Metall. 6, 731.

Lachenmann R. and Schultz H. 1973, Scripta Metall. 7, 155.

Lau S.S. and Dorn J.E. 1968, Scripta Metall. 2, 335.

Loomis B.A. and Gerber S.B. 1970, Scripta Metall. 4, 921.

Luft A. 1970, Phys. Stat. Sol. 42, 429.

Luft A. and Kaun L. 1969, Phys. Stat. Sol. 34, 135.

Luft A. and Kaun L. 1973, Phys. Stat. Sol. 18, 109.

Ma Y. and Son J. 1964, Acta Metall. Sinica 7, 68.

Matsui H. and Kimura H. 1973, Scripta Metall. 7, 905.

Matsui H. and Kimura H. 1974, Scripta Metall. 8, 463.

Matsui H., Saka H., Noda K., Kimura H. and Imura T. 1974, Scripta Metall. 8, 467.

Meyerhoff R.W. 1971, J. Electrochem. Soc. 118, 997.

Minami F., Kuramoto E. and Takeuchi S. 1972, Phys. Stat. Sol. 12a,581.

Nakada Y. and Keh A.S. 1968, Acta Metall. 16, 903.

Nakonechnikov A.J., Pavlinov L.V. and Bykov V.N. 1966, Fiz. Metal. Metalloved 22, 234.

Ohba Y., Tamura Y. and Fujii T. 1971, J. Jap. Inst. Metals 12, 348.

Ono K. and Sommer A.W. 1970, Met. Trans. 1, 877.

Oppermann H., Weise G., Barthel J. and Berthel K.H. 1967, Phys. Stat. Sol. 22, K151.

Piguzov V.Yu., Werner W.D. and Rzhevskaya I.Ya. 1967, Fiz. Met. Metalloved 24, 560.

Pink E. 1973, Phys. Stat. Sol. 16, 633.
Powers R.W. and Doyle M.V. 1959, J. Appl. Phys. 30, 514.

Prekel H.L., Lawley A. and Conrad H. 1968, Acta Metall. 16, 337.

Ravi K.V. and Gibala R. 1970, Acta Metall. 18, 623.

Ravi K.V. and Gibala R. 1972, Met. Trans. 3, 3081.

Richter J. 1971, Phys. Stat. Sol. 46, 203.

Rose R.M., Ferris D.P. and Wulff J. 1962, Trans. AIME 224, 981.

Rudman P.S. 1967, Trans. AIME 239, 1949.

Saka H., Noda K. and Imura T. 1973, Crystal Lattice Defects 4, 45.

Schultz H. 1964, Acta Metall. 12, 649.

Schultz H. 1968, Material Science and Engineering 3, 189.

Scrivastava S.C. and Seigle L.L. 1974, Met. Trans. 5, 49.

Sestak B. and Seeger A. 1973, Proc. 3rd Int. Conf. on Strength of Metals and Alloys, Cambridge, ASM, p.563.

Seybolt A.U. 1954, Trans. AIME 200, 770.

Sharp J.V. 1964, D. Phil. Thesis, Oxford University.

Smialek R.L. and Mitchell T.E. 1970a, Phil. Mag. 22, 1105.

Smialek R.L. and Mitchell T.E. 1970b, Proc. 2nd Int. Conf. on Strength of Metals and Alloys, Asilomar, ASM, p.73.

Smith J.V. (ed.) 1960, X-ray Powder Data File, ASTM.

Snoek J.L. 1941, Physica 8, 711.

Solomon H.D. and McMahon C.J. 1968, Advances in Materials Research 2, 311.

Speiser R, Spretnak J.W., Few W.E. and Park R.M. 1952, J. of Metals 4, 275.

Statham C.D. 1968, D. Phil. Thesis, Oxford University.

Stein D.F. 1967, Can. J. Phys. 45, 1063.

Stein D.F. 1968, Dislocation Dynamics, McGraw-Hill, New York, p.453.

Stein D.F. and Low J.R. 1960, J. Appl. Phys. 31, 362.

Stein D.F. and Low J.R. 1966, Acta Metall. 14, 1183.

Stein D.F., Low J.R. and Seybolt A.V. 1963, Acta Metall. 2, 1253.

Stein D.F., Wang Chen C.P. and Ayres R.A. 1973, Inhomogeneity of Plastic Deformation, ASM, p.55.

Stokes R.J. and Cottrell A.H. 1954, Acta Metall. 2, 343.

Szkopiak Z.C. 1970, J. Less-Com. Metals 21, 383.

Takeuchi T. 1969, J. Phys. Soc. Jap. 27, 436.

Takeuchi T. 1973, J. Phys. Soc. Jap. 35, 1149.

Takeuchi S., Taoka T. and Yoshida H. 1967, Trans ISIJ 9, 105.

Takeuchi S., Kuramoto E. and Suzuki T. 1972, Acta Metall. 20, 909.

Taylor A. and Doyle N.J. 1967a, J. Less-Com. Metals 13, 313.

Taylor A. and Doyle N.J. 1967b, J. Less-Com. Metals 13, 399.

Taylor A. and Doyle N.J. 1967c, J. Less-Com. Metals 13, 511.

Taylor G. 1965, D. Phil. Thesis, Oxford University.

Taylor G. 1973, J. Phys. (E), 6, 513.

Taylor G. 1974, Scripta Metall. 8, 459.

Taylor G. and Bowen D.K. 1970, Proc. 2nd Int. Conf. on Strength of Metals and Alloys, Asilomar, ASM, p.78.

Taylor G. and Bowen D.K. 1975, to be published.

Taylor G. and Christian J.W. 1965, Acta Metall. 13, 1216.

Taylor G. and Christian J.W. 1967, Phil. Mag. 15, 873.

Taylor G., Bajaj R. and Carlson O.N. 1973, Phil. Mag. 28, 1035.

Taylor G., Vesely D. and Christian J.W. 1973a, Proc. 3rd Int. Conf. on Strength of Metals and Alloys, Cambridge, ASM, p.1.

Taylor G.I. 1928, Proc. Roy. Soc. A118, 1.

Thornley J.C. 1968, Material Science Research Report, University of Bradford, p.111.

Touboul J., Minel L. and Langeron J. 1971, C.R. Acad. Sci. Paris t272, Series C, 1109.

Touboul J., Minel L. and Langeron J. 1973, J. Less-Com. Metals 30, 279.

Trenzinger K., Jung P. and Schilling W. 1974, Acta Metall. 22, 937.

Ulitchny M.G. Sagues A.A. and Gibala R. 1972, Proc. Int. Discussion Meeting on Defects in Refractory Metals, Mol, CEN/SCK, p.245.

VanTorne L.I. and Thomas G. 1966, Acta Metall. 14, 621.

Vaughan D.A., Stewart O.M. and Schwartz Ch.M. 1961, Trans. AIME 221, 937.

Vesely D. 1968a, Phys. Stat. Sol. 29, 675.

Vesely D. 1968b, Phys. Stat. Sol. 29, 685.

Vesely D. 1972, Scripta Metall. 6, 753.

Vesely D. 1973a, Phil. Mag. 27, 607.

Vesely D. 1973b, J. of Microscopy 97, 191.

Vesely D. 1974, Proc. 3rd Int. Conf. on HVEM, Oxford, Academic, p.189.

Vitek V. 1968, Phil. Mag. 18, 773.

Vitek V. 1970, Phil. Mag. 21, 1275.

Vitek V. 1974, Crystal Lattice Defects, 5, 1.

Vitek V. and Kroupa F. 1969, Phil. Mag. 19, 265.

Vitek V. and Yamaguchi M. 1973, J. of Phys. (F) 3, 537.

Vitek V., Perrin R.C. and Bowen D.K. 1970, Phil. Mag. 21, 1049.

Vreeland T. and Turner A.P.L. 1969, Scripta Metall. 3, 193.

Weaver D.E. 1972, Ph.D. Thesis, Davis UCLA.

Webb G.L., Gibala R. and Mitchell T.E. 1973, Proc. 3rd Int. Conf. on Strength of Metals and Alloys, Cambridge, ASM, p.155.

Welsch G., Gibala R. and Mitchell T.E. 1975, Phys. Stat. Sol. 30, 117.

Wynblatt P. and Dorn J.E. 1966, Trans. AIME 236, 1451.

Yamaguchi M. and Vitek V. 1973, J. Phys. (F) 3, 523.